Technical Report SL-94-2
February 1994

US Army Corps
of Engineers
Waterways Experiment
Station

AD--A277 879

(2)

DNA/WES Ground Motion Test Facility–Results and Analysis of Impact Tests Against Masonry and Socorro Plaster Sand Testbeds

by *Howard G. White*
Structures Laboratory

John T. Byrne
IIT Research Institute

DTIC
ELECTE
APR 05 1994
S B D

WES

Approved For Public Release; Distribution Is Unlimited

94-10189

94 4 4 109

DTIC QUALITY INSPECTED 3

Prepared for Defense Nuclear Agency, Headquarters
and Defense Nuclear Agency, Field Command

The contents of this report are not to be used for advertising, publication, or promotional purposes. Citation of trade names does not constitute an official endorsement or approval of the use of such commercial products.

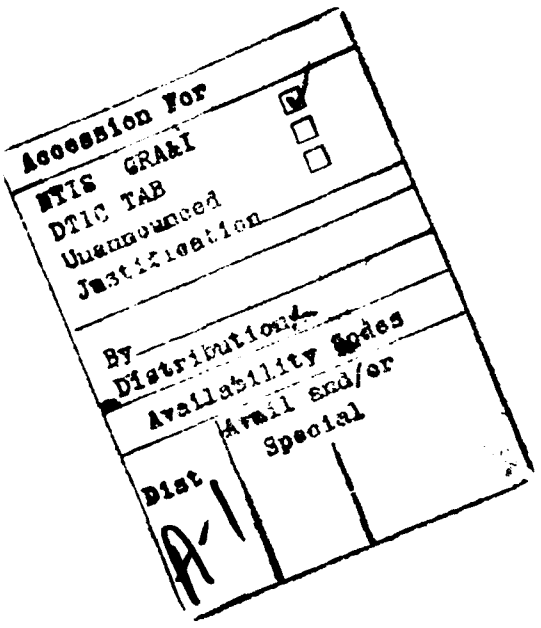

PRINTED ON RECYCLED PAPER

Technical Report SL-94-2
February 1994

DNA/WES Ground Motion Test Facility– Results and Analysis of Impact Tests Against Masonry and Socorro Plaster Sand Testbeds

by Howard G. White
Structures Laboratory

U.S. Army Corps of Engineers
Waterways Experiment Station
3909 Halls Ferry Road
Vicksburg, MS 39180-6199

John T. Byrne
IIT Research Institute
10 West 35th Street
Chicago, IL 60616

Final report

Approved for public release; distribution is unlimited

DTIC QUALITY INSPECTED 3

Prepared for Defense Nuclear Agency, Headquarters
6801 Telegraph Road
Alexandria, VA 22510-3398

and Defense Nuclear Agency, Field Command
Kirtland Air Force Base, NM 87115-5000

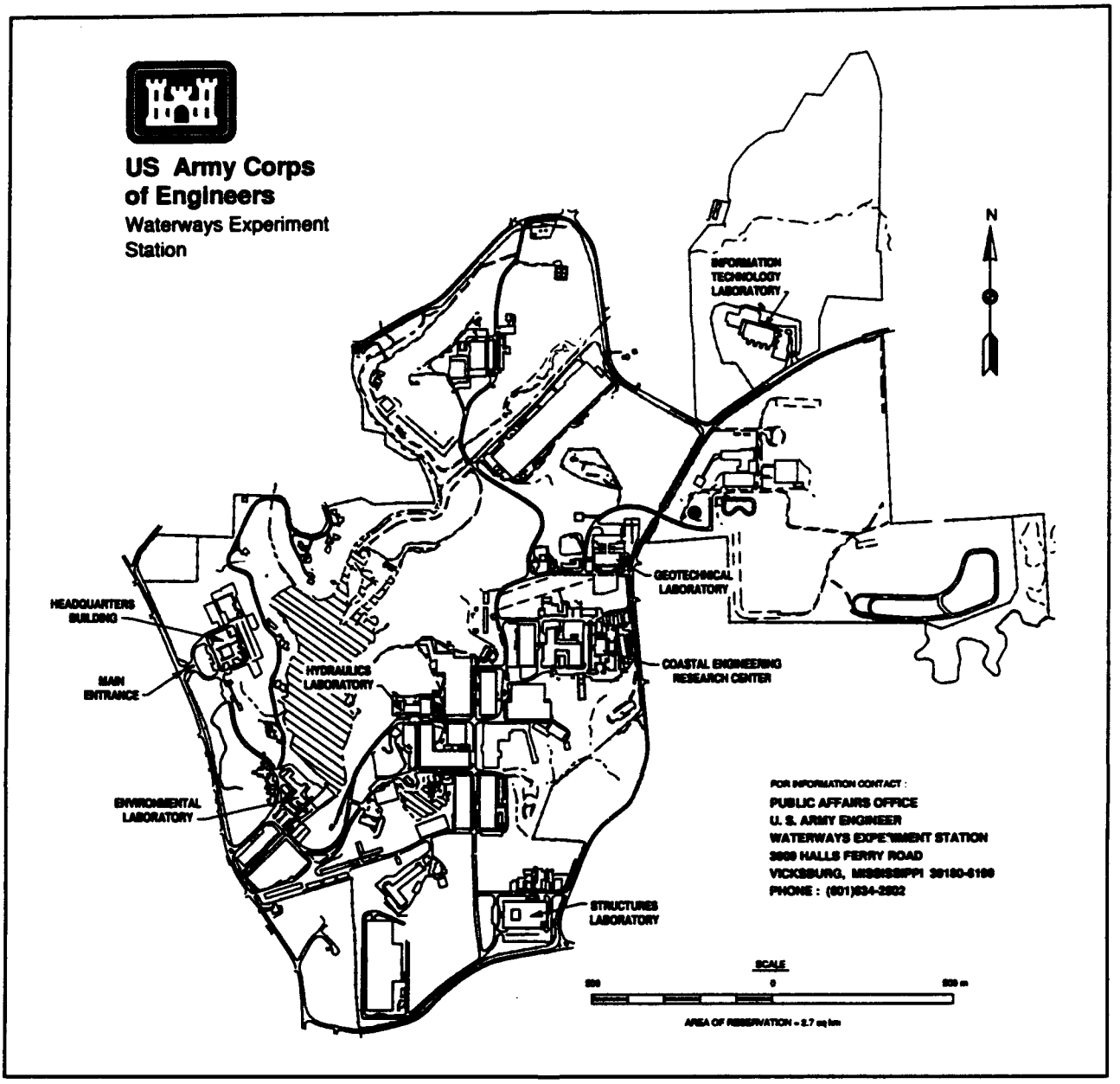

Waterways Experiment Station Cataloging-in-Publication Data

White, Howard G.

DNA/WES Ground Motion Test Facility—results and analysis of impact tests against masonry and socorro plaster sand testbeds / by Howard G. White [and] John T. Byrne ; prepared for Defense Nuclear Agency, Headquarters, and Defense Nuclear Agency, Field Command.

153 p. : ill. ; 28 cm. — (Technical report ; SL-94-2)

Includes bibliographical references.

1. Projectiles — Testing. 2. Penetration mechanics — Testing. 3. Impact — Testing. I. Byrne, John T. II. United States. Defense Nuclear Agency. III. U.S. Army Engineer Waterways Experiment Station. IV. Title. V. Series: Technical report (U.S. Army Engineer Waterways Experiment Station) ; SL-94-2.

TA7 W34 no.SL-94-2

Contents

Preface ix

1—Introduction 1

Background 1
Description of Ground Motion Test Facility 1
Objectives 4
Scope 4

2—Experiment Description 5

Testbed Construction 5
Typical Instrumentation Layout 5
Testing Procedure 9

3—Experiment Data 13

Testbed Material Data 13
Active Measurement Data 13
Time-of-Arrival Data 14
Determination of Propagation Velocity of Rarefaction Wave 29
Graphical Method 29
Analytic Method 29

4—Analysis of Nonnormal Impacts 38

Requirement 38
Description of Nonnormal Impact 38
Description of CLAP Code 41
Determination of First Point of Impact on the Surface of the Testbed and Angle of Impact 41
Determination of the Loading Wave Speed in the Testbed Using TOA Measurements at the Surface of the Testbed 43
Determination of the Loading Wave Speed in the Testbed on a Trial and Error Basis 54

5—Conclusion and Recommendations 58

Conclusions 58

Recommendations 58

References 60
Appendix A: Notation A1
Appendix B: Gage Locations for Tests in Sand B1
Appendix C: Wet Density and Moisture Content Profiles for Tests in Sand C1
Appendix D: Active Measurement Data for Tests in Sand D1

List of Tables

Table 1. Stress Gages Used for Tests in Sand 6
Table 2. Velocity Gages Used for Tests in Sand 6
Table 3. Test Pressure Level, Projectile Mass, and Projectile Velocity for Tests in Sand 10
Table 4. Average Wet Density and Moisture Content for Sand Testbeds 14
Table 5. Propagation Velocity of Loading Shock Wave for Tests in Sand 28
Table 6. Unloading Wave Speed, C_u, as Determined by the Analytic Method for Test 22, Assuming a Constant Loading Wave Speed 34
Table 7. Unloading Wave Speed, C_u, as Determined by the Analytic Method for Test 22, Assuming a Varying Loading Wave Speed 37
Table 8. Comparison of Loading Wave Speed Determined by Graphical Procedure and by Trial and Error CLAP Calculation 57
Table B1. Gage Locations for Tests in Sand B2

List of Figures

Figure 1. DNA/WES Ground Motion Test Facility 2
Figure 2. Schematic of the 4-ft-diameter gas gun 3
Figure 3. Typical layout for testbed instrumentation 7

Figure 4. Cross section of the gas gun projectile and container of target material 8

Figure 5. Recording setup for tests with the 4-ft gas gun 11

Figure 6. Control panel used in operating the gas gun 11

Figure 7. Fill system used for conducting tests with the gas gun 12

Figure 8. Typical target geometry for tests in sand 15

Figure 9. Time-of-arrival vs. distance for Test 6 16

Figure 10. Time-of-arrival vs. distance for Test 7 17

Figure 11. Time-of-arrival vs. distance for Test 8 18

Figure 12. Time-of-arrival vs. distance for Test 10 19

Figure 13. Time-of-arrival vs. distance for Test 11 20

Figure 14. Time-of-arrival vs. distance for Test 12 21

Figure 15. Time-of-arrival vs. distance for Test 13 22

Figure 16. Time-of-arrival vs. distance for Test 14 23

Figure 17. Time-of-arrival vs. distance for Test 15 24

Figure 18. Time-of-arrival vs. distance for Test 16 25

Figure 19. Time-of-arrival vs. distance for Test 17 26

Figure 20. Time-of-arrival vs. depth for Test 22 27

Figure 21. Schematic of canister positions at TOA of the loading and unloading waves 30

Figure 22. Stress measurements at the two instrumented depths from Test 22, indicating TOA of the loading (T1 and T2) and unloading (T3 and T4) waves 31

Figure 23. Graphical determination of the unloading wave speed, C_u 32

Figure 24. Determination of a varying loading wave speed through the depth of the target 36

Figure 25. Schematic of nonnormal impact 40

Figure 26. Schematic of parameters used to determine the first point of impact on the testbed surface for nonnormal impacts 42

Figure 27. Orientation of coordinate system used to determine the loading wave speed 44

Figure 28. Elevation view indicating "depths" used in determining the loading wave speed 45

Figure 29. Introductory screen of the CLAP code 46

Figure 30. CLAP screen listing data used for determining the equation of the plane of the projectile and the calculated coefficients of the plane 47

Figure 31. CLAP screen indicating the first point of impact onto the surface of the testbed and the angle of impact 48

Figure 32. CLAP screen listing the data used to determine the initial loading wave speed (with no iterations in CLAP) 49

Figure 33. CLAP screen listing regression data for the least squares curve fit through the TOA vs. depth data (prior to iterating with CLAP) 50

Figure 34. CLAP screen showing TOA vs. depth data (prior to iterating with CLAP) 51

Figure 35. CLAP screen listing regression data for the least squares curve fit through the TOA vs. depth data (after a single iteration with CLAP) 52

Figure 36. CLAP screen showing TOA vs. depth data (after a single iteration with CLAP) 53

Figure 37. CLAP screen showing TOA vs. depth data for a modified input data set (after a single iteration with CLAP) 55

Figure C1. Wet density and moisture content profiles for Test 6 . . . . . C2

Figure C2. Wet density and moisture content profiles for Test 7 . . . . . C3

Figure C3. Wet density and moisture content profiles for Test 8 . . . . . C4

Figure C4. Wet density and moisture content profiles for Test 10 . . . . C5

Figure C5. Wet density and moisture content profiles for Test 11 . . . . C6

Figure C6. Wet density and moisture content profiles for Test 12 . . . . C7

Figure C8. Wet density and moisture content profiles for Test 14 . . . . C9

Figure C9. Wet density and moisture content profiles for Test 15 . . . . C10

Figure C10. Wet density and moisture content profiles for Test 16 . . . . C11

Figure C11. Wet density and moisture content profiles for Test 17 . . . . C12

Figure C12. Wet density and moisture content profiles for Test 22 . . . . C13

Figure D1. Stress and impulse wave forms from Test 6 . . . . . D2

Figure D2. Stress and impulse wave forms from Test 7 . . . . . D4

Figure D3. Stress and impulse wave forms from Test 8 . . . . . D6

Figure D4. Stress and impulse wave forms from Test 10 . . . . . D8

Figure D5. Stress and impulse wave forms from Test 11 . . . . . D10

Figure D6. Stress and impulse wave forms from Test 12 . . . . . D12

Figure D7. Stress and impulse wave forms from Test 13 . . . . . D14

Figure D8. Stress and impulse wave forms from Test 14 . . . . . D16

Figure D9. Stress and impulse wave forms from Test 15 . . . . . D18

Figure D10. Stress and impulse wave forms from Test 16 . . . . . D20

Figure D11. Stress and impulse wave forms from Test 17 . . . . . D22

Figure D12. Stress and impulse wave forms from Test 22 . . . . . D24

Figure D13. Acceleration, velocity, and displacement wave forms from Test 6 . . . . . D26

Figure D14. Acceleration, velocity, and displacement wave forms from Test 7 . . . . . D29

Figure D15. Acceleration, velocity, and displacement wave forms from Test 8 . . . . . D32

Figure D16. Acceleration, velocity, and displacement wave forms from Test 10 . . . . . D35

Figure D17. Acceleration, velocity, and displacement wave forms from Test 11 . . . . . D38

Figure D18. Acceleration, velocity, and displacement wave forms from Test 12 . . . . . D41

Figure D19. Acceleration, velocity, and displacement wave forms from Test 13 . . . . . D44

Figure D20. Acceleration, velocity, and displacement wave forms from Test 14 . . . . . D47

Figure D21. Acceleration, velocity, and displacement wave forms from Test 15 . . . . . D50

Figure D22. Acceleration, velocity, and displacement wave forms from Test 16 . . . . . D53

Figure D23. Acceleration, velocity, and displacement wave forms from Test 17 . . . . . D56

Figure D24. Acceleration, velocity, and displacement wave forms from Test 22 . . . . . D60

Preface

The work described in this report was sponsored jointly by the Headquarters, Defense Nuclear Agency (HQ, DNA) and Field Command, Defense Nuclear Agency (FC, DNA). Funding was provided from HQ, DNA, under MIPR's 90-594, 91-571, and 92-573, with Mr. Mark Flohr, DNA/TDTR, Project Manager. Funding was provided from FC, DNA, under MIPR HD1102-1-A45V25, Work Unit Code 82372, with Dr. Eric Rinehart, DNA/TTSP, Project Manager.

This study was conducted by the Explosion Effects Division (EED), Structures Laboratory (SL), U.S. Army Engineer Waterways Experiment Station (WES), Vicksburg, MS.

This effort was performed under the overall direction of Dr. C. R. Welch. Mr. Howard G. White was the Principal Investigator. Field work was supervised by Mr. R. N. Walters, assisted by Messrs. G. E. Logan and R. D. Wood, WES Engineering and Construction Services Division. Mr. John T. Byrne, IIT Research Institute, Chicago, IL, wrote the computer code CLAP and assisted in the analysis of the test data. The report was coauthored by Messrs. White and Byrne.

Laboratory calibration support was provided by Mr. C. N. Thompson, WES Instrumentation Services Division (ISD). Field instrumentation support was also provided by Mr. Thompson, with the assistance of Messrs. J. O. Holder and W. C. Strahan, ISD. The instrumentation support was under the overall supervision of Mr. B. C. Barker, ISD. During this investigation, Mr. L. K. Davis was Chief, EED, and Mr. Bryant Mather was Director, SL.

At the time of publication of this report, Director of WES was Dr. Robert W. Whalin. Commander was COL Bruce K. Howard, EN.

1 Introduction

Background

The Defense Nuclear Agency funded the Explosion Effects Division (EED) of the USAE Waterways Experiment Station (WES) to develop a large-bore (4-ft-diameter) vertical gas gun. The primary purpose of the gas gun is to simulate ground shock environments in a manner suitable for testing ground shock measurement devices. An additional purpose for the gun is to obtain dynamic material properties data from relatively large geologic samples.

Description of the DNA/WES Ground Motion Test Facility

Design

The facility was designed over a 24-month period beginning in 1988 (see White et al. 1991). An artist's rendering of the facility is shown in Figure 1, and a schematic of the gun is shown in Figure 2. The gun consists of a large annular pressure vessel surrounding a vertical barrel. A series of orifices are machined in the upper barrel wall. These allow the compressed air from the vessel to expand into the barrel. When the gun is in the cocked position, a projectile, with o-rings placed at the top and bottom, straddles the orifices, and prevents the compressed air from being released into the barrel. The projectile is held in place by a quick-release trigger mechanism. A water reaction mass fills the top portion of the barrel above the trigger mechanism. This mass is used to reduce the reaction of the gun to the pressure driving the projectile. The bottom of the barrel may be sealed with a diaphragm to allow a partial vacuum to be created in the barrel section below the projectile. (Note: none of the tests reported here utilized a vacuum in the lower portion of the barrel.)

Operation

To fire the gun, the projectile is released. The weight of the projectile causes it to move downward. As the top o-ring clears the orifices, the

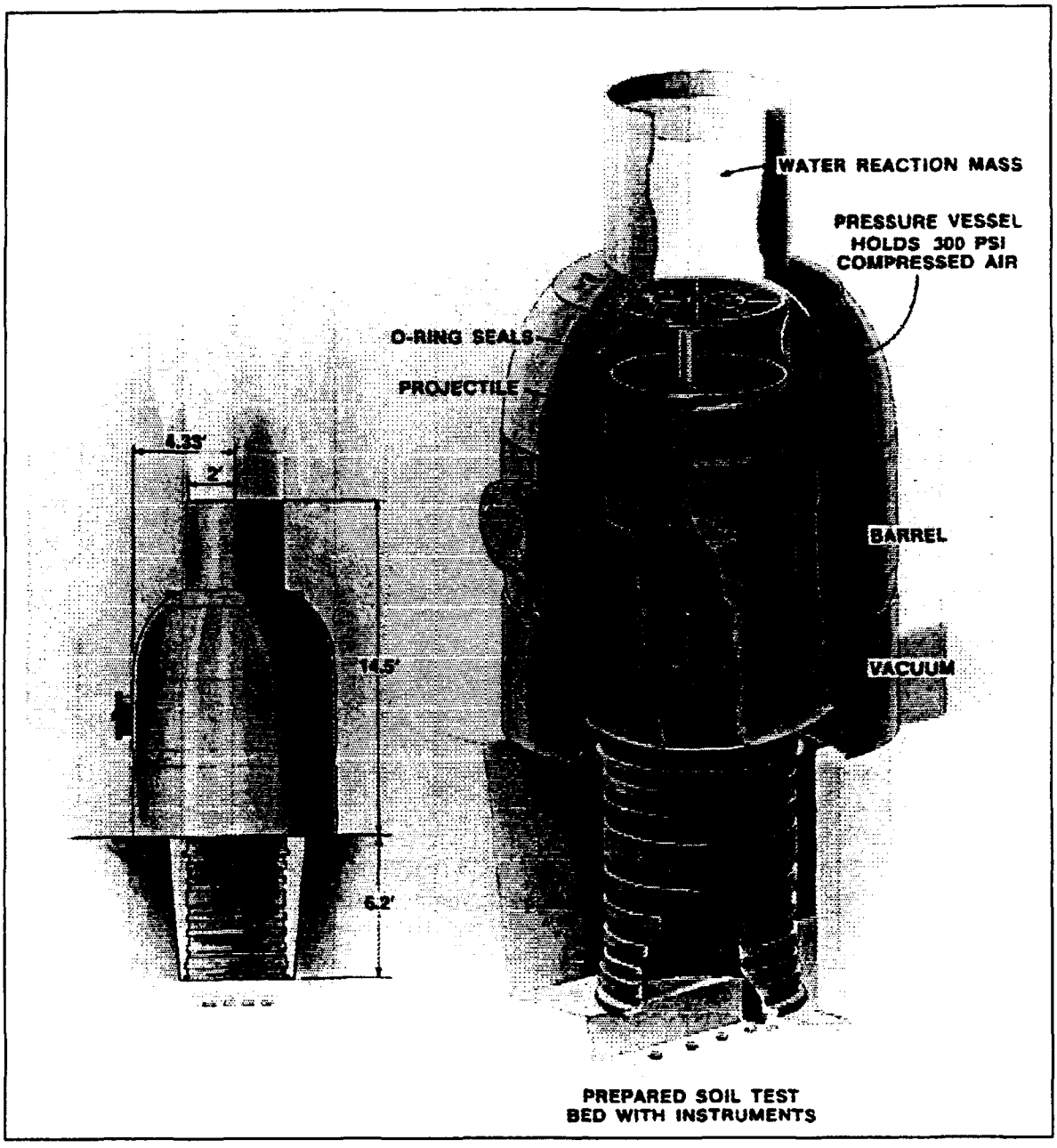

Figure 1. WES 4-ft-Diameter Vertical Gas Gun

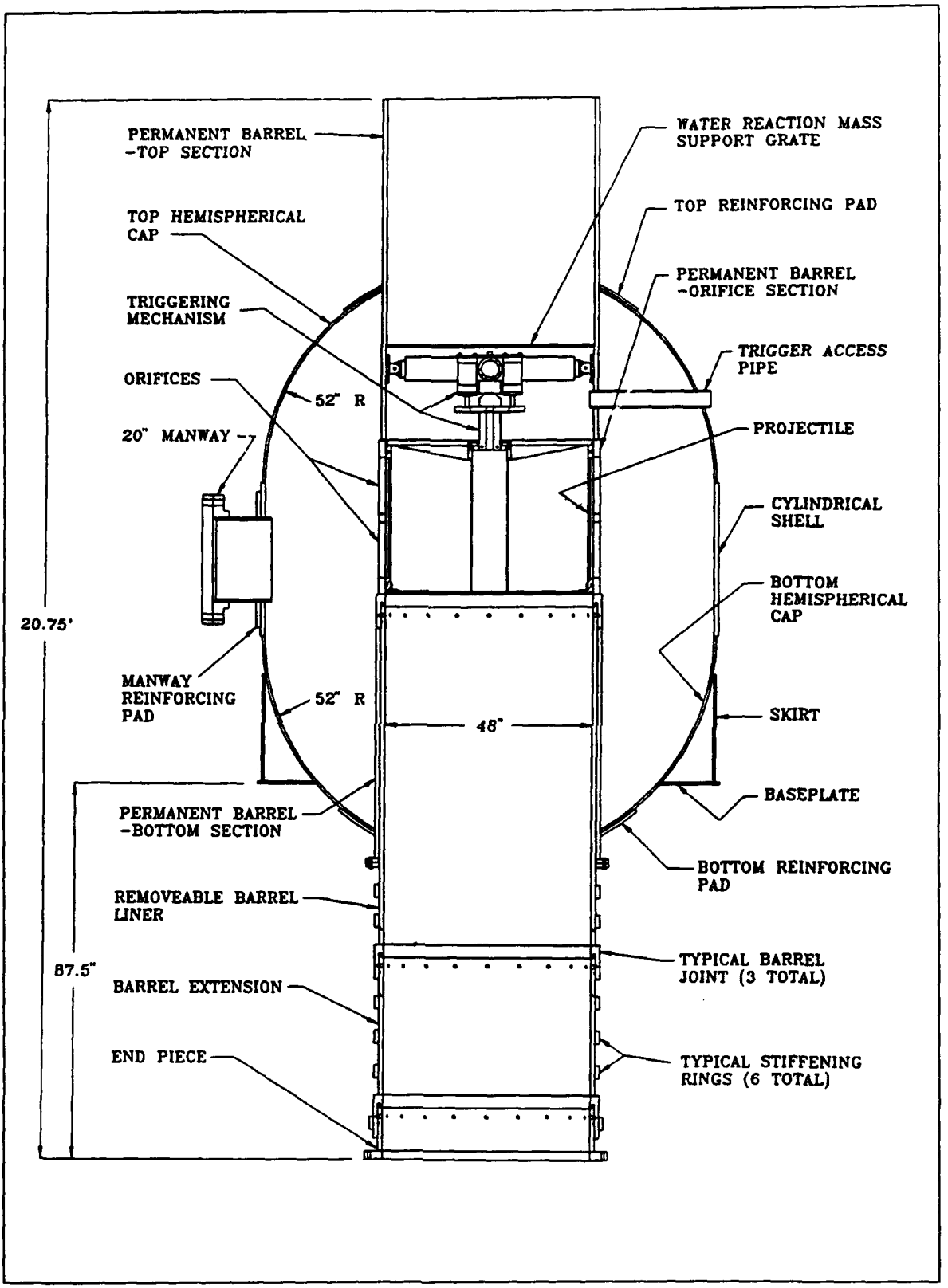

Figure 2. Schematic of the 4-ft-diameter gas gun

compressed air expands into the barrel. The incoming air simultaneously drives the projectile downward and the water reaction mass upward. Theoretically, the mass of the water can be adjusted so that the "bottom" of the mass of water will exit the top of the barrel at the same time that the projectile clears the bottom of the barrel. This would maintain maximum pressure on the projectile for as long as it was in the barrel. The maximum operating range is 2,070 kPa, which produces a projectile velocity of 71 mps.

Objectives

The primary objectives for all tests were to develop safe procedures for testing and to determine the operating characteristics of the gun (e.g., determination of projectile velocity, far-field ground motion and nuisance noise levels as a function of vessel pressure). The performance aspects of testing with the 4-ft gun with regard to the primary objectives have been reported by White (1993).

The primary objectives of the development program for the gas gun could have been met without including testbeds on each test. However, to take full advantage of the gun, testbeds were included when possible. This, in turn, led to a secondary set of objectives being associated with these testbeds. These objectives included the initial dynamic testing of new ground shock instruments for use in the HUSKY JAGUAR and the Seismic Hard-Rock In Situ test programs, and the development of testing procedures and equipment for routine use with the gun. The inclusion of a target on a test never became the driving force of the gas gun program; however, its role increased in importance as testing progressed. Of the twenty-two tests conducted under this program, twelve of these tests included an instrumented testbed.

Scope

This report describes the testbed construction and test procedures. Stress and velocity histories are presented from each test. Analysis of the data includes determination of the propagation velocity of the loading wave for the two types of sand used as a backfill. Two methods for determining the propagation velocity of the rarefaction wave are discussed. Two methods for analyzing impact angle and planarity are also presented. Conclusions are drawn on the results of the development program to date.

2 Experiment Description

Testbed Construction

Twelve tests were conducted using a sand testbed as a target beneath the gun during the period addressed by this report (January 1990 - December 1992). Nine of the tests used masonry sand and three of the tests used Socorro Plaster sand as the backfill material. The disposable target container was a 1.37-m diameter by 0.76-m high corrugated 12-gauge steel pipe with a welded 12-gauge steel bottom.

The target for each test was constructed by placing four lifts (typically 15-20 cm) of sand in the steel container. Each lift was compacted using a vibratory compactor to obtain a maximum density. The wet density and moisture content were measured, using a nuclear densitometer, at two locations in each of the three lower lifts. For several tests, the moisture content was also measured by weighing samples of the sand before and after drying in a microwave oven (called the oven dry method). The last test, Test 22, was constructed to meet specifications for density and moisture content. The construction methods used for the other tests were designed primarily to produce a uniform testbed, as opposed to specific densities or moisture contents.

The time required to build a testbed, once all materials were on hand (gages, sand, vibrator, microwave oven, tools, etc.), was approximately one day per test. An efficient method for testing with the gun was to prepare several samples at a time, since objectives for subsequent tests were not contingent on results from previous tests. For this series, two or three testbeds were prepared (in a sheltered area) on successive days. Using a fork lift, they were moved to the facility as required for testing. Approximately two to three days were required for conducting a test.

Typical Instrumentation Layout

The total depth of each target was 61 cm. Two depths in a target were typically instrumented. These two depths (15.2 cm and 30.5 cm) included a variety of the stress and velocity instruments (Tables 1 and 2). The common

Table 1
Stress Gages Used for Tests in Sand

Instrument	Common Name
High-Range SE gage	HRSE
Old Column-Based Stress gage	OCBS
New Column-Based Stress gage	NCBS
Stress and Velocity gage	S&V or CCBS

Table 2
Velocity Gages Used for Tests in Sand

Instrument/Canister	Common Name
Log Shock-Isolated Accelerometer canister	AV-L
Wedge Shock-Isolated Accelerometer canister	AV-W
Micro Hard-Mounted Accelerometer canister	AV-M
HIFI Accelerometer canister	AV-N or SHMA
Stress and Velocity gage	S&V or CSHMA
Sunburst Recovery, Inc. Constant Pitch Electromagnetic gage	SC
Sunburst Recovery, Inc. Variable Pitch Electromagnetic gage	SV

name used to describe each instrument is also listed in the tables. A representative example of the gage layout is presented in Figure 3. Gages were placed in the correct lift as the testbed was being built. The instruments located at the 30.5 cm depth were typically placed at a radius of 15.2 cm, and the instruments at the 15.2 cm depth were placed at a radius of 30.5 cm (see Figure 4). For some tests a gage was placed in the center of the testbed at one of the two levels. A short length of cable was routed from each gage, through the testbed, and terminated just outside of the target container. The gages used in each testbed and their locations are listed in Appendix B.

Diagnostic measurements were included for each test. Two pressure gages were located in the reservoir of the gas gun. One served as a direct readout gage used to monitor system pressure, prior to firing, at the control panel for the gun. The second gage was used to monitor the pressure drop in the vessel during a test. An accelerometer was mounted on the base of the gun to monitor acceleration levels in the vertical direction. Six piezoelectric pins at the bottom of the barrel of the gun were used to measure the projectile velocity and planarity as the forward face exited the barrel. A triaxial seismic station and microbarograph gage were fielded at three different ranges on several tests to monitor far-field ground motions and airblast. Sound pressure

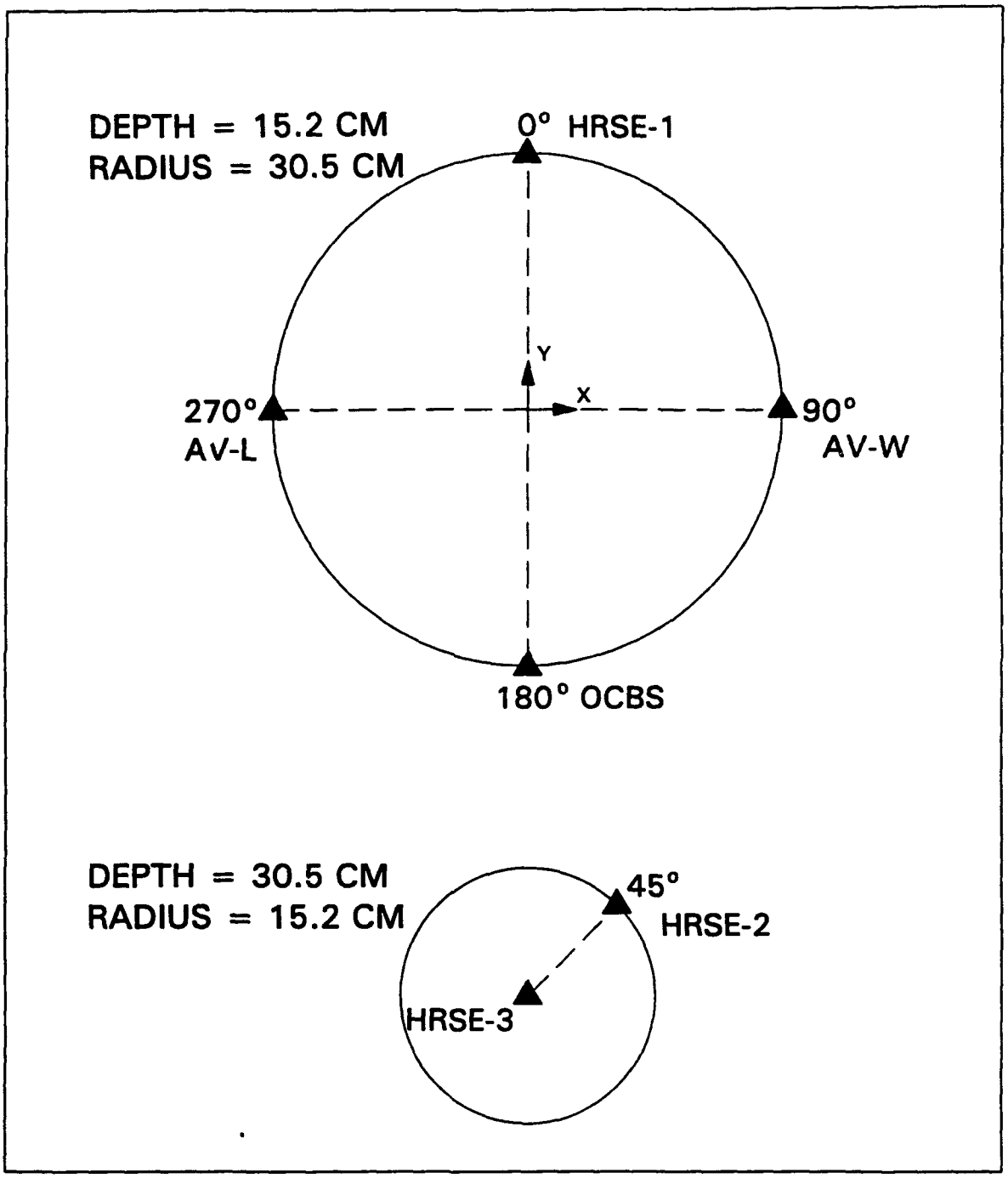

Figure 3. Typical layout for testbed instrumentation

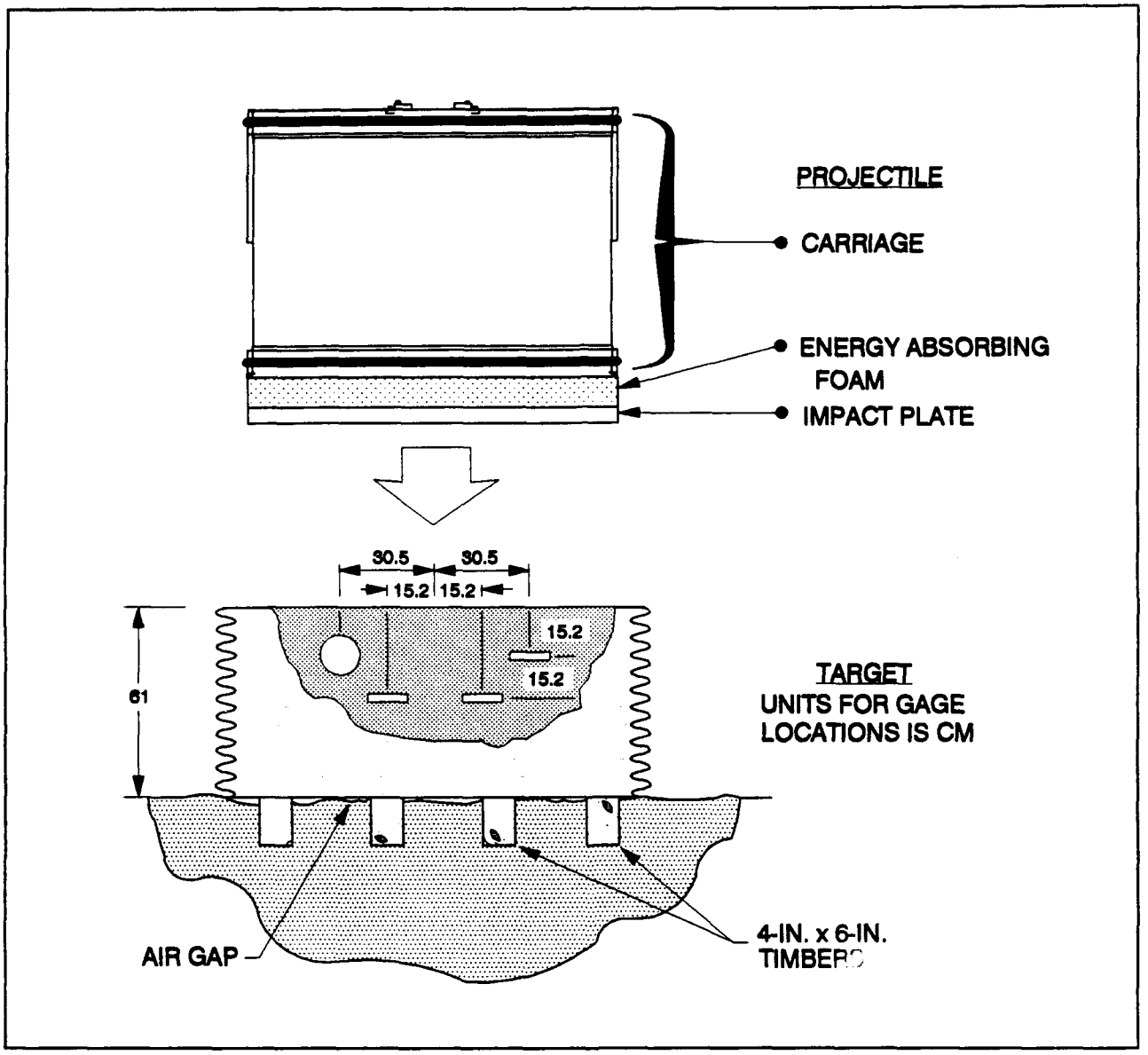

Figure 4. Cross section of the gas gun projectile and container of target material

level measurements were made at five ranges on most tests, and a video camera was used to photograph each test. The results of the diagnostic measurements have been reported by White (1993).

Testing Procedure

For these tests, the projectile was loaded into the gun prior to moving the testbed beneath the barrel of the gun. The projectile was raised into its cocked position via a chain hoist attached to a tripod at the top of the barrel. Two chains were used to lift the projectile, and two were used as safety chains during the loading process. The two safety chains remained in place after the projectile was locked into position with the quick-release trigger mechanism.

The configuration of the projectile varied depending on the vessel pressure planned for the test (see Figure 4). As test levels increased (higher vessel pressures and projectile velocities), thicker pieces of foam were required at the base of the projectile to absorb the impact energy, and thus protect the carriage from damage. The mass of the projectile varied slightly as a result of changing the foam thickness. The mass of the projectile for most tests was 1,482 kg. The vessel pressure for these twelve tests varied from 345 to 1,379 kPa and the projectile velocity (as the leading edge exited the barrel) varied from 27.9 to 59 mps. The location of the target was typically 120 cm below the end of the barrel. The test level, projectile mass, and projectile velocity for each test is listed in Table 3.

Sand was placed over the earthen portion of the trench bottom located directly beneath the barrel of the gun. Several timbers (4-in. by 6-in.) were placed in the sand base to support the sample. The sample was moved into position beneath the barrel of the gun via a trolley that ran along channels cast into the concrete walls on either side of the trench. The sample was centered beneath the gun using a plumb bob suspended from crosshairs at the bottom of the barrel. Final leveling of the testbed was achieved using a carpenter level to guide placement of shims between the steel bottom of the sample and the timbers. An advantage of supporting the sample with timbers is that it essentially provides a "free" surface at its base. The shock wave reflecting off this free surface may be seen in the stress wave forms, and thus may be used to investigate the unloading wave speed of the testbed material.

After the testbed was positioned beneath the gun, instrument cables were spliced to cables running to the Control Trailer. After all electrical checkouts were completed, the safety chains on the projectile were removed. A 1-mm-thick fiberglass diaphragm and plastic liner, used for containing the water reaction mass, were placed above the quick-release trigger mechanism in the upper portion of the barrel. The depth of the water reaction mass for all tests was 1.35 m, which corresponds to a mass of 1,570 kg. After placing the reaction mass, the firing system for the trigger mechanism was enabled by supplying pressurized gas to the system and by connecting battery power to a solenoid valve used to control the flow of gas.

Table 3
Test Pressure Level, Projectile Mass, and Projectile Velocity for Tests in Sand

Test No.	Vessel Pressure kPa	Projectile Mass kg	Projectile Velocity mps
6	345	1,452	27.9
7	517	1,482	37.1
8	517	1,482	35.5
10	862	1,489	47.2
11	1,014	1,475	50.3
12	662	1,482	41.8
13	1,027	1,482	52.8
14	1,207	1,482	55.7
15	1,379	1,482	59.0
16	841	1,482	46.3[1]
17	1,165	1,482	54.9[1]
22	862	1,472	46.8

[1] Calculated value (no experiment data)

Instrument recording and remote operation of the gun were performed at the Control Trailer, located approximately 50 m away. A picture of the recording setup is shown in Figure 5. The control panel used for operating the "fill system" for the gun is shown in Figure 6. The fill system (illustrated in Figure 7) is comprised of three components; the pressure system, the vacuum system, and the firing system. None of the tests reported here used a vacuum in the lower section of the barrel. The pressure vessel was filled by a high-pressure, high-volume air compressor. After the desired testing level was reached, the air compressor was stopped. The time required to pressurize the gun for these tests varied between 13 and 54 minutes. A master switch was then used to ensure all components of the pressure system were in their proper state; i.e., all valves closed and the air compressor shut off. The master switch also provided power to the firing system. After sounding a warning siren and a final check with instrumentation personnel, the gun was fired by energizing the 4-way solenoid valve in the firing system. This allowed gas pressure to activate the quick-release trigger mechanism, which released the projectile. On average, approximately 450 msec were required for the trigger mechanism to release the projectile. The additional time required for the projectile to travel the length of the barrel was anywhere between 100 and 400 msec, depending on the test level and length of the projectile.

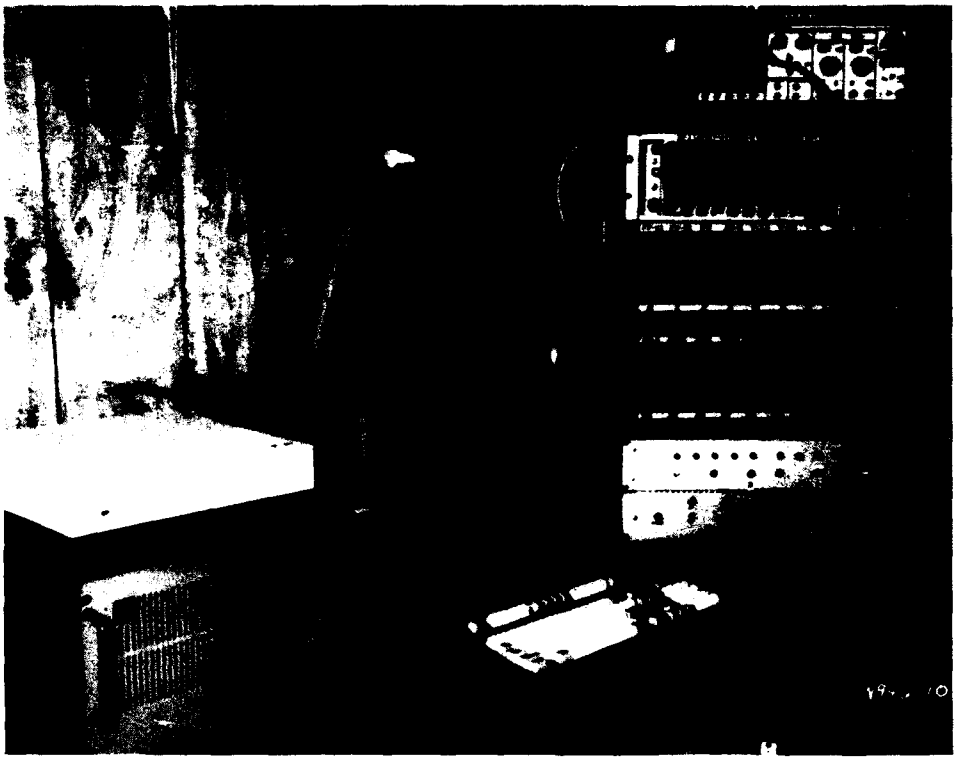

Figure 5. Recording setup for tests with the 4-ft gas gun

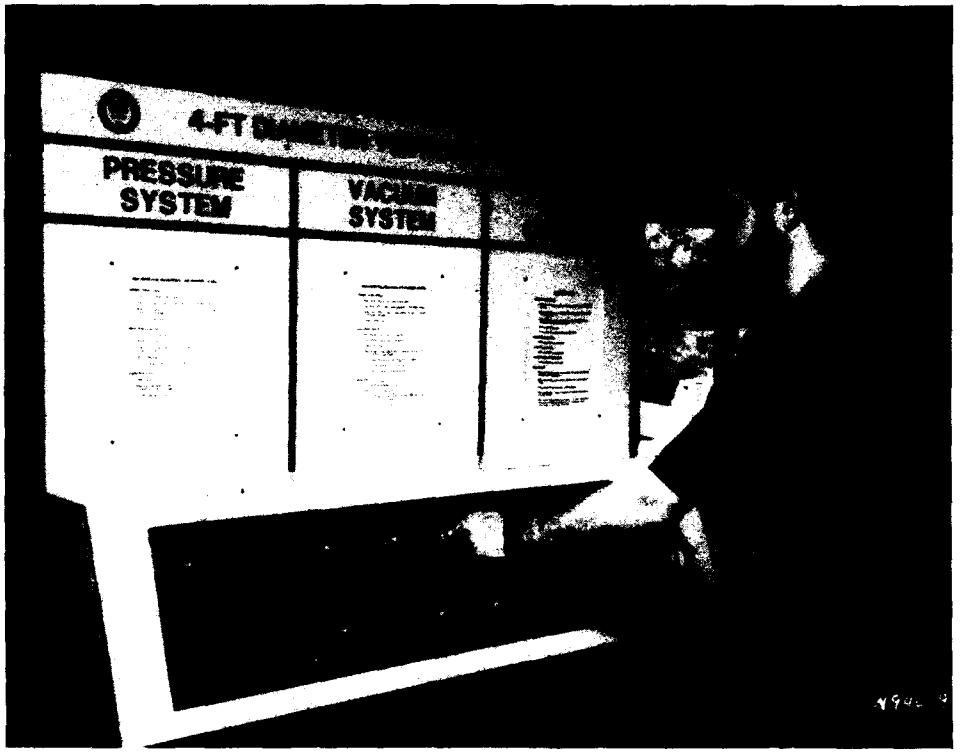

Figure 6. Control panel used in operating the gas gun

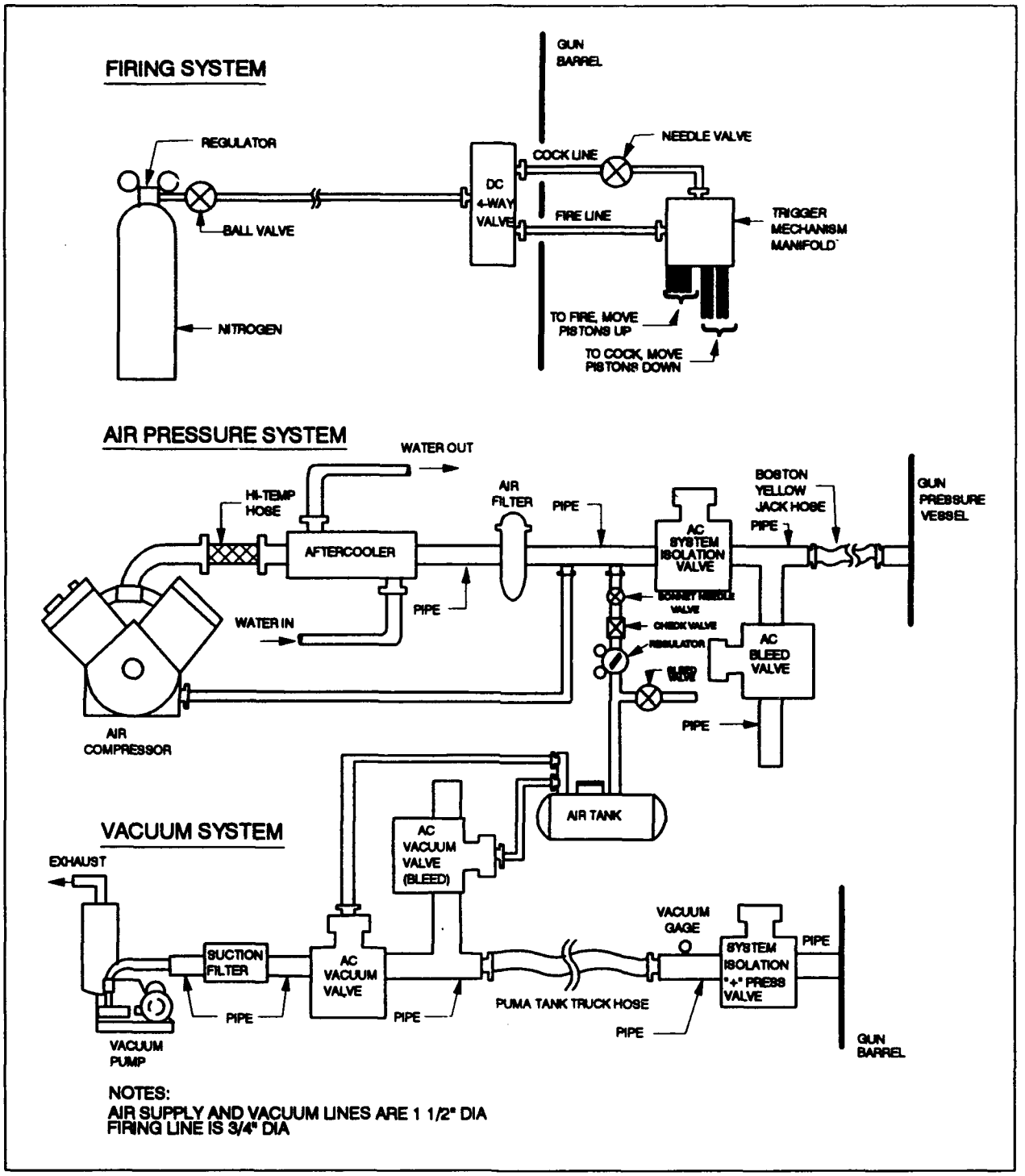

Figure 7. Fill system used for conducting tests with the gas gun

3 Experiment Data

Testbed Material Data

The wet density and moisture content of the test materials were measured at two locations in each of the three lower lifts of a testbed using a nuclear densitometer. The accuracy of the nuclear densitometer for measuring moisture content is questionable, however, because the source and receiver are both in the base of the gage, and experience has shown that the moisture content is only measured to a depth of approximately 5 cm. For that reason, the moisture content was also measured for several tests by weighing samples of the sand before and after drying in a microwave oven (oven dry method).

A summary of the average wet density and moisture content of the entire testbed is presented in Table 4. Presented in Appendix C are profiles of the wet density and moisture content for each testbed. The values presented in the appendix represent the average of two measurements at each depth. Where moisture content measurements were made with both the nuclear densitometer and the oven dry method, the oven dry method (as the more accurate) is presented. Considering the average moisture content of the entire testbed, the oven drying method indicated values anywhere between 0.4 and 1.8 percent higher than those determined using the nuclear densitometer.

Active Measurement Data

Stress and impulse measurements from each test are presented in Figures D1-D12, contained in Appendix D. Acceleration records and the integrated velocity and displacement records are presented in Figures D-13 through D-24. Data return from the tests was very good. The average peak stresses produced in the test materials varied between 7 and 27 MPa. The average peak particle velocities varied from 18 to 34 mps.

Table 4
Average Wet Density and Moisture Content for Sand Testbeds

Test No.	Sand Type	Average Wet Density g/cc	Average Moisture Content percent
6	Masonry	1.61	4.9[OD]
7	Masonry	1.59	3.6[OD]
8	Masonry	1.61	5.2[OD]
10	Masonry	1.60	3.5[OD]
11	Masonry	1.62	3.8[OD]
12	Masonry	1.58	3.0[OD]
13	Masonry	1.58	1.4[ND]
14	Masonry	1.59	2.8[ND]
15	Masonry	1.60	3.1[ND]
16	Socorro Plaster	1.69	2.4[ND]
17	Socorro Plaster	1.70	2.5[ND]
22	Socorro Plaster	1.67	4.0[OD]

[OD] Oven dry method
[ND] Nuclear densitometer

Time-of-Arrival Data

The propagation velocity of the shock wave in sand was determined by noting the time-of-arrival (TOA) at known depths within the testbed. For eleven of the tests (all but Test 22), instruments were located at only two depths within the testbed (15.2 cm and 30.5 cm). The centerline of each gage/canister was placed at the designated depth (see Figure 8). After the shock wave reached the upper edge of a canister, the time required for it to traverse to the sensing element was negligible compared to the time required for the shock wave in sand to traverse a like distance. As a result, the relative "distance" between the top surface of the various instruments was used to determine the "depth" over which the shock wave propagated between the TOA at each location.

Each test in sand (except Test 22) included a Log shock-isolated accelerometer (SIA) canister (AV-L) at the 15.2 cm depth. This canister had the largest thickness of those used in the tests, and for planar impacts should indicate the first TOA. Presented in Figures 9 through 19 is the TOA at each instrument location for the first eleven tests in sand. The x-axis for these figures is labeled as "distance," since the values presented are the relative distance between the top surface of a Log canister and other gages/canisters in the testbed. For Test 22, TOA crystals were placed at the surface and throughout the depth of the testbed. The TOA data presented in Figure 20 is

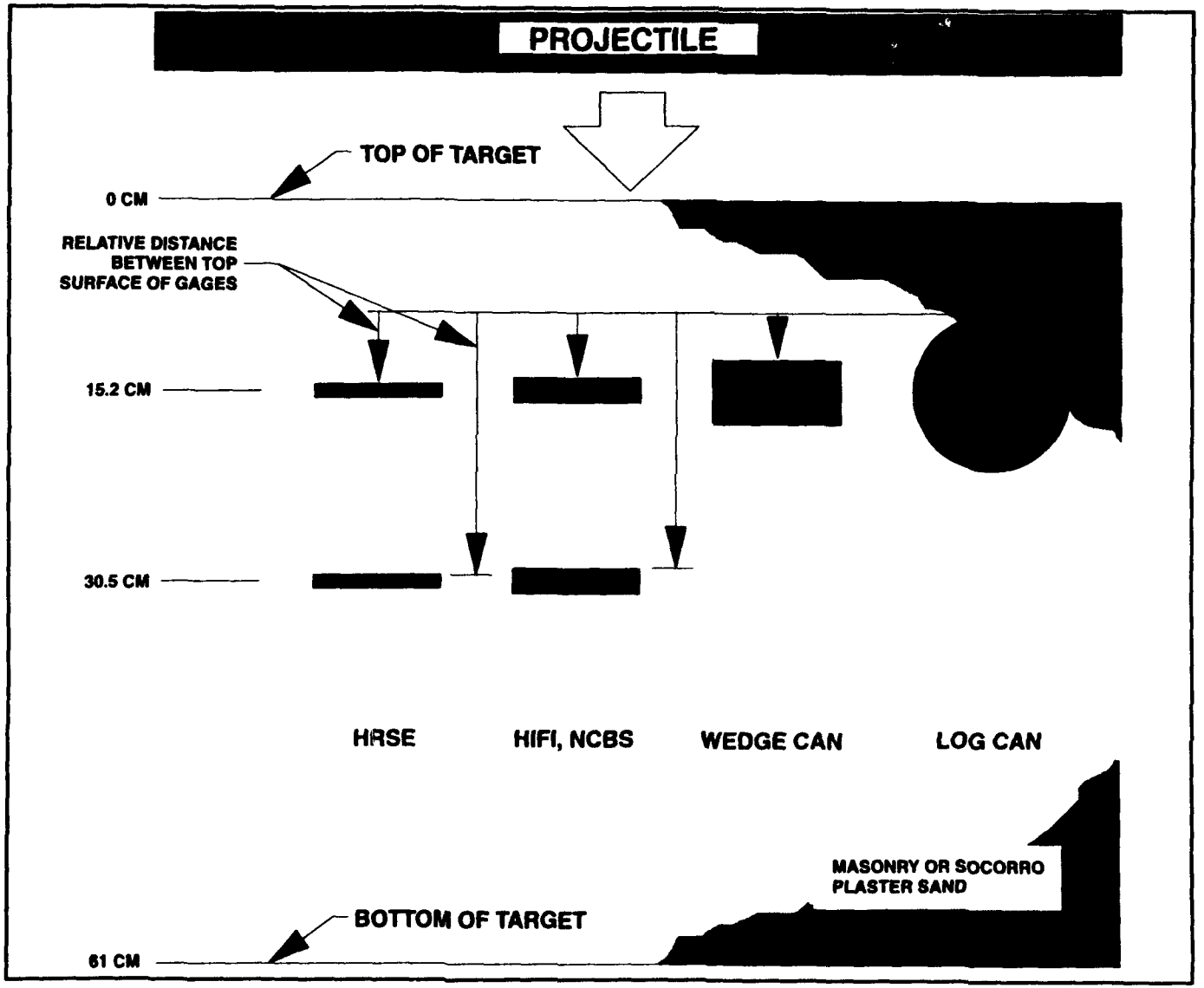

Figure 8. Typical target geometry for tests in sand

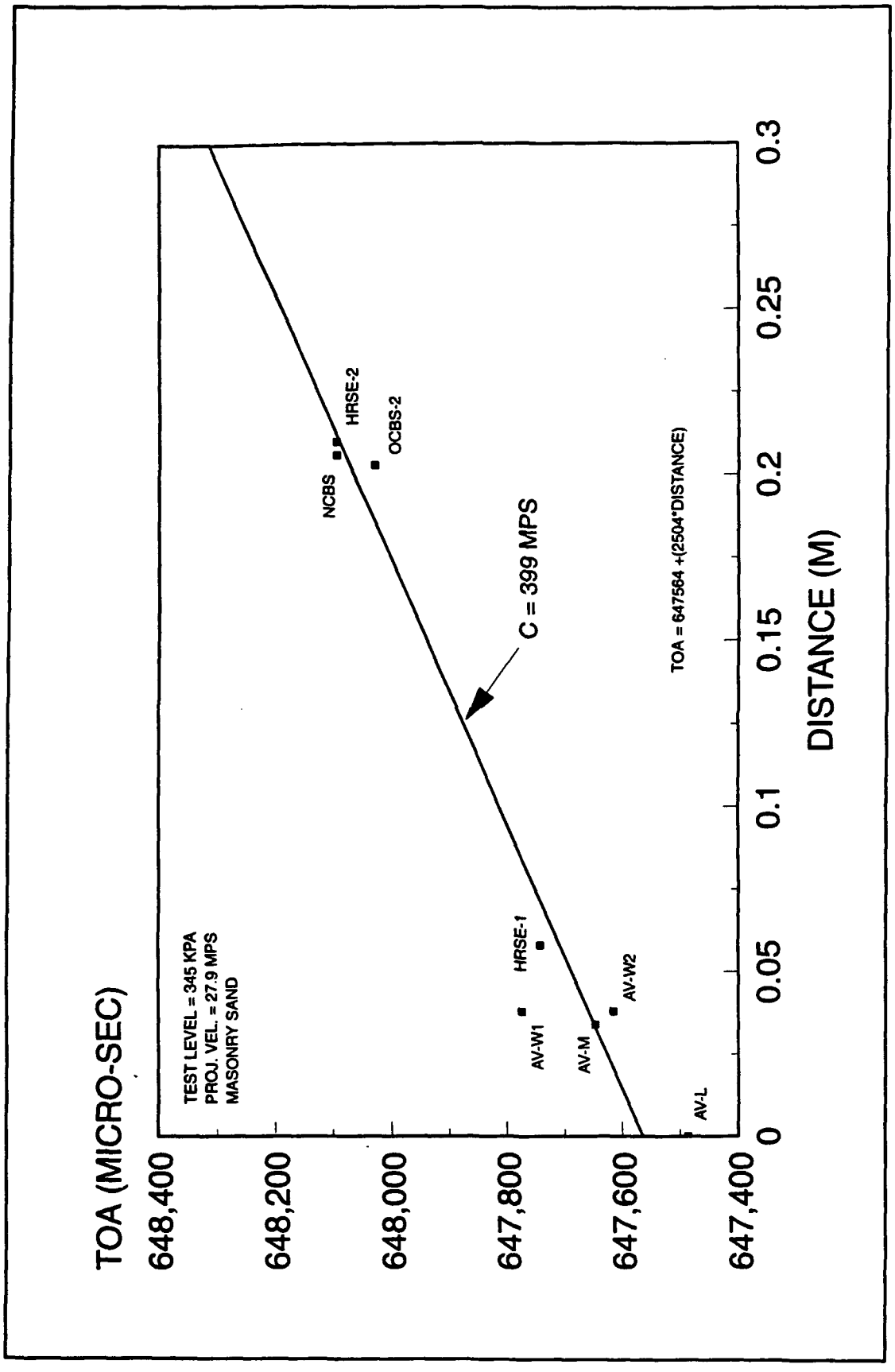

Figure 9. Time-of-arrival vs. distance for Test 6

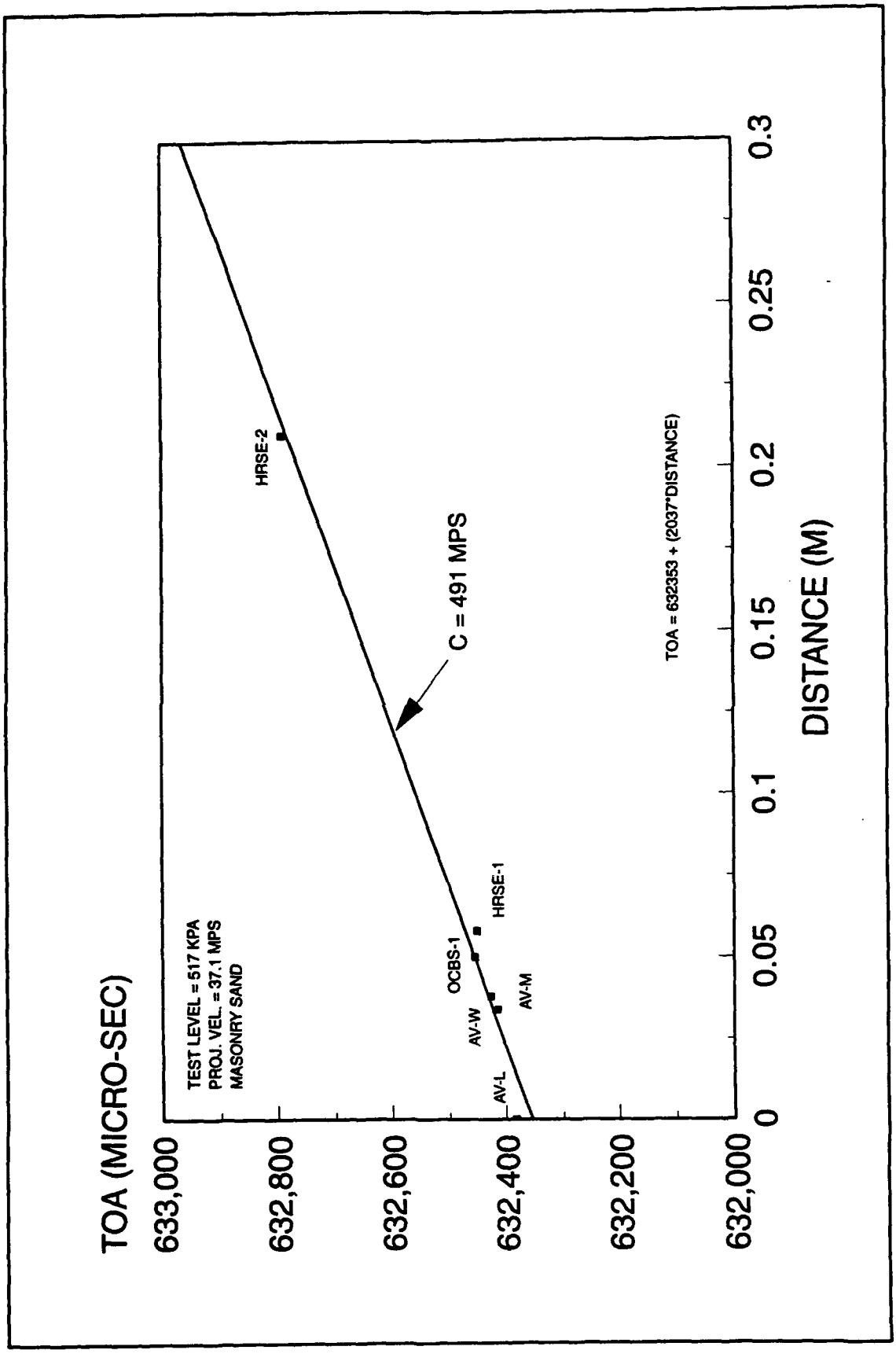

Figure 10. Time-of-arrival vs. distance for Test 7

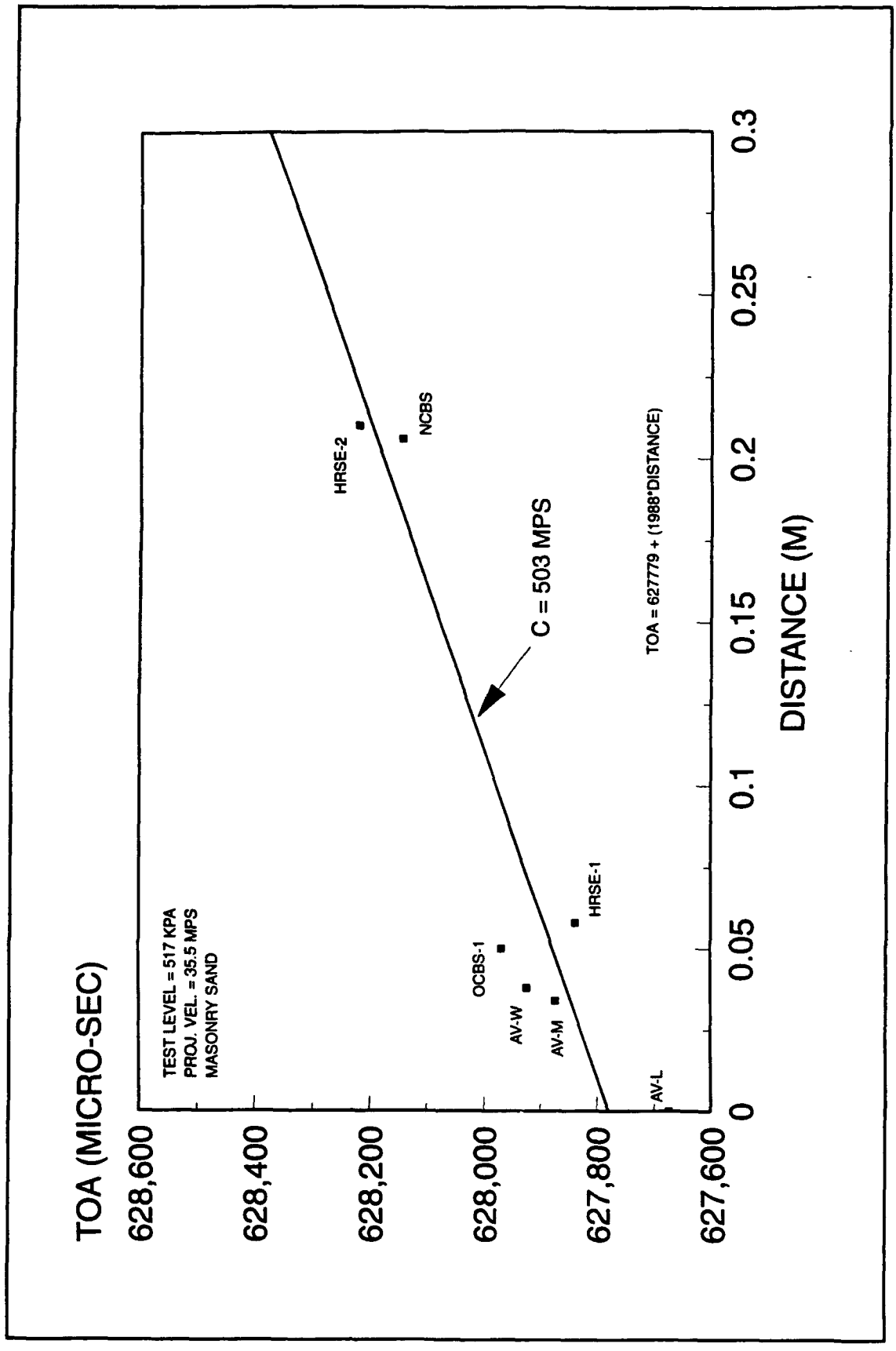

Figure 11. Time-of-arrival vs. distance for Test 8

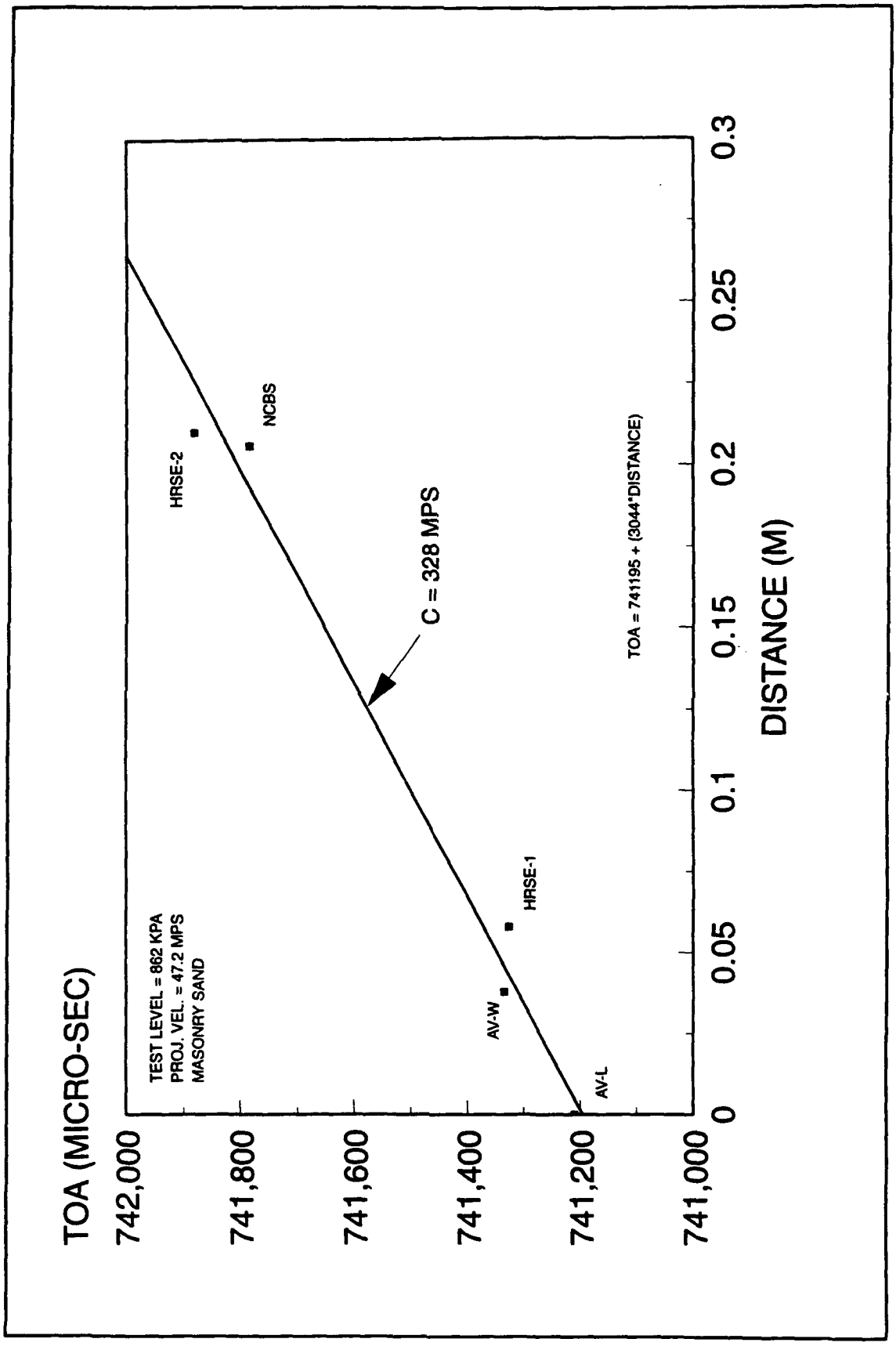

Figure 12. Time-of-arrival vs. distance for Test 10

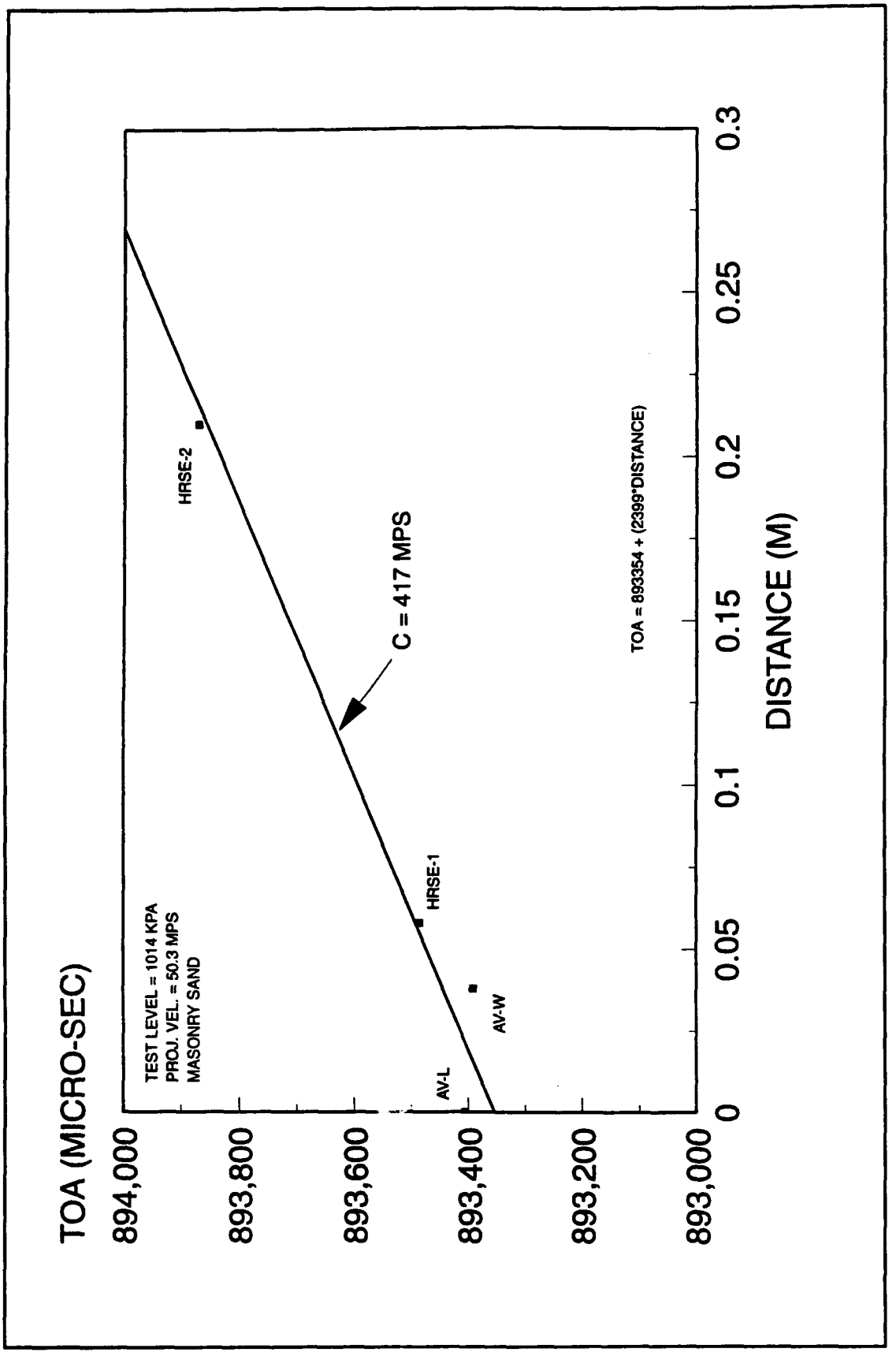

Figure 13. Time-of-arrival vs. distance for Test 11

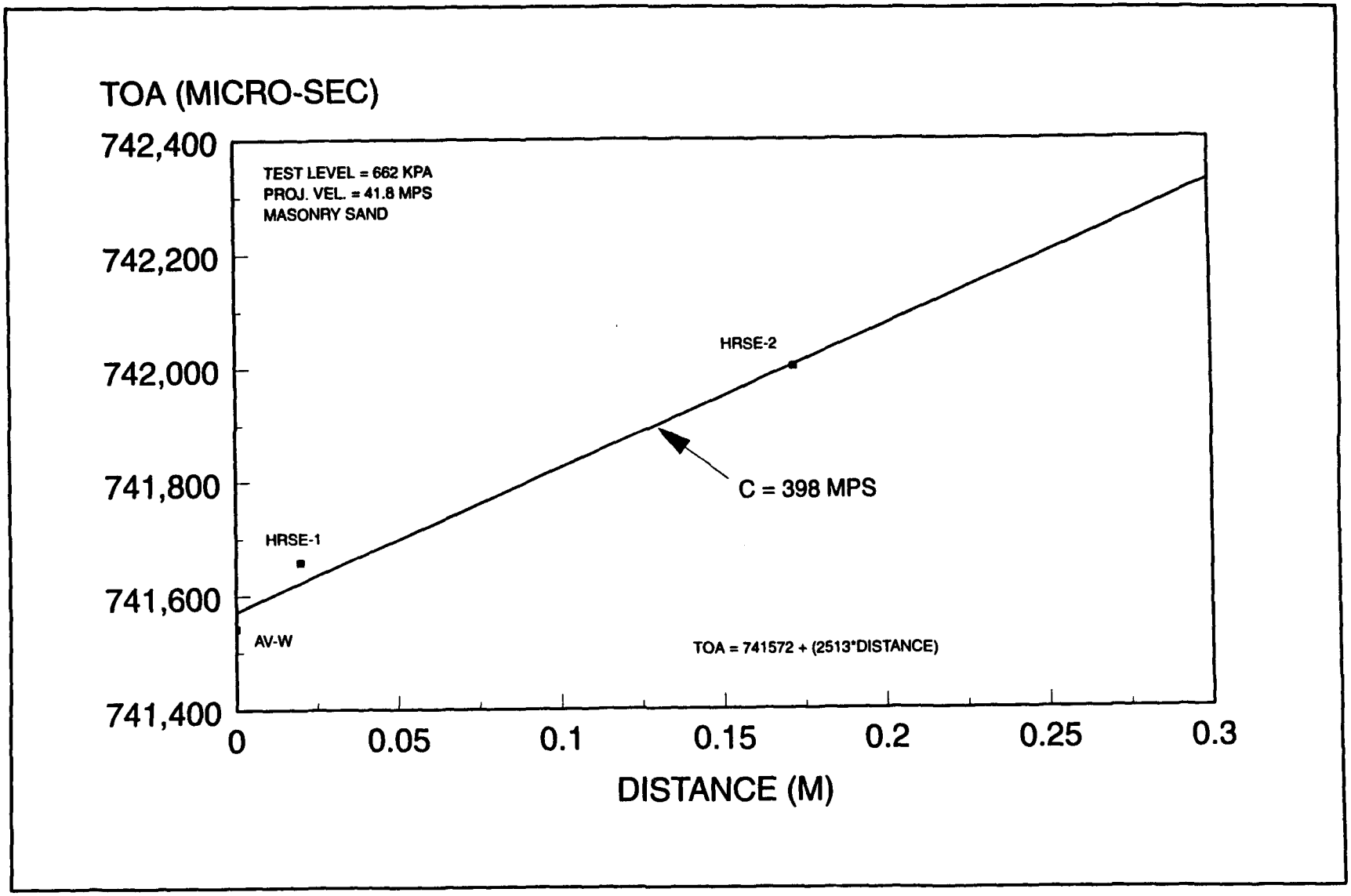

Figure 14. Time-of-arrival vs. distance for Test 12

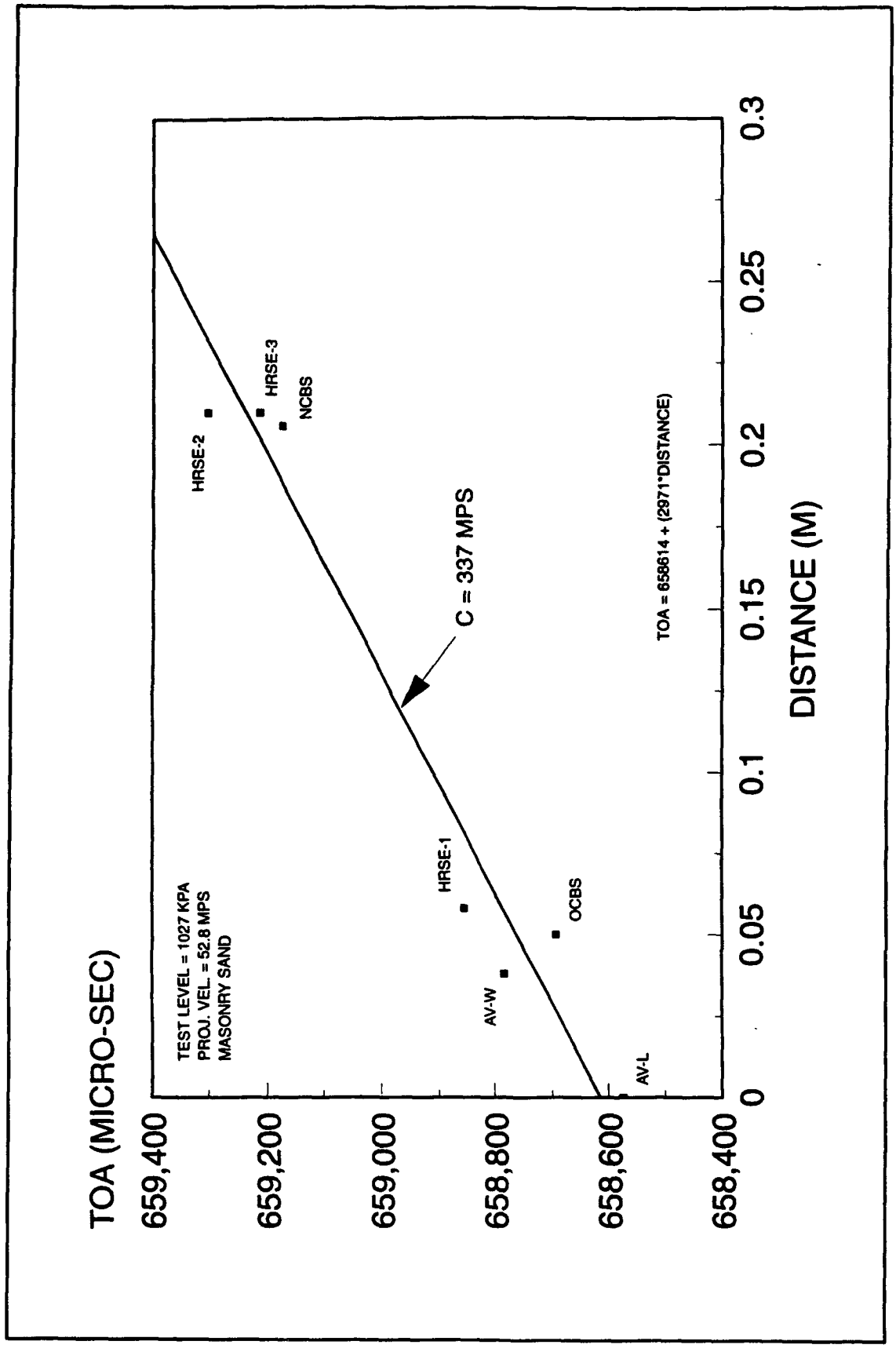

Figure 15. Time-of-arrival vs. distance for Test 13

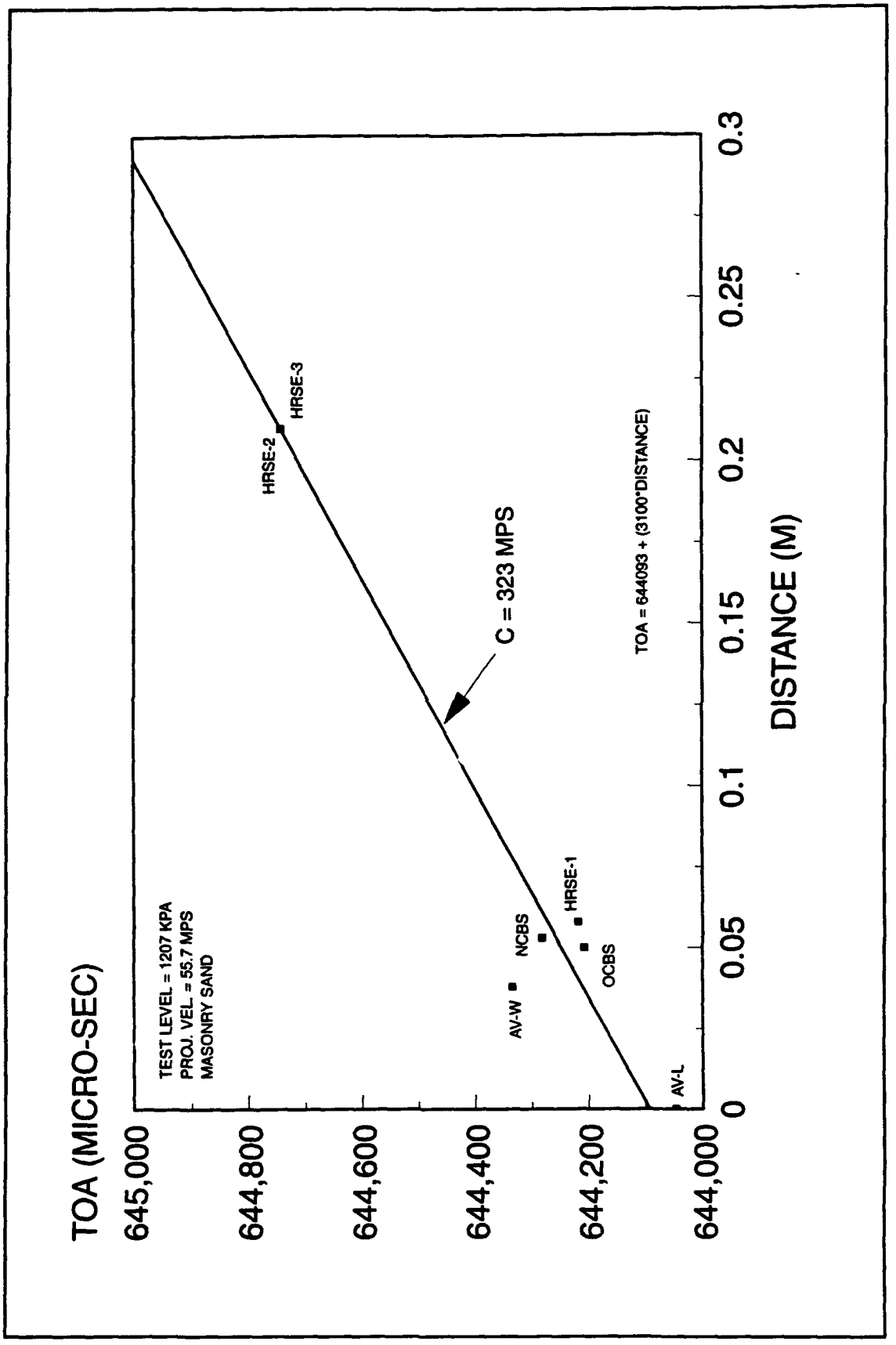

Figure 16. Time-of-arrival vs. distance for Test 14

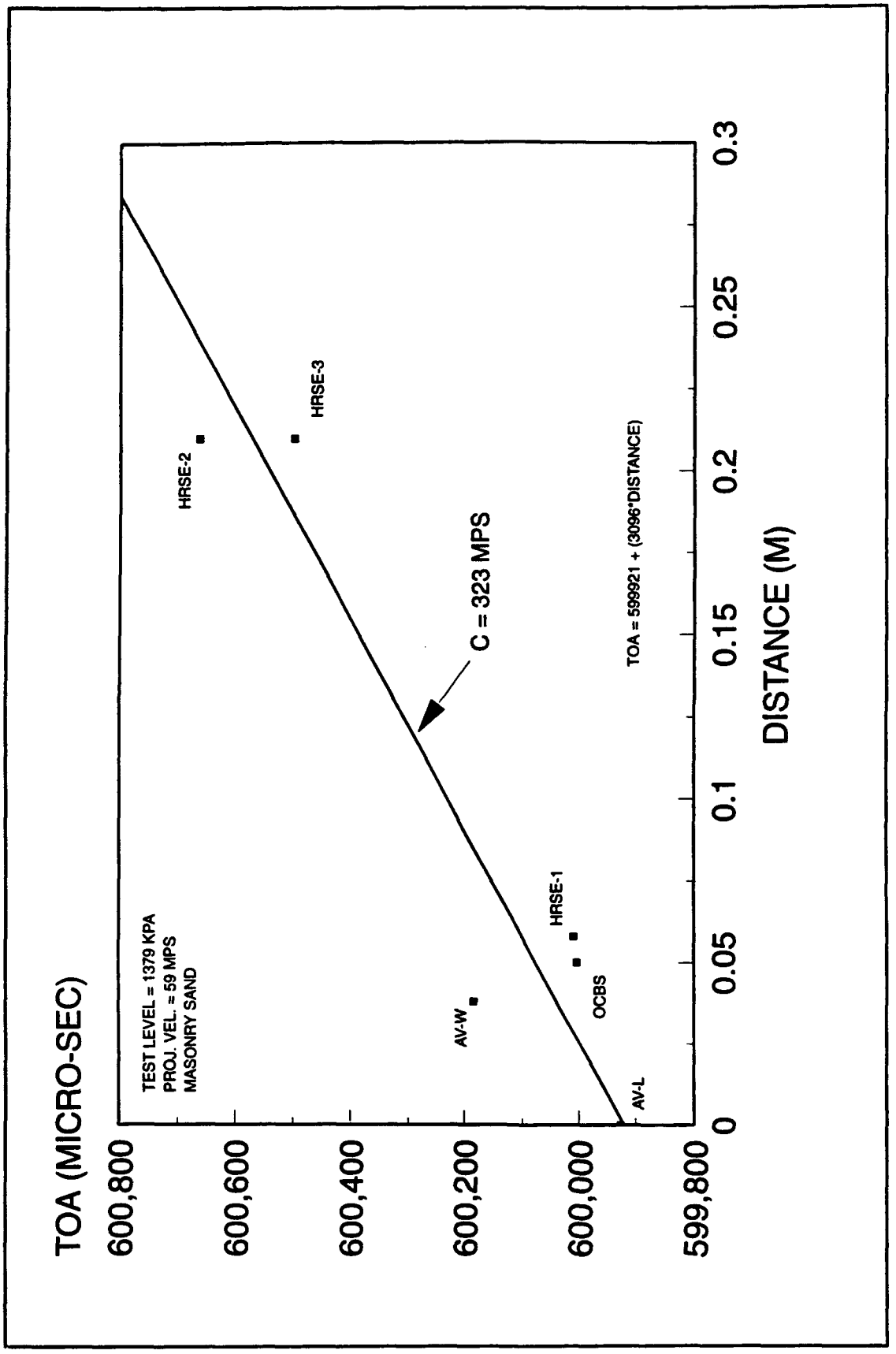

Figure 17. Time-of-arrival vs. distance for Test 15

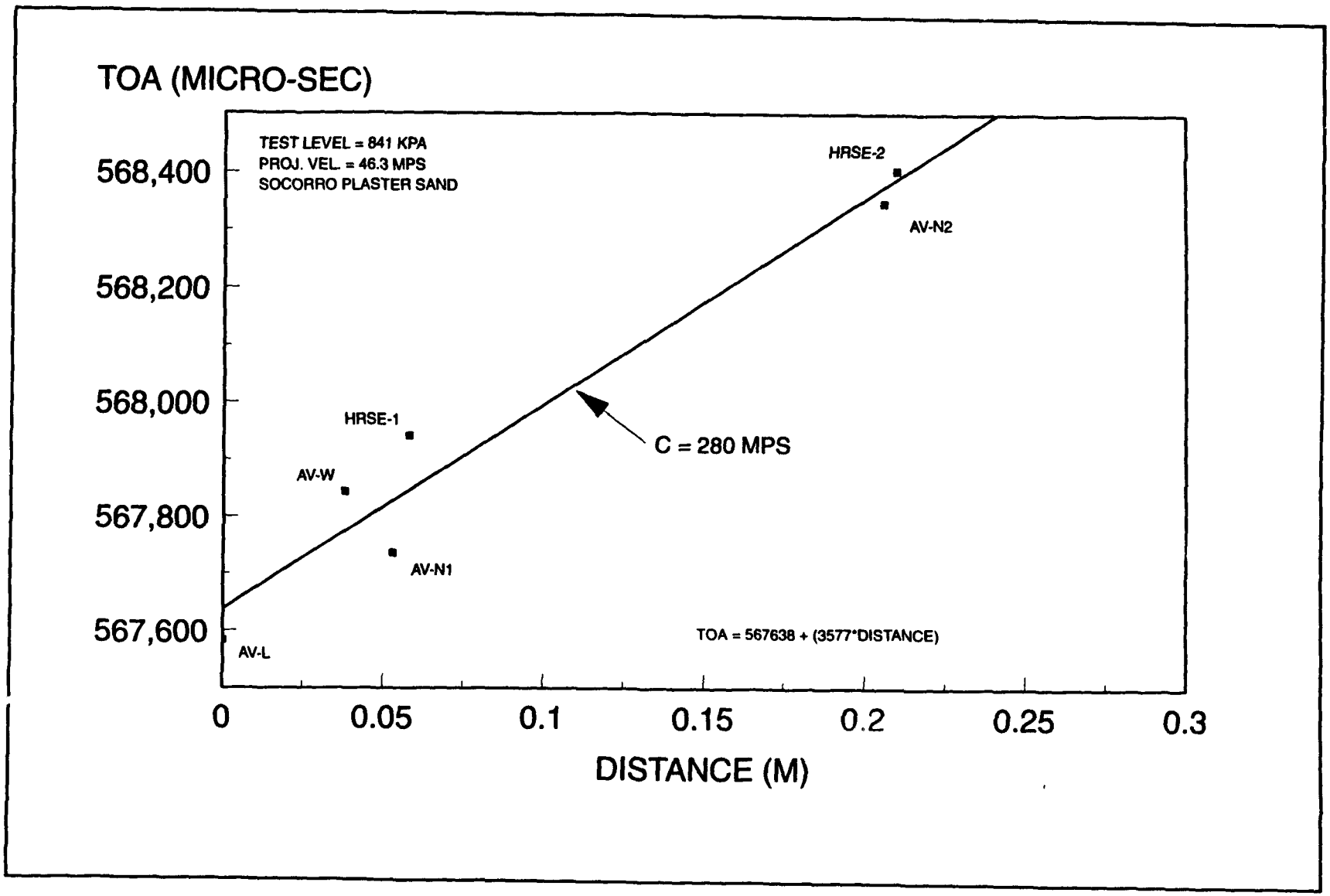

Figure 18. Time-of-arrival vs. distance for Test 16

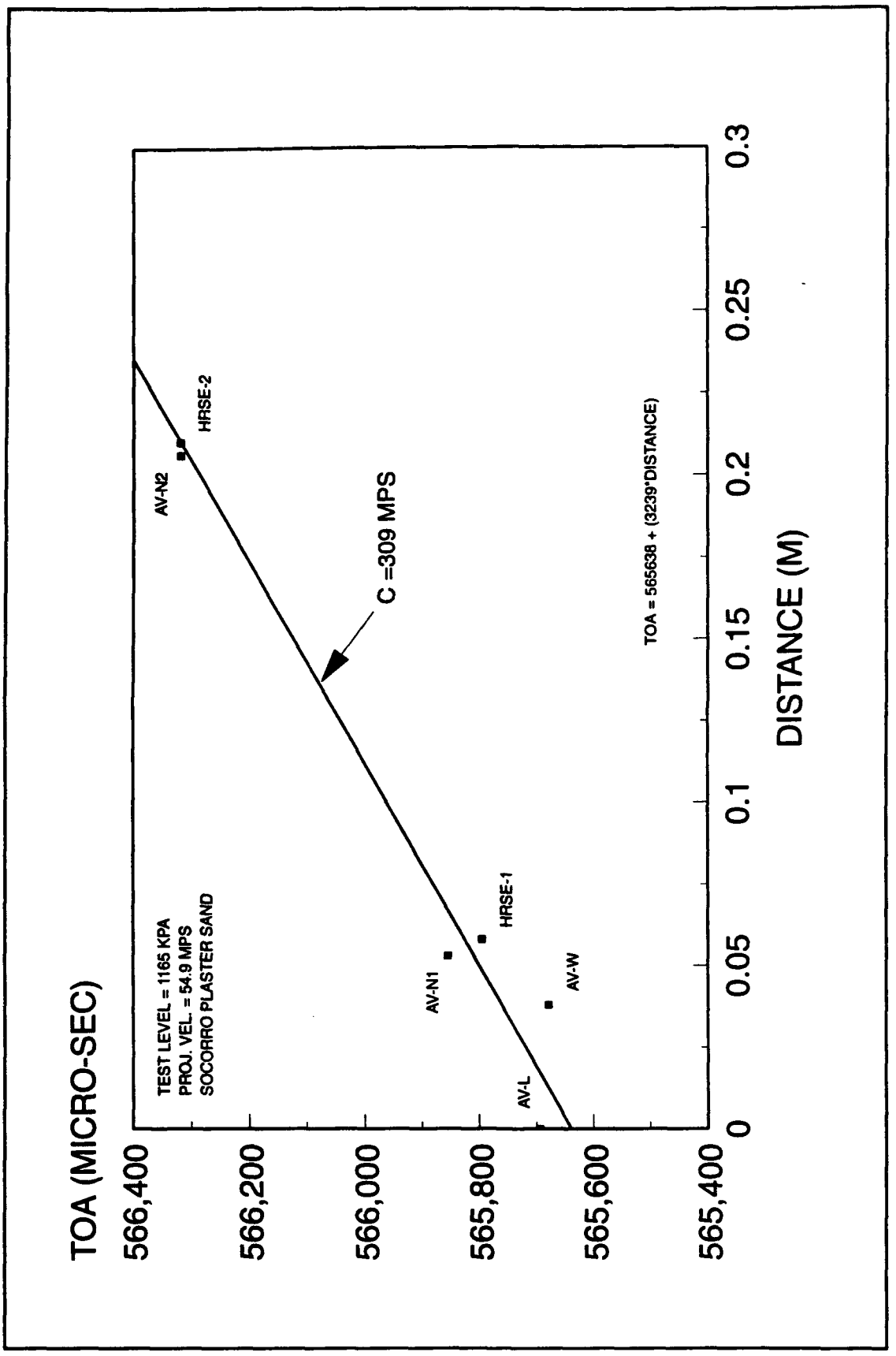

Figure 19. Time-of-arrival vs. distance for Test 17

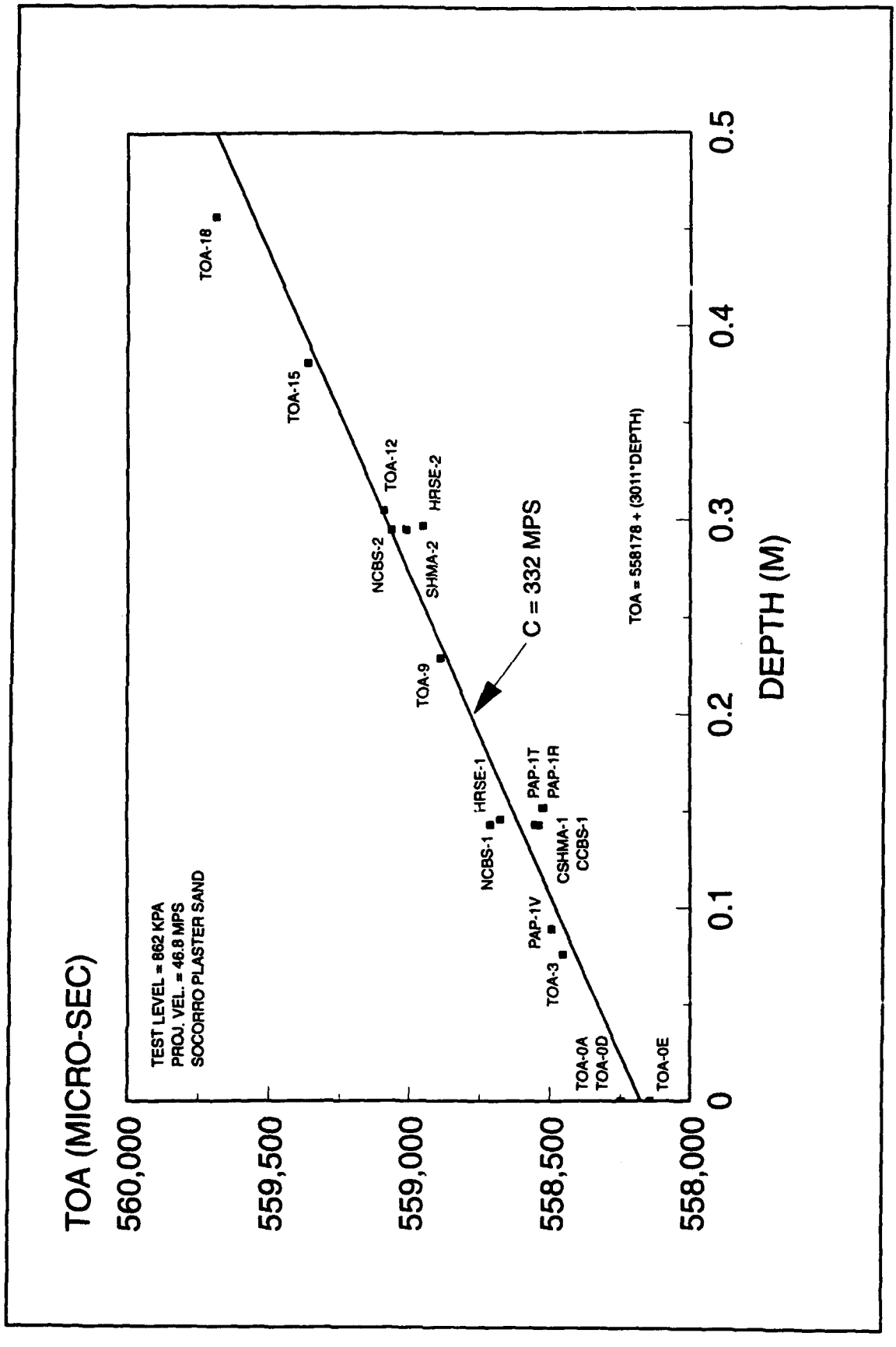

Figure 20. Time-of-arrival vs. distance for Test 22

plotted against the depth (from the surface of the testbed) to the top surface of each gage. The inverse slope (P-wave velocity) of the best linear fit through the data is shown in the figures and is tabulated in Table 5 below.

Table 5
Propagation Velocity of Loading Shock Wave for Tests in Sand

Test No.	Sand Type	Vessel Pressure kPa	Projectile Velocity mps	Wave Propagation Velocity mps
6	Masonry	345	27.9	399
7	Masonry	517	37.1	491
8	Masonry	517	35.5	503
10	Masonry	862	47.2	328
11	Masonry	1,014	50.3	417
12	Masonry	662	41.8	398
13	Masonry	1,027	52.8	337
14	Masonry	1,207	55.7	323
15	Masonry	1,379	59.0	323
16	Socorro	841	46.3[1]	280
17	Socorro	1,165	54.9[1]	309
22	Socorro	862	46.8	332

[1] Calculated value (no experiment data)

In these tests, perfectly normal impacts are unlikely. Nonnormal impacts can result in apparent inconsistancies in the time-of-arrival versus depth-to-top-of-canister data. For instance, in most tests the Wedge SIA canister was placed 180° from the Log SIA canister, and at the same depth. If a nonnormal impact occurred where the projectile impacted the side of the testbed near the Wedge canister first, the shock wave could be witnessed by the Wedge canister before the Log canister. This is seen in Test 11 (Figure 13). Notice the TOA at AV-W occurs prior to that at AV-L. This is possibly the explanation for several cases where gages at slightly lower depths witnessed shock arrival prior to gages at higher locations in the testbed. Other explanations for this might include accuracy of gage placements and variability in the soil conditions across the diameter of the testbed.

Determination of Propagation Velocity of Rarefaction Wave

A rarefaction wave was generated in each testbed by the interaction of the shock wave with the free surface at the bottom of container (and the sides as well). Two methods were used to determine the propagation velocity of the rarefaction wave (or unloading wave) for several tests in sand. Both methods hinged on witnessing the TOA of the unloading wave on individual stress records. The displacement of a stress gage was assumed to be identical to the displacement of an accelerometer canister located at the same depth. Discussion of these results is limited to Test 22.

Graphical Method

A schematic of the depths of the stress and velocity gages fielded in Test 22 in their original position and at a later time is presented in Figure 21. Representative stress records from the 15.2 and 30.5-cm depths are shown in Figure 22. The TOA of the rarefaction wave at each gage location is noted in the figure. The displacement of the accelerometer canister, at each depth, at the arrival time of the relief wave is measured from the double-integrated acceleration history. This displacement is added to the original gage position to determine the location of the gage at the arrival time of the relief wave. The location of each stress gage at the arrival time of the rarefaction wave is plotted in Figure 23. The slope of the linear fit through this data indicates an unloading propagation velocity of 966 mps.

If the loading and unloading wave velocities were constant throughout the depth of the testbed, then the two lines representing the best fit through the loading TOA and unloading TOA should meet at the bottom of the testbed (i.e., at the 61-cm depth). The nominal stress at the 15.2-cm depth as recorded by HRSE-1 was 27.1 MPa, and the value at the 30.5-cm depth, as recorded by HRSE-2, was 16.6 MPa. This difference in the stress levels could cause changes in the loading or unloading wave velocities. Other potential reasons for the non-intersection of the lines at the 61-cm depth include experiment error in placing the gages in the testbed, or uncertainty in the absolute depth of the testbed.

Analytic Method

The second method used to determine the propagation velocity of the rarefaction wave in the soil is based on the geometry of the testbed and the determined loading wave velocity. After the shock wave impacted a stress gage, it continued until it impacted the free surface at the bottom of the testbed. The distance over which the shock wave traveled at the loading wave speed is known. The reflected wave then traveled back though the testbed at the unloading wave speed. The distance over which the rarefaction wave traveled

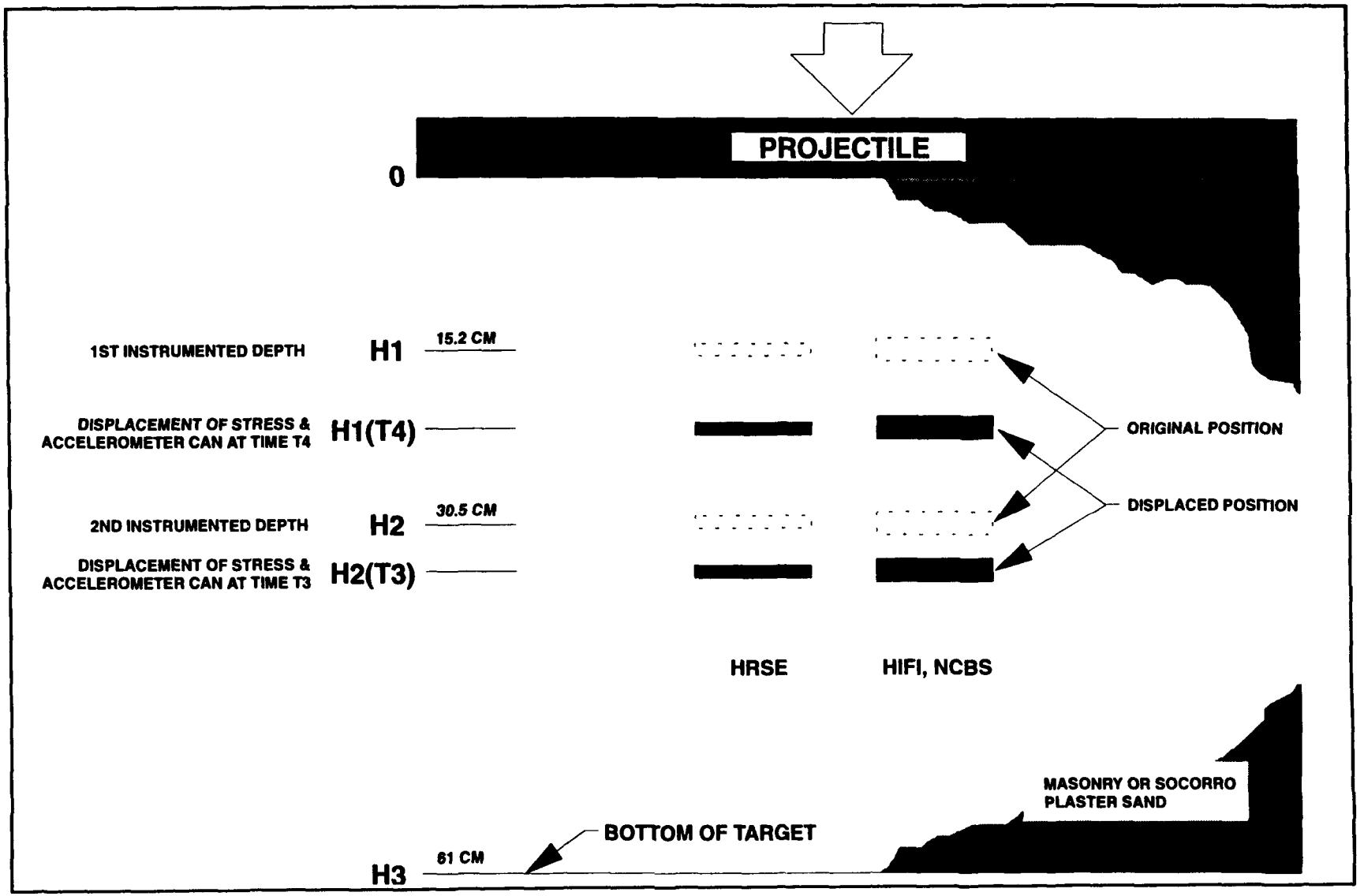

Figure 21. Schematic of canister positions at TOA of the loading and unloading waves

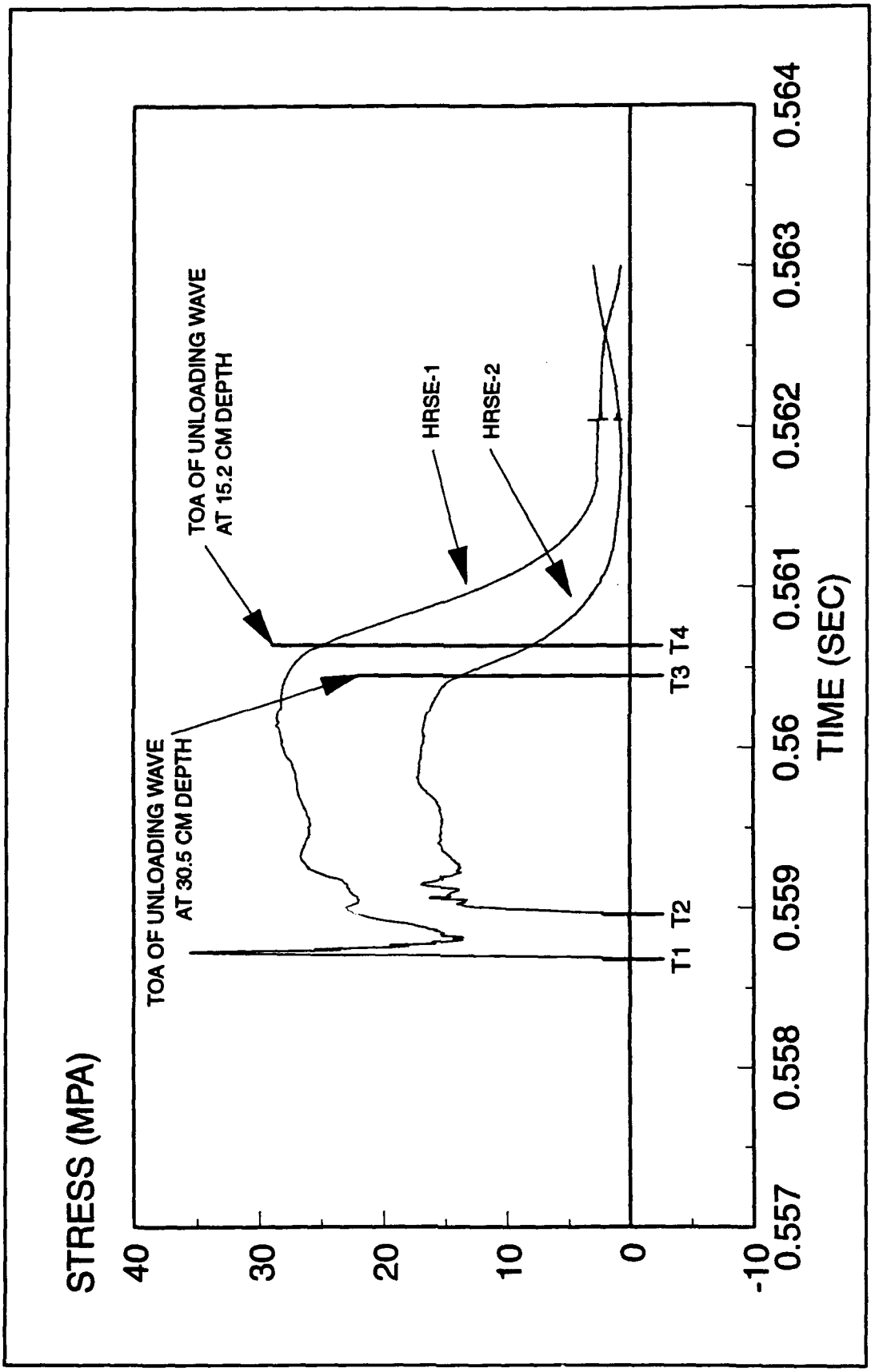

Figure 22. Stress measurements at the two instrumented depths from Test 22, indicating TOA of the loading (T1 and T2) and unloading (T3 and T4) waves

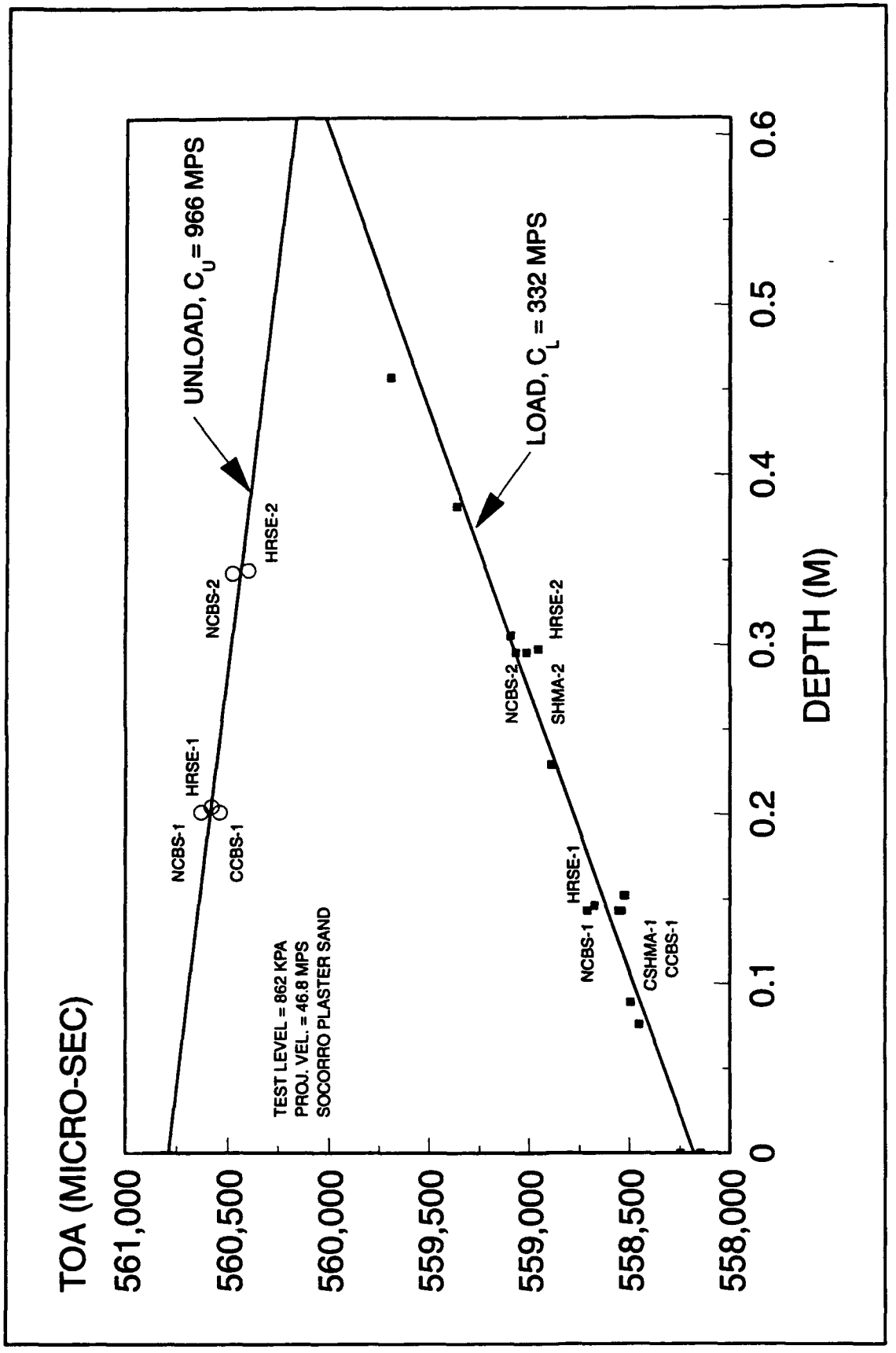

Figure 23. Graphical determination of the unloading wave speed, C_U

until it impacted the stress gage was determined by assuming that displacement of the stress gage was identical to that of an accelerometer canister at the same depth. The velocity of the loading and unloading waves was assumed to be constant over the distance traveled.

In Figure 21 the original positions of gages at the upper and lower depths are denoted by *H1* and *H2*, respectively. The displaced positions at TOA of the relief wave are denoted by *H1(T4)* and *H2(T3)*, respectively. The location of the bottom of the target is denoted by *H3*. In Figure 22 the initial TOA of the shock wave at each gage depth is labeled as *T1* and *T2*. The TOA of the relief wave at the lower and upper depths is labeled *T3* and *T4*, respectively. Given the time for a shock wave to travel these two known distances, and knowing the velocity over one of those distances, the velocity over the second distance may be determined. At the upper depth and lower depths (respectively), the difference in time between loading and unloading wave arrival is given by:

$$(T4 - T1) = \frac{H3 - H1}{C_L} + \frac{H3 - H1(T4)}{C_U}$$

$$(T3 - T2) = \frac{H3 - H2}{C_L} + \frac{H3 - H2(T3)}{C_U}$$

where

C_L = the loading wave velocity

C_U = the unloading wave velocity

These equations may be rearranged to solve for the unloading wave velocity. For gages located at the upper depth,

$$C_U = \frac{H3 - H1(T4)}{(T4 - T1) - \left[\frac{H3 - H1}{C_L}\right]} \qquad (1)$$

For gages located at the lower depth, the unloading wave velocity may be determined from

$$C_U = \frac{H3 - H2(T3)}{(T3 - T2) - \left[\frac{H3 - H2}{C_L}\right]} \qquad (2)$$

Equation (1) was applied to the stress records at the upper depth and Equation (2) was applied to the stress records at the lower depth for Test 22. The results are presented in Table 6. The loading wave speed, C_L, used in these calculations was that determined by the linear fit to the TOA data; i.e., 332 mps (see Figure 20). The thickness of the gage was also considered in these calculations.

Table 6
Unloading Wave Speed, C_U, as Determined by the Analytic Method for Test 22, Assuming a Constant Loading Wave Speed

Gage Name	Depth, cm	C_U, mps
HRSE-1	15.2	810
NCBS-1	15.2	670
CCBS-1	15.2	777
HRSE-2	30.5	506
NCBS-2	30.5	555

The variation in the determined unloading wave speed may be attributed to experiment error in placing gages in the testbed, or the assumption that the displacement of the stress gage is identical to that of an adjacent accelerometer canister. However, the most plausible explanation is perhaps the error in assuming the loading wave travels at constant velocity through the depth of the testbed. This may be seen in the values of the C_U determined by the stress gages at the lower depth. If a slower loading wave velocity is chosen for the depths where stresses are lower, the determined unloading wave speed will be larger.

This premise was investigated for the data of Test 22. A loading wave speed, C_{L1}, was determined for that portion of the testbed between the two instrumented depths by considering only the TOA data at the two depths. A different loading wave speed, C_{L2}, was determined by the linear fit through the TOA data at, and below, the lower instrumented depth. For gages at the upper depth, the mathematical description of the time required for the shock wave to make the round trip is,

$$(T4 - T1) = \frac{H2 - H1}{C_{L1}} + \frac{H3 - H2}{C_{L2}} + \frac{H3 - H1(T4)}{C_U}$$

where

C_{L1} = the loading wave speed between the upper and lower instrumented depths

C_{L2} = the loading wave speed between the lower depth and the bottom of the sample

This may be rearranged to solve for C_U,

$$C_U = \frac{H3 - H1(T4)}{(T4 - T1) - \left[\frac{H2 - H1}{C_{L1}} + \frac{H3 - H2}{C_{L2}}\right]} \quad (3)$$

Equation (3) is used to determine C_U from the stress records for the three gages at the upper depth. Equation (2) is still applicable for the two stress gages at the lower depth by substituting C_{L2} for C_L. The dashed line presented in Figure 24 is the linear fit through the TOA data at the two instrumented depths. The loading wave speed determined by the slope of this line (364 mps) is the assumed C_{L1} over the distance from H1 to H2 within the testbed. The solid line in Figure 24 is a linear fit through instruments at and below the lower depth. The wave speed determined from a linear fit through this data is 242 mps. This is substituted as C_{L2} in Equation (3) and as C_L in Equation (2) to determine the unloading wave speed. The results of this analysis are presented in Table 7.

While this analysis does not yield a unique value for the unloading wave speed in the testbed, it does provide insight on how future tests may be instrumented in order to determine the changing loading wave speed through the depth of the testbed. An advantage of the S&V canister for this type of analysis is that the stress and velocity measurements are made in the same canister; therefore the displacement of the stress gage is known as a function of time.

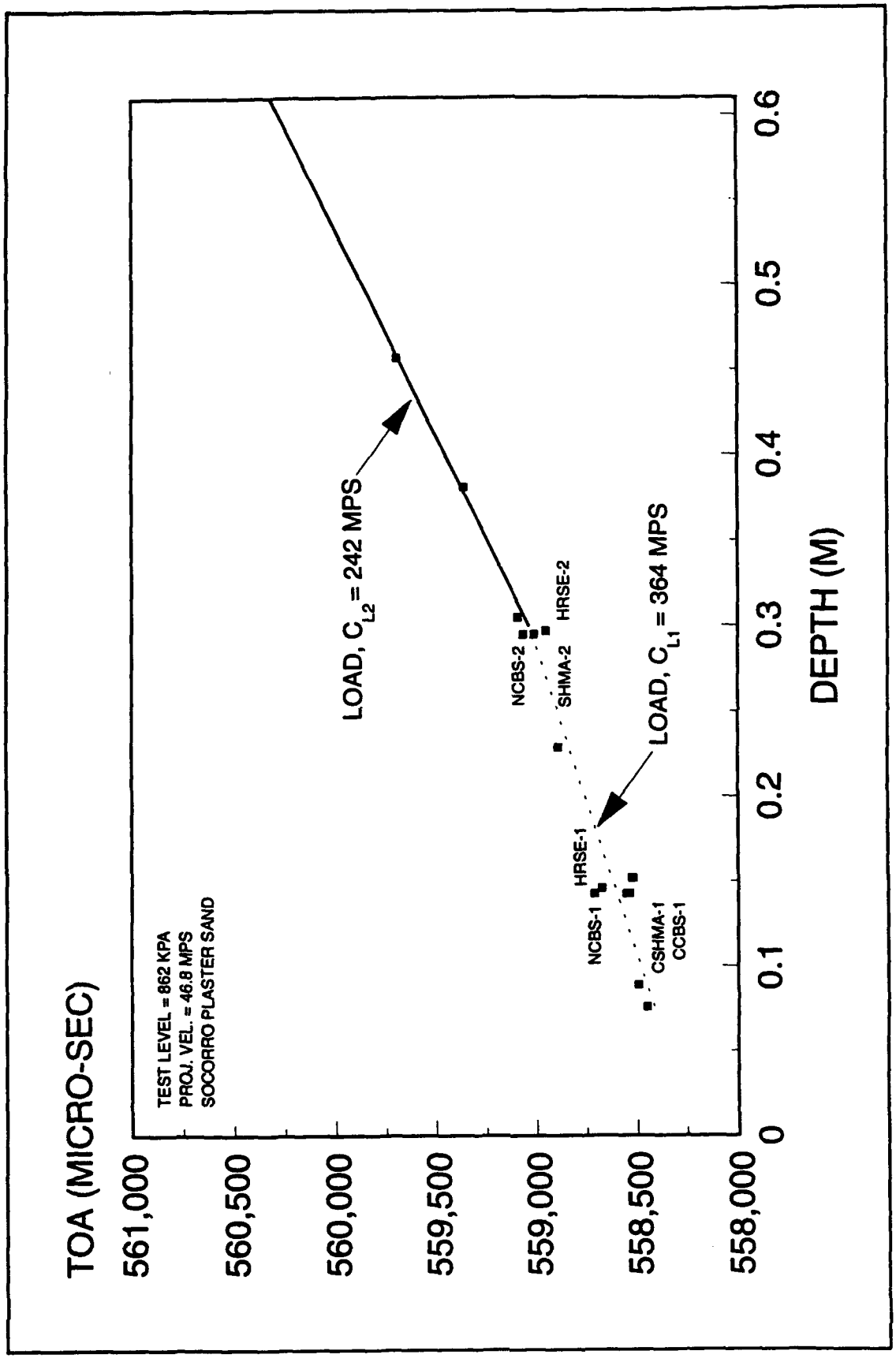

Figure 24. Determination of a varying loading wave speed through the depth of the target

Table 7
Unloading Wave Speed, C_u, as Determined by the Analytic Method for Test 22, Assuming a Varying Loading Wave Speed

Gage Name	Depth, cm	C_u, mps
HRSE-1	15.2	1977
NCBS-1	15.2	1253
CCBS-1	15.2	1685
HRSE-2	30.5	1389
NCBS-2	30.5	1712

4 Analysis of Nonnormal Impacts

Requirement

As mentioned in Section 3, it is not probable to have a completely normal impact between the projectile and sample when testing with a 4-ft diameter projectile. A full understanding of the interaction between the projectile and the sample is required in order to use the large diameter gas gun for dynamic material properties testing.

In the analysis of TOA measurements presented earlier, it was assumed that the projectile impacted the testbed in a perfectly normal fashion. In order to determine the propagation velocity of the shock front, the TOA at each gage location was plotted against the relative distance between the top surfaces of different instruments (for the first eleven tests). For Test 22, the TOA was plotted against the actual depth to the top surface of each instrument in the testbed. The wave speed in the sample was then determined by the inverse slope of the linear fit through this data. For this type of analysis, the value to be plotted as "depth" is the perpendicular distance between the gage and the loading shock front. For a perfectly normal impact, this distance is simply the vertical distance from the top of the testbed to the top surface of the instrument. For a nonnormal impact, however, the gage depth is a function of the projectile velocity, the angle of impact, and the propagation velocity of the loading wave.

Description of Nonnormal Impact

Several assumptions are required for the analysis of nonnormal impacts. These are:

- The surface of the impacting plate is flat.
- The surface of the testbed is flat.

- The surface of the testbed is perpendicular to the centerline axis of the testbed.
- The centerlines of the projectile impact plate and the testbed are collinear.
- The projectile does not rotate after initial contact with the testbed.
- The loading wave velocity, C_L, is a constant.

In a nonnormal impact, a single point at the outer edge of the projectile impact plate strikes the top surface of the testbed first (see Figure 25). The projectile continues to be driven into the test sample. The last part of the impact plate to come into contact with the sample is the point on the face of the plate diametrically opposed to the first point of impact. The time delay, ΔT, between the first point of impact and the last point of impact is a function of the projectile velocity, Vel_p, the projectile diameter, D, and the impact angle, θ, according to the relation,

$$\Delta T = \frac{D * Sin(\theta)}{Vel_p}$$

The loading wave in the sample emanates from the first point of impact, but does not become fully developed until the last point on the projectile impacts the surface of the testbed. The angle, α, at which the normal loading wave propagates through the testbed is a function of the propagation velocity, C_L, in the testbed; the difference in time, ΔT, between the first and last points of impact of the projectile; and the angle of impact (θ) of the projectile; according to the relation,

$$\alpha = Tan^{-1}\left[\frac{C_L * \Delta T}{D * Cos(\theta)}\right]$$

Substituting for ΔT from above, this expression becomes

$$\alpha = Tan^{-1}\left[\frac{C_L * Tan(\theta)}{Vel_p}\right] \quad (4)$$

From this equation, it is evident that as the projectile impact velocity increases, the angle at which the wave propagates through the sample is

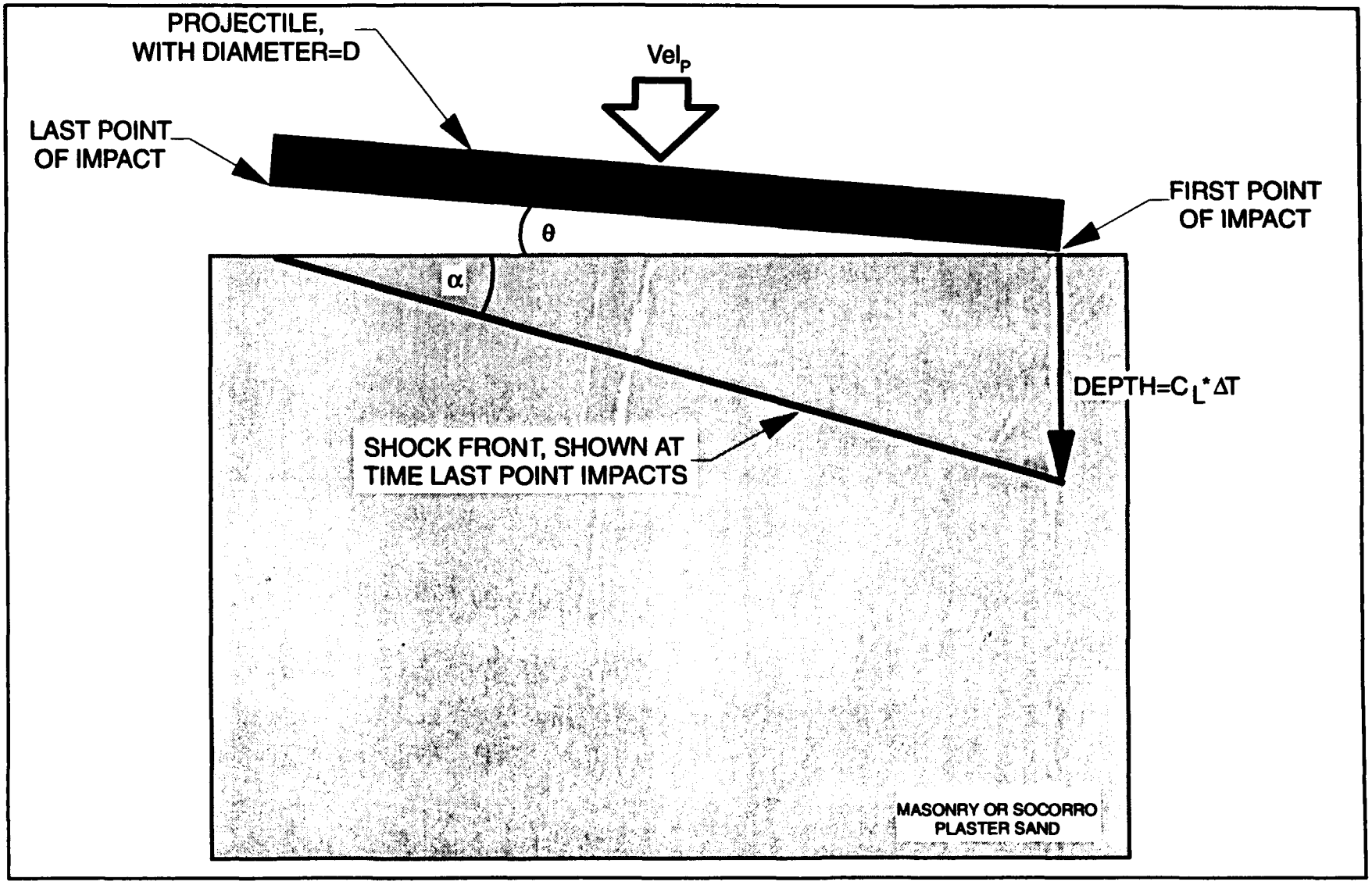

Figure 25. Schematic of nonplanar impact

minimized, for a given angle of impact, θ. On the other hand, for testbed materials with a higher loading wave speed, the effect is increased.

Description of CLAP Code

A computer code was written (in BASIC) to assist in the analysis of non-normal impacts. The code name, CLAP, is an acronym for loading wave (C_L) angle (A) program (P). The code is used to calculate the first point of impact on the testbed surface, the angle of impact of the projectile, and the loading wave speed in the testbed.

Determination of First Point of Impact on the Surface of the Testbed and Angle of Impact

For Test 22, three piezoelectric crystals were placed on the surface of the testbed to determine the angle of projectile impact. The differences in TOA for the crystals were calculated using the first crystal impacted as the reference for the remaining crystals. Assuming that the crystals lie in a horizontal plane perpendicular to the centerline of the testbed, differences in the TOA's for the three crystals indicates that the projectile was tilted as it impacted the testbed (see Figure 26). At the time the last crystal was impacted, the product of the impact velocity and the difference in TOA yields the relative height of the projectile (at the crystal locations) with respect to the testbed surface, assuming the projectile does not rotate after impact. With the centerlines of the projectile and testbed aligned, the (x,y) coordinates of the crystals may be transferred to the face of the projectile. Three points on the projectile's impacting surface are now defined, with the origin of the coordinate system at the top center of the testbed surface. The equation of the plane through these three points is then determined.

Using the equation describing the plane of the impact plate, the first point of contact onto the testbed surface is determined. The impact plate is divided into 1440 equal segments (¼ degree increments). For each increment, the z coordinate at the outer radius of the plate is calculated. The increment which results in the minimum z represents the first point of impact at the surface of the testbed. The angle formed by the horizontal testbed surface and the line from the first point of impact through the center of the impact plate is the angle of impact, θ (see Figure 26).

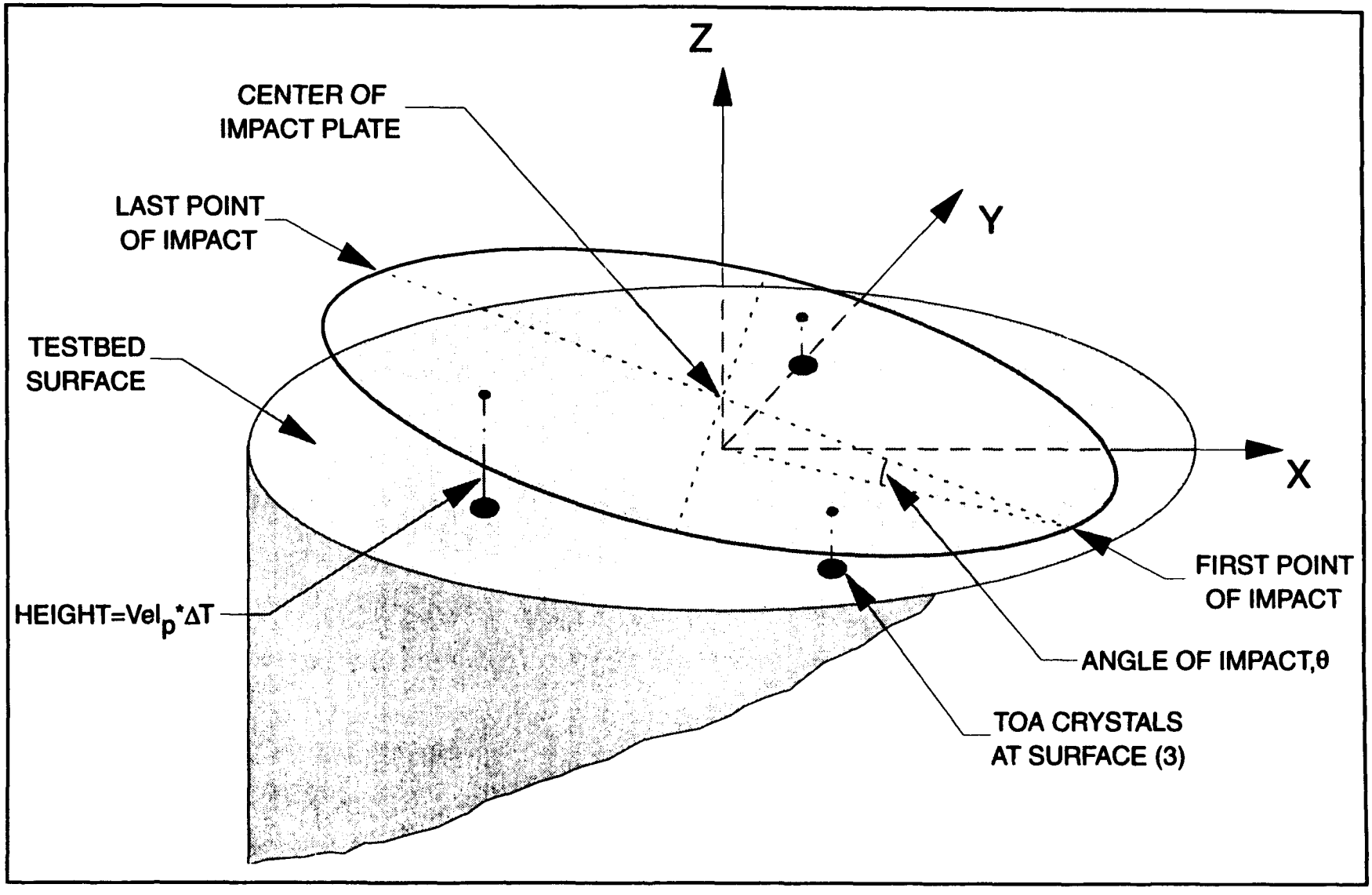

Figure 26. Schematic of parameters used to determine the first point of impact on the testbed surface for nonplanar impacts

Determination of the Loading Wave Speed in the Testbed Using TOA Measurements at the Surface of the Testbed

To begin, the loading wave speed is determined by the procedure described in Section 3. That is, a normal impact is assumed and the loading wave speed is the inverse slope of a linear fit through the TOA versus depth plot. A correlation coefficient is determined that represents the quality of the linear fit through the experiment data. For a perfect fit this coefficient is 1. For any case other than a perfect fit this coefficient is less than 1. Using Equation (4), the angle (α) at which the normal loading wave propagates through the testbed is calculated. The "depth" of each gage location is recalculated as the perpendicular distance between the gage location and the new, fully-developed loading wave (with angle α). This is illustrated in Figure 27.

A new loading wave speed is determined from the linear fit through a plot of TOA versus (recalculated) depth. The correlation coefficient is also calculated. As the values of depth are adjusted for each gage location, the data falls more closely on a line, and thus increases the correlation coefficient. Using the new value for the loading wave velocity, Equation (4) is used once again to determine the angle at which the plane wave propagates through the testbed. The "depth" of each gage is recalculated, and a new loading wave velocity is determined as before. This iterative process continues until the correlation coefficient converges to a constant value.

Test 22 was the only test that used TOA crystals at the surface of the testbed to determine the angle of impact. CLAP was used to evaluate the angle of impact (θ), the first point of impact, the angle at which the loading wave travelled through the testbed (α), and the loading wave velocity (C_L), as described above. A series of screen dumps from the code are included as Figures 28 through 35. Figure 28 is an introductory screen allowing the user to select one of two methods of analysis. The first selection is described above and the second selection is a trial and error method, described below. Data required by the program (e.g., gage locations, TOAs, etc.) may be entered through the keyboard or by a data file. Figure 29 lists the data used to calculate the equation of the plane through the impact plate. Also presented are the coefficients for the equation of the plane. Figure 30 indicates the first point of impact of the projectile onto the testbed surface. Figure 31 lists the coordinates of the gage locations in the testbed. This coordinate system defines the origin at the top center of the testbed, with the positive x-axis pointing due east when looking at a plan view of the testbed (see Figure 3). The values for z indicate the depth to the top surface of the gage (note: this is a left handed coordinate system). Figure 32 lists the least squares curve fit data for the data set of Figure 31. The plot of Figure 33 is identical to the TOA versus depth plot of Figure 20. Figure 34 lists the least squares curve fit data after one iteration on the angle at which the loading wave propagates. The plot of Figure 35 shows the TOA data plotted against the recalculated values for the depth of the gages. The loading wave speed changed from 332 mps to 336 mps after one iteration, and the correlation coefficient decreased from 0.98222 to 0.97923. Further iterations do not significantly

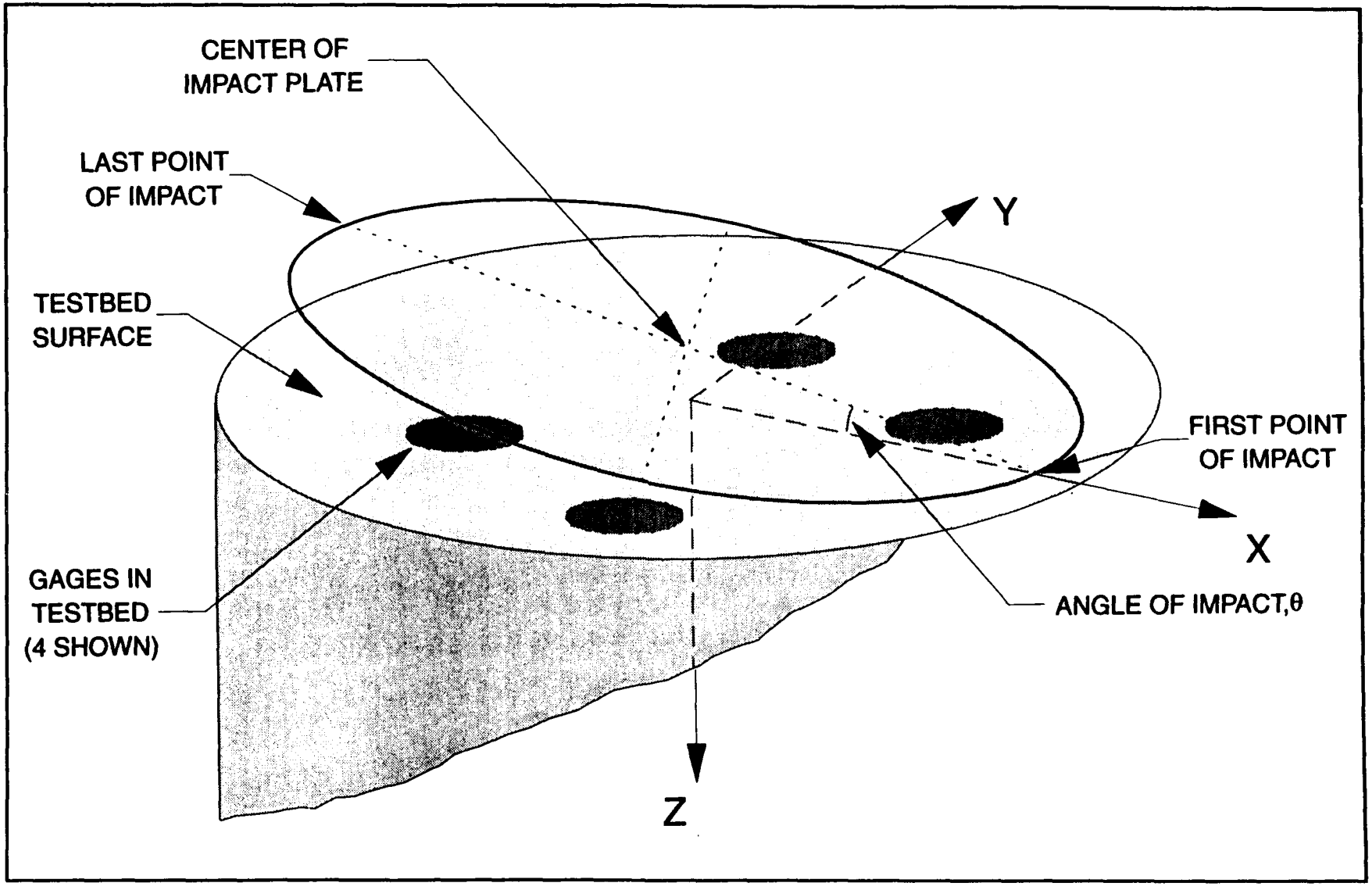

Figure 27. Orientation of coordinate system used to determine the loading wave speed

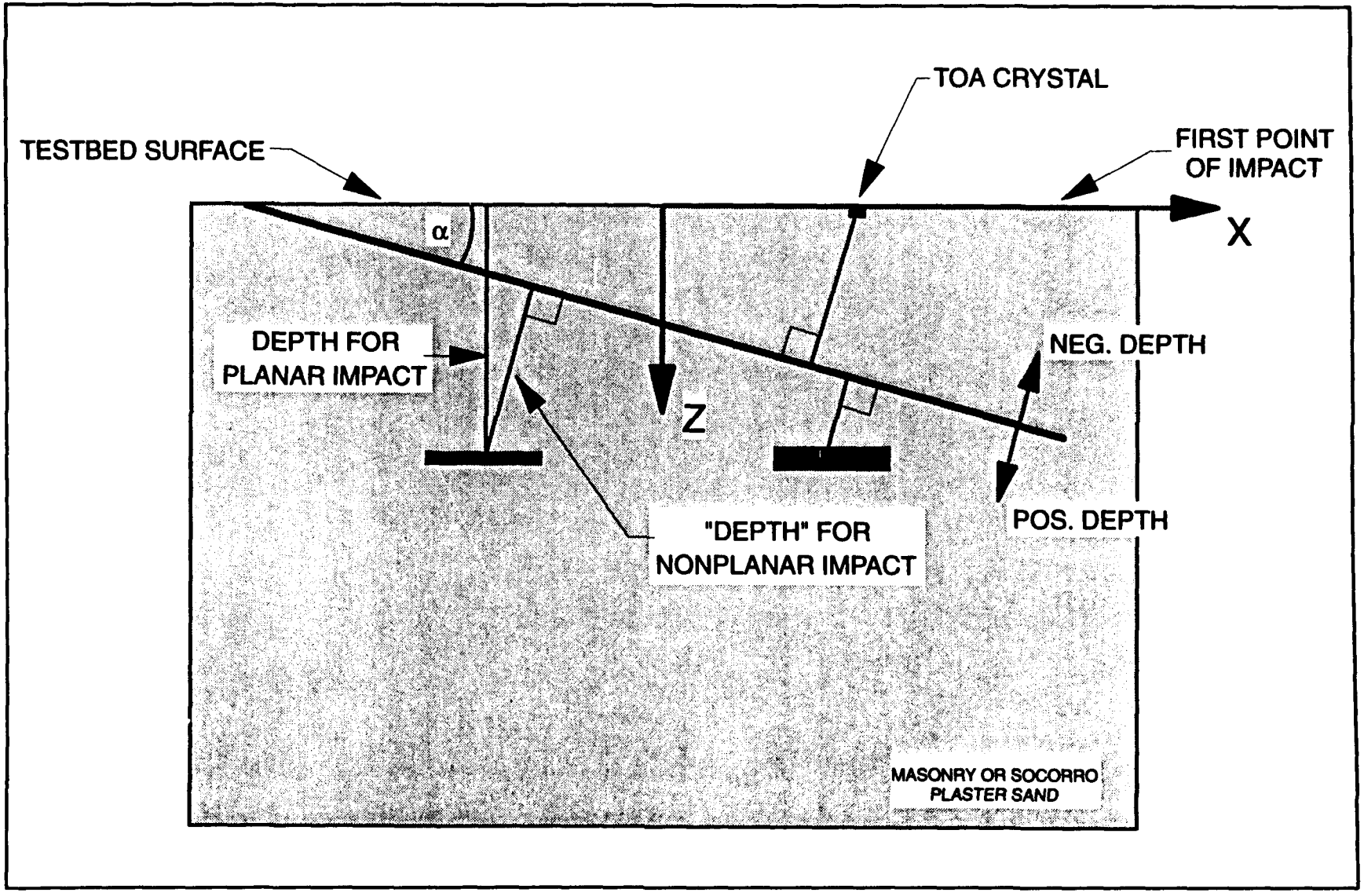

Figure 28. Elevation view indicating "depths" used in determining the loading wave speed

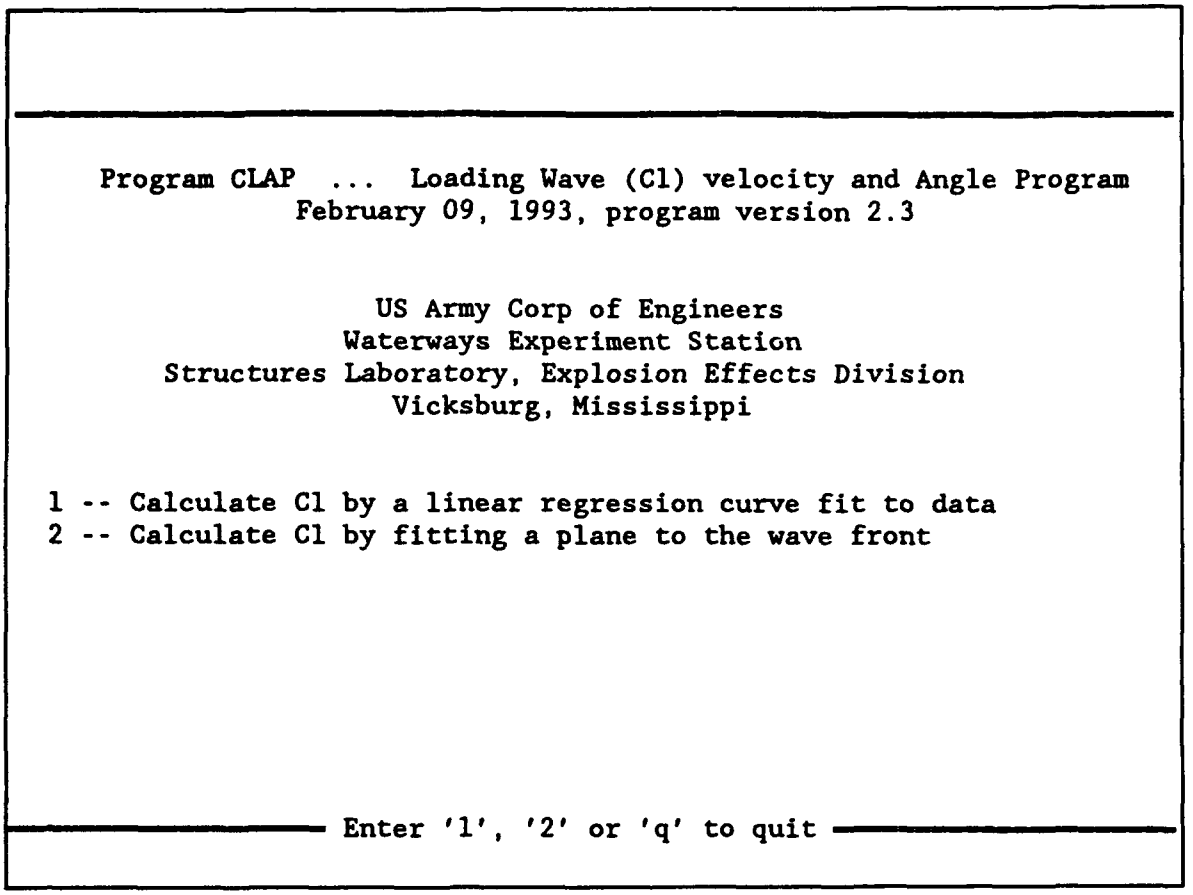

Figure 29. Introductory screen of the CLAP code

```
Entered Impact Plate Data

The following data has been entered

Test name: test 22
Location of TOA gage 1 = ( 0 , .1524 )
Location of TOA gage 2 = ( .32385 ,-.32385 )
Location of TOA gage 3 = (-.32385 ,-.32385 )
Time of arrival for TOA gage 1 = 558.247  msec
Time of arrival for TOA gage 2 = 558.246  msec
Time of arrival for TOA gage 3 = 558.145  msec
Projectile velocity = 50  m/sec

The general equation for the equation of a plane is Ax+By+Cz+D=0

The following coefficients have been calculated for the projectile
A =-2.402651E-03
B =-1.668394E-03
C = .3084671
D =-8.609789

strike 'c' to continue or 'q' to quit
```

Figure 30. CLAP screen listing data used for determining the equation of the plane of the projectile and the calculated coefficients of the plane

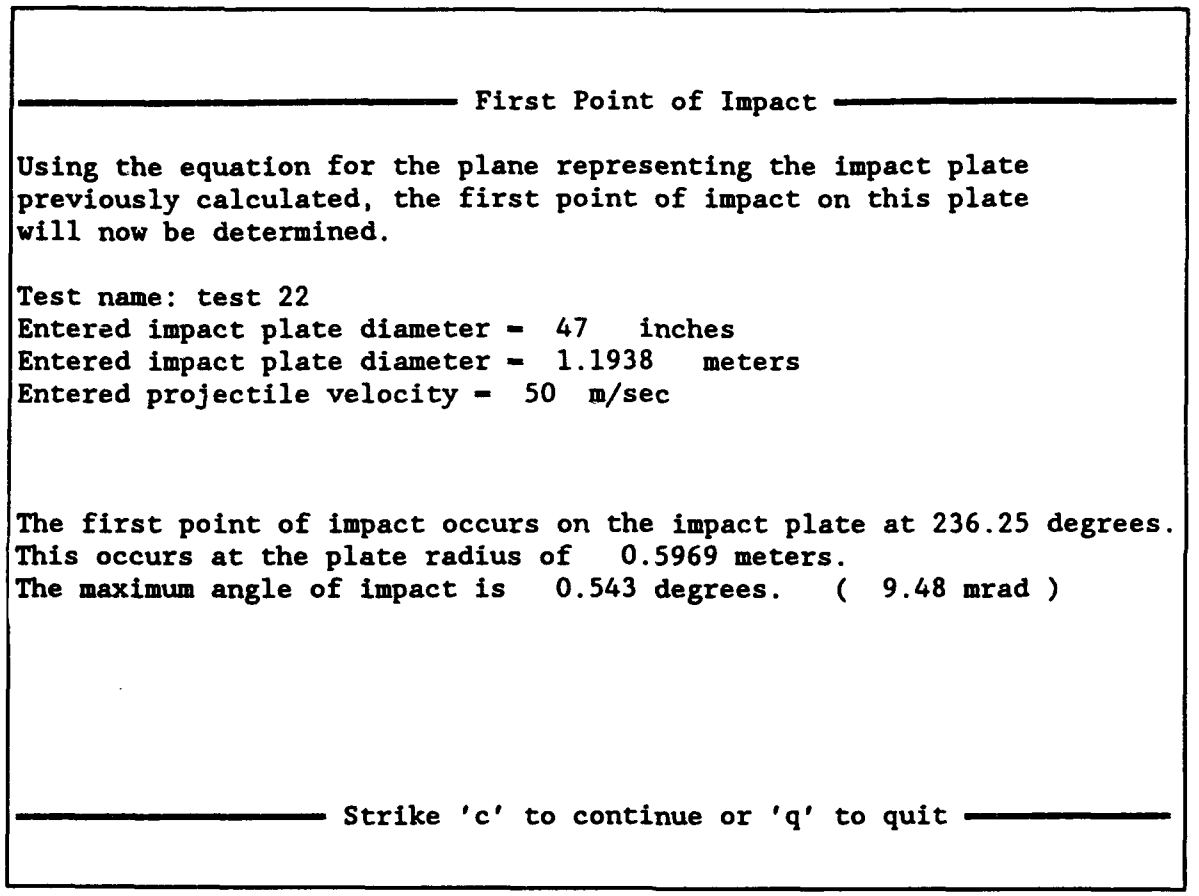

Figure 31. CLAP screen indicating the first point of impact onto the surface of the testbed and the angle of impact

```
                    Entered gage Data

Gage TOA-0A    X =  0.000    Y =  0.152    Z =  0.000    TOA= 558.247
Gage TOA-0D    X =  0.324    Y = -0.324    Z =  0.000    TOA= 558.246
Gage TOA-0E    X = -0.324    Y = -0.324    Z =  0.000    TOA= 558.145
Gage HRSE-1A   X =  0.000    Y =  0.305    Z =  0.146    TOA= 558.674
Gage NCBS-1    X =  0.305    Y =  0.000    Z =  0.143    TOA= 558.710
Gage CCBS-1    X = -0.305    Y =  0.000    Z =  0.143    TOA= 558.538
Gage CSHMA-1   X = -0.305    Y =  0.000    Z =  0.143    TOA= 558.551
Gage PAP-1V    X =  0.216    Y =  0.216    Z =  0.089    TOA= 558.494
Gage PAP-1R    X =  0.216    Y =  0.216    Z =  0.152    TOA= 558.526
Gage PAP-1T    X =  0.216    Y =  0.216    Z =  0.152    TOA= 558.522
Gage HRSE-2    X =  0.146    Y =  0.042    Z =  0.297    TOA= 558.951
Gage NCBS-2    X = -0.108    Y = -0.108    Z =  0.295    TOA= 559.063
Gage SHMA-2    X =  0.042    Y =  0.146    Z =  0.295    TOA= 559.010
Gage TOA-3     X =  0.000    Y =  0.051    Z =  0.076    TOA= 558.452
Gage TOA-9     X =  0.000    Y = -0.051    Z =  0.229    TOA= 558.890
Gage TOA-12    X = -0.051    Y =  0.000    Z =  0.305    TOA= 559.089
Gage TOA-15    X =  0.000    Y =  0.051    Z =  0.381    TOA= 559.358
Gage TOA-18    X =  0.051    Y =  0.000    Z =  0.457    TOA= 559.687

              strike 'c' to continue or 'q' to quit
```

Figure 32. CLAP screen listing the data used to determine the initial loading wave speed (with no iterations in CLAP)

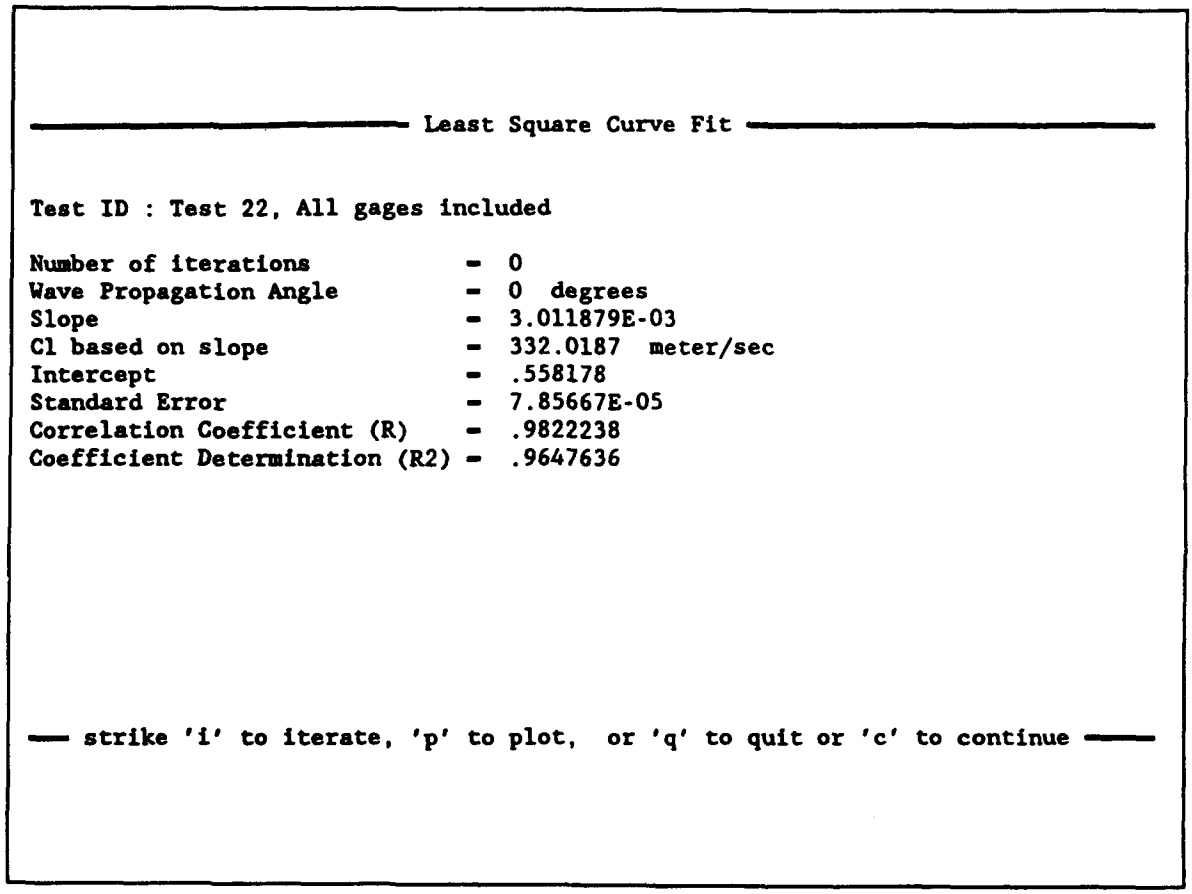

Figure 33. CLAP screen listing regression data for the least squares curve fit through the TOA vs. depth data (prior to iterating with CLAP)

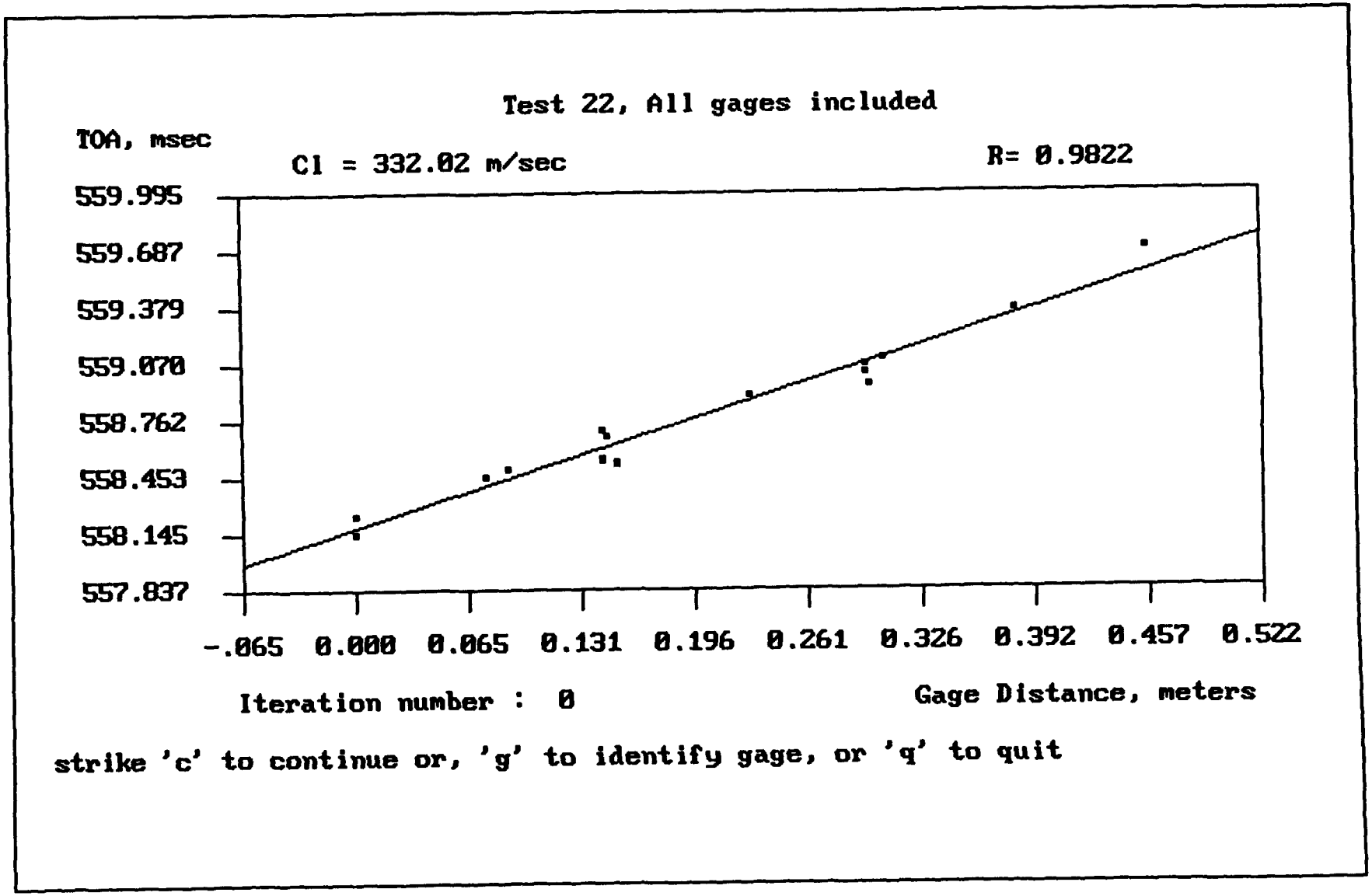

Figure 34. CLAP screen showing TOA vs. depth data (prior to iterating with CLAP)

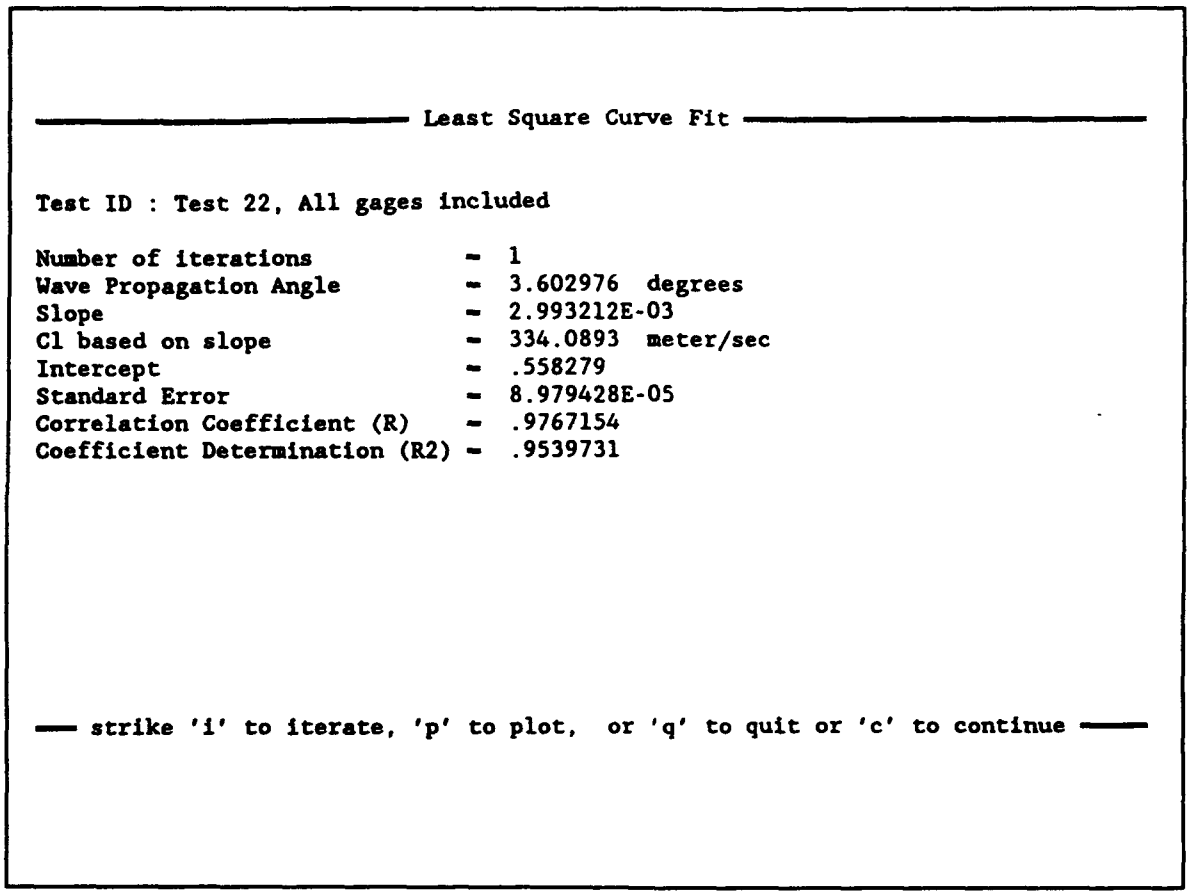

Figure 35. CLAP screen listing regression data for the least squares curve fit through the TOA vs. depth data (after a single iteration with CLAP)

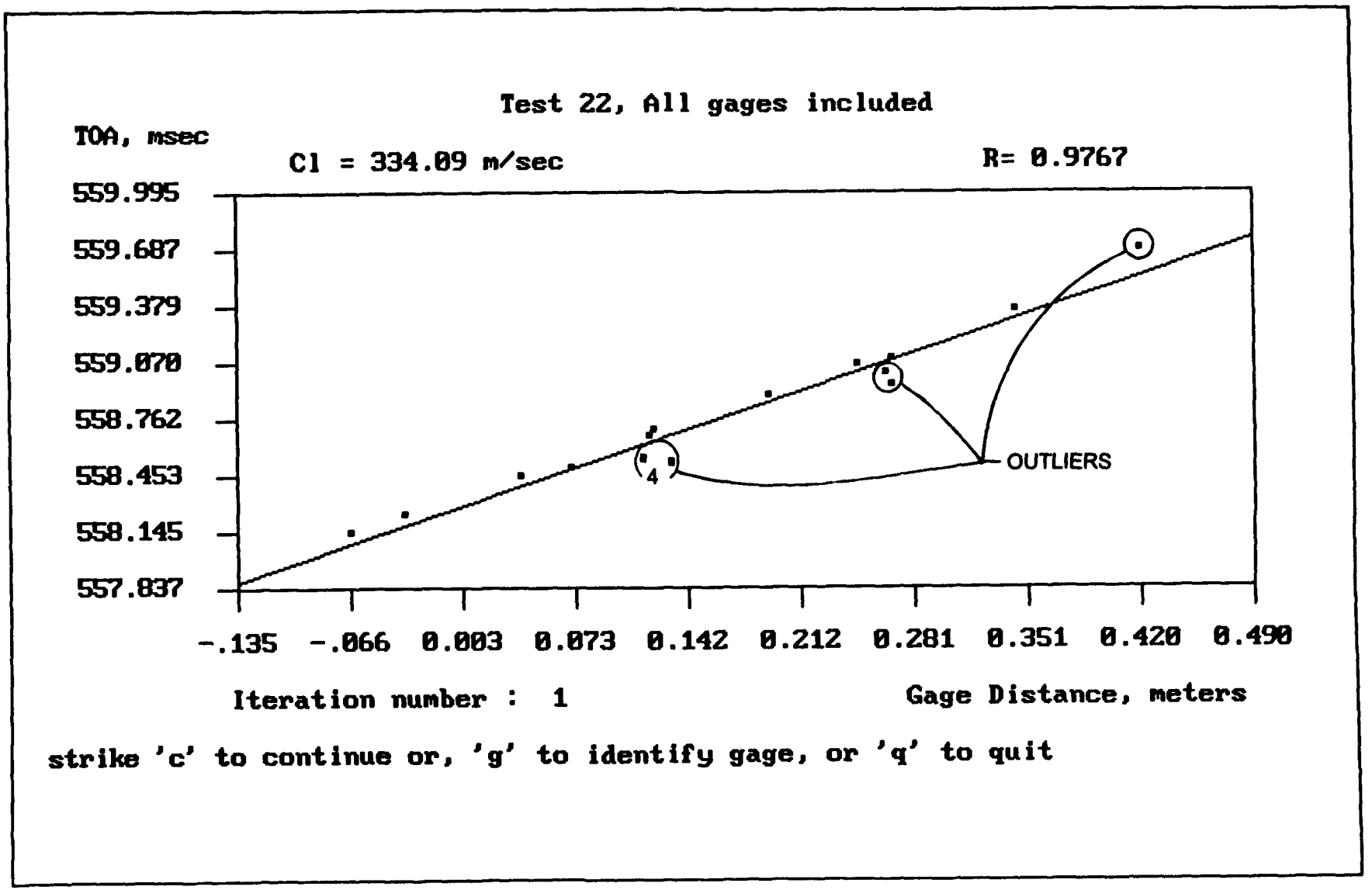

Figure 36. CLAP screen showing TOA vs. depth data (after a single iteration with CLAP)

change the loading wave speed or the correlation coefficient. For example, after an additional four iterations the determined loading wave speed is 336 mps and the correlation coefficient is 0.97913. The angle at which the wave propagated through the testbed was determined to be 3.65 degrees.

As a result of this analysis, the stated locations of several gages in the testbed appear to contain errors. This is because the correlation coefficient should increase after each iteration, and for this data set the coefficient decreased. Several factors could result in inaccurate gage locations: 1) gages were not placed properly in the testbed, 2) gages locations were not measured or recorded properly, or 3) the gage locations changed when the testbed was relocated from the preparation area to the gas gun facility. An additional source of error could simply be the tolerance at which the gages were placed in the testbed (± 3 mm).

From the plot of Figure 35, it is noted that, with the exception of five TOA measurements, the data set is quite linear. These five measurements are indicated as "outliers" in the figure. As an exercise, CLAP was used to evaluate a modified data set that removed these measurements. A plot of this data set after a single iteration is shown in Figure 36. The loading wave speed determined using this reduced data set was 340 mps. The angle at which the wave propagated through the sample was determined to be 3.71 degrees. The correlation coefficient increased to 0.99766, indicating a tighter data set than that of Figure 35.

By accounting for nonnormal impact, the loading wave speed increased by 0.6 percent when considering the entire data set, and increased by 3 percent when considering a modified data set. This difference is not significant in either case. What is significant, however, is that this analysis provides an independent check on the location of the gages. It will also assist in determining the required placement tolerances on future tests.

Determination of the Loading Wave Speed in the Testbed on a Trial and Error Basis

If the angle of impact of the projectile is not known or cannot be determined, the CLAP code uses a trial and error method for determining the loading wave speed in the soil. This method tries different combinations of first points of impact and loading wave propagation angles (α) to determine which condition will produce the highest correlation coefficient from the linear regression curve fit.

To do this, CLAP sets the first point of impact at 0 degrees. Then the angle between the loading wave and the testbed surface is varied from 0 to 12 degrees in ¼-degree increments. For each increment, the perpendicular distance (or depth) between the gage location and the loading wave plane is calculated, as described above. A linear fit through the TOA-versus-depth data is made and the correlation coefficient is recorded. The first point of

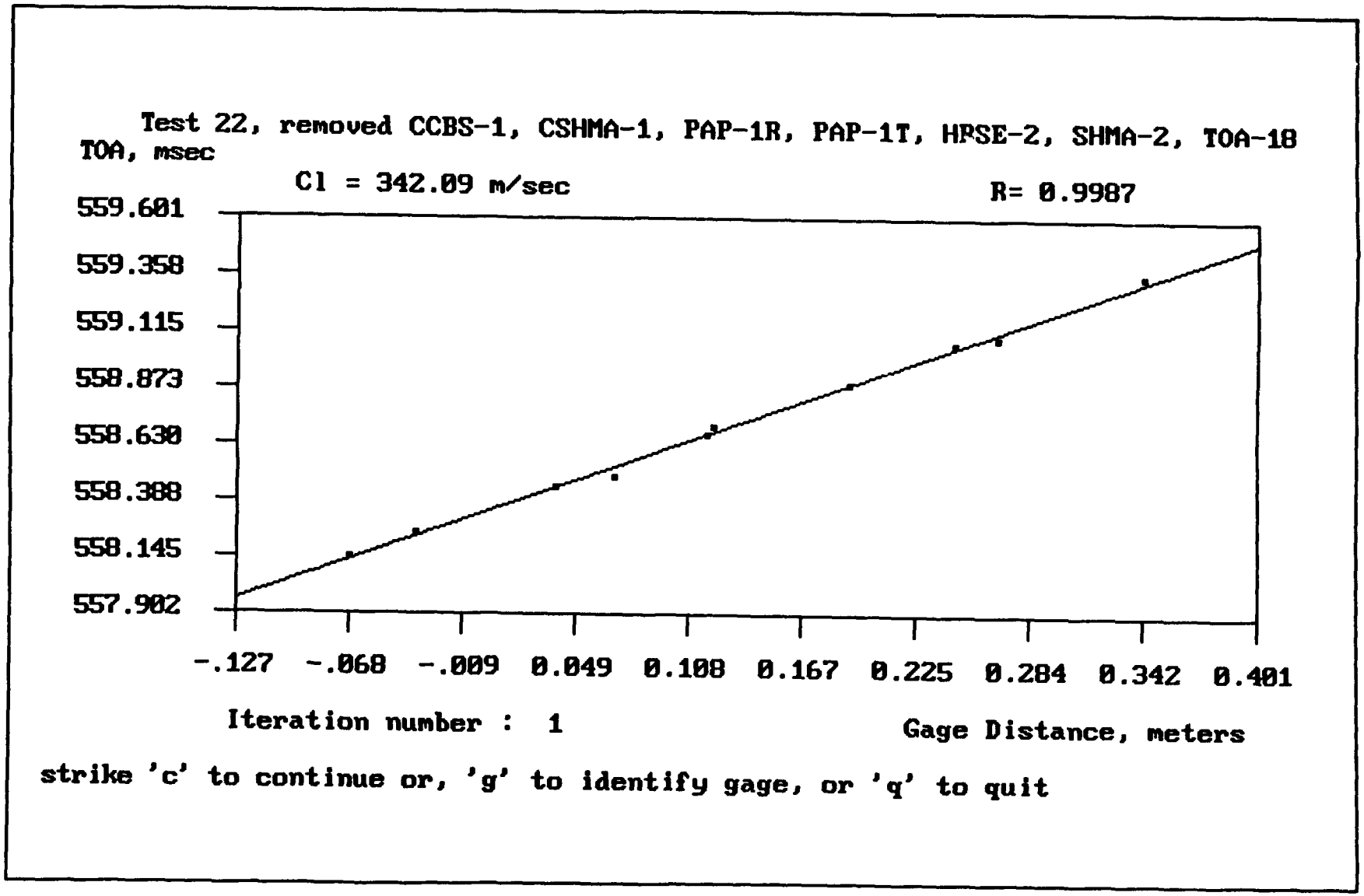

Figure 37. CLAP screen showing TOA vs. depth data for a modified input data set (after a single iteration with CLAP)

impact is then incremented by 1 degree. As before, the angle between the loading wave and the testbed surface in incremented. A linear fit is made and the correlation coefficient for each increment is calculated. This procedure is continued as the first point of impact varies from 0 to 359.75 degrees. The combination of the first point of impact and the angle of the loading wave which produced the best (or highest) correlation coefficient is said to represent the actual test condition. The inverse slope of the linear fit through the data for this combination is reported as the loading wave speed.

The graphical procedure for determining the loading wave speed, presented in Section 3, is very sensitive to the accuracy of the gage placement. The difference in height between the top surface of some gage types (at the same level) is on the same order as the placement tolerances. A comparison of values for the loading wave speed as determined by the graphical procedure, versus those determined by the CLAP trial and error procedure, can better describe actual test conditions.

Agreement between the loading wave speed determined by the CLAP code and the value determined by the graphical procedure (discussed in Section 3) would indicate normal impact. However, large values for alpha would not necessarily indicate a large impact angle, since the angle at which the wave propagates through the sample is a function of the projectile velocity.

Repeated in Table 8 is the value of the loading wave speed determined by the graphical method presented in Table 5, Section 3. The trial and error procedure within CLAP was used to determine the loading wave speed and angle of propagation for the tests where the angle of impact could not be determined (all except Test 22). The results are presented in Table 8. The correlation coefficient for each method is listed in the table. Note that in each instance the wave speed decreases or remains constant and the correlation coefficient increases. Using Equation (4), Section 4, the angle of impact (θ) was calculated to check the consistency of the values for C_L and α determined using CLAP. The values presented in Table 8 are consistent and similar to the value measured on Test 22. Hence the trial and error method used within CLAP provides a mechanism to analyze the geometry of impact without surface TOA measurements.

Table 8
Comparison of Loading Wave Speed Determined by Graphical Procedure and by Trial and Error CLAP Calculation

Test No.	Sand Type	Graphical Method		CLAP, Trial and Error Method			
		C_L, mps	Correlation Coefficient	C_L, mps	Correlation Coefficient	α, deg	θ, milliradians
6	Masonry	399	0.93697	363	0.95152	3.99	5.4
7	Masonry	491	0.98723	465	0.99941	3.24	4.5
8	Masonry	503	0.85381	506	0.93056	8.65	10.7
10	Masonry	328	0.98176	275	0.99986	4.73	14.2
11	Masonry	417	0.96161	341	1.0	5.72	14.8
12	Masonry	398	0.98081	349	1.0	10.09	21.3
13	Masonry	337	0.95557	333	0.99608	5.72	15.9
14	Masonry	323	0.94881	296	0.96274	3.74	12.3
15	Masonry	323	0.89308	288	0.98996	7.44	26.7
16	Socorro	280	0.95149	276	0.97939	8.65	25.5
17	Socorro	309	0.97052	270	0.97786	1.50	5.3

5 Conclusions and Recommendations

Conclusions

Twelve tests were conducted with the DNA/WES Ground Motion Test Facility with sand testbeds as targets. Nine tests used Masonry sand and three tests used Socorro Plaster sand as the target testbed material. A variety of stress and motion transducers were included in each testbed to investigate the environment in the testbeds, and to determine the robustness of the various instruments.

These experiments provided valuable information on the mechanics of testing with the gun. Analysis of the data provided insight for instrumentation requirements and placement procedures/tolerances for future tests. The results indicate that the facility is a viable tool for conducting dynamic tests for instrumentation development and material properties studies.

Recommendations

Future tests with the gun will incorporate more diagnostic measurements in the testbed. These will include time-of-arrival (TOA) measurements at the surface of the testbed to determine the velocity and angle of impact of the projectile. The TOA of the shock wave at various depths in the sample will be measured (as was done for Test 22) to supplement the TOA measured at the active gage locations. The inclusion of additional TOA measurements will allow for more exact determination of the propagation velocity of the loading and unloading waves in the sample. Also, the S&V canister will be fielded to allow for more precise determination of the displacement of a stress sensor, which will in turn allow a more definitive calculation of the unloading wave speed.

In order to make optimum use of the gun to validate or test ground motion sensors in granular materials, a testbed material is required that will have consistent and predictable properties. WES is investigating the selection of a

standard granular material (perhaps synthetic) and the development of emplacement procedures which will provide a testbed with well-controlled and consistent properties.

References

White, Ohrt, Welch, and Joachim. (1991). "Design and Testing Experiences with the WES 12-in. and 4-ft Diameter Vertical Gas Guns," *Proceedings of the Defense Nuclear Agency Instrumentation for Nuclear Weapons Effects Testing (INWET) Conference, 16-19 April 1991. Volume 1-General Session and Sessions I and II*, DASIAC-TR-91-001-V1, Defense Nuclear Agency, Alexandria, VA.

White, Howard G. (1993). "Performance Tests with the WES 4-ft Diameter Vertical Gas Gun," Technical Report SL-93-11. U.S. Army Engineer Waterways Experiment Station, Vicksburg, MS.

Appendix A
Notation

C_L	Average loading wave velocity in a testbed (velocity of disturbance caused by projectile impact)
C_{L1}	Loading wave velocity between the two instrumented depths in a testbed
C_{L2}	Loading wave velocity between the lower instrumented depth and bottom of a testbed
C_U	Unloading wave velocity in a testbed (wave resulting from reflection from bottom of testbed)
D	Projectile diameter
H1	Upper instrumented depth in a testbed
H1(T3)	Location of an instrument originally in the upper depth, at TOA of relief wave
H2	Lower instrumented depth in a testbed
H2(T4)	Location of an instrument originally in the lower depth, at TOA of relief wave
TOA	Time-of-arrival (of shock waves)
T1	Initial TOA at a gage in the upper depth
T2	Initial TOA at a gage in the lower depth
T3	TOA of the relief wave at a gage in the lower depth
T4	TOA of the relief wave at a gage in the upper depth

ΔT	Difference in time between the first and last points of impact of the projectile onto the surface of a testbed
Vel_p	Projectile velocity
α	angle at which the loading wave propagates through the testbed
θ	angle at which the projectile impacts the testbed

Appendix B
Gage Locations for Tests in Sand

Table B1
Gage Locations for Tests in Sand

Test No.	Gage Name	Depth = 15.2 cm Radius = 30.5 cm	Depth = 30.5 CM Radius = 15.2 CM
6	HRSE-1	✓	
	OCBS-1	✓	
	AV-W1	✓	
	AV-W2	✓[1]	
	AV-L	✓	
	AV-M	✓	
	HRSE-2		✓
	OCBS-2		✓
	NCBS		✓
7	HRSE-1	✓	
	OCBS-1	✓	
	AV-W	✓	
	AV-L	✓	
	AV-M	✓	
	HRSE-2		✓
	HRSE-3[2]		✓
	NCBS		✓
8	HRSE-1	✓	
	OCBS-1	✓	
	AV-W	✓	
	AV-L	✓	
	AV-M	✓	
	HRSE-2		✓
	HRSE-3[2]		✓
	NCBS		✓

(Sheet 1 of 4)

[1] Located in center of testbed (radius = 0 cm)
[2] Oriented horizontally

Table B1 (Continued)

Test No.	Gage Name	Depth = 15.2 cm Radius = 30.5 cm	Depth = 30.5 CM Radius = 15.2 CM
10	HRSE-1	✓	
	OCBS[3]	✓	
	AV-W	✓	
	AV-L	✓	
	HRSE-2		✓
	HRSE-3[2,3]		✓
	NCBS		✓
11	HRSE-1	✓	
	OCBS[3]	✓	
	AV-W	✓	
	AV-L	✓	
	HRSE-2		✓
	HRSE-3[2]		✓
	NCBS		✓
12	HRSE-1	✓	
	AV-W	✓	
	HRSE-2		✓
13	HRSE-1	✓	
	OCBS	✓	
	AV-W	✓	
	AV-L	✓	
	HRSE-2		✓
	HRSE-3		✓[1]
	NCBS		✓

(Sheet 2 of 4)

[1] Located in center of testbed (radius = 0 cm)
[2] Oriented horizontally
[3] No data

Table B1 (Continued)

Test No.	Gage Name	Depth = 15.2 cm Radius = 30.5 cm	Depth = 30.5 CM Radius = 15.2 CM
14	HRSE-1	✓	
	OCBS	✓	
	NCBS	✓	
	AV-W	✓	
	AV-L	✓	
	HRSE-2		✓
	HRSE-3		✓[1]
15	HRSE-1	✓	
	OCBS	✓	
	AV-W	✓	
	AV-L	✓	
	HRSE-2		✓
	HRSE-3		✓[1]
16	HRSE-1	✓	
	AV-W	✓	
	AV-L	✓	
	AV-N1	✓	
	SC-S1	✓	
	SV-S1	✓	
	HRSE-2		✓
	AV-N2[3]		✓
	SC-S2		✓
	SV-L1		✓[1]

(Sheet 3 of 4)

[1] Located in center of testbed (radius = 0 cm)
[2] Oriented horizontally
[3] No data

Table B1 (Concluded)

Test No.	Gage Name	Depth = 15.2 cm Radius = 30.5 cm	Depth = 30.5 CM Radius = 15.2 CM
17	HRSE-1	✓	
	AV-W	✓	
	AV-L	✓	
	AV-N1	✓	
	SC-S1	✓	
	SV-S1	✓	
	HRSE-2		✓
	AV-N2		✓
	SC-S2		✓
	SV-L1		✓[1]
22	HRSE-1	✓	
	NCBS-1	✓	
	CCBS-1[4]	✓	
	CSHMA-1[5]	✓	
	HRSE-2		✓
	NCBS-2		✓
	SHMA-2		✓

(Sheet 4 of 4)

[1] Located in center of testbed (radius = 0 cm)
[2] Oriented horizontally
[3] No data
[4] NCBS in canister with HIFI
[5] HIFI in canister with NCBS

Appendix C
Wet Density and Moisture Content Profiles for Tests in Sand

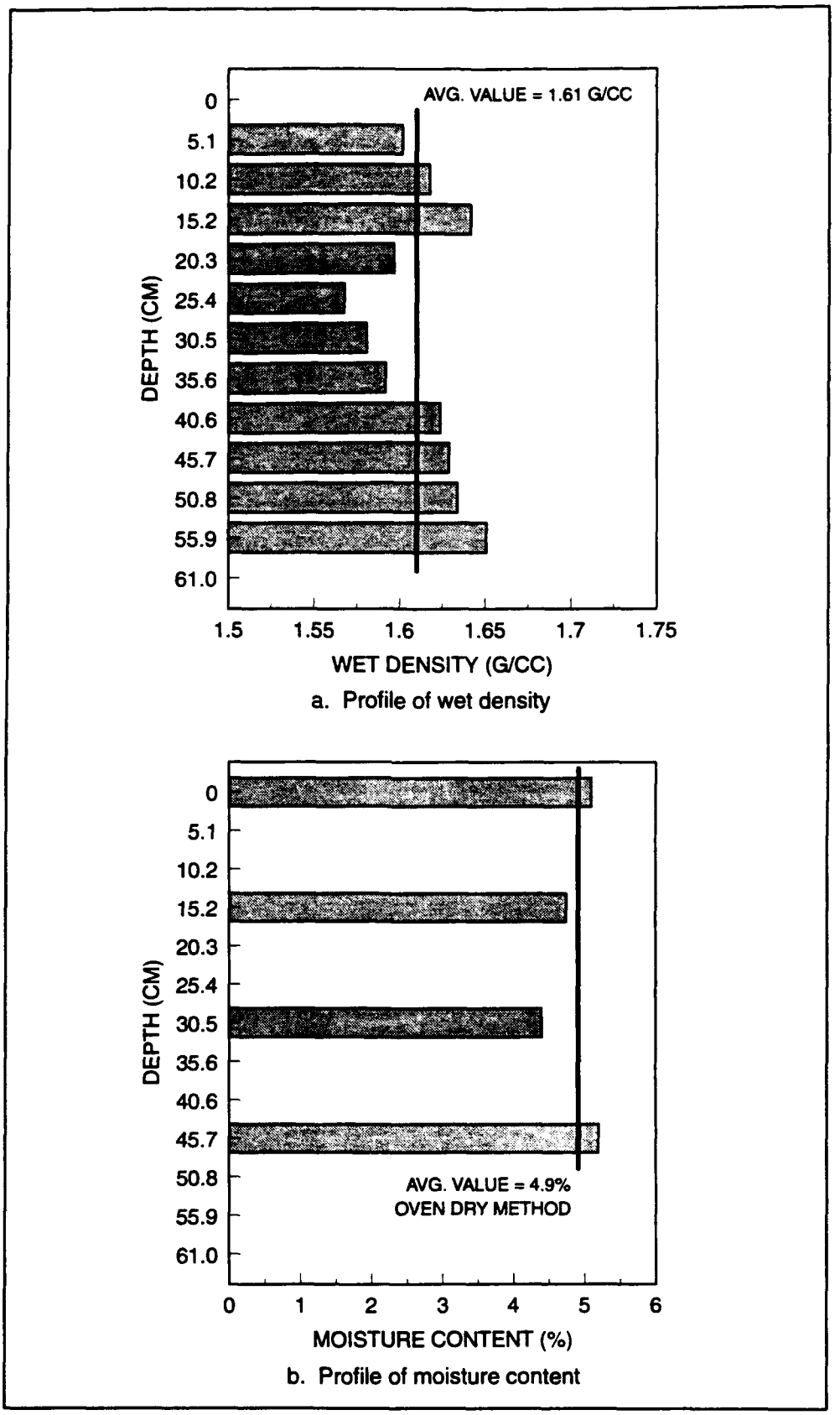

Figure C1. Wet density and moisture content profiles for Test 6

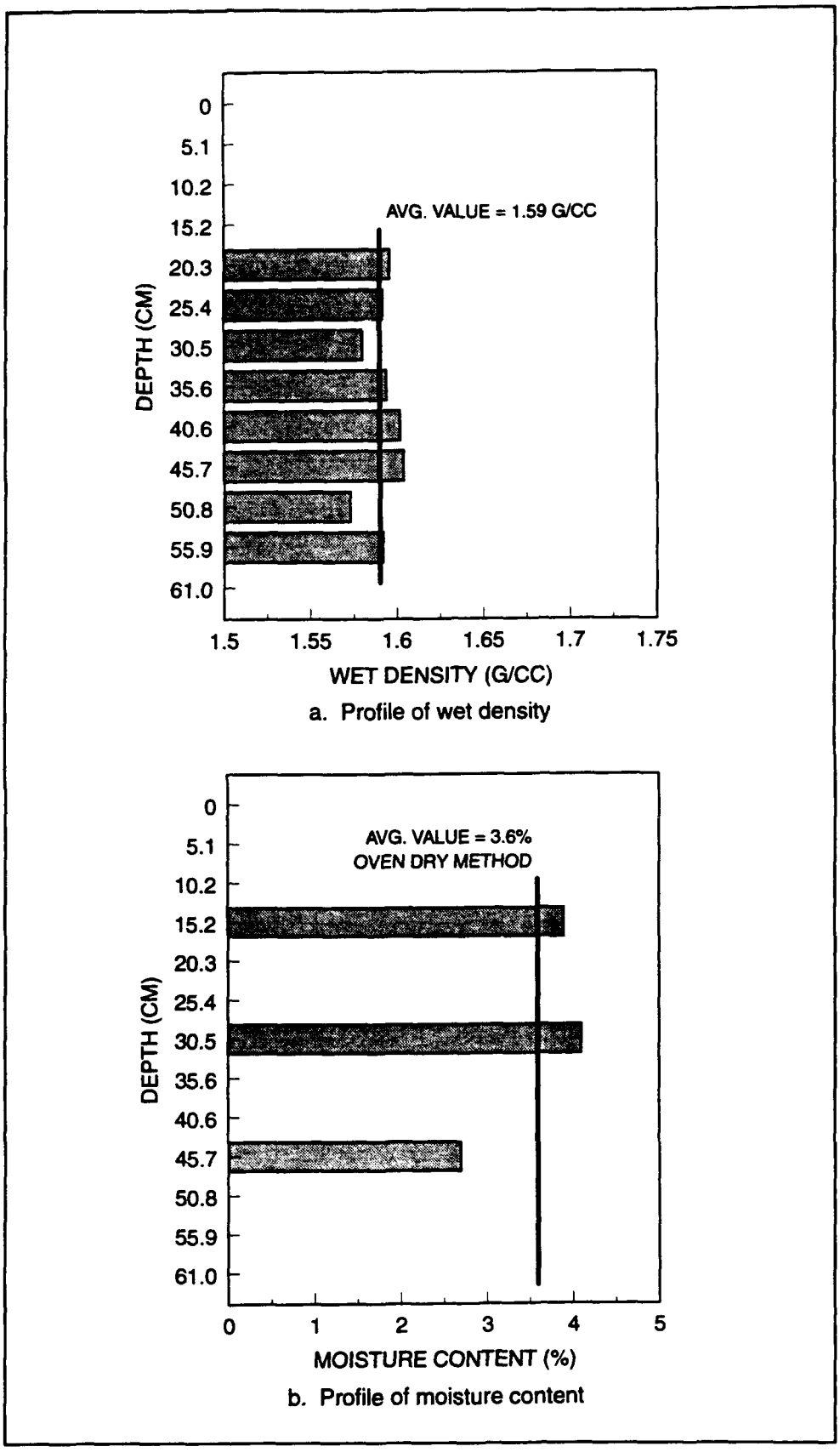

Figure C2. Wet density and moisture content profiles for Test 7

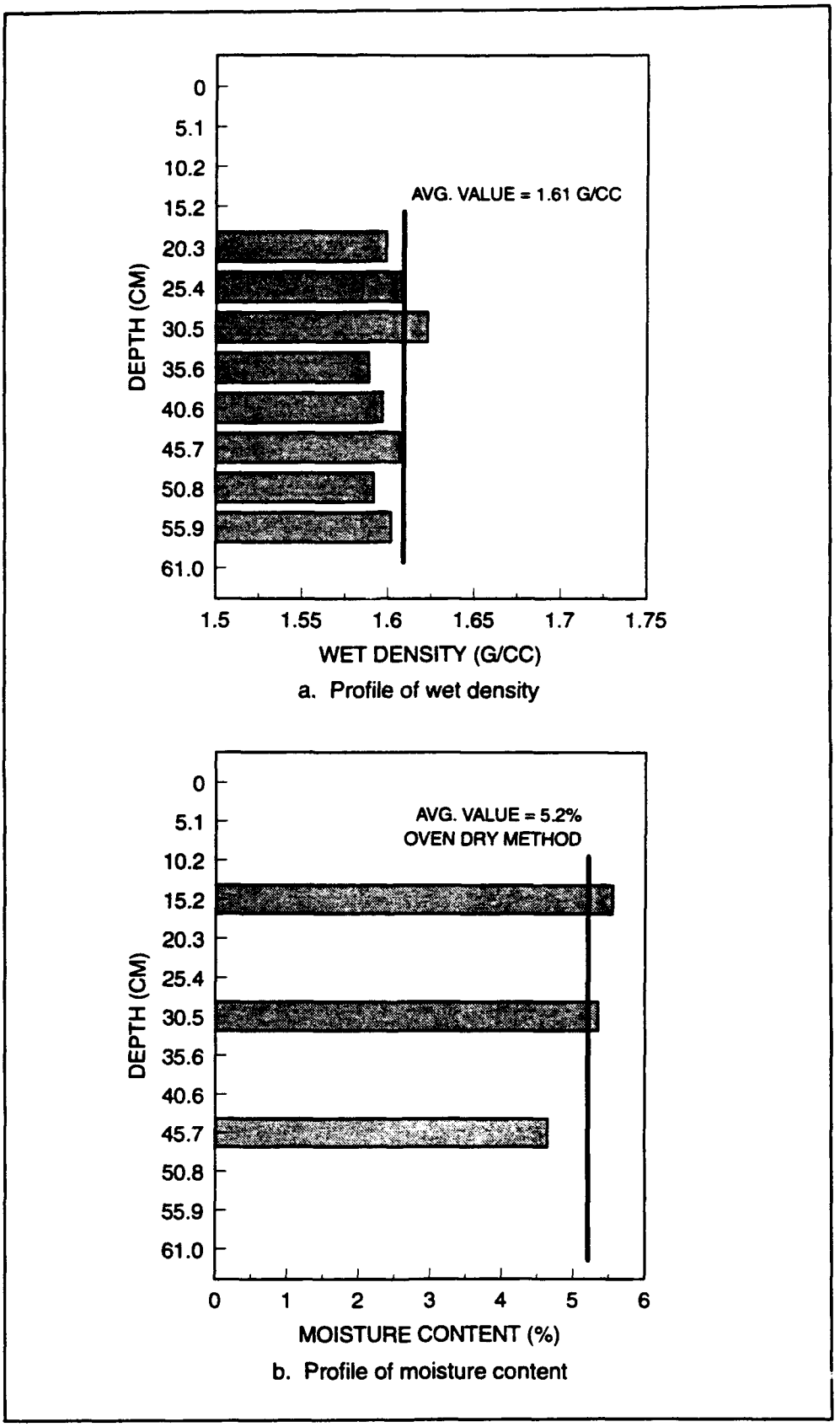

Figure C3. Wet density and moisture content profiles for Test 8

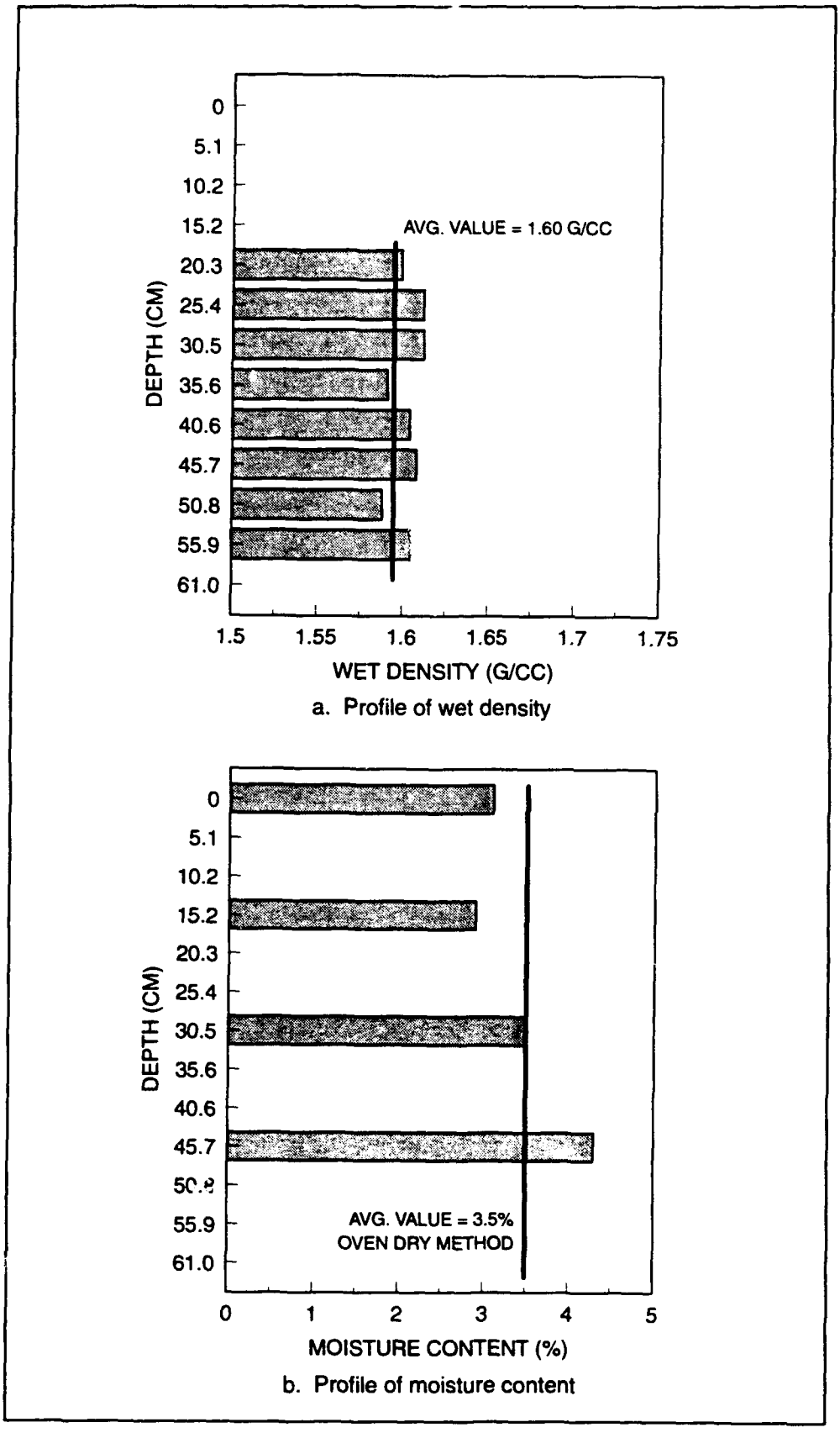

Figure C4. Wet density and moisture content profiles for Test 10

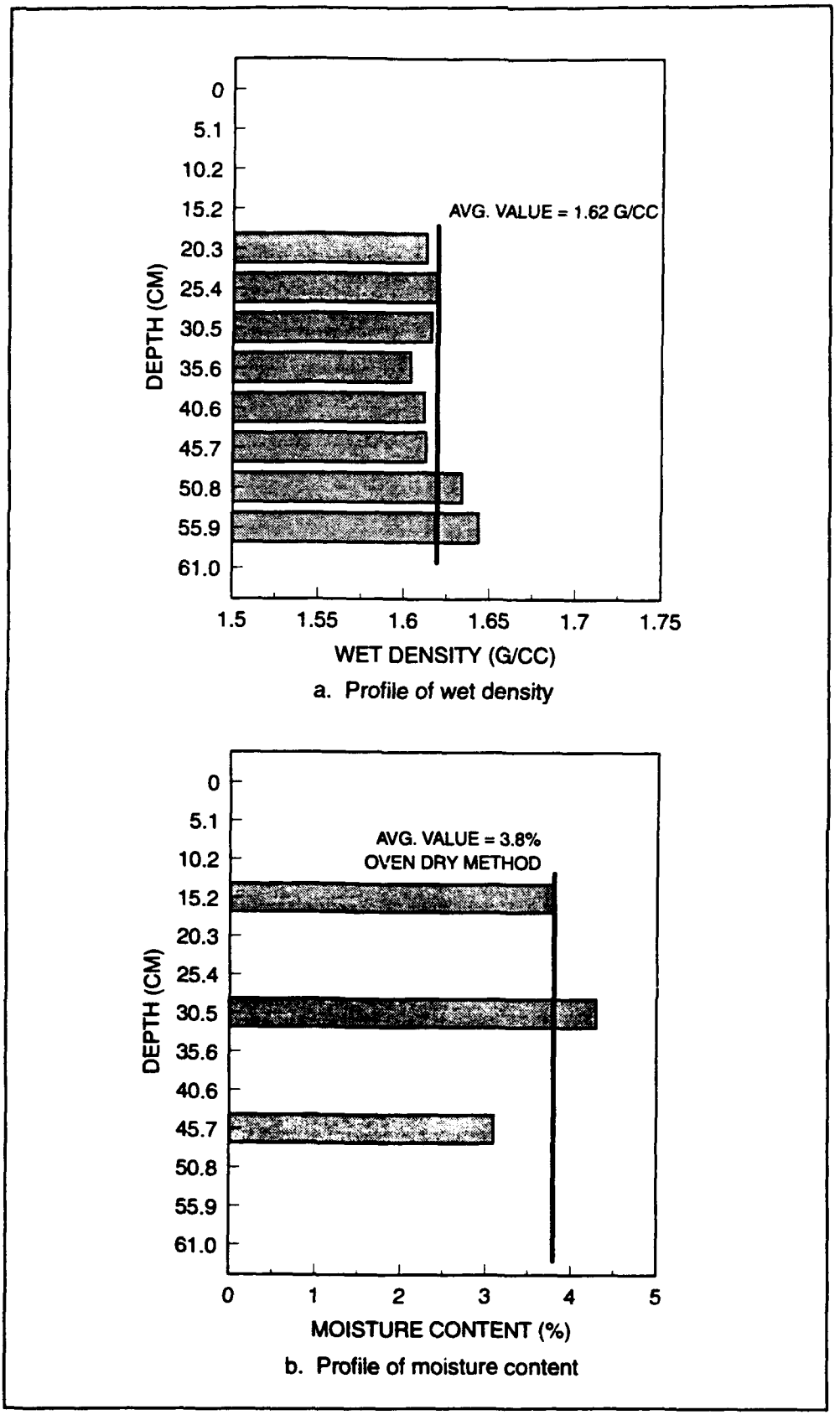

Figure C5. Wet density and moisture content profiles for Test 11

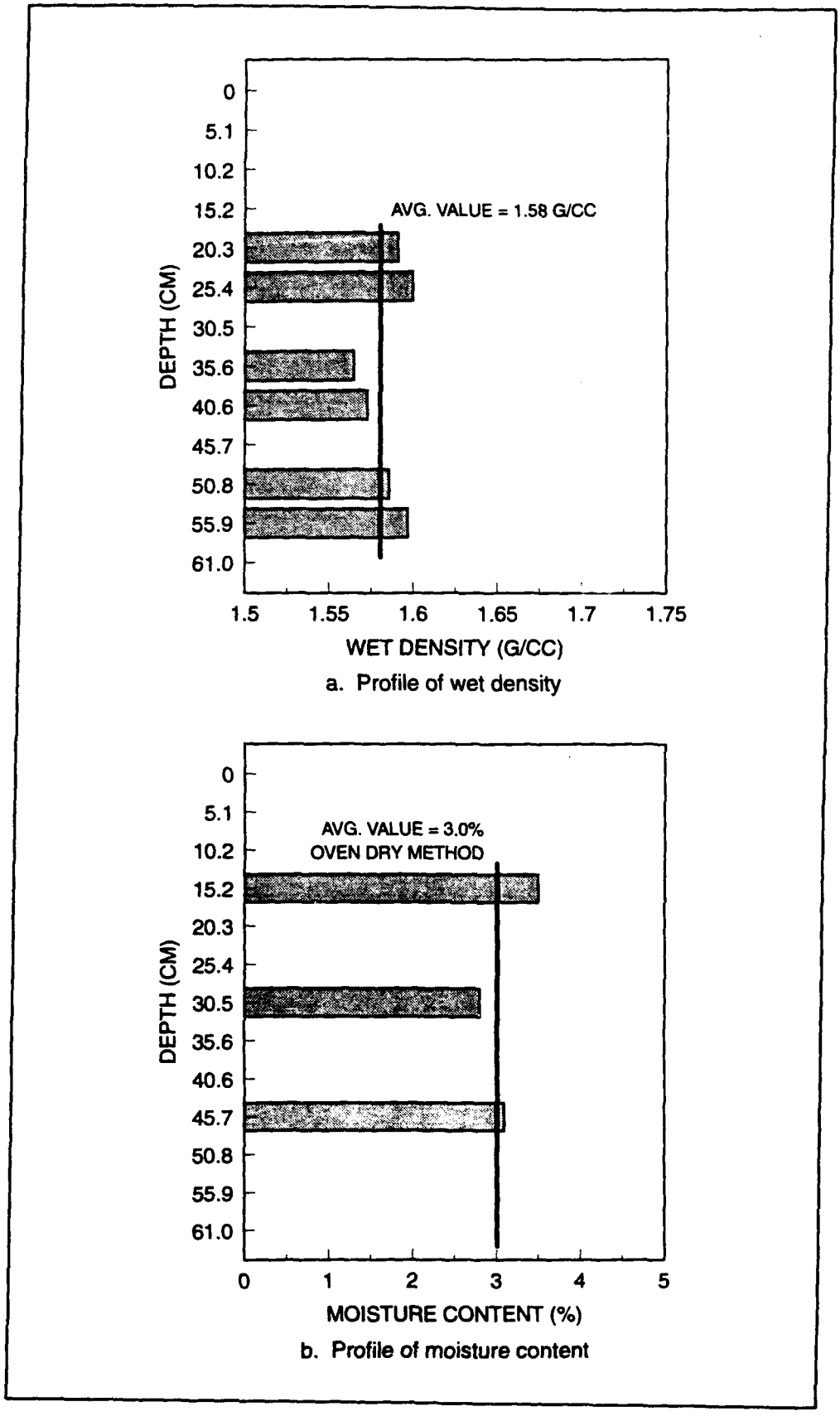

Figure C6. Wet density and moisture content profiles for Test 12

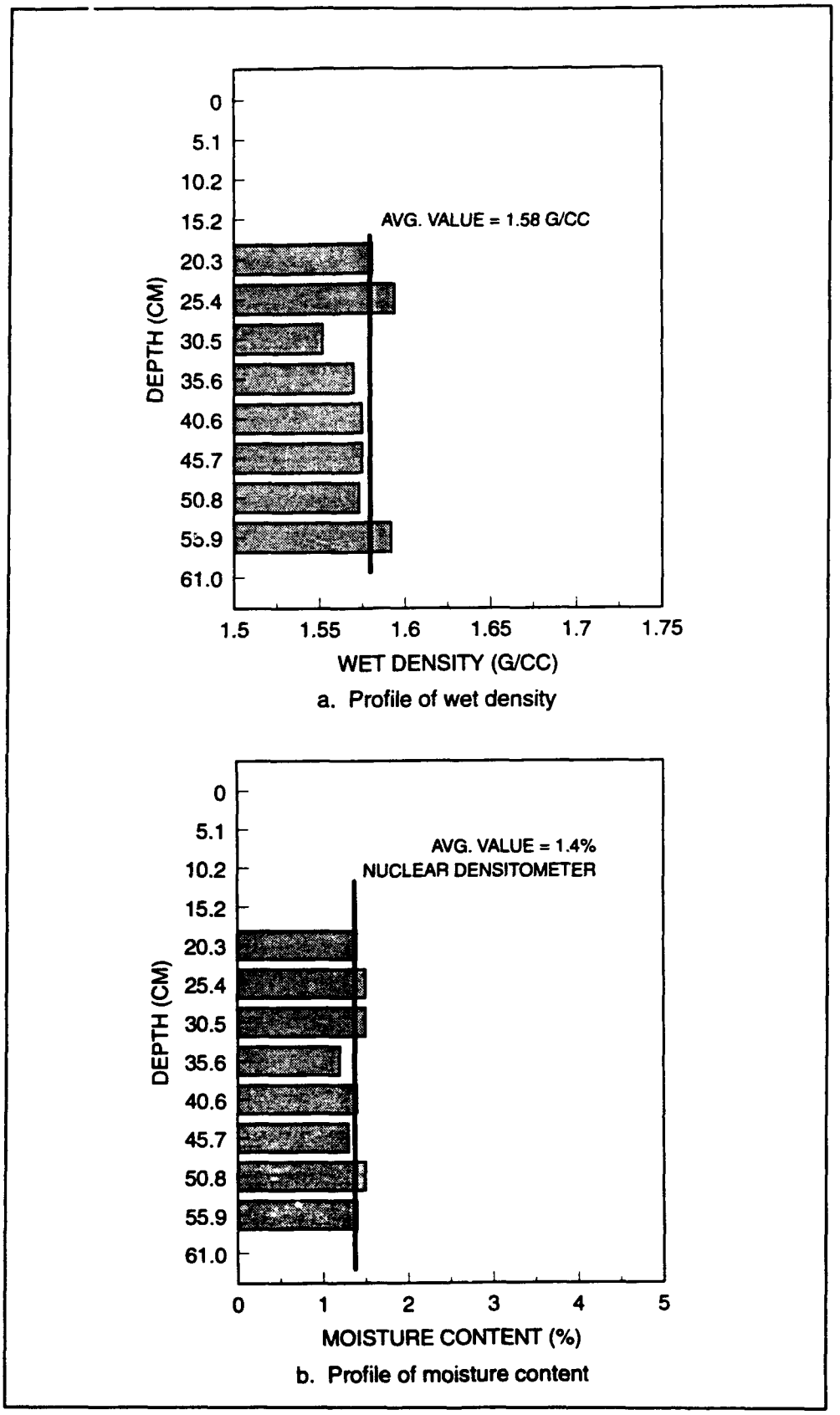

Figure C7. Wet density and moisture content profiles for Test 13

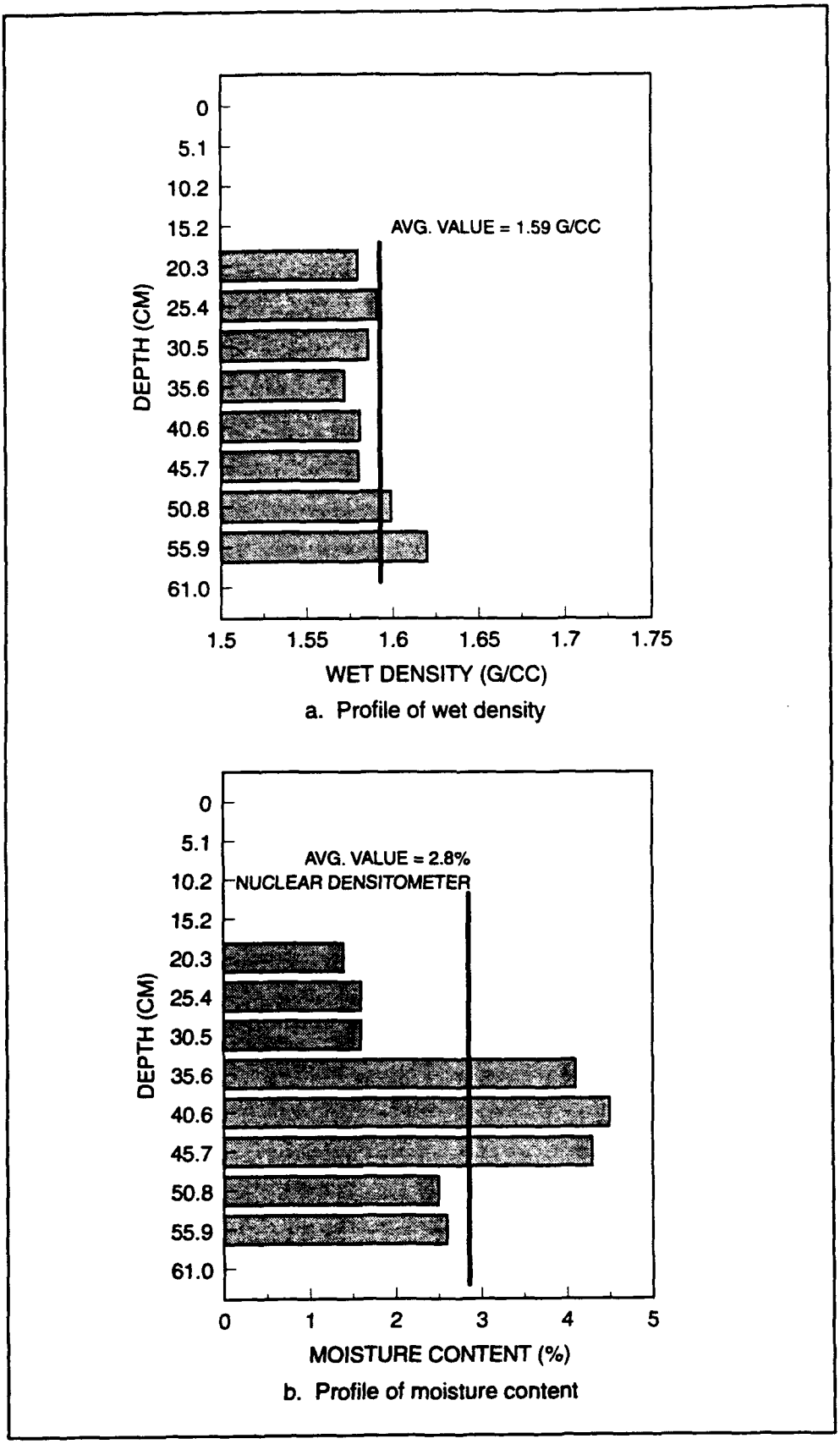

Figure C8. Wet density and moisture content profiles for Test 14

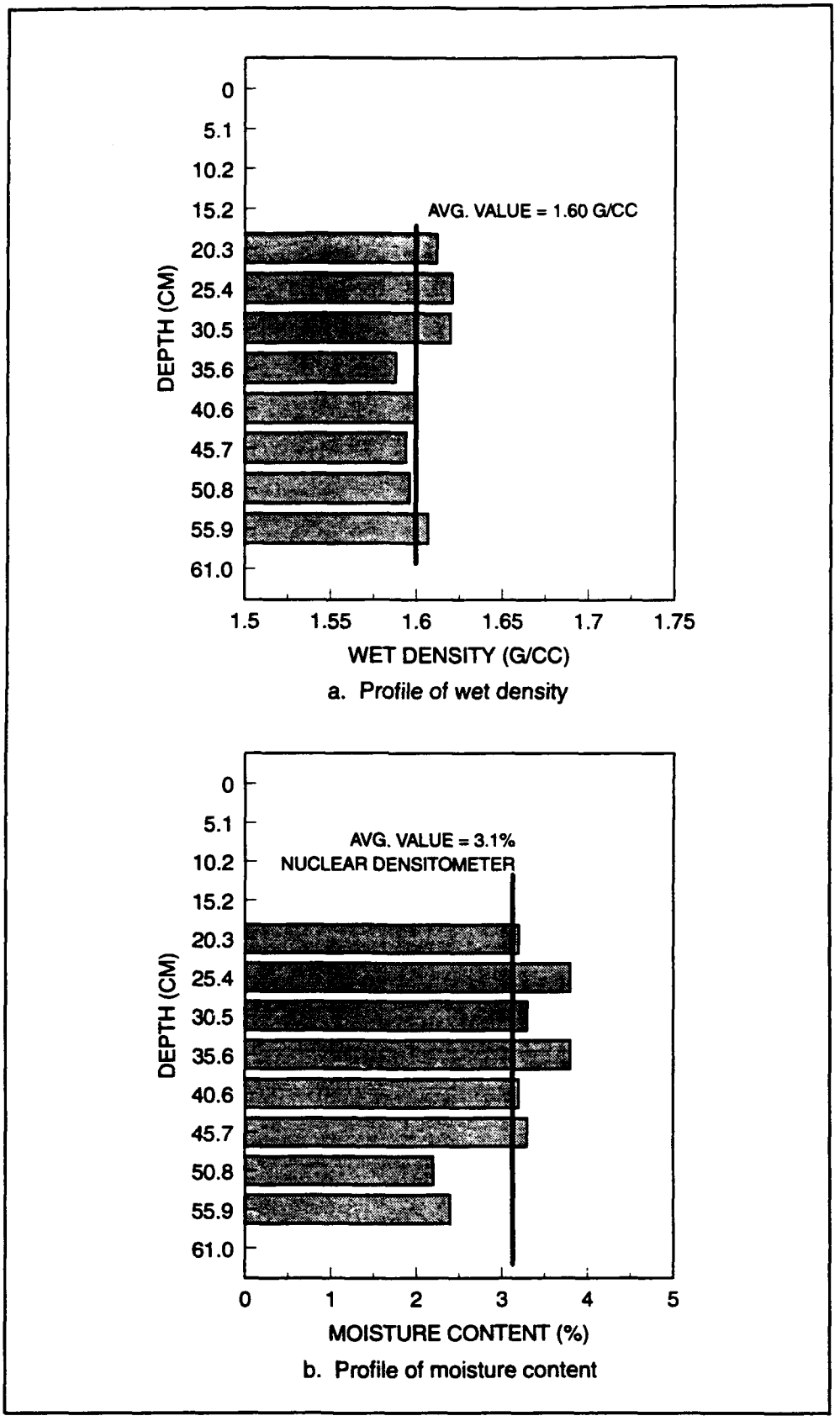

Figure C9. Wet density and moisture content profiles for Test 15

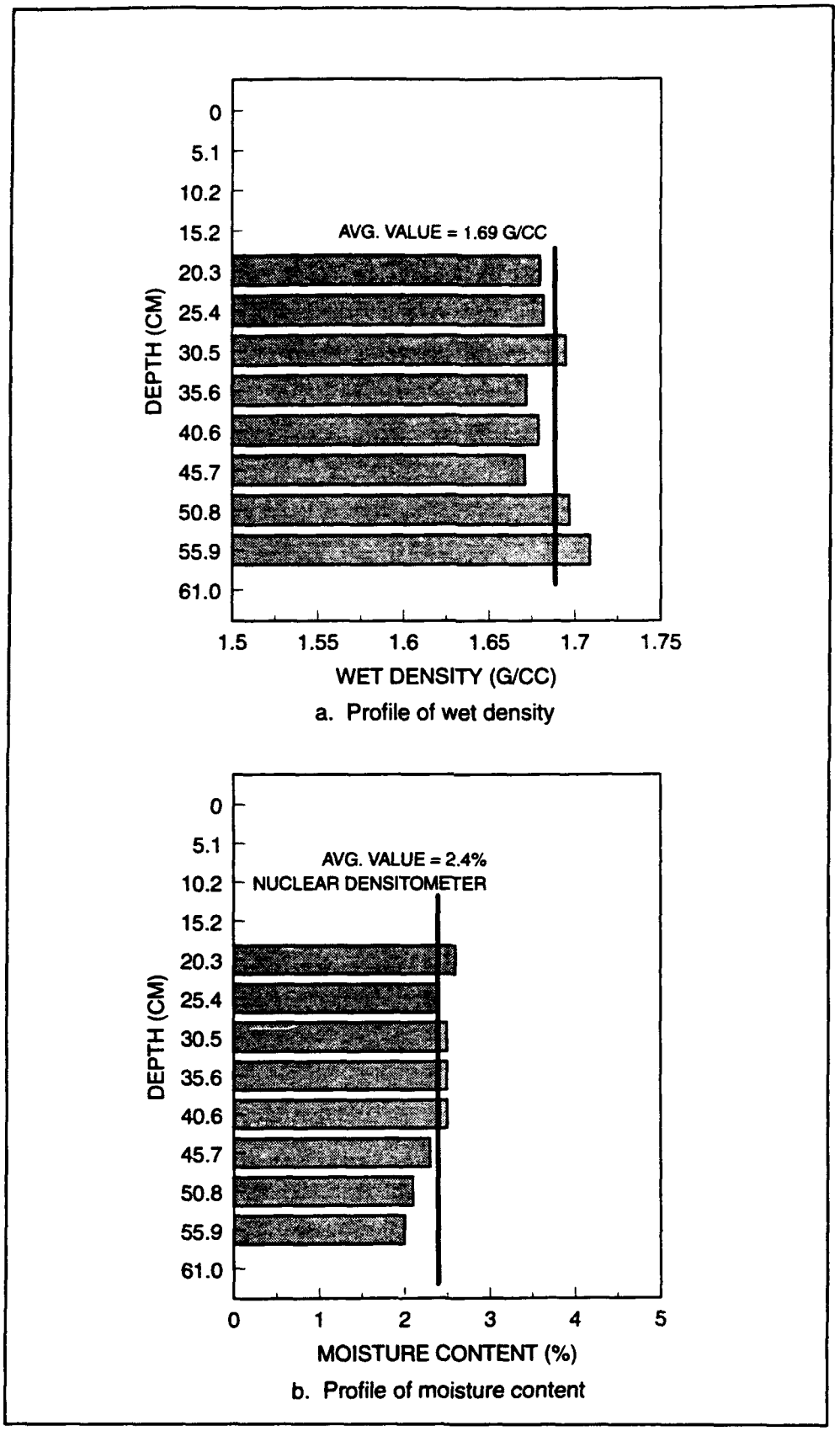

Figure C10. Wet density and moisture content profiles for Test 16

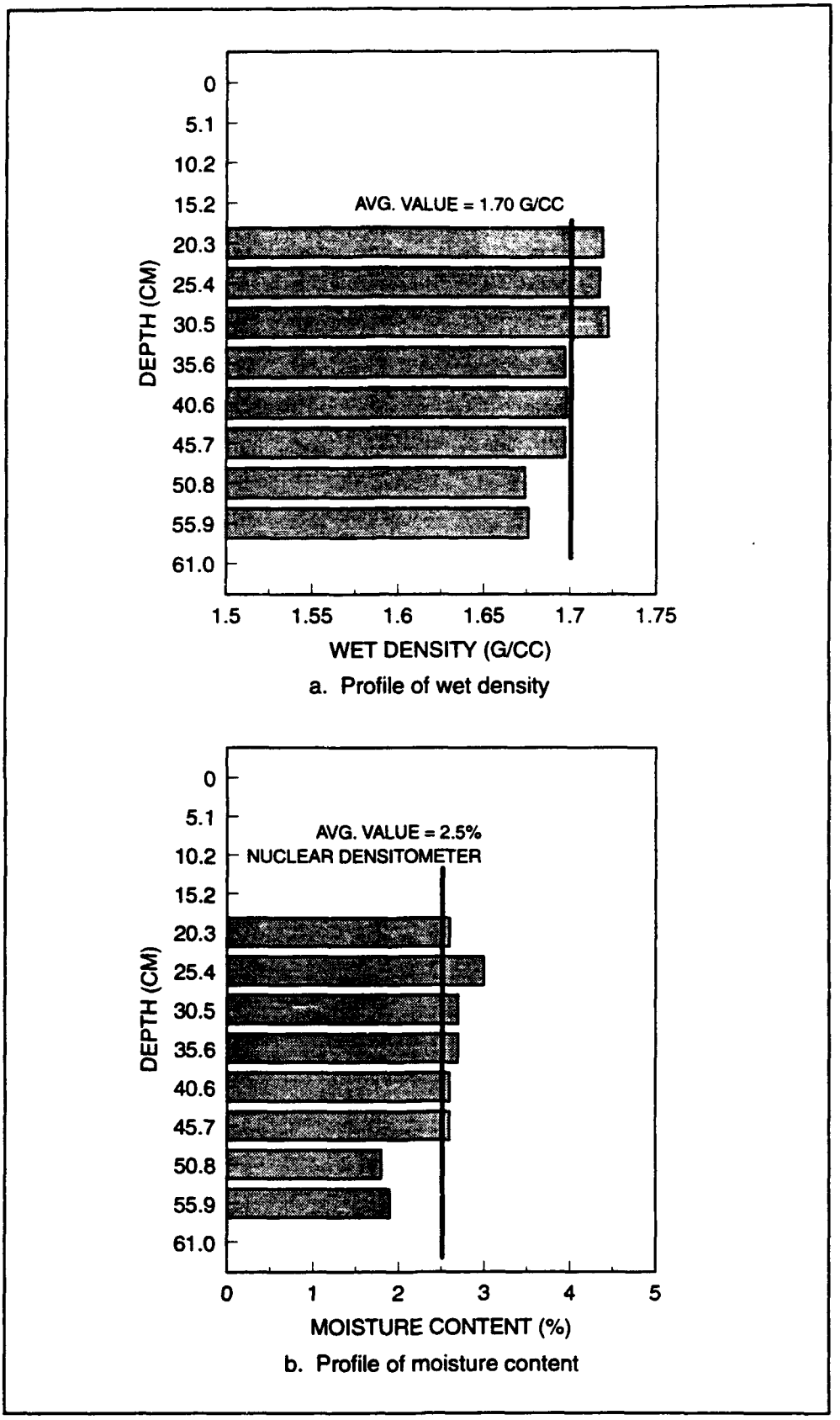

Figure C11. Wet density and moisture content profiles for Test 17

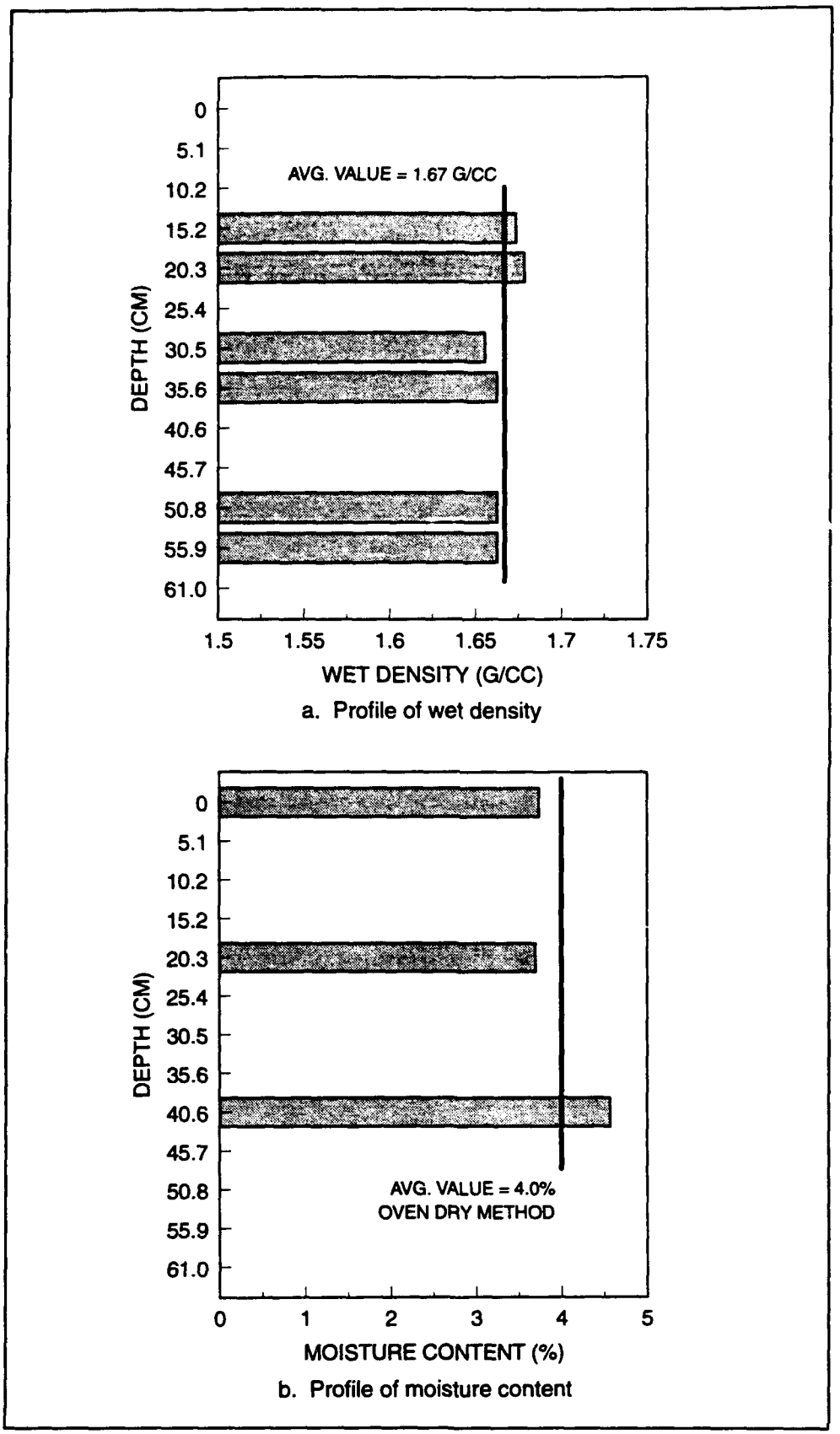

Figure C12. Wet density and moisture content profiles for Test 22

Appendix D
Active Measurement Data for Tests in Sand

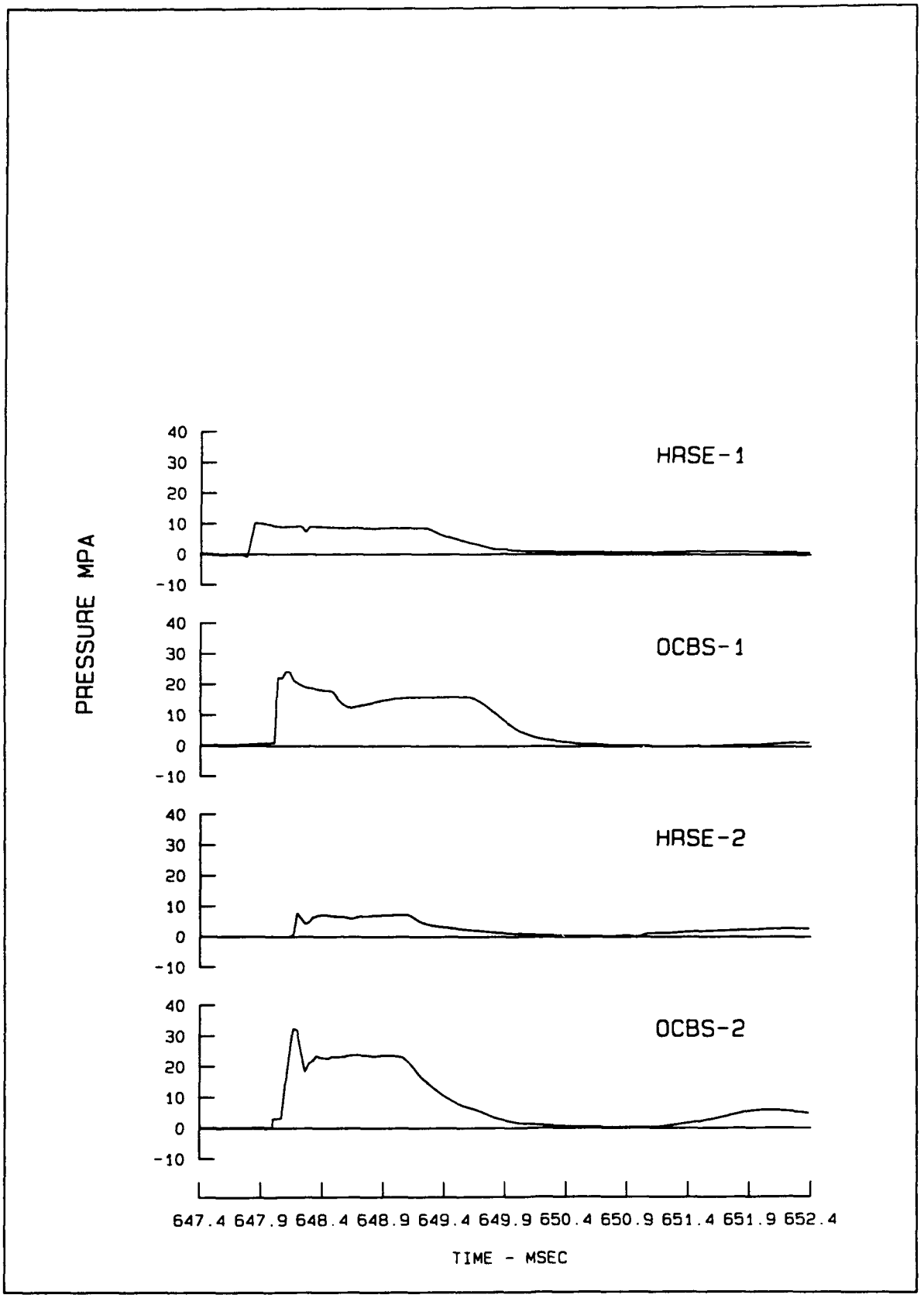

Figure D1. Stress and impulse wave forms from Test 6 (Continued)

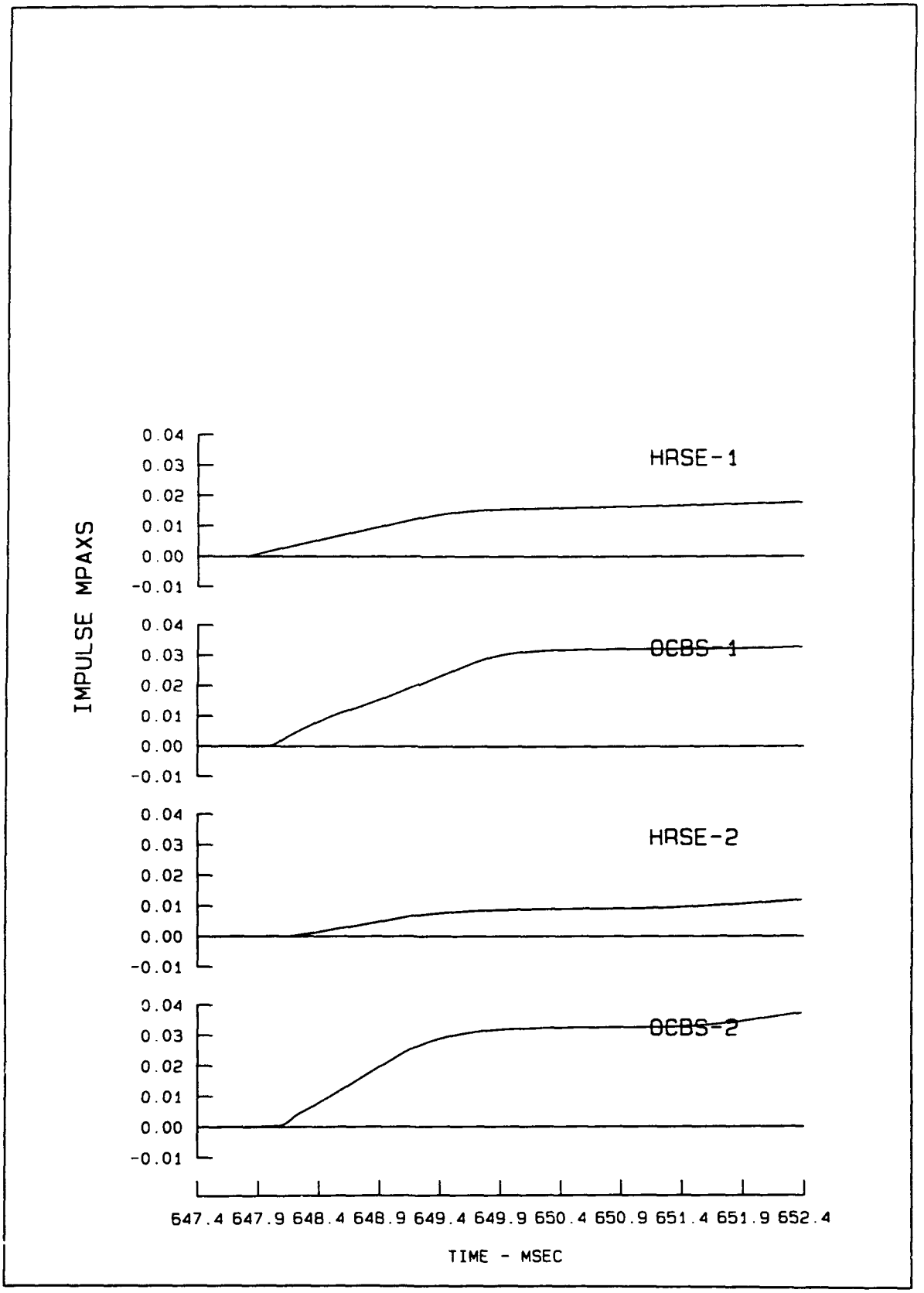

Figure D1. (Concluded)

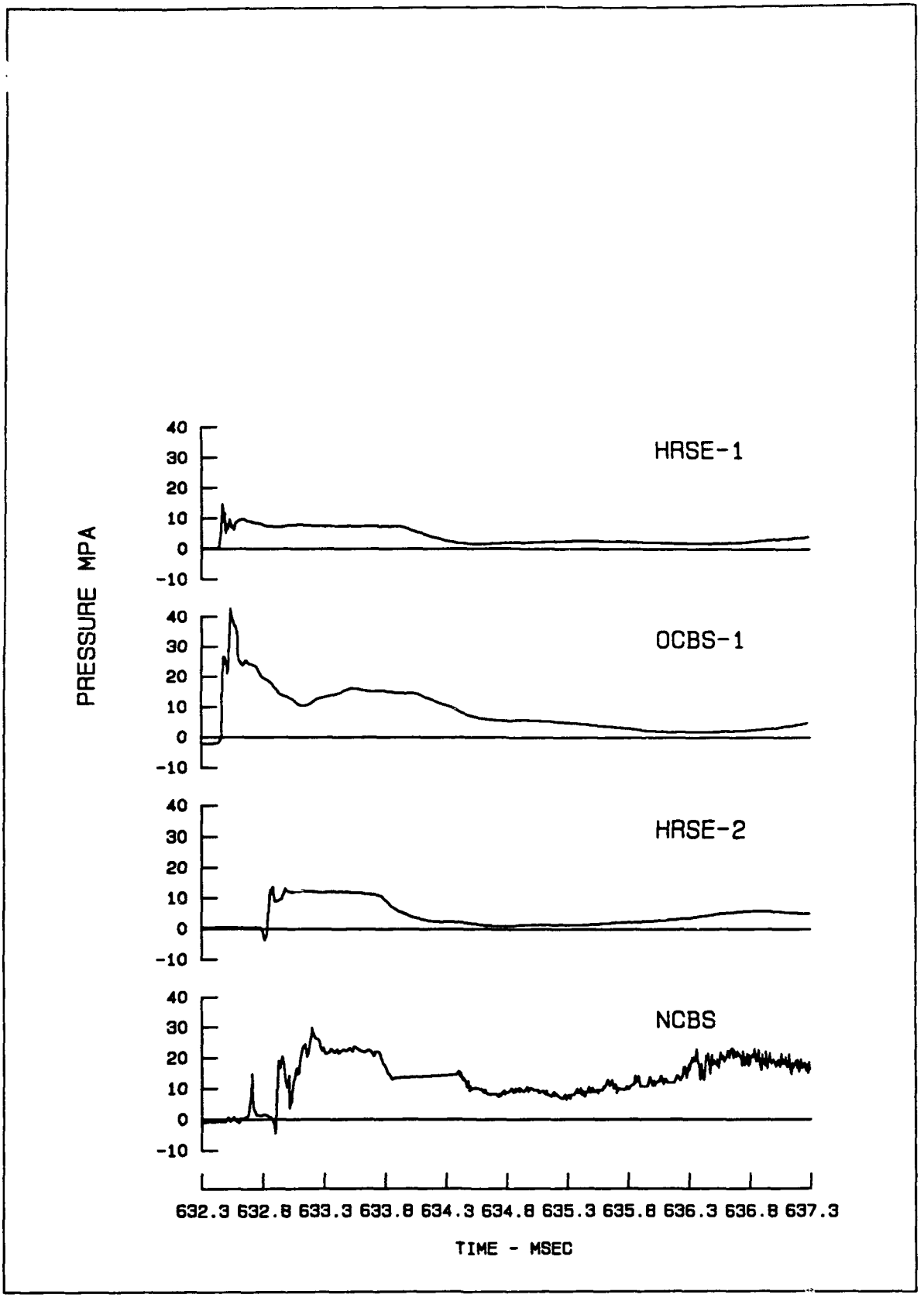

Figure D2. Stress and impulse wave forms from Test 7 (Continued)

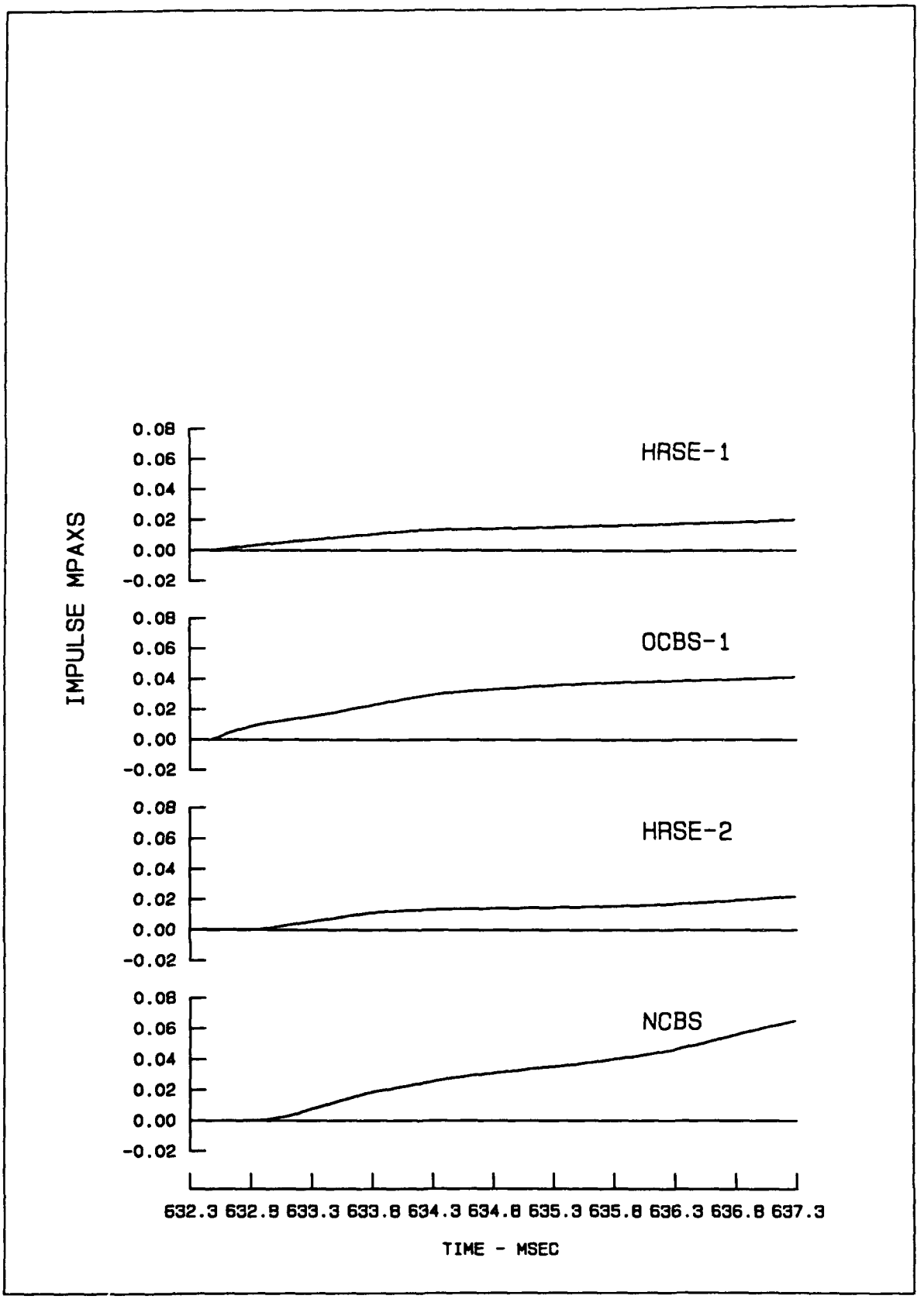

Figure D2. (Concluded)

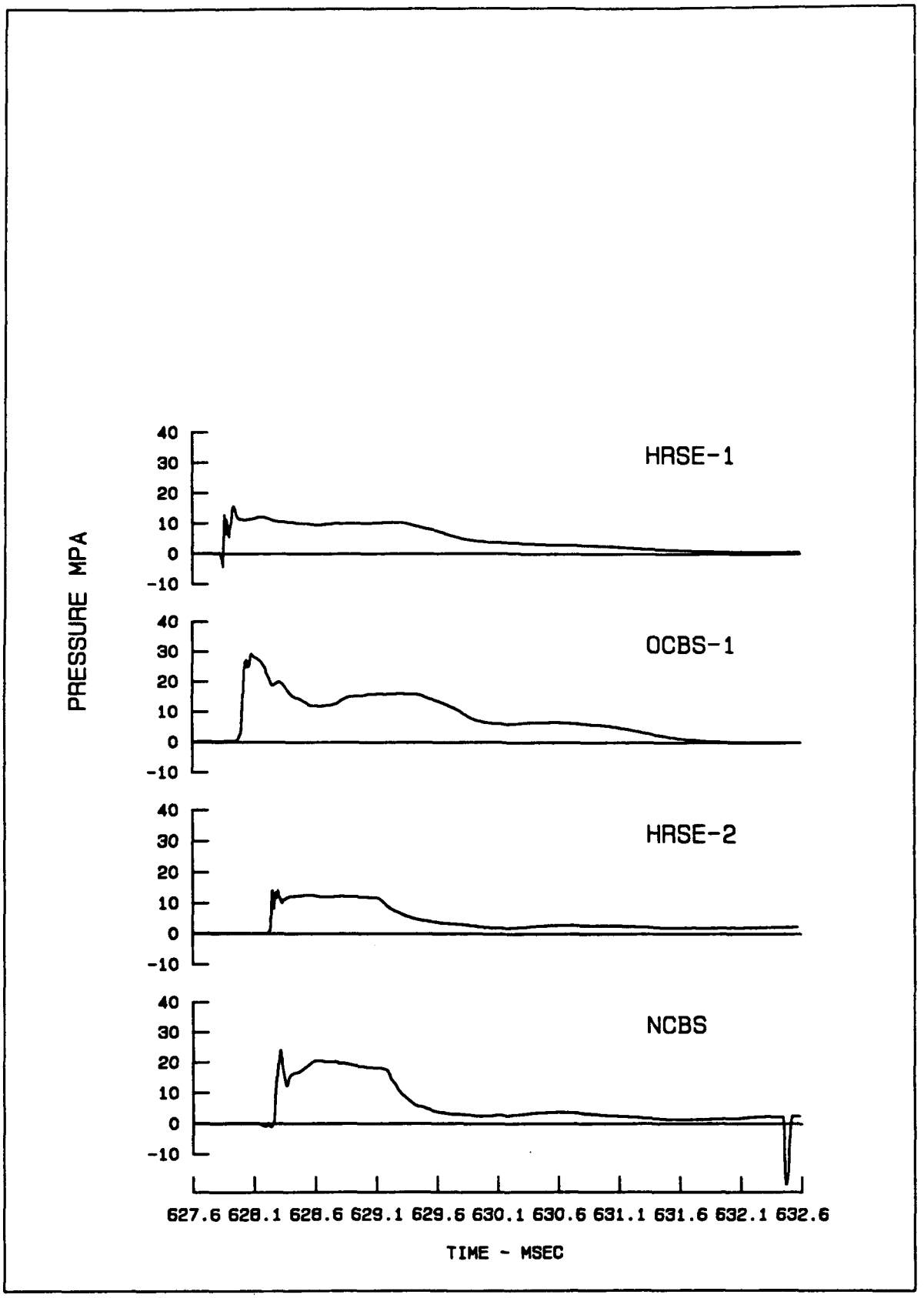

Figure D3. Stress and impulse wave forms from Test 8 (Continued)

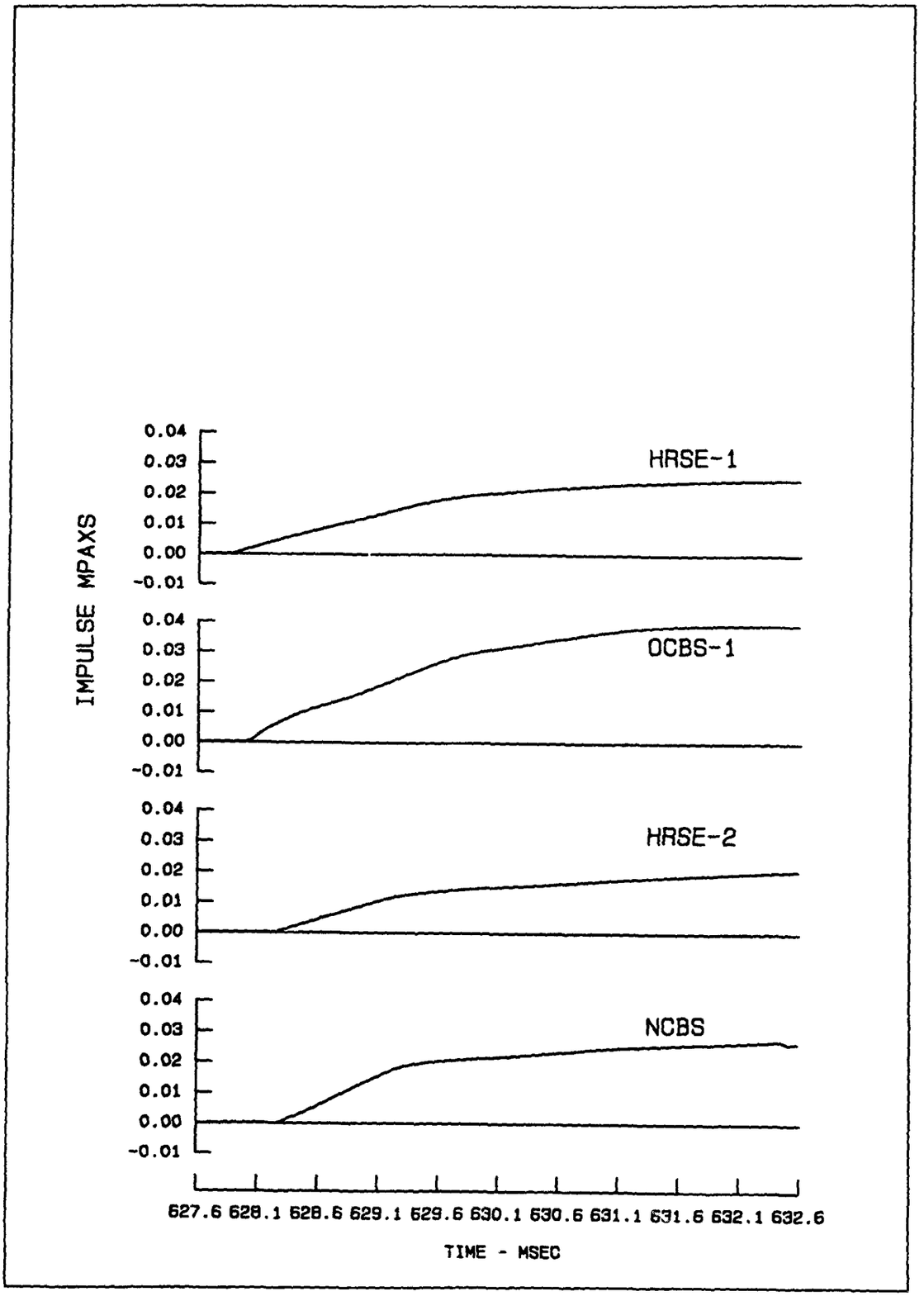

Figure D3. (Concluded)

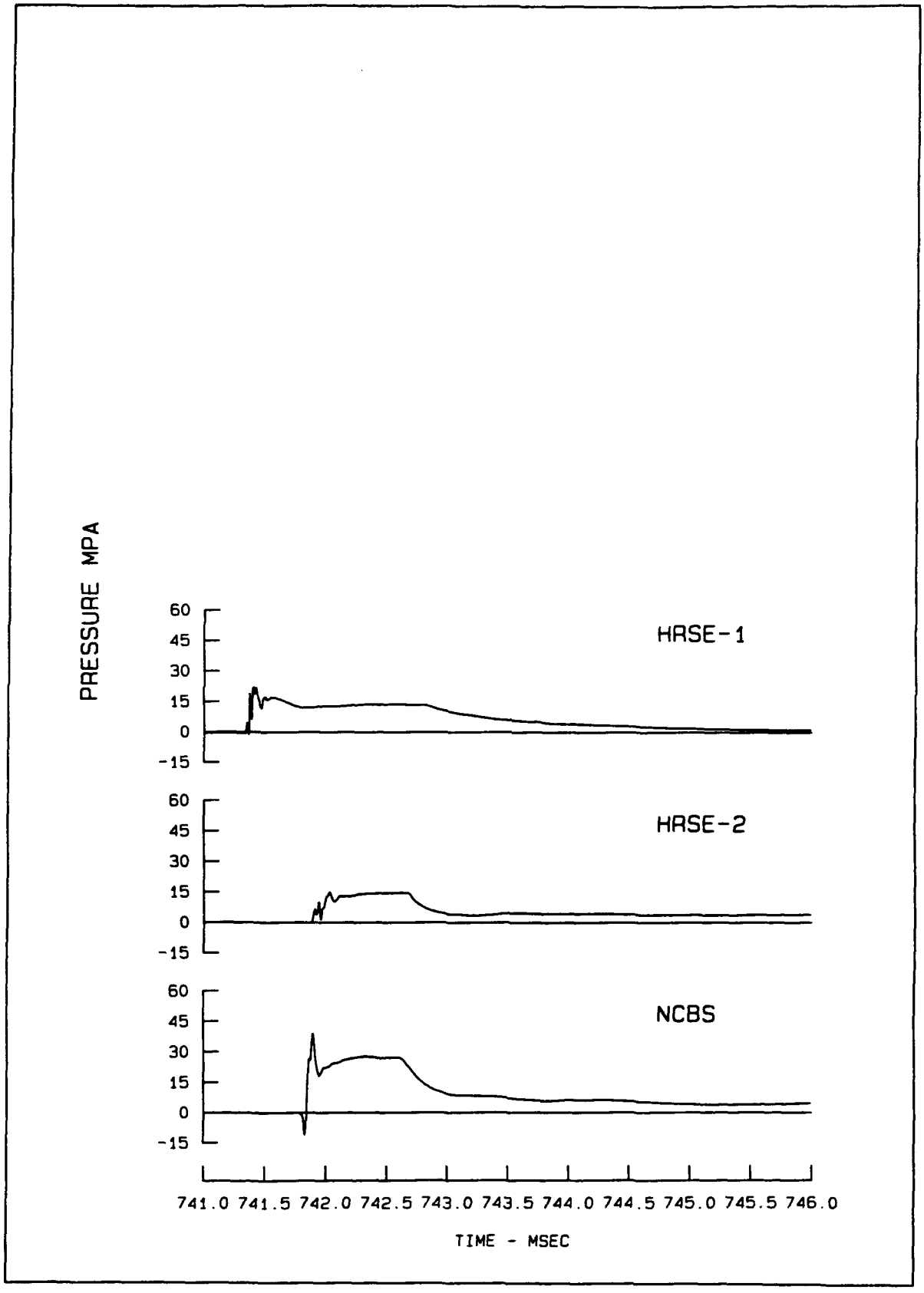

Figure D4. Stress and impulse wave forms from Test 10 (Continued)

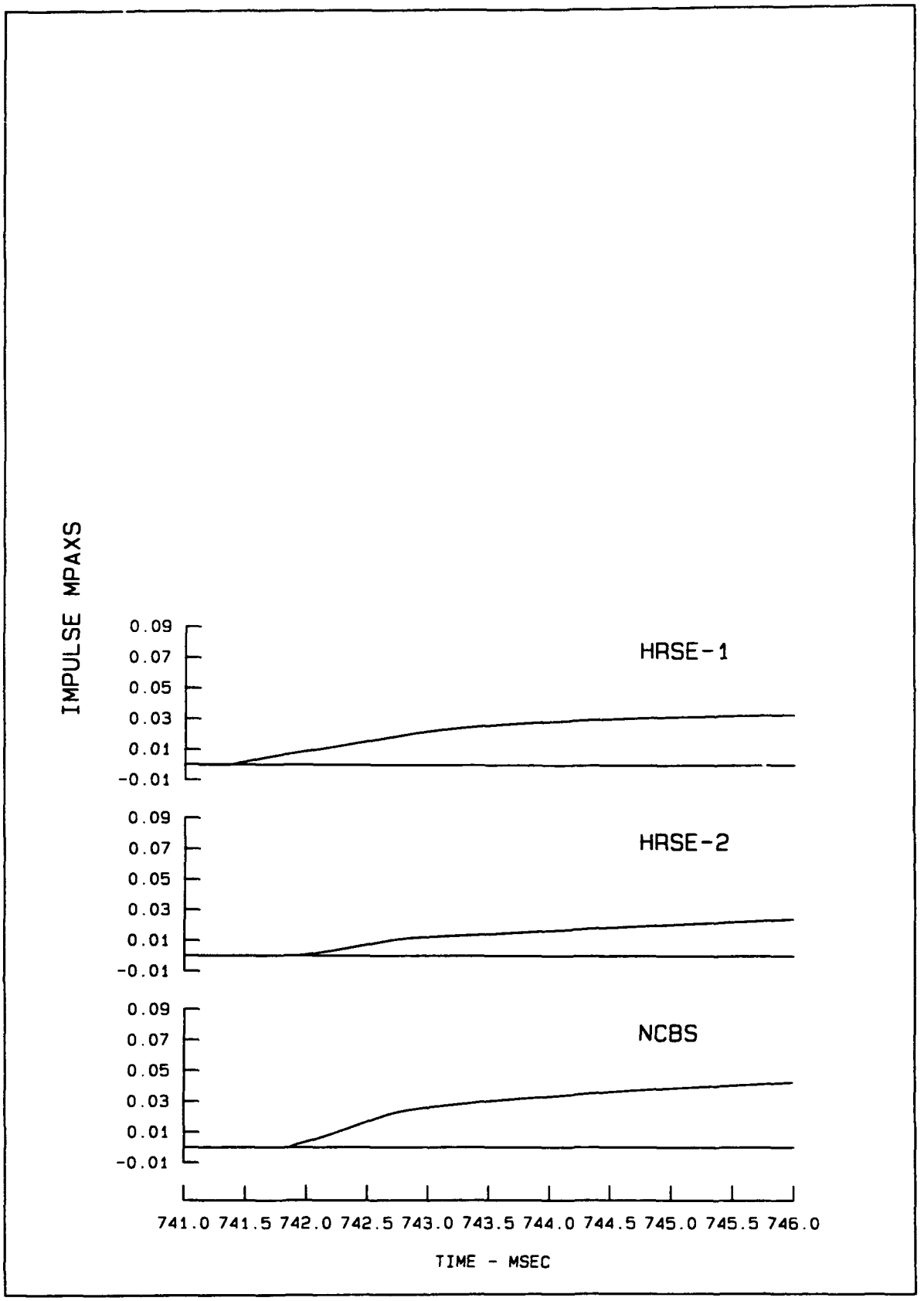

Figure D4. (Concluded)

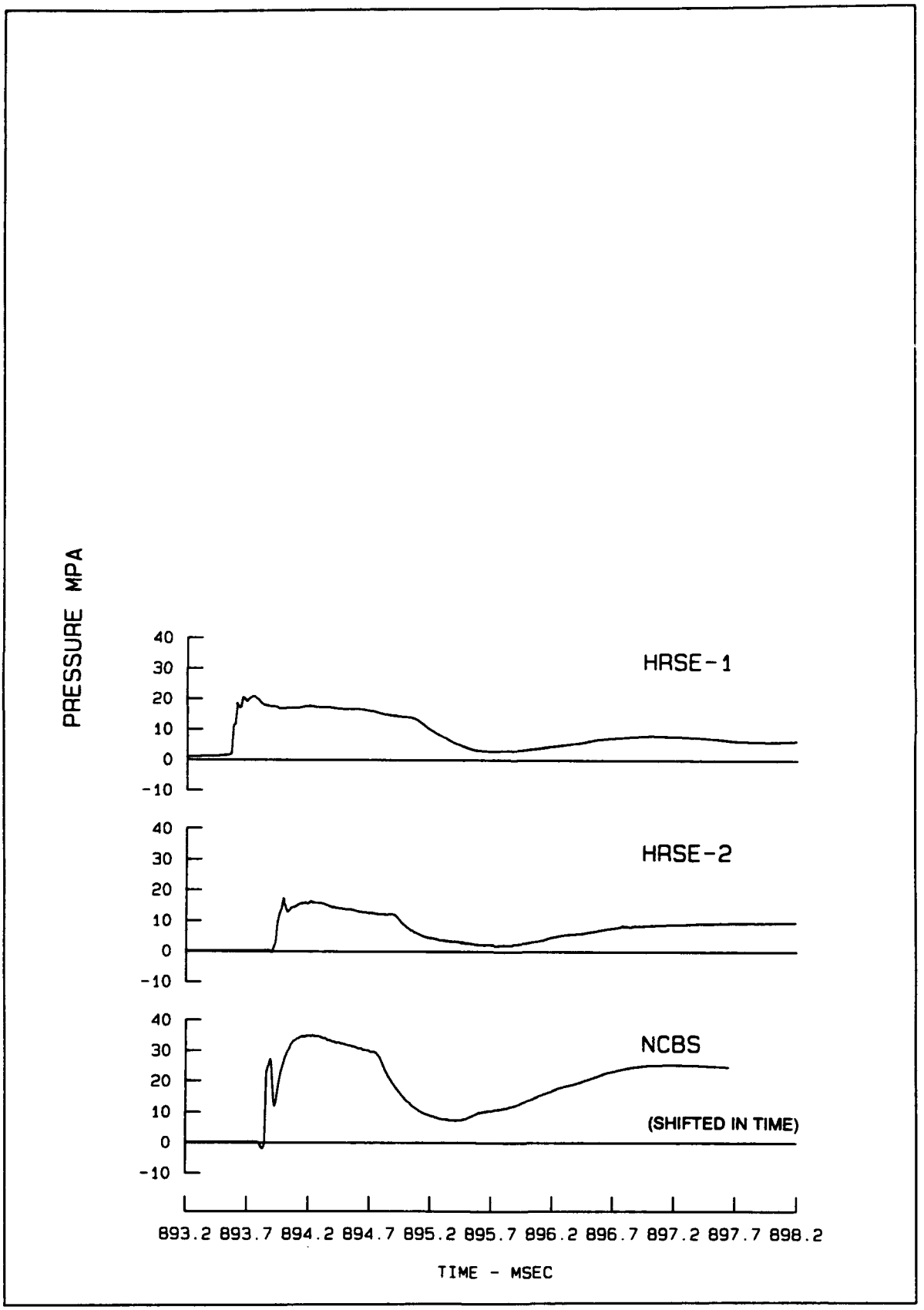

Figure D5. Stress and impulse wave forms from Test 11 (Continued)

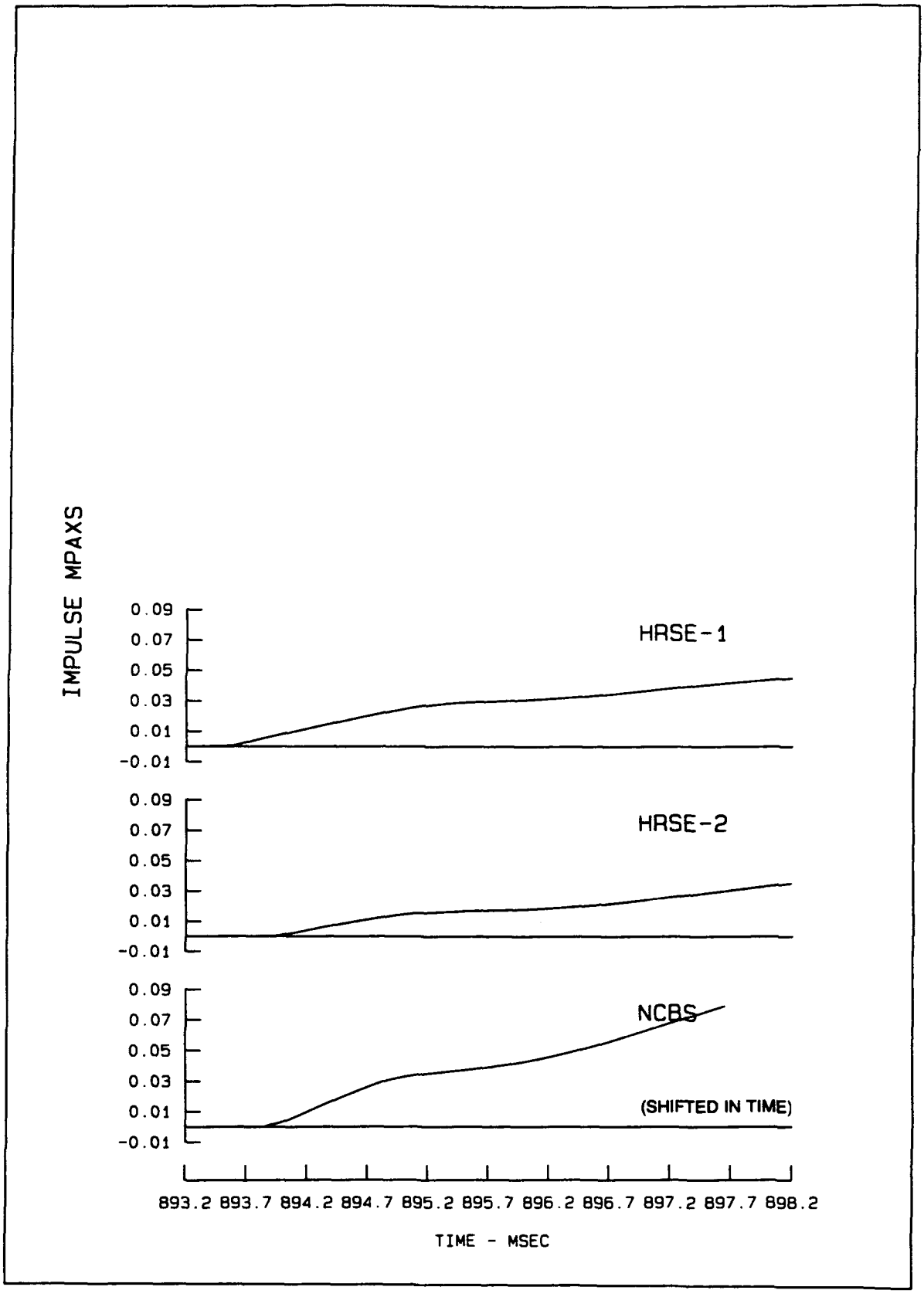

Figure D5. (Concluded)

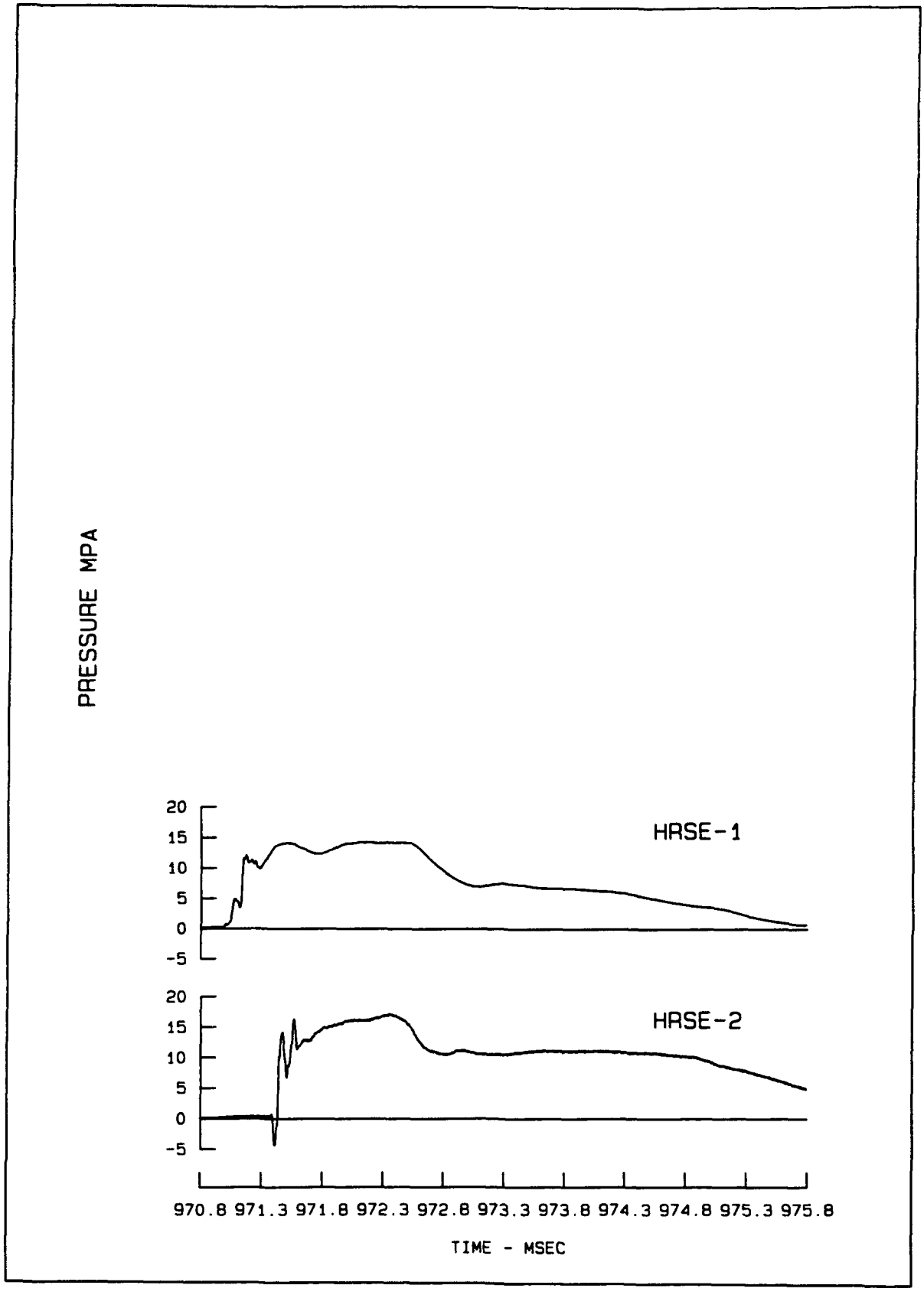

Figure D6. Stress and impulse wave forms from Test 12 (Continued)

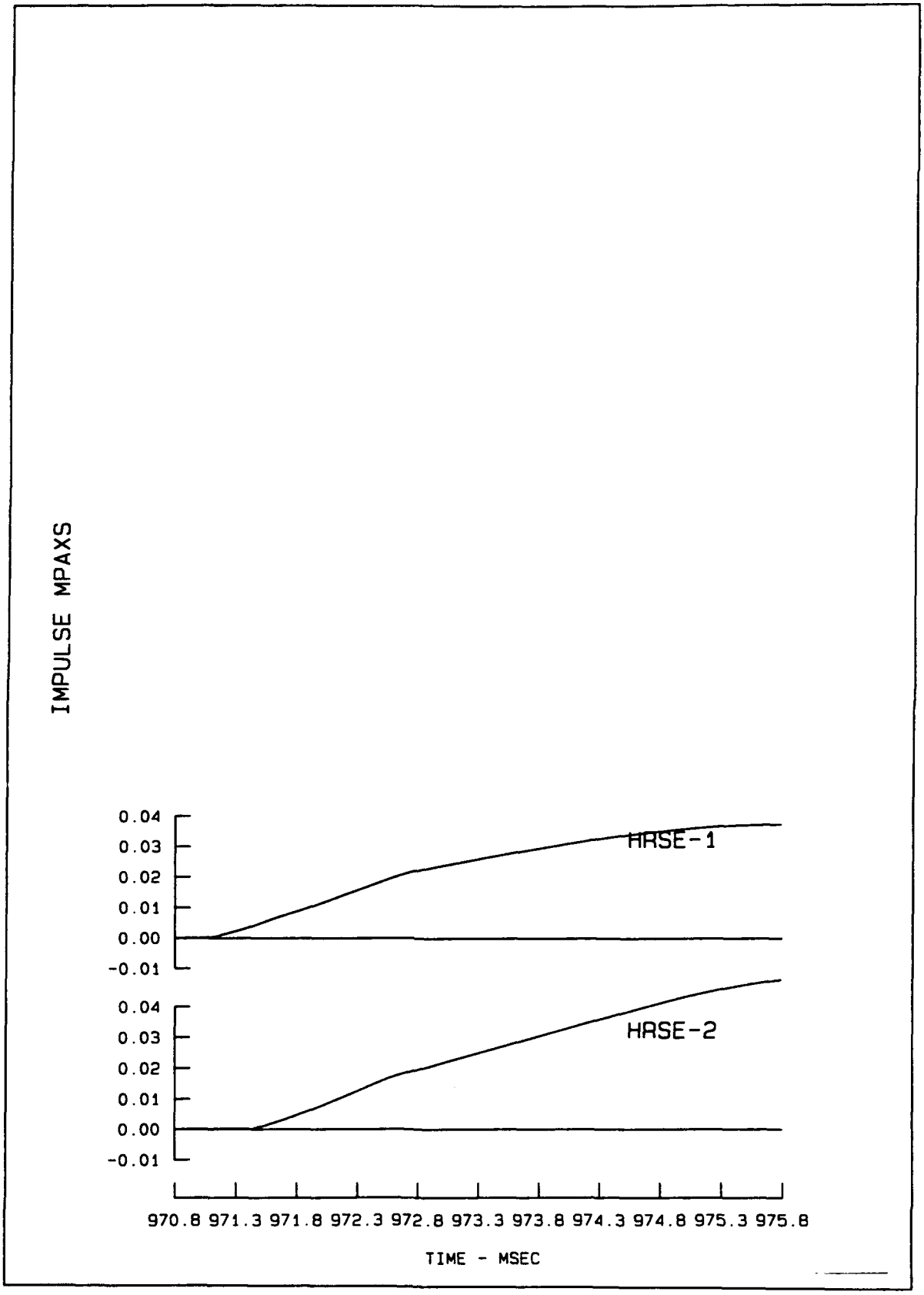

Figure D6. (Concluded)

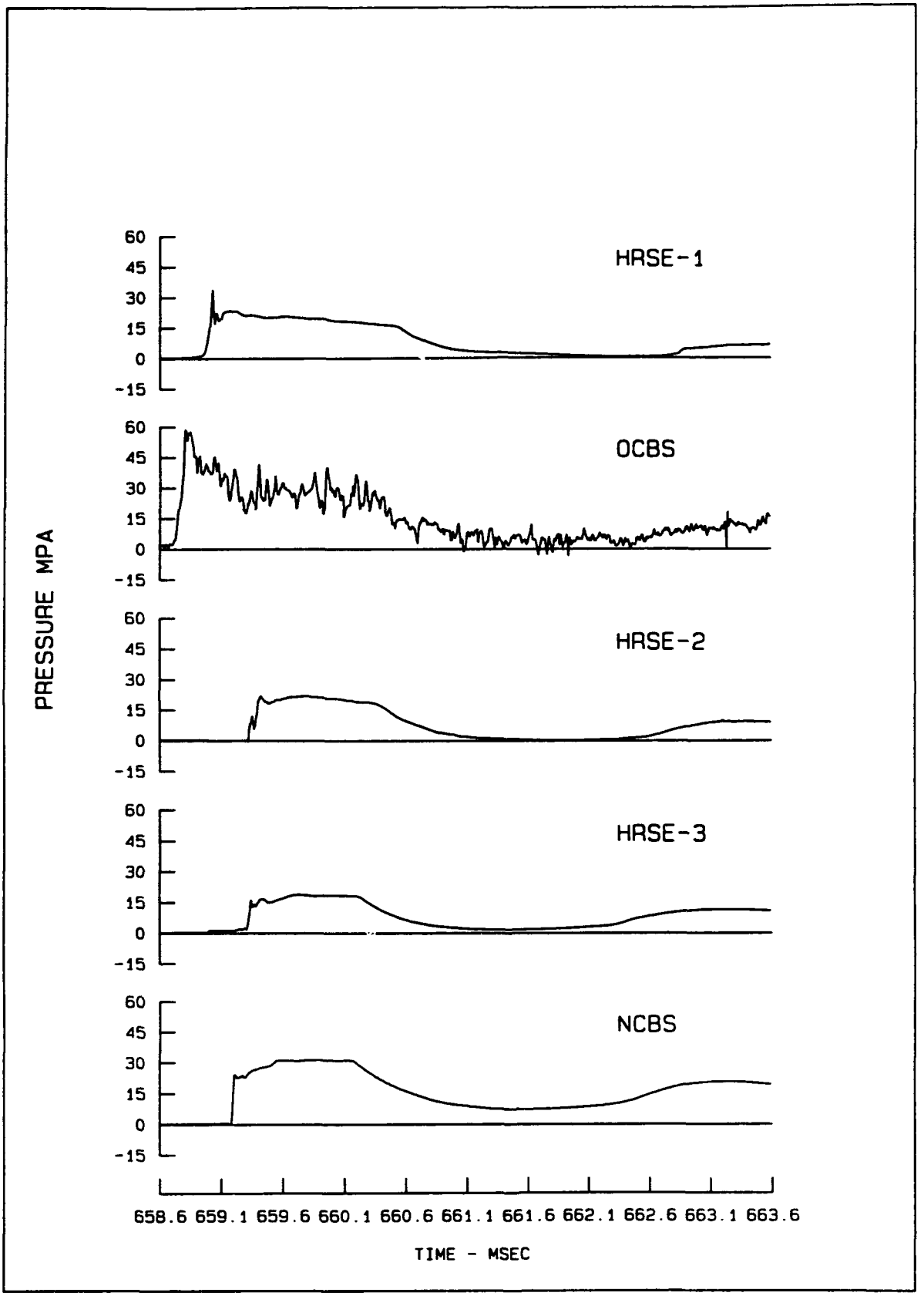

Figure D7. Stress and impulse wave forms from Test 13 (Continued)

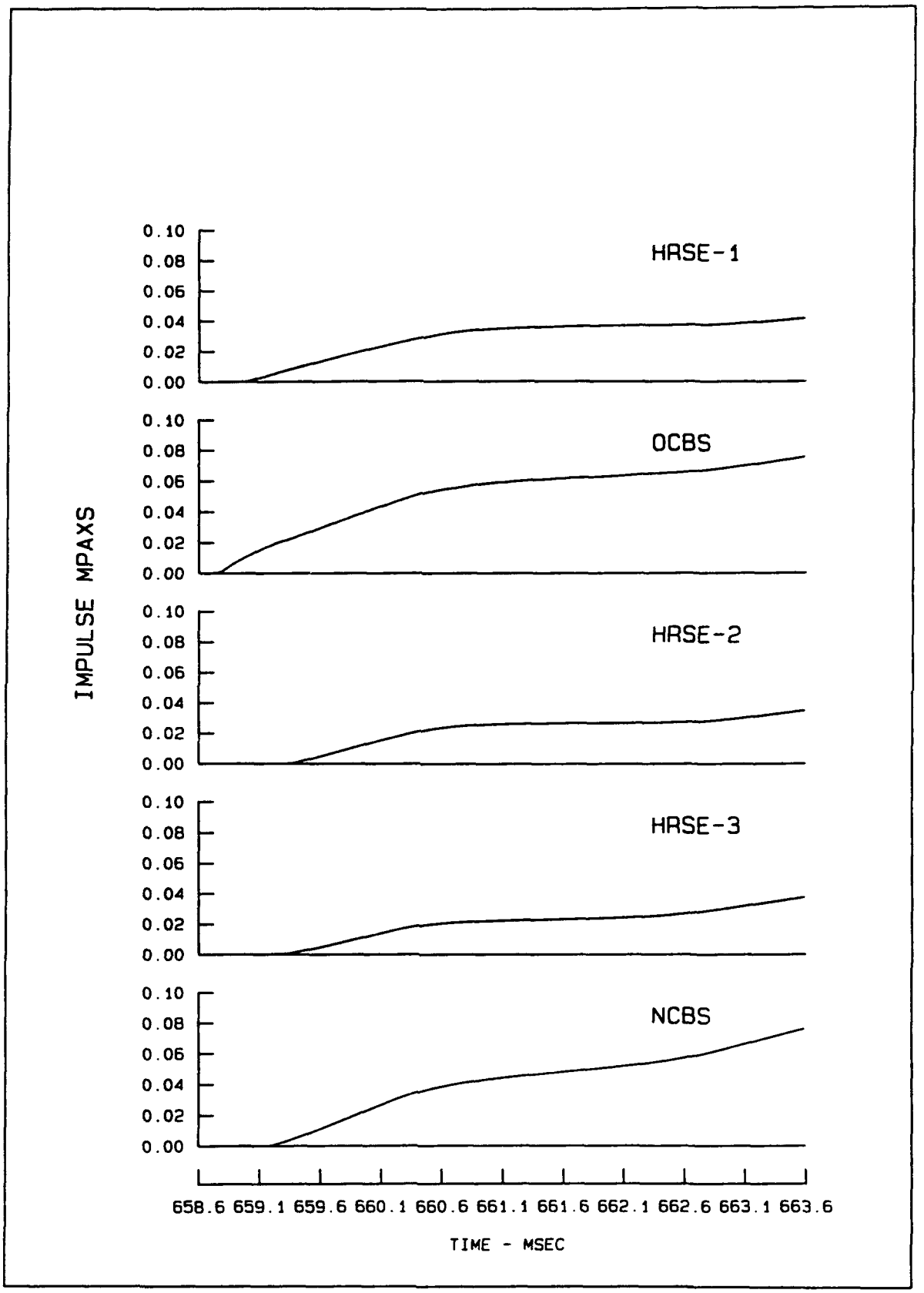

Figure D7. (Concluded)

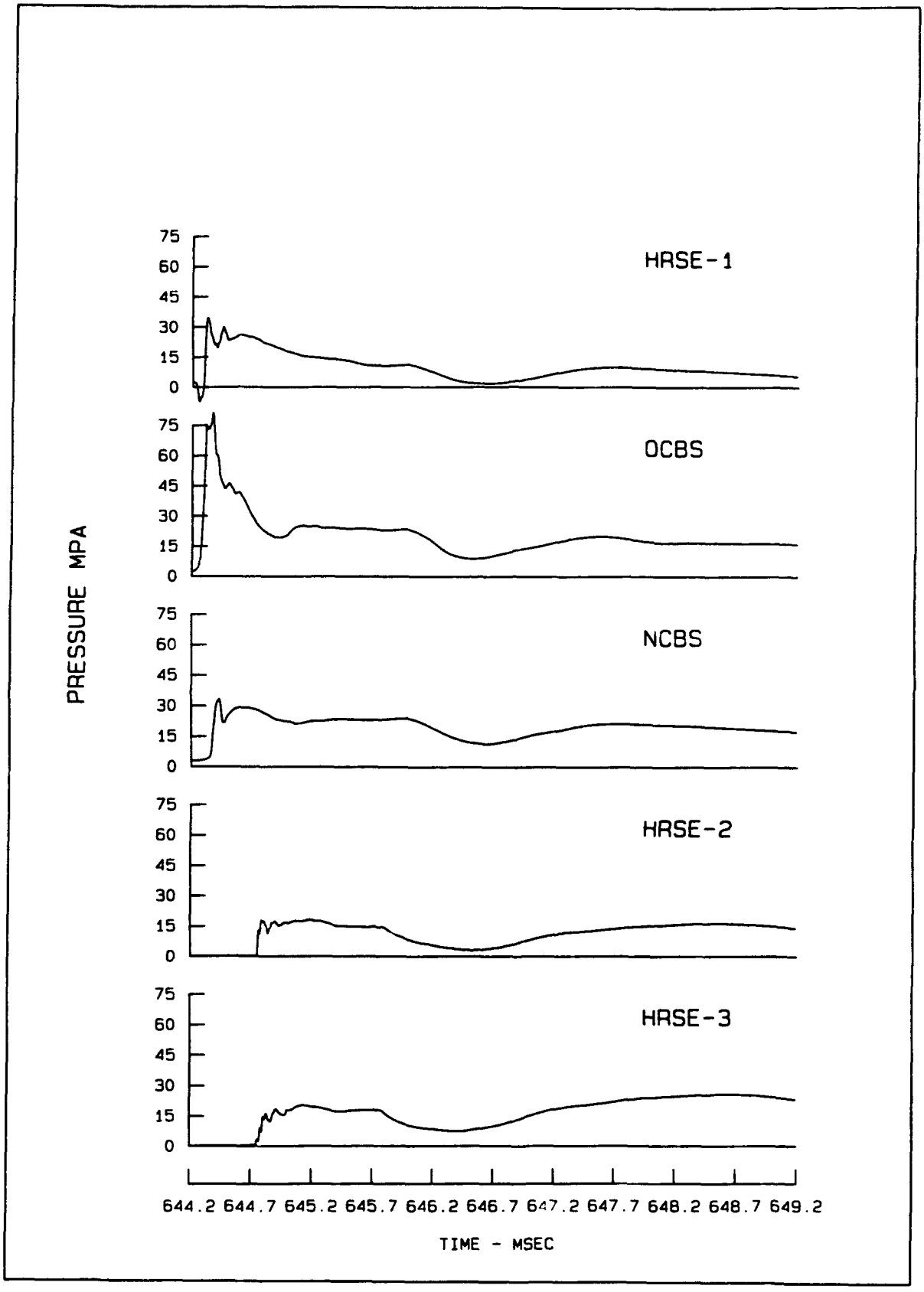

Figure D8. Stress and impulse wave forms from Test 14 (Continued)

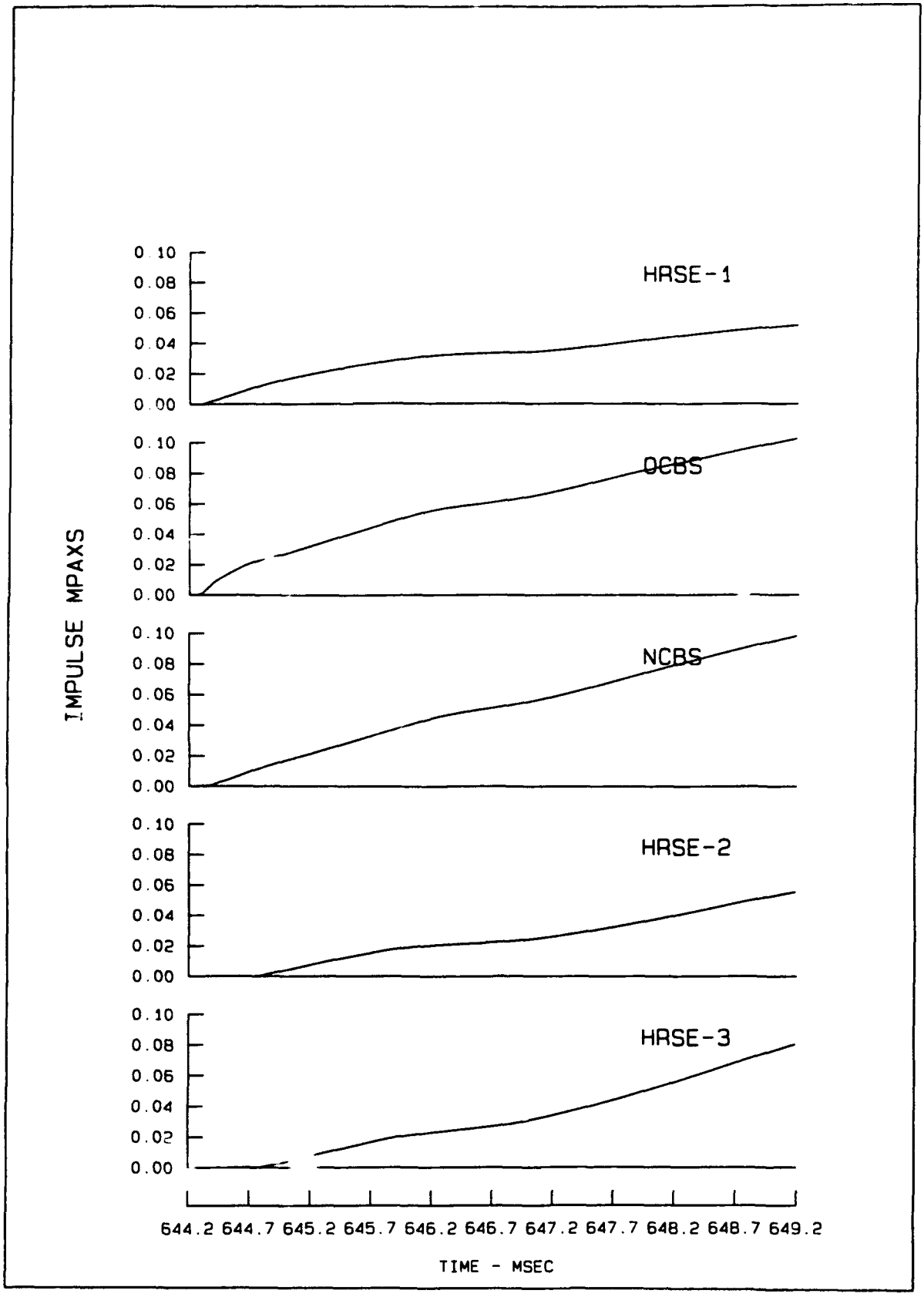

Figure D8. (Concluded)

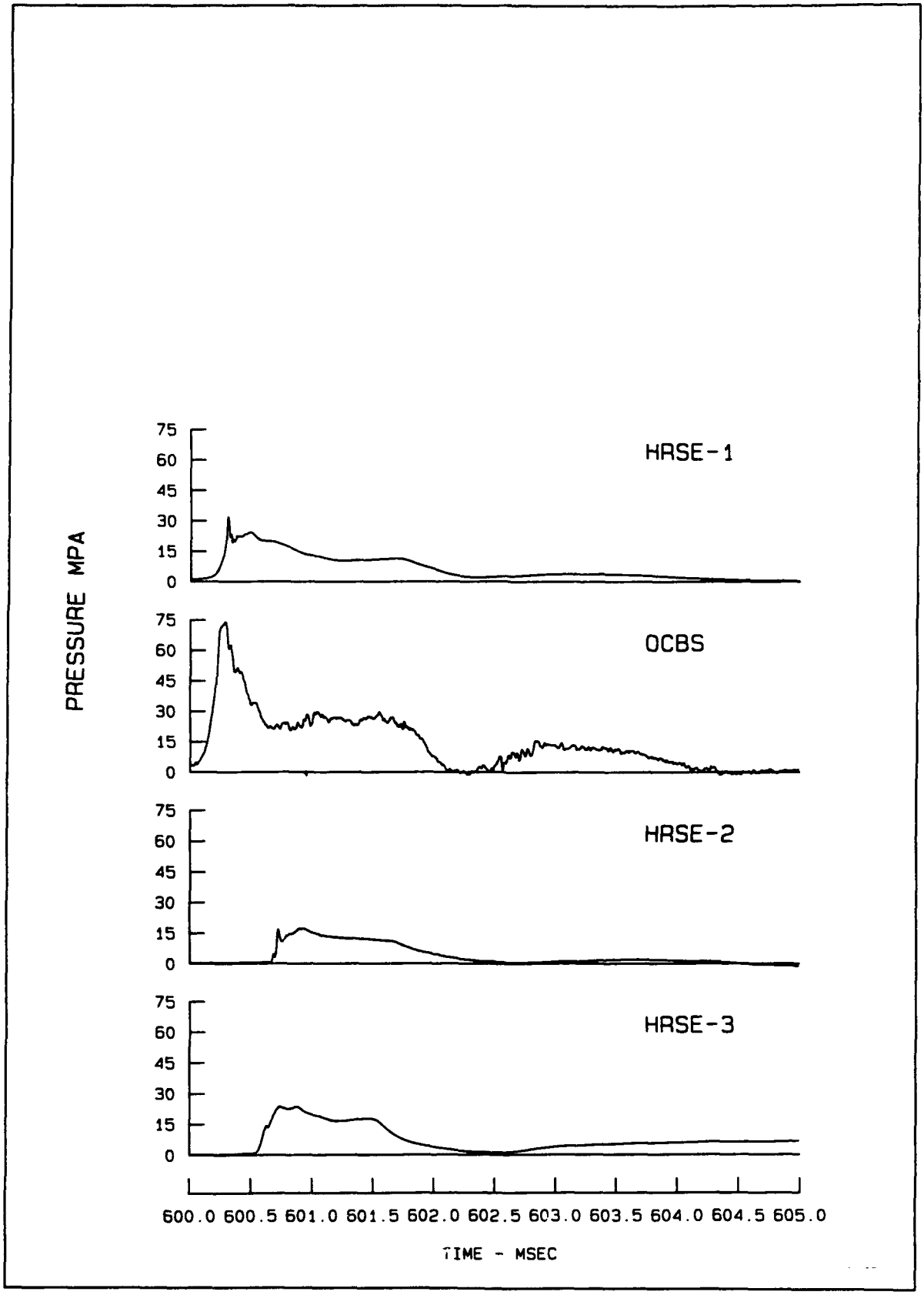

Figure D9. Stress and impulse wave forms from Test 15 (Continued)

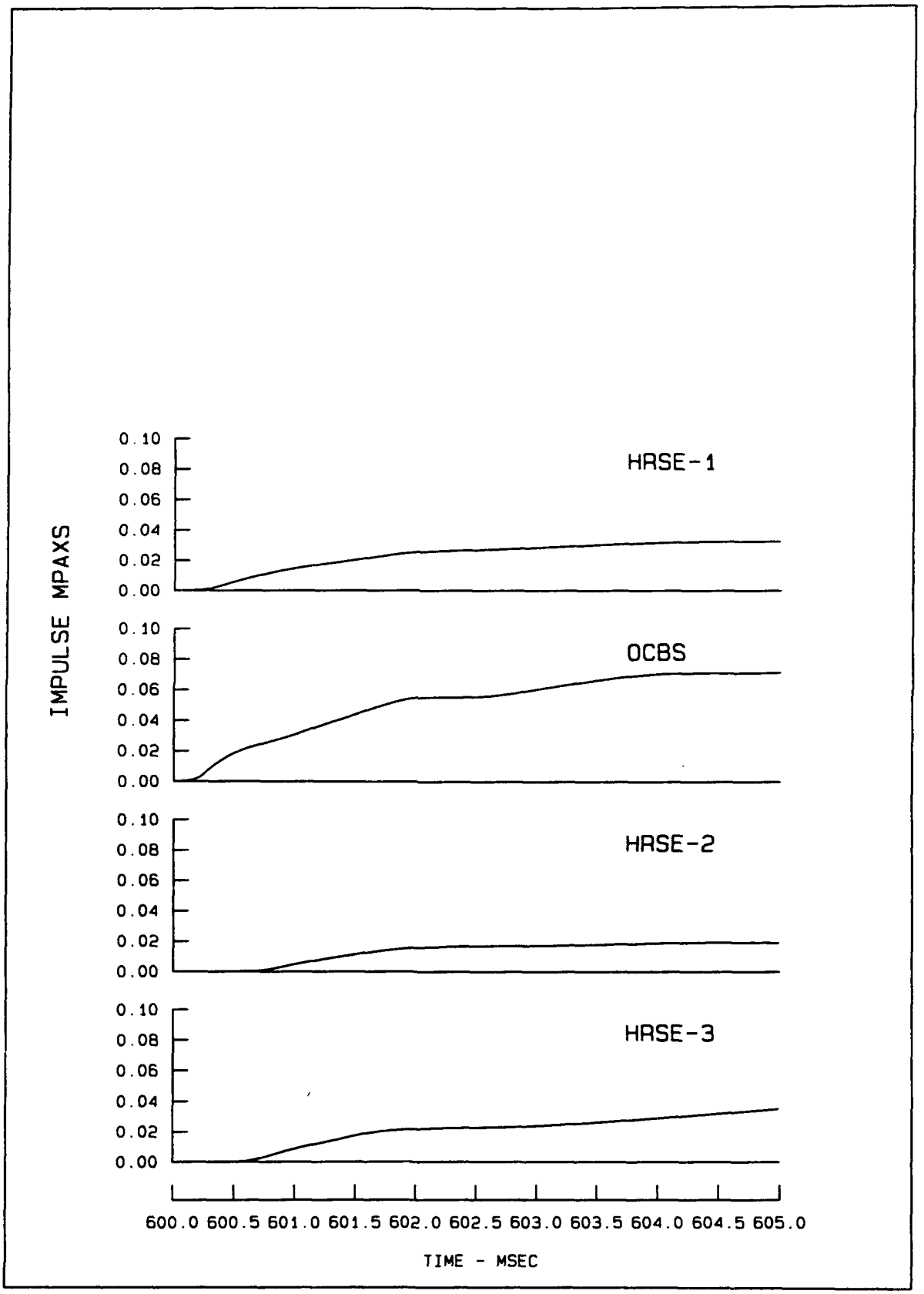

Figure D9. (Concluded)

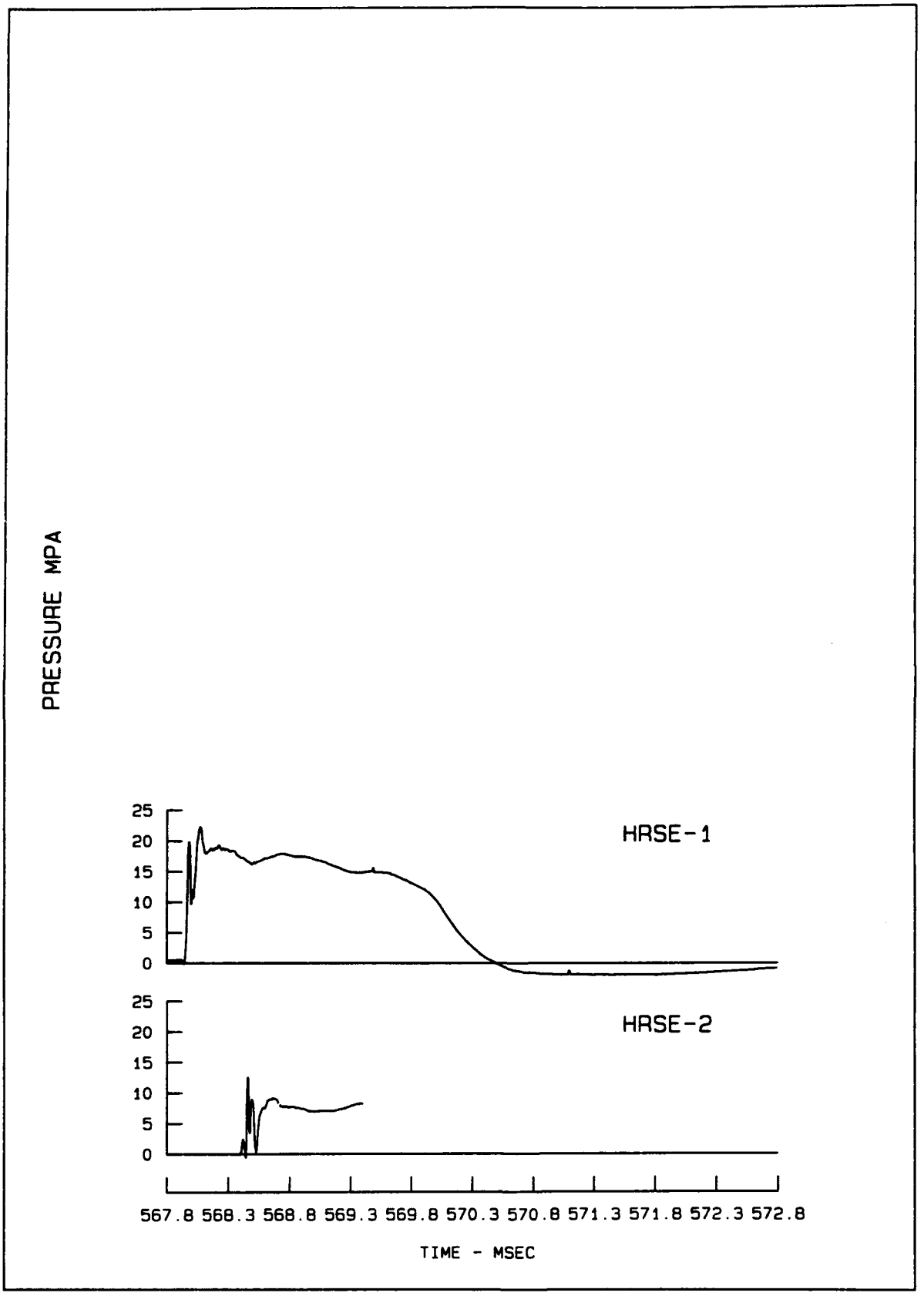

Figure D10. Stress and impulse wave forms from Test 16 (Continued)

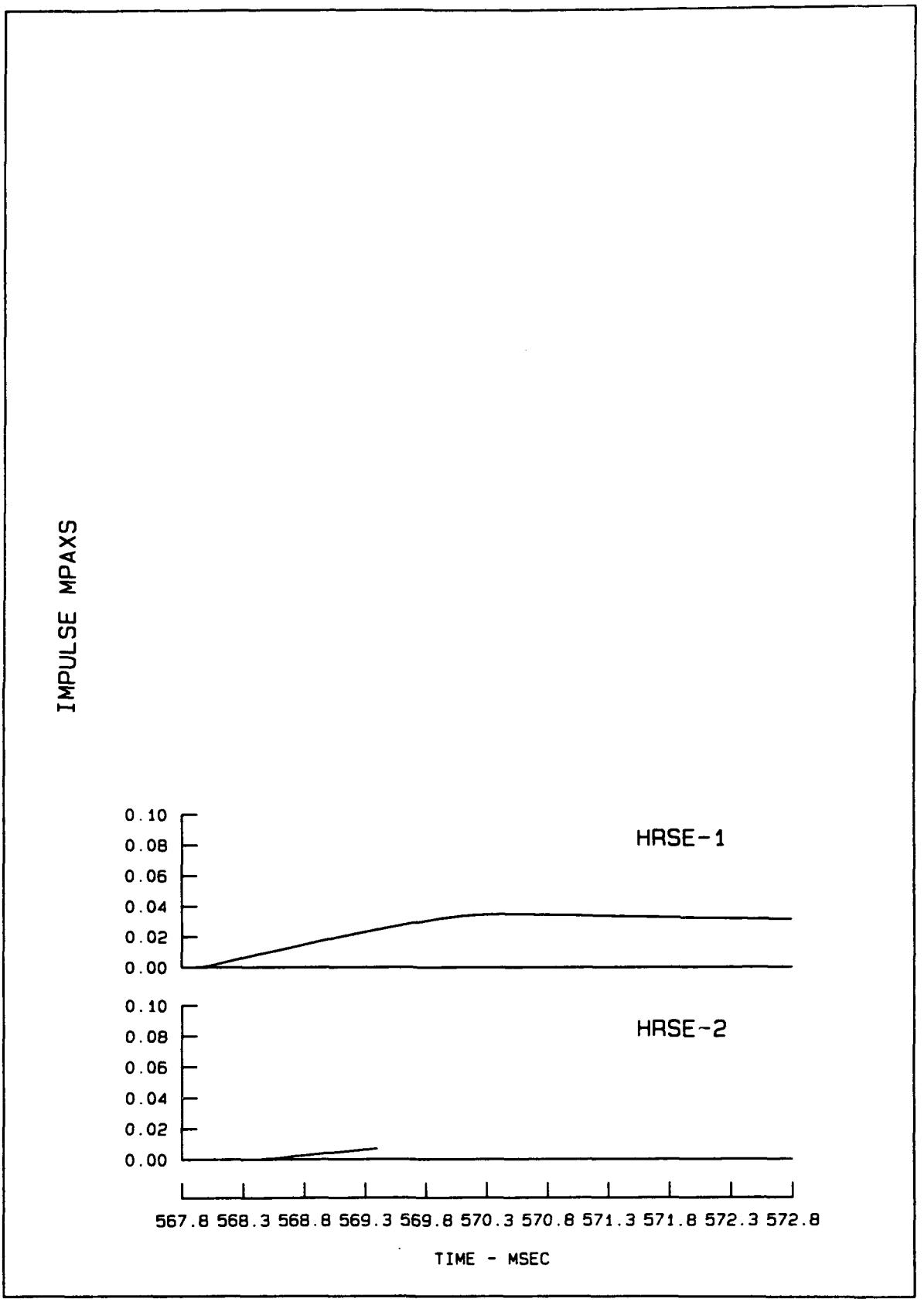

Figure D10. (Concluded)

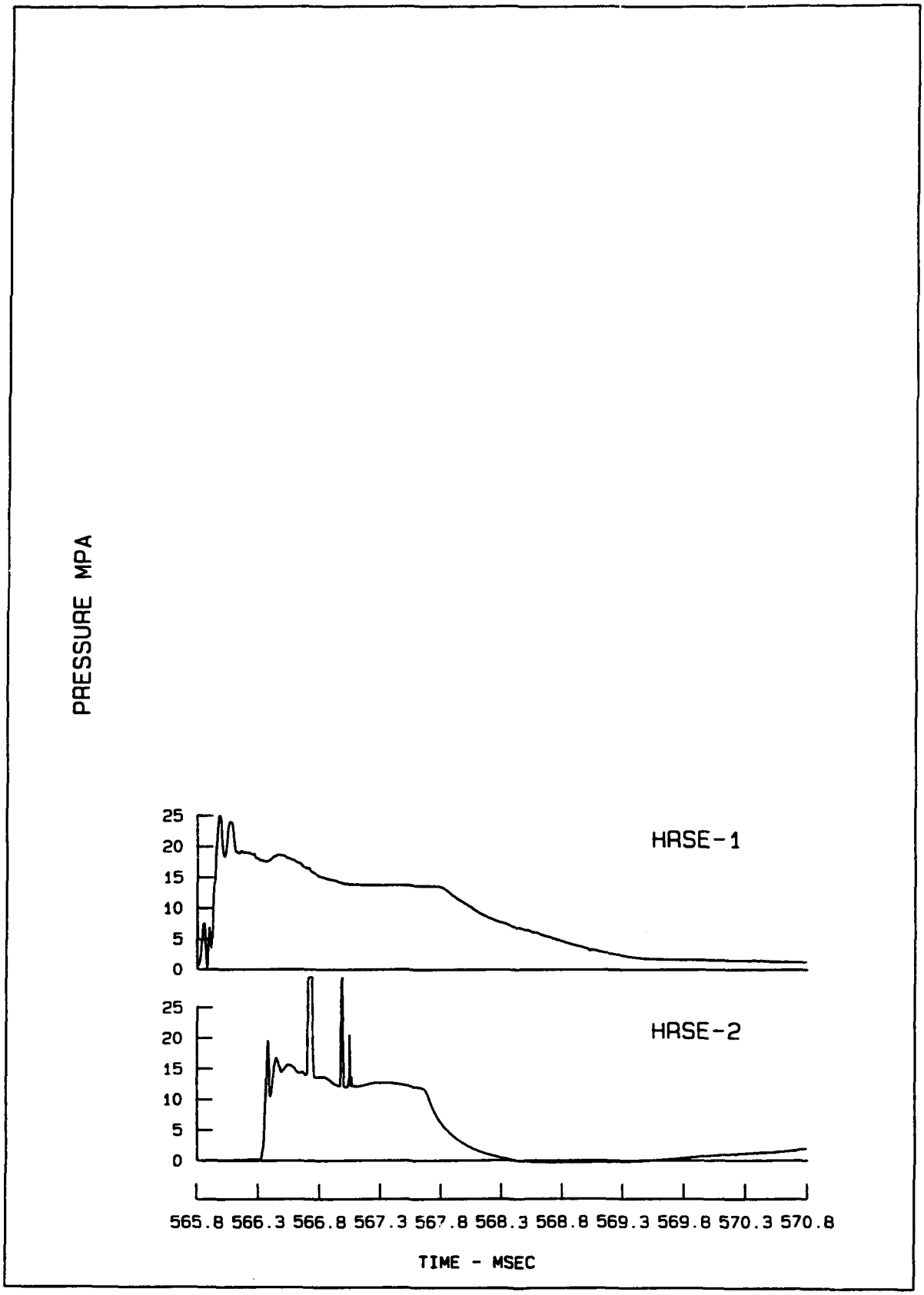

Figure D11. Stress and impulse wave forms from Test 17 (Continued)

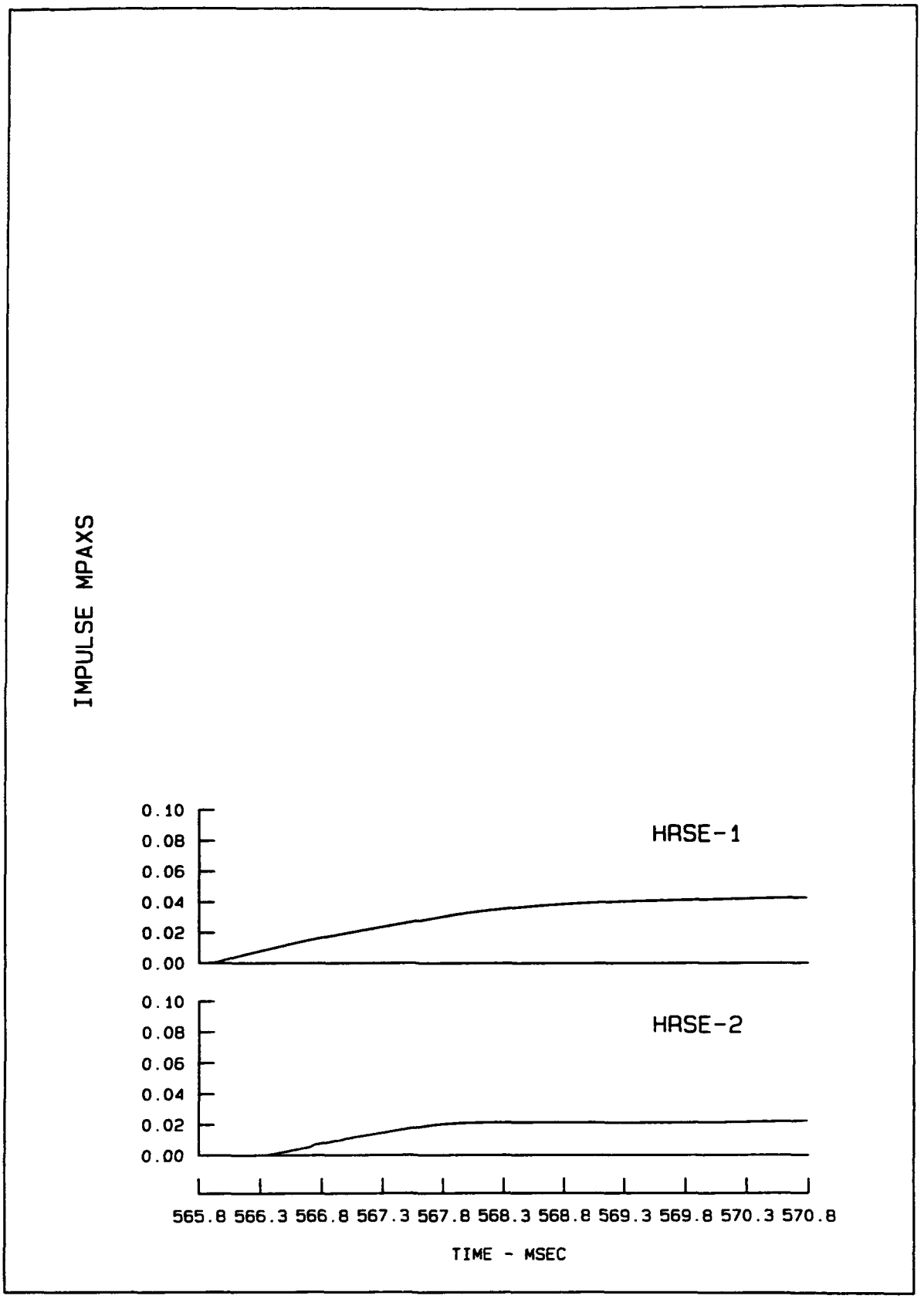

Figure D11. (Concluded)

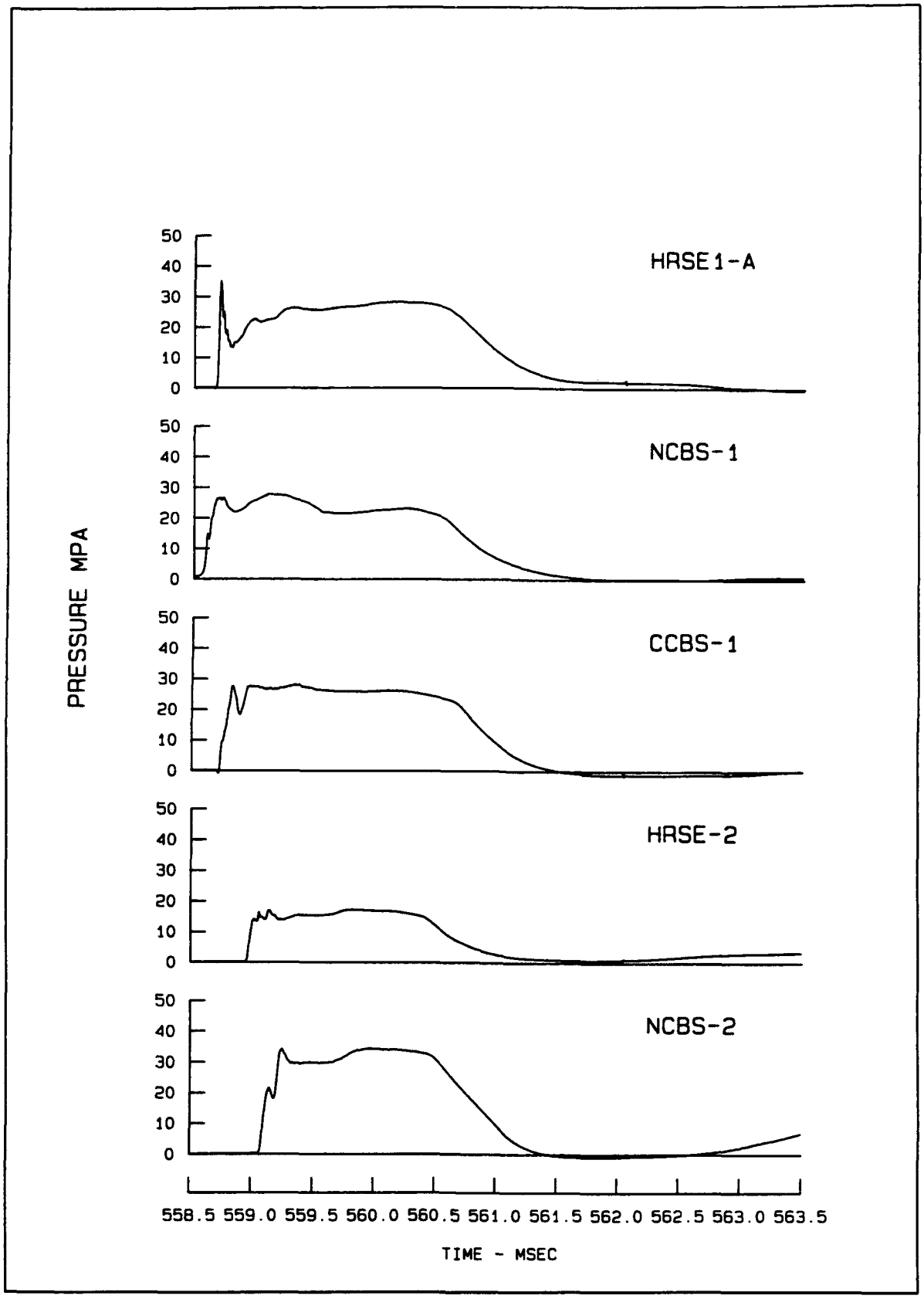

Figure D12. Stress and impulse wave forms from Test 22 (Continued)

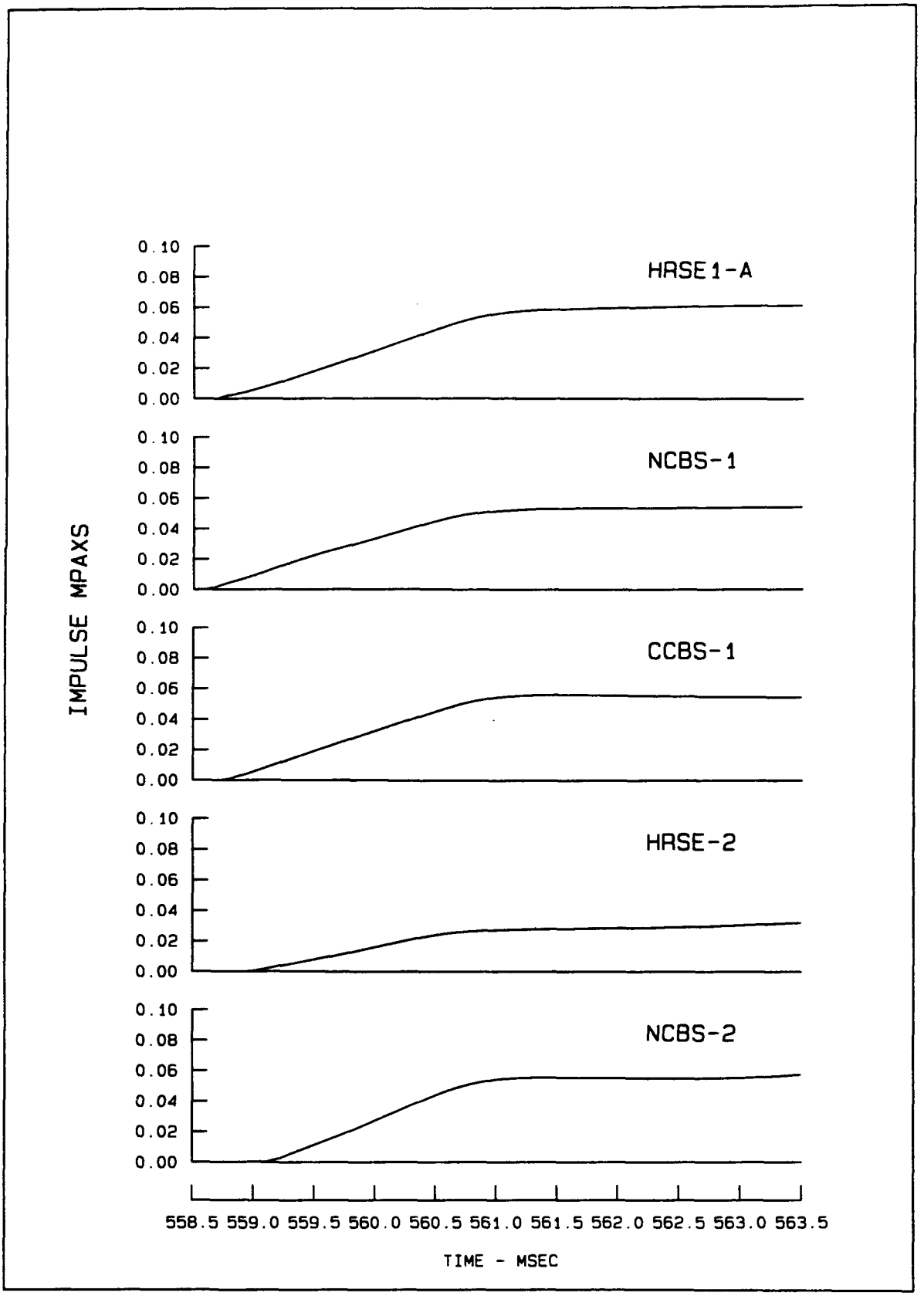

Figure D12. (Concluded)

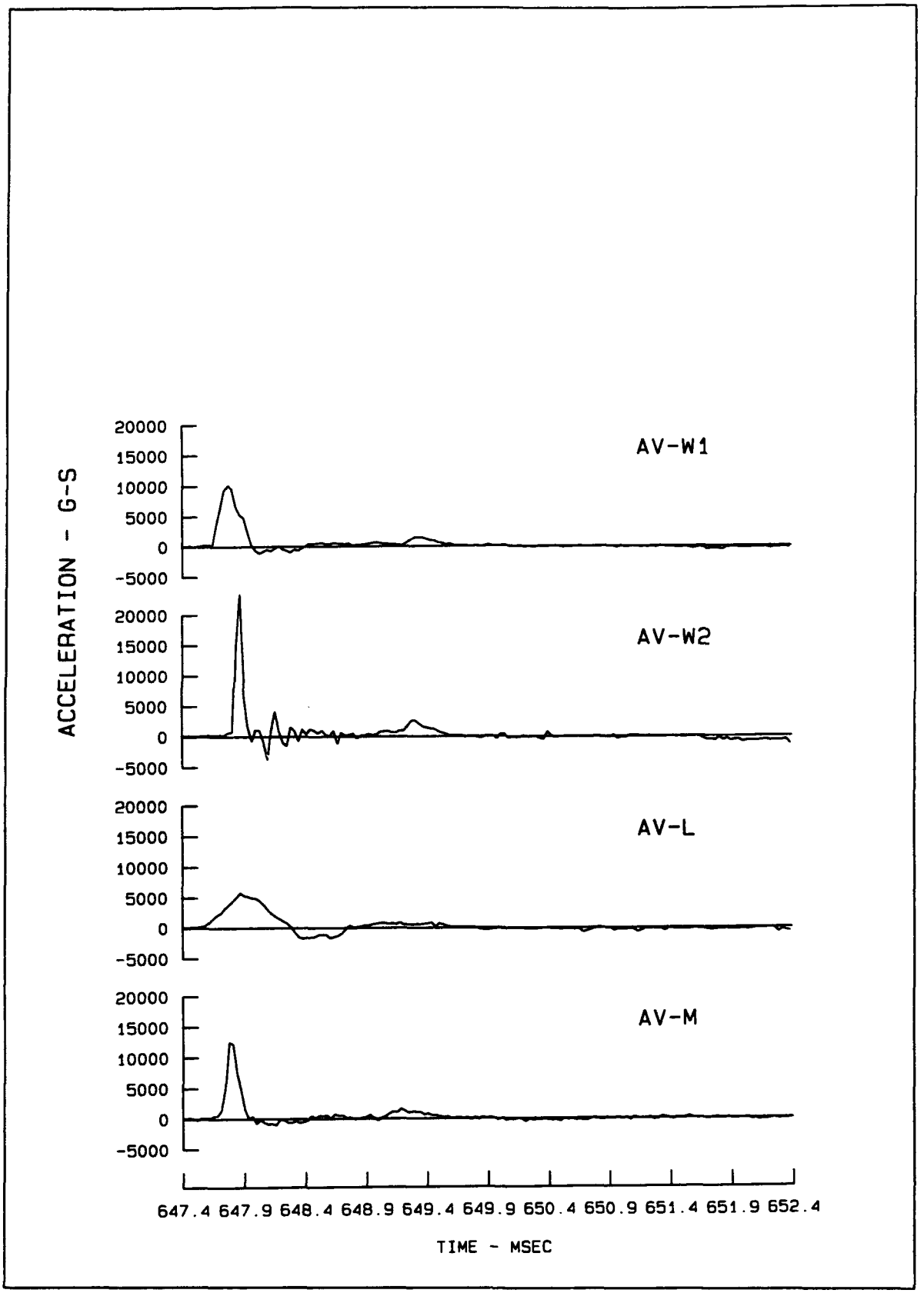

Figure D13. Acceleration, velocity, and displacement wave forms from Test 6 (Sheet 1 of 3)

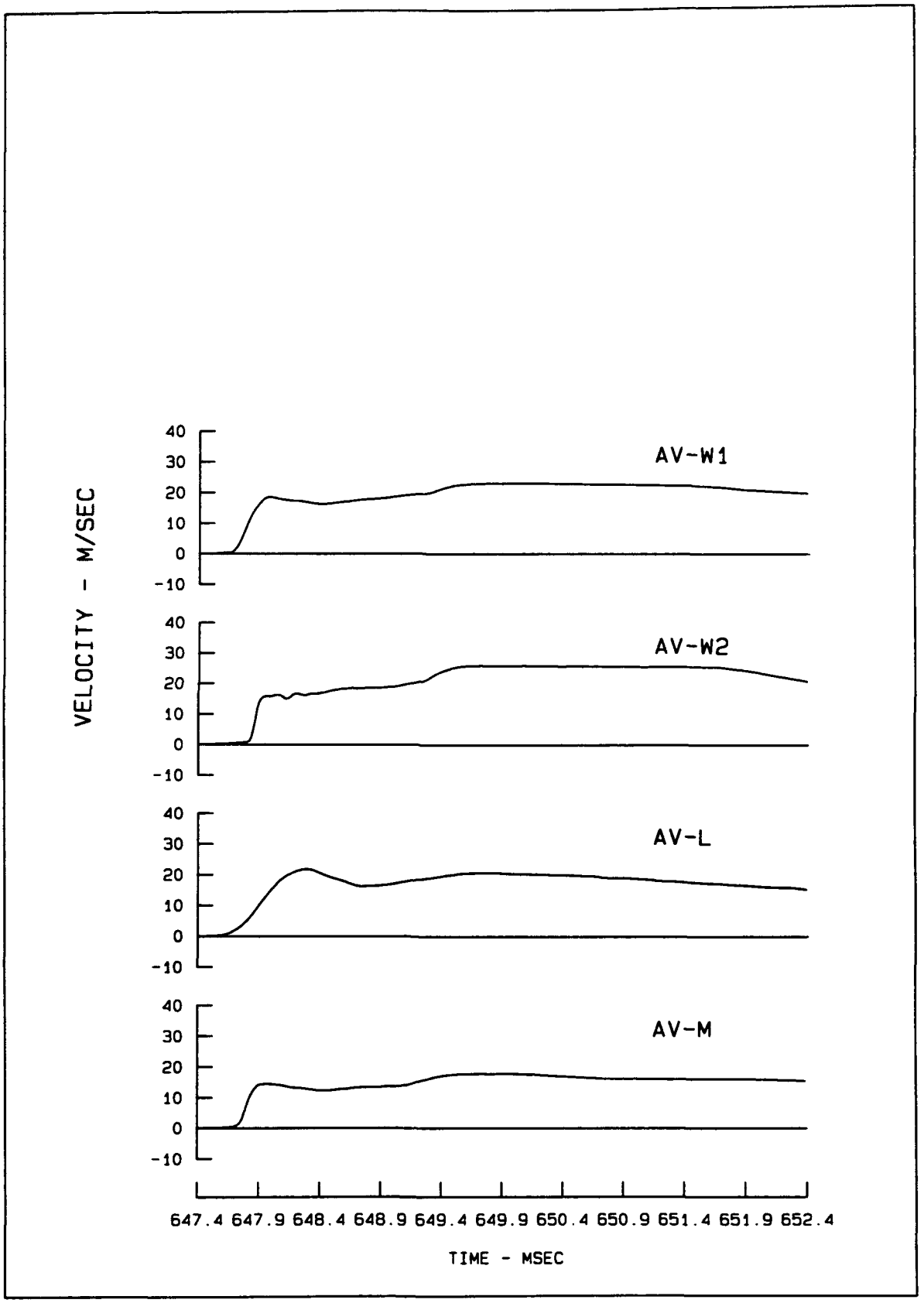

Figure D13. (Sheet 2 of 3)

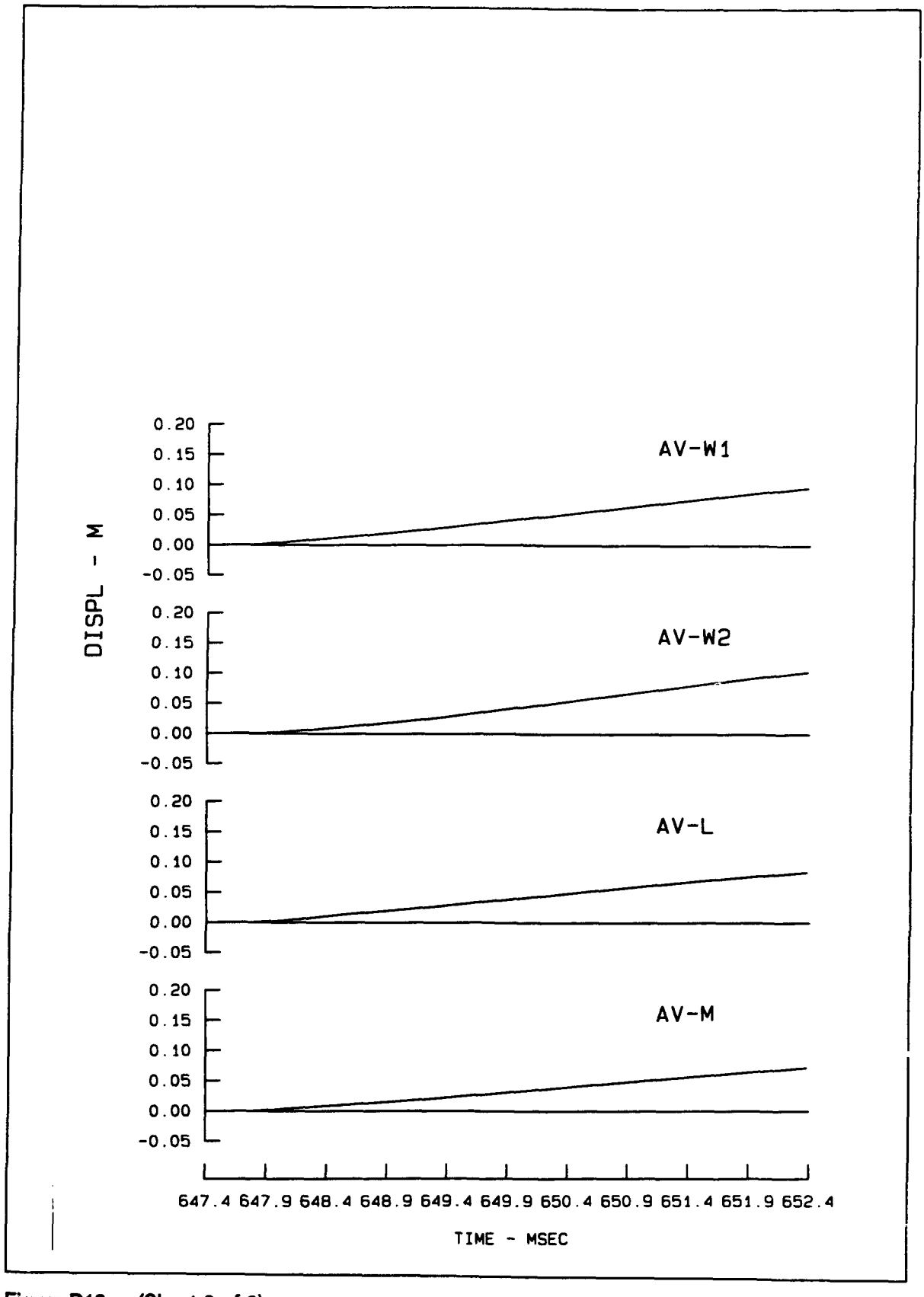

Figure D13. (Sheet 3 of 3)

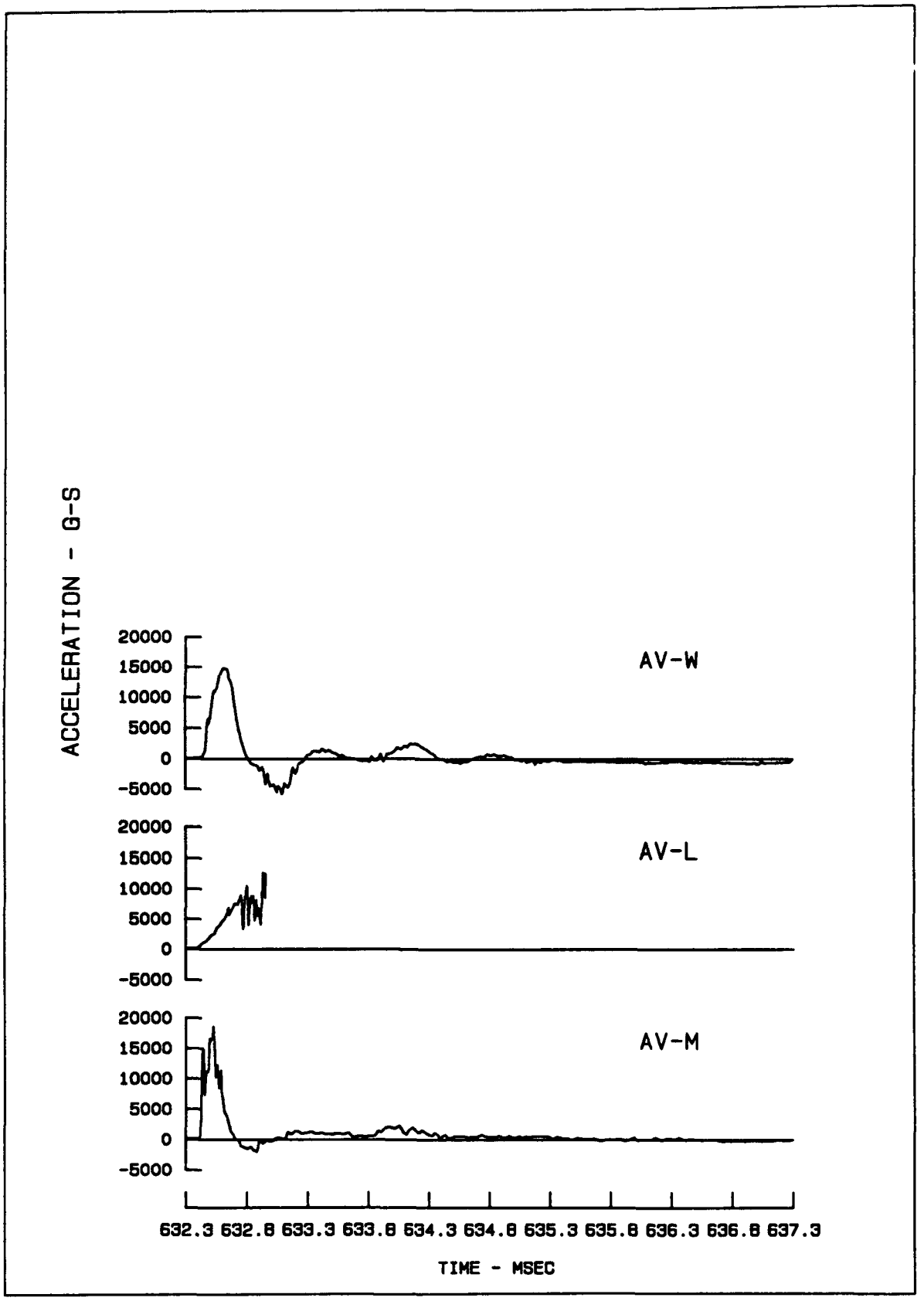

Figure D14. Acceleration, velocity, and displacement wave forms from Test 7 (Sheet 1 of 3)

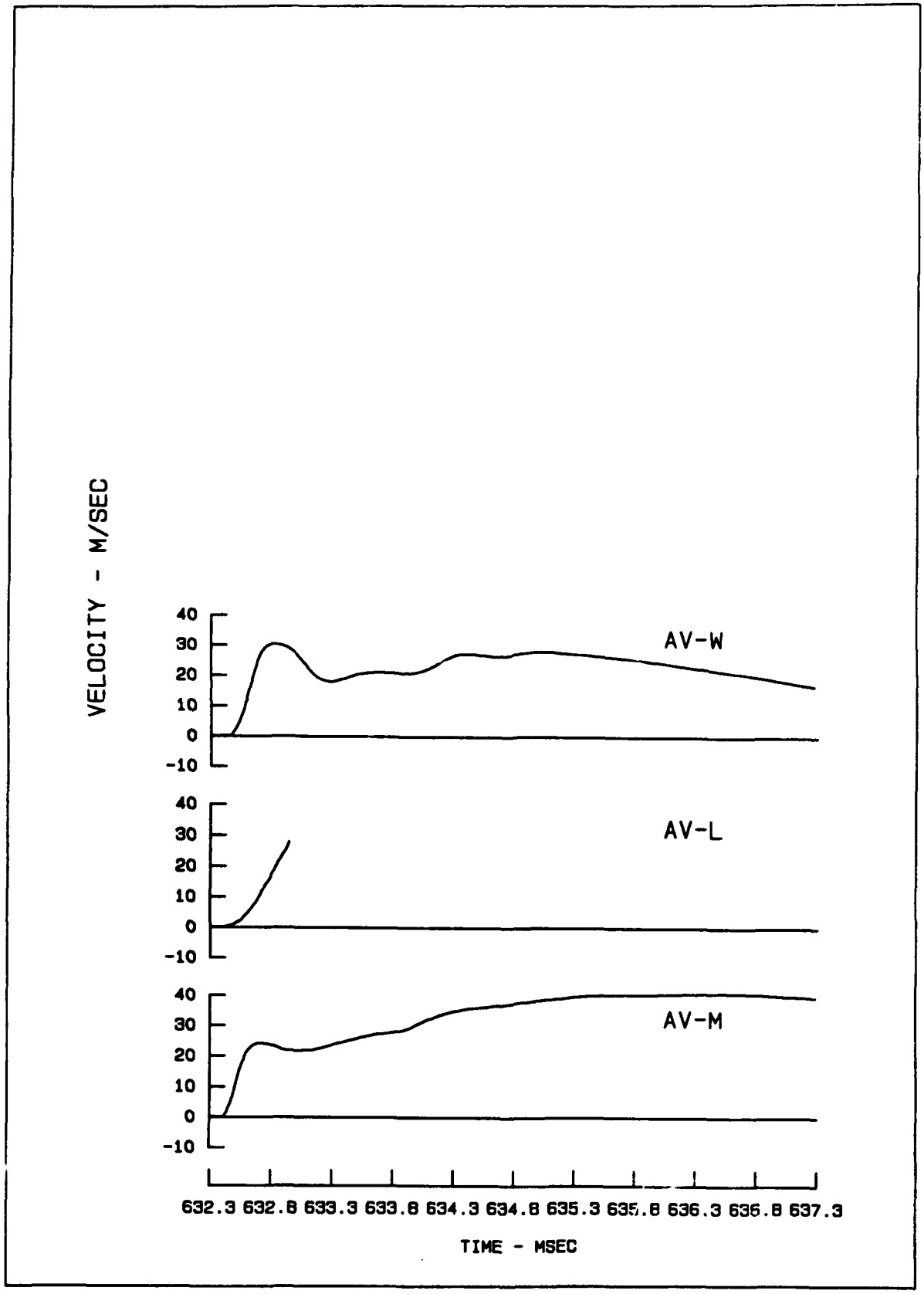

Figure D14. (Sheet 2 of 3)

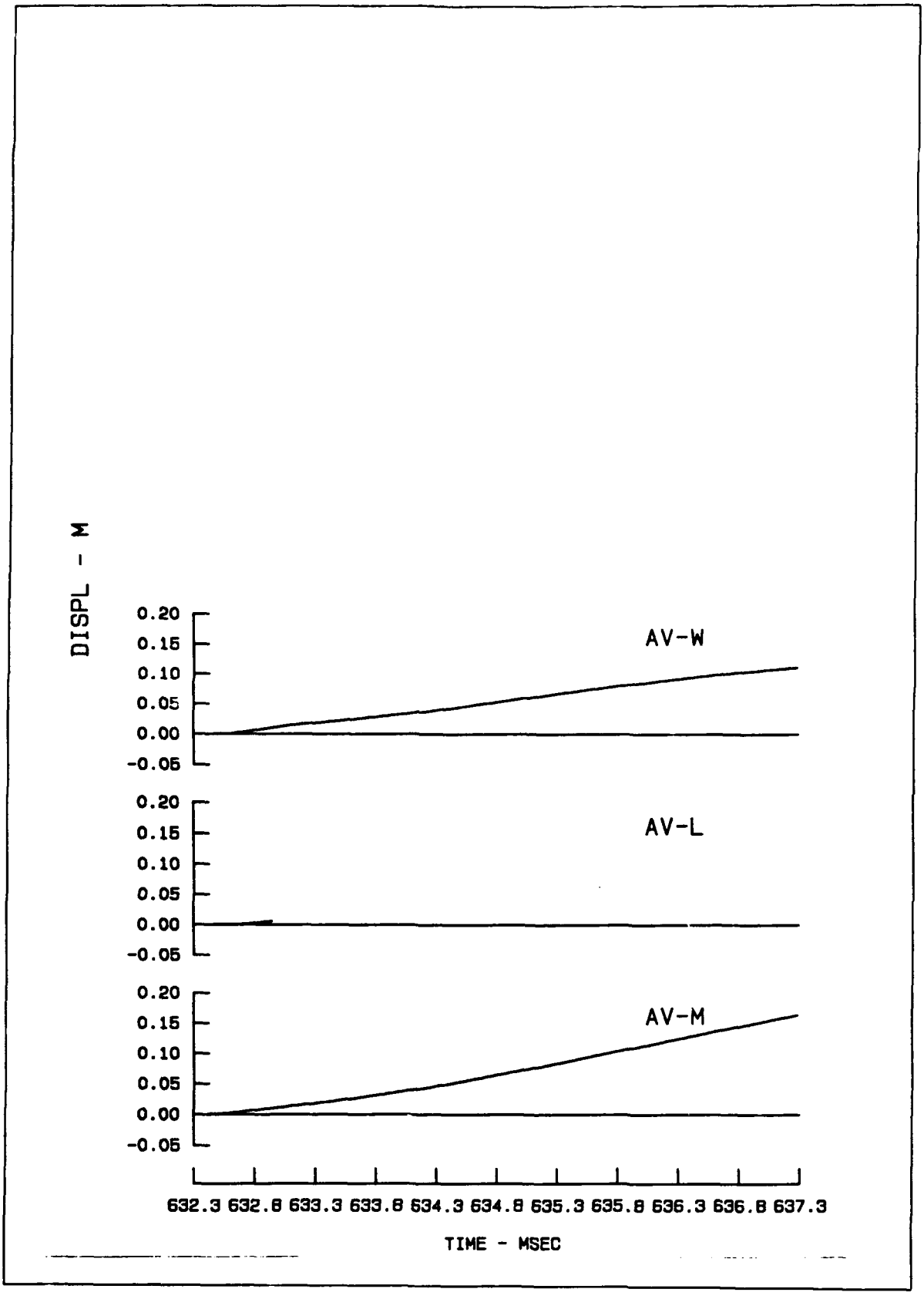

Figure D14. (Sheet 3 of 3)

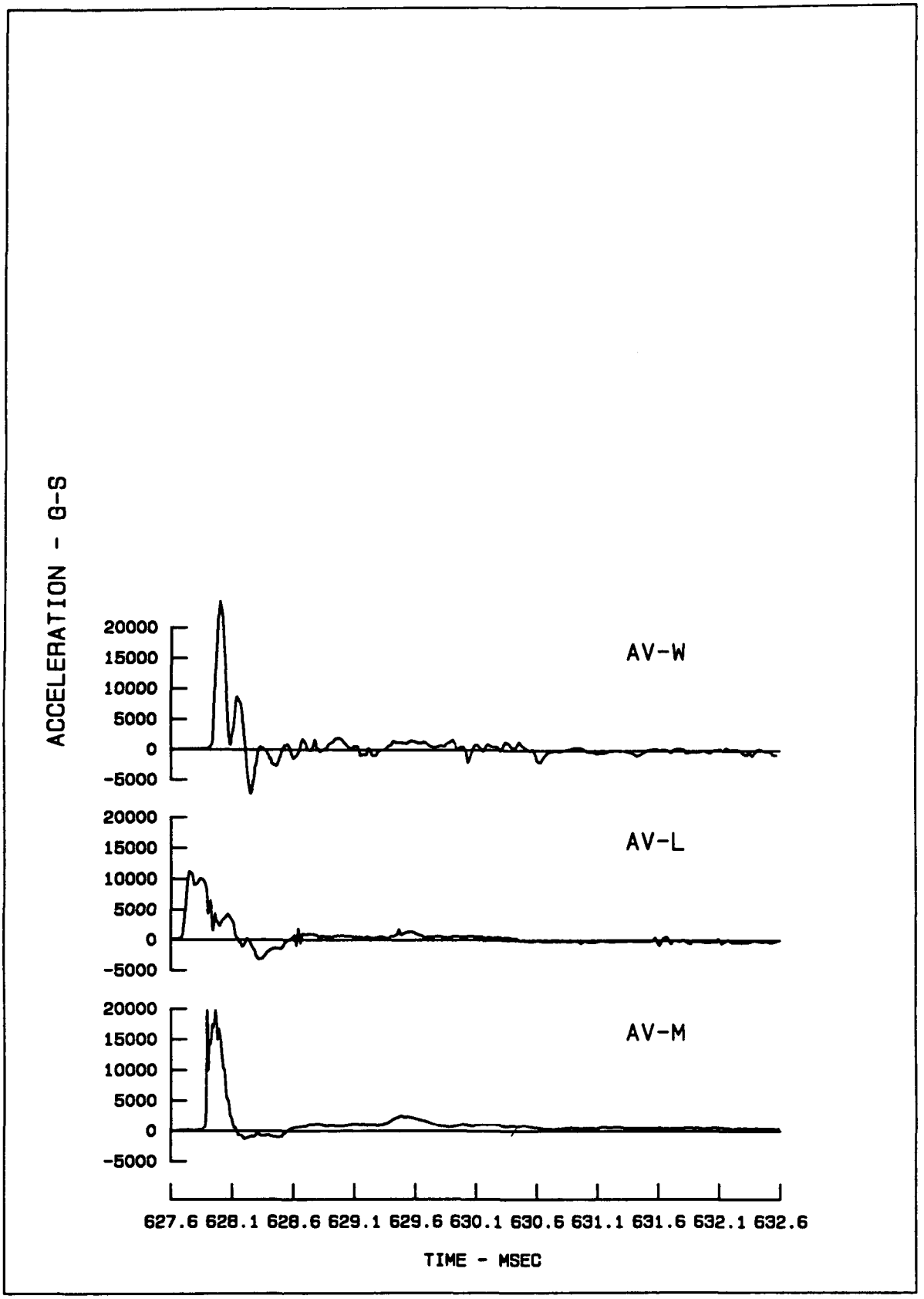

Figure D15. Acceleration, velocity, and displacement wave forms from Test 8 (Sheet 1 of 3)

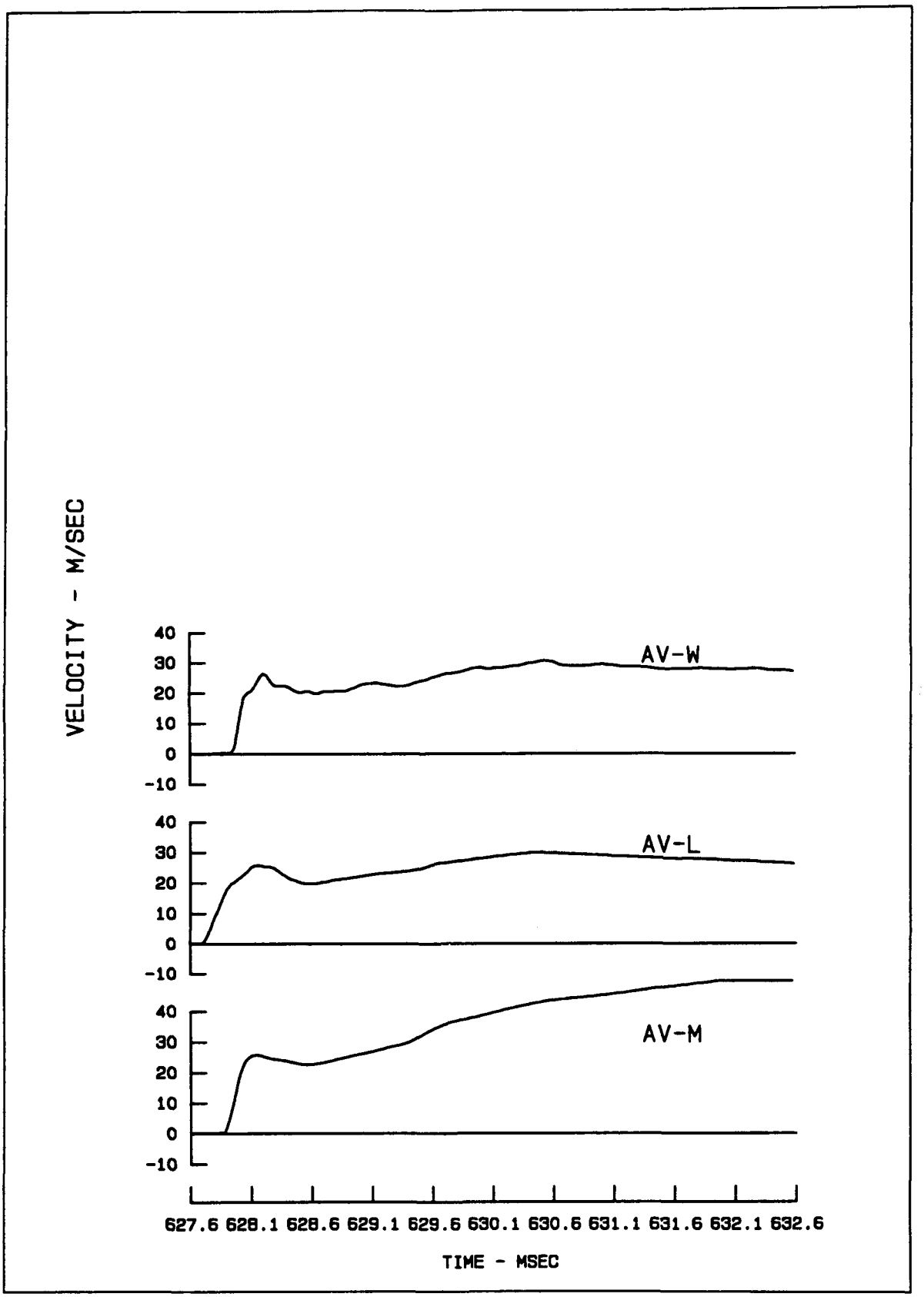

Figure D15. (Sheet 2 of 3)

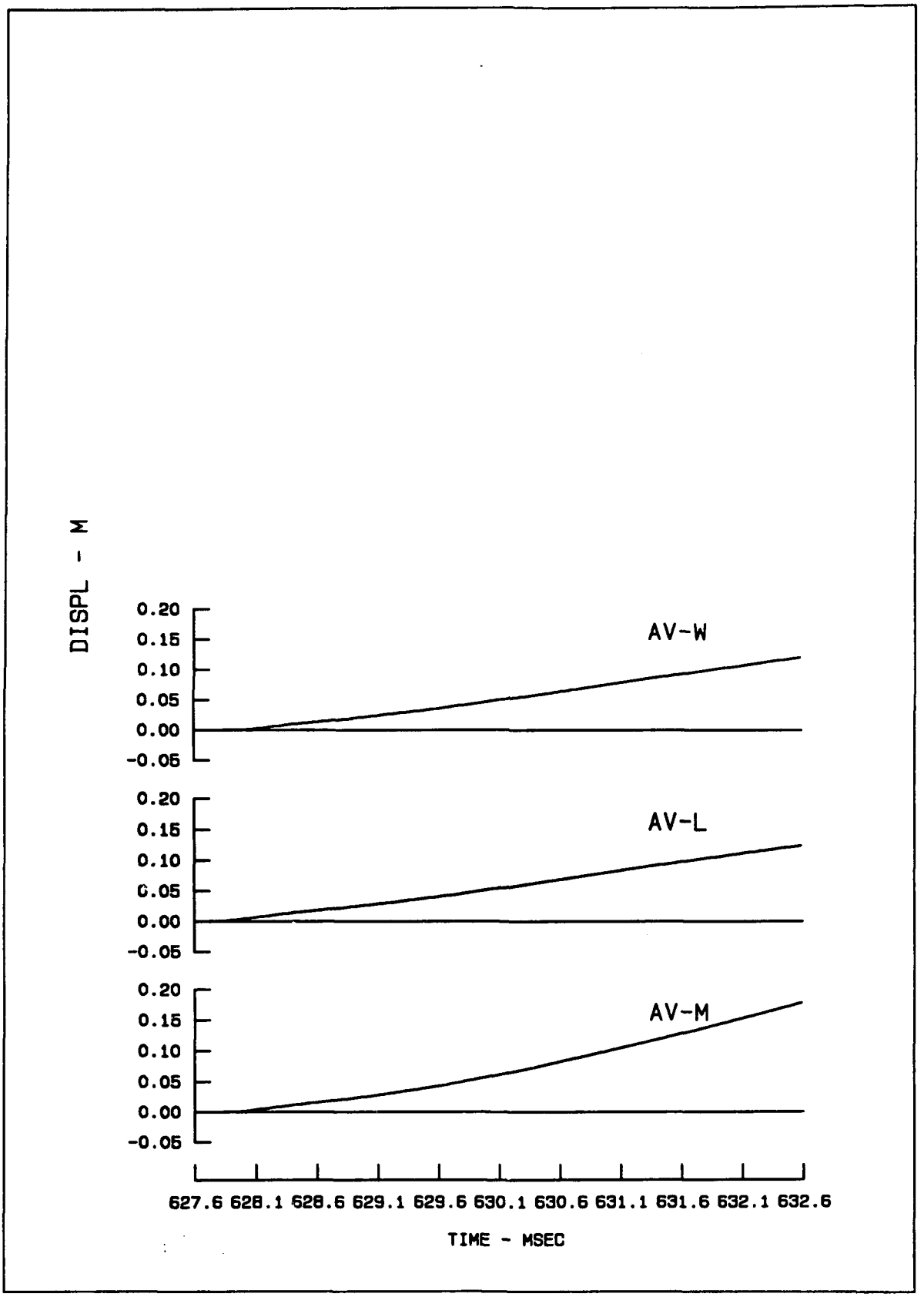

Figure D15. (Sheet 3 of 3)

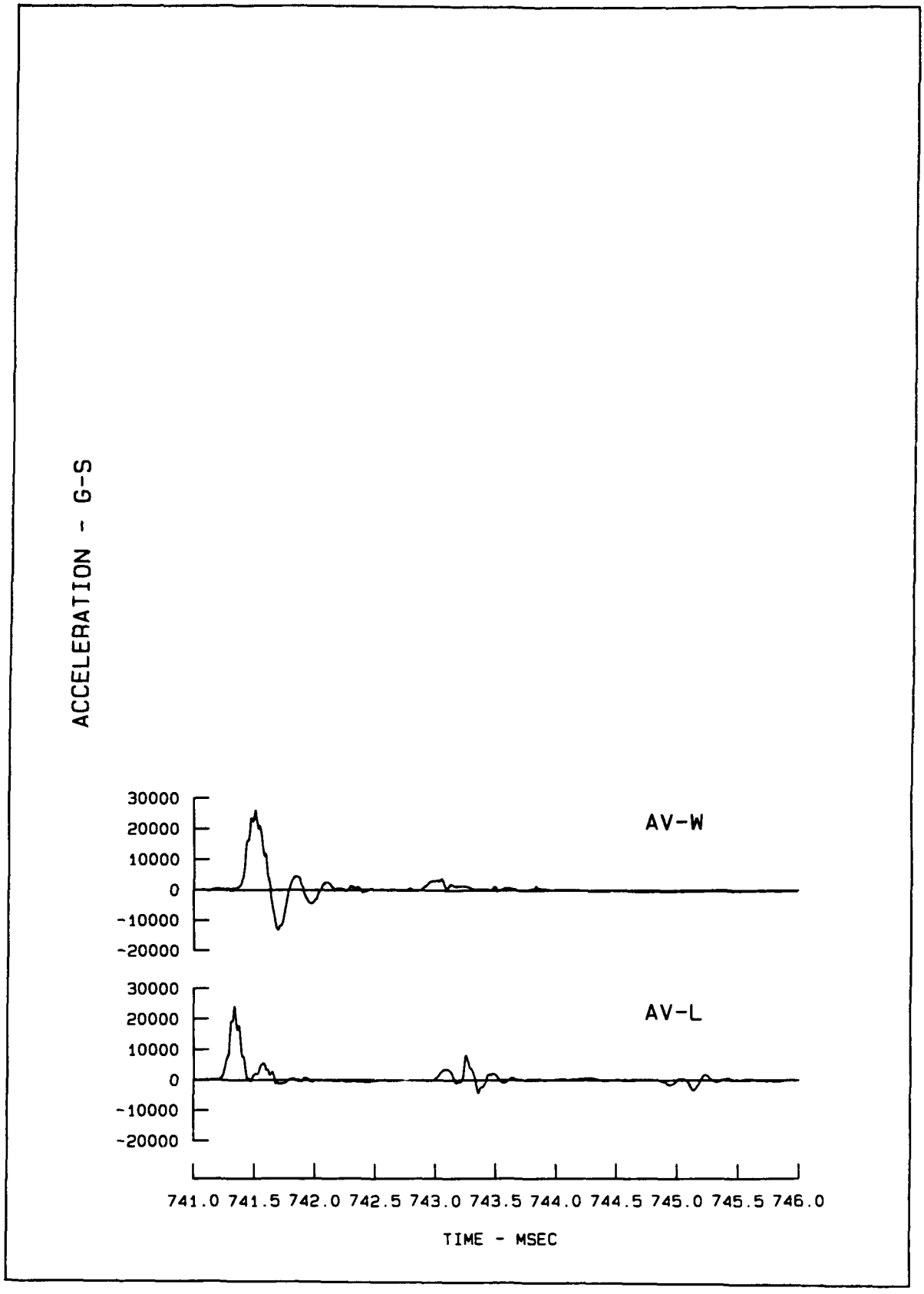

Figure D16. Acceleration, velocity, and displacement wave forms from Test 10 (Sheet 1 of 3)

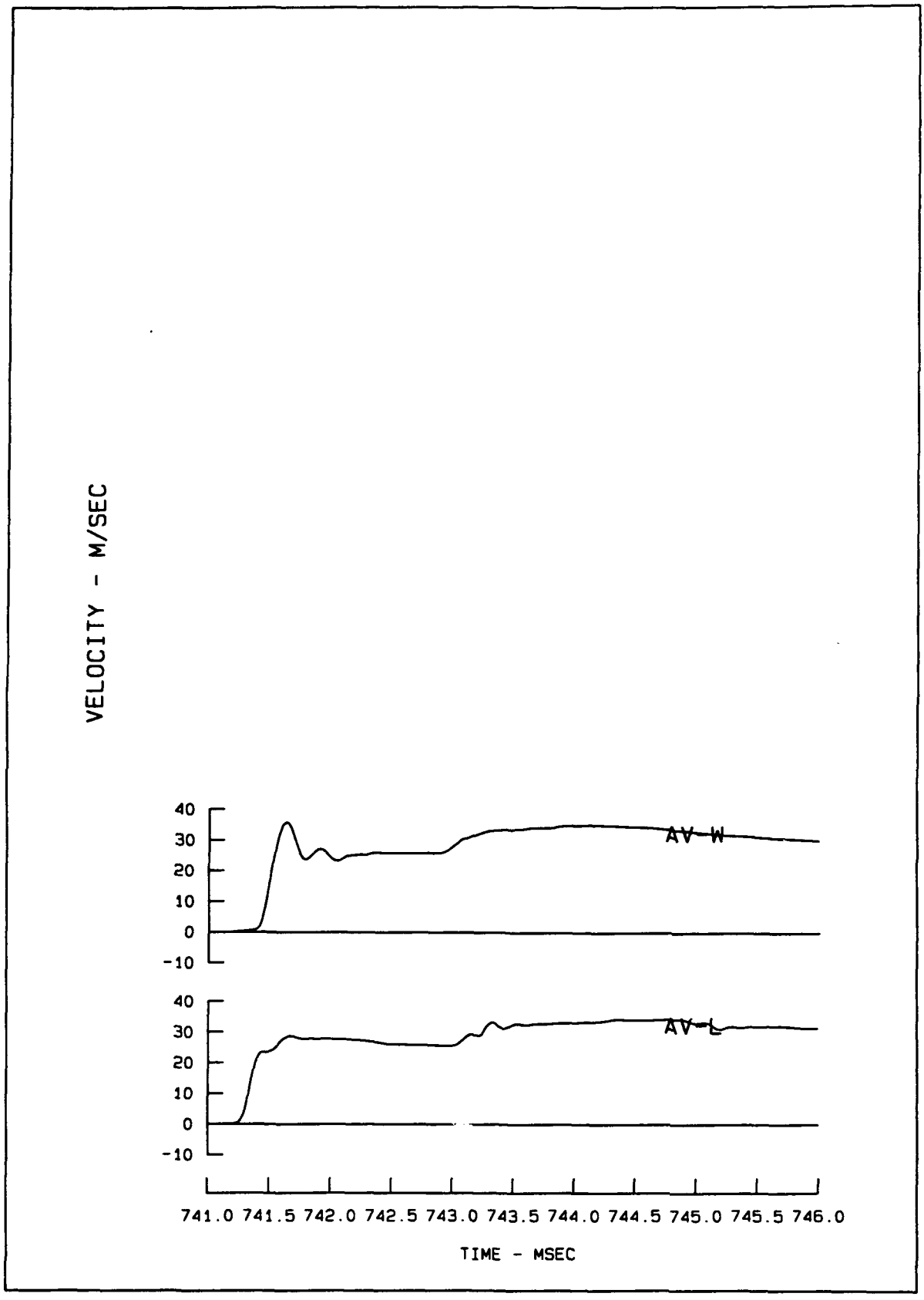

Figure D16. (Sheet 2 of 3)

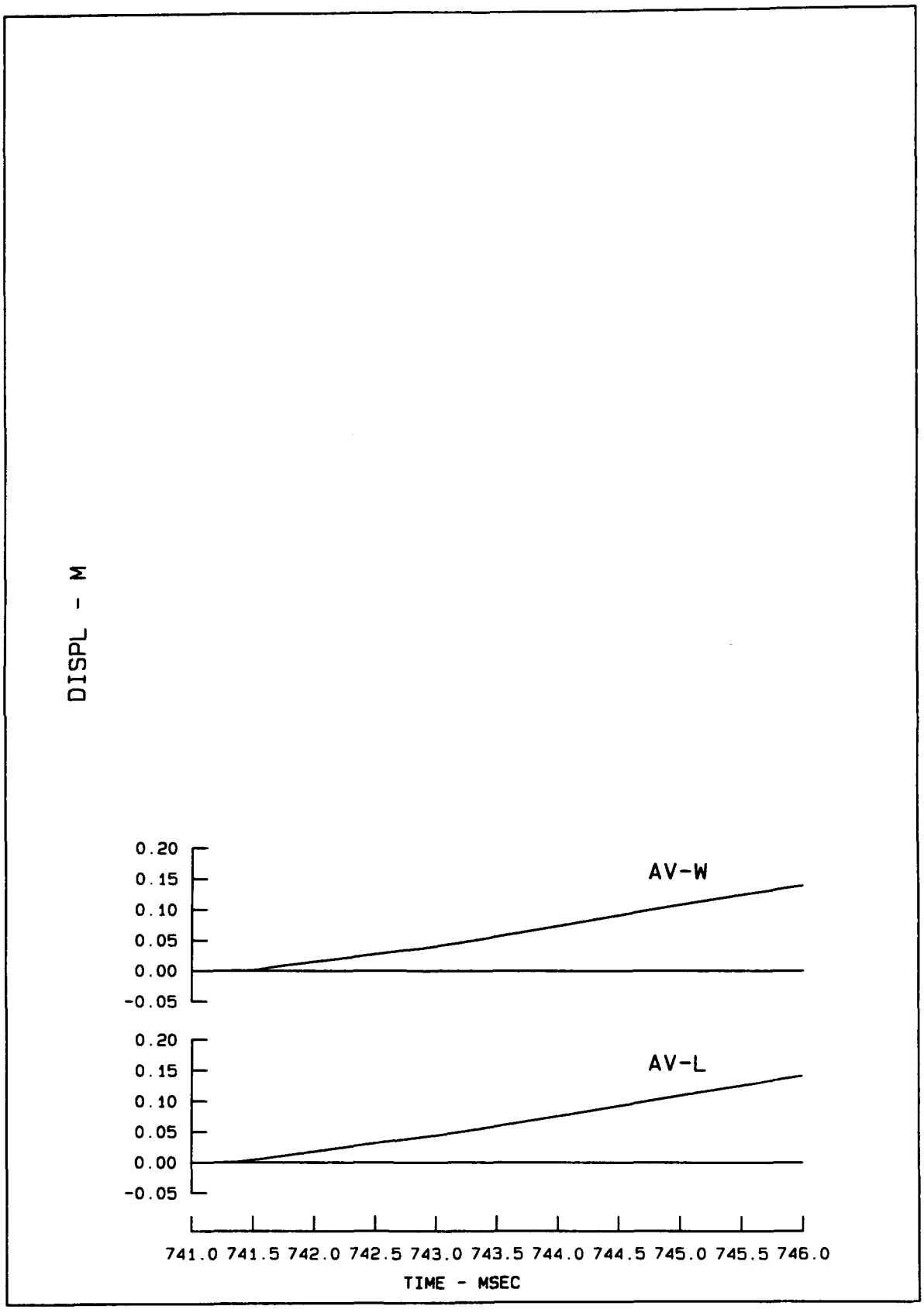

Figure D16. (Sheet 3 of 3)

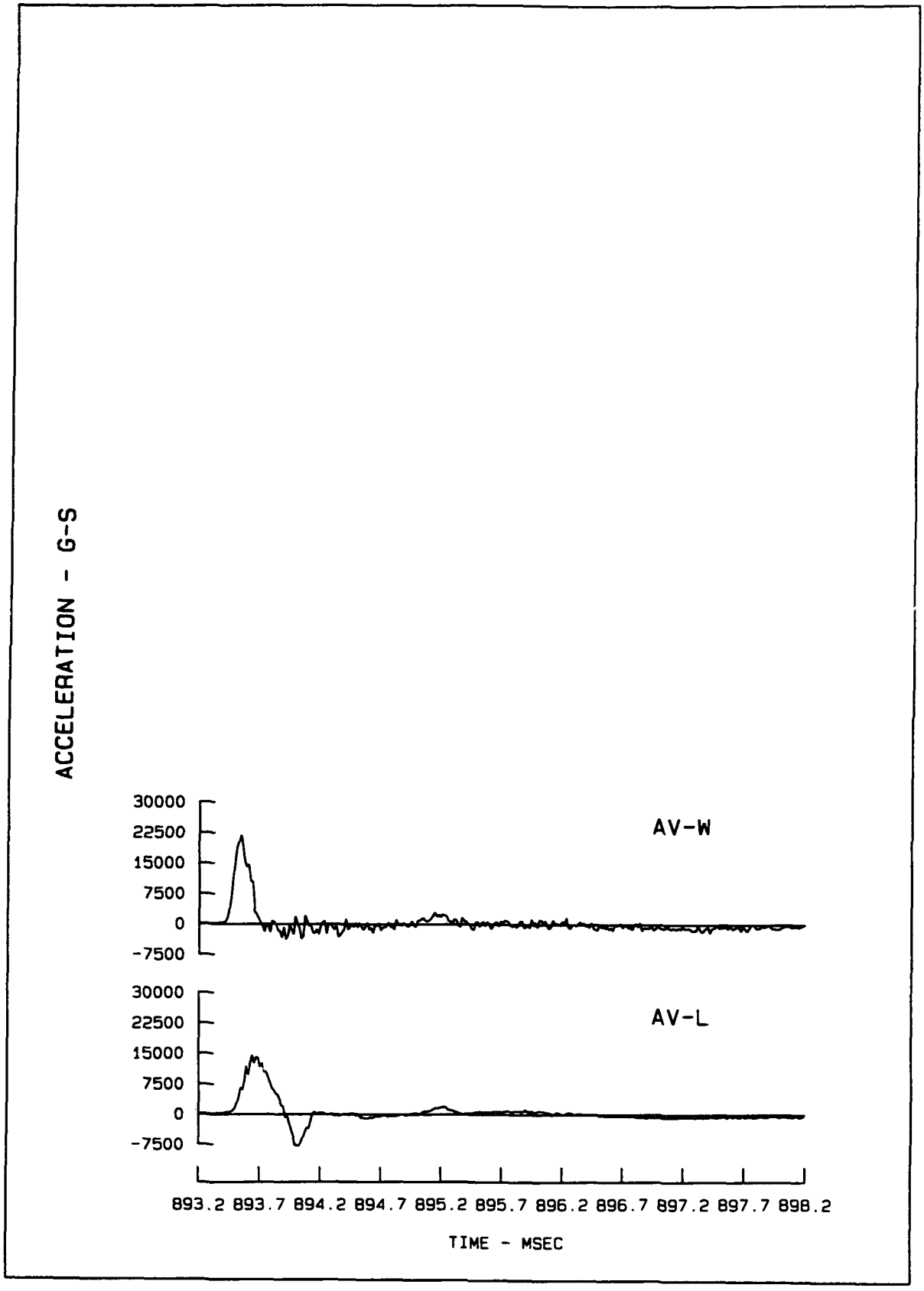

Figure D17. Acceleration, velocity, and displacement wave forms from Test 11 (Sheet 1 of 3)

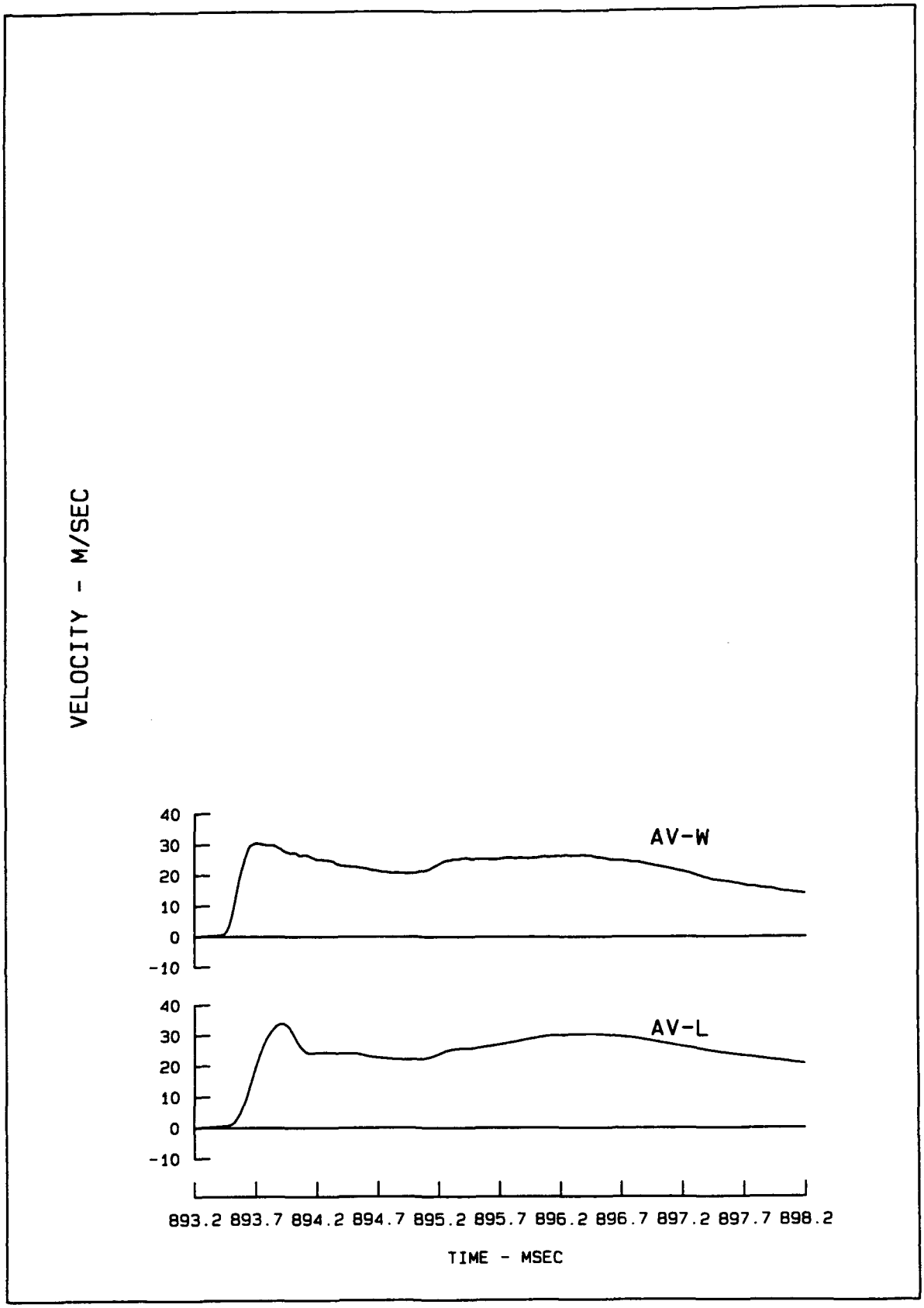

Figure D17. (Sheet 2 of 3)

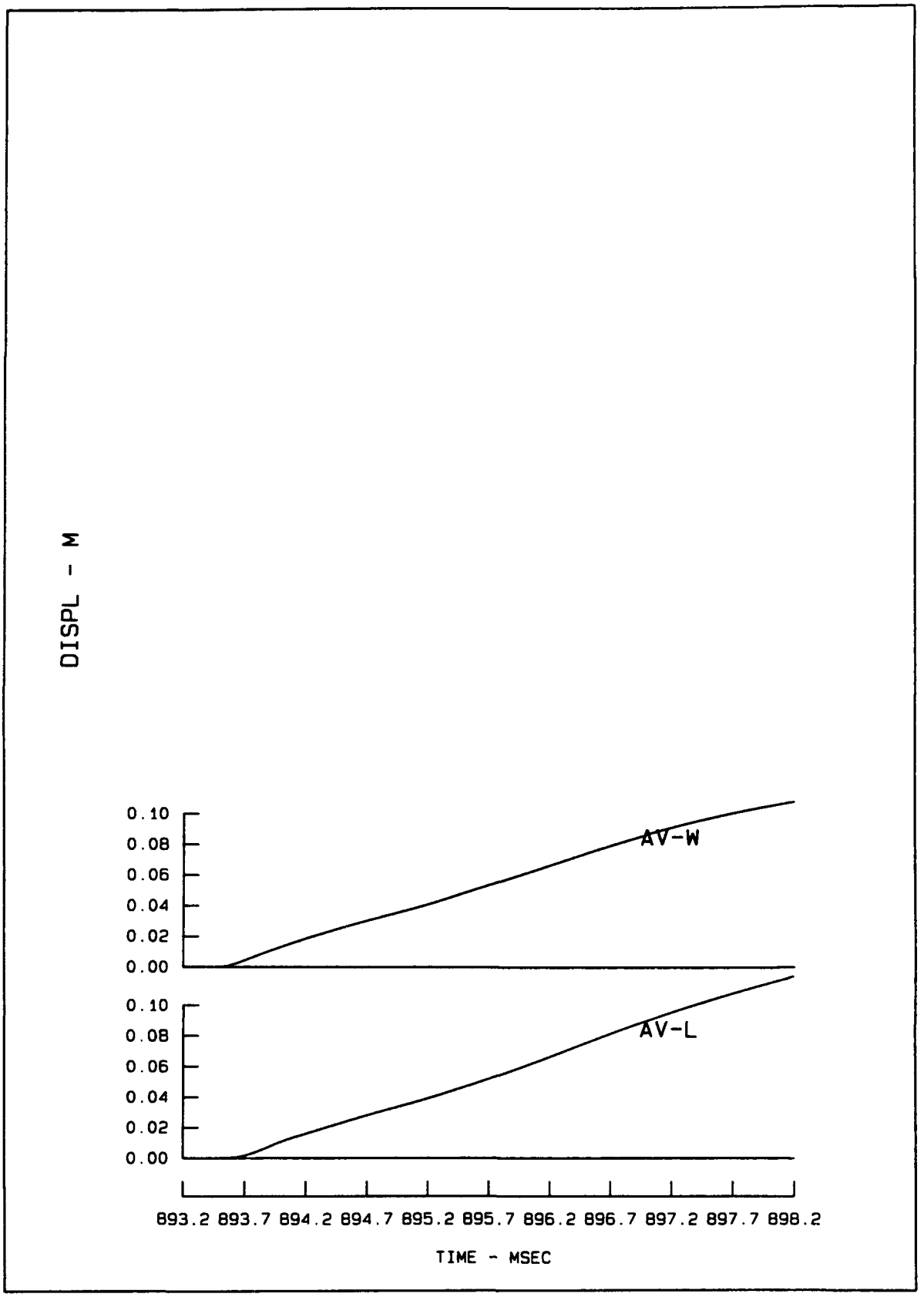

Figure D17. (Sheet 3 of 3)

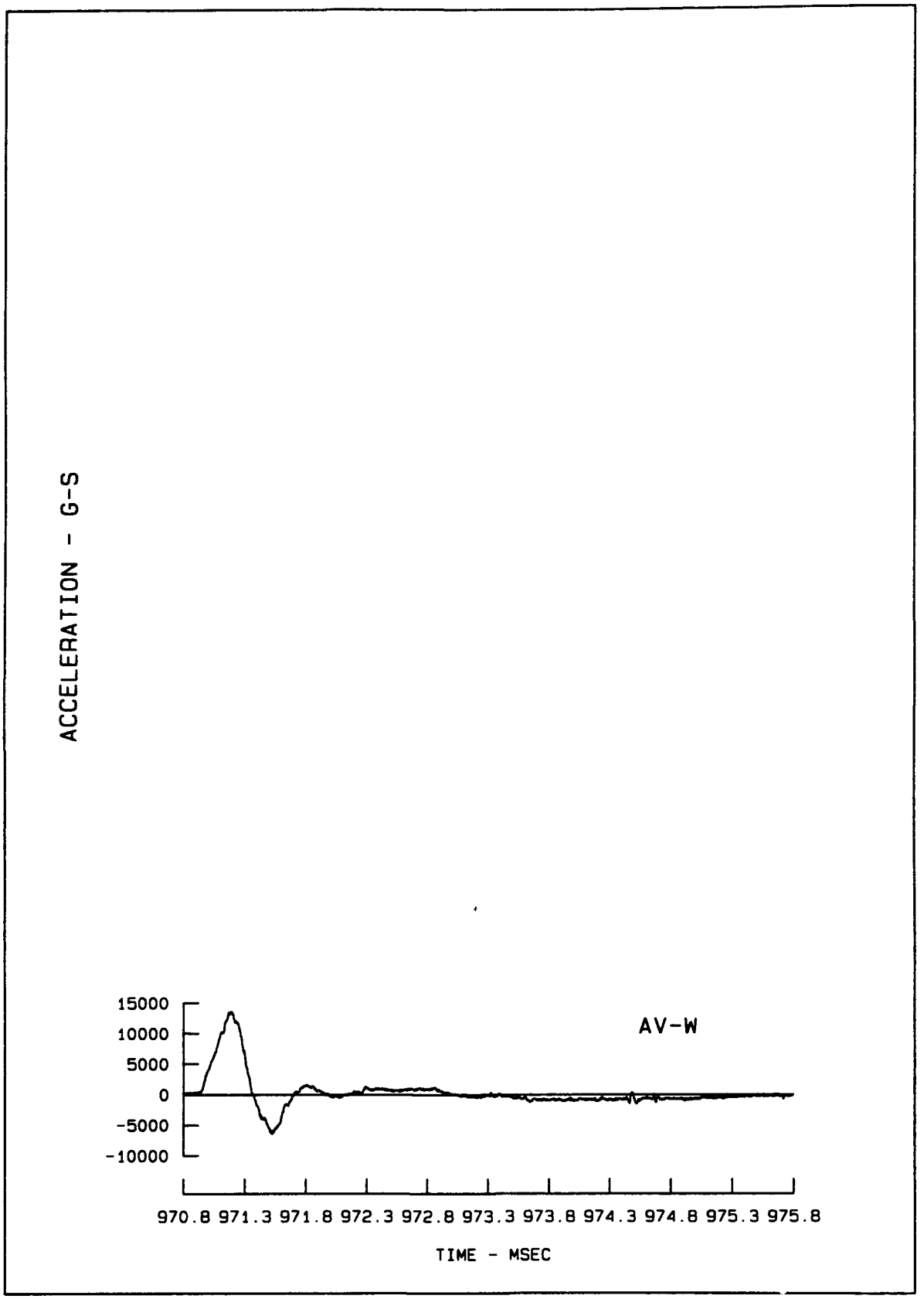

Figure D18. Acceleration, velocity, and displacement wave forms from Test 12 (Sheet 1 of 3)

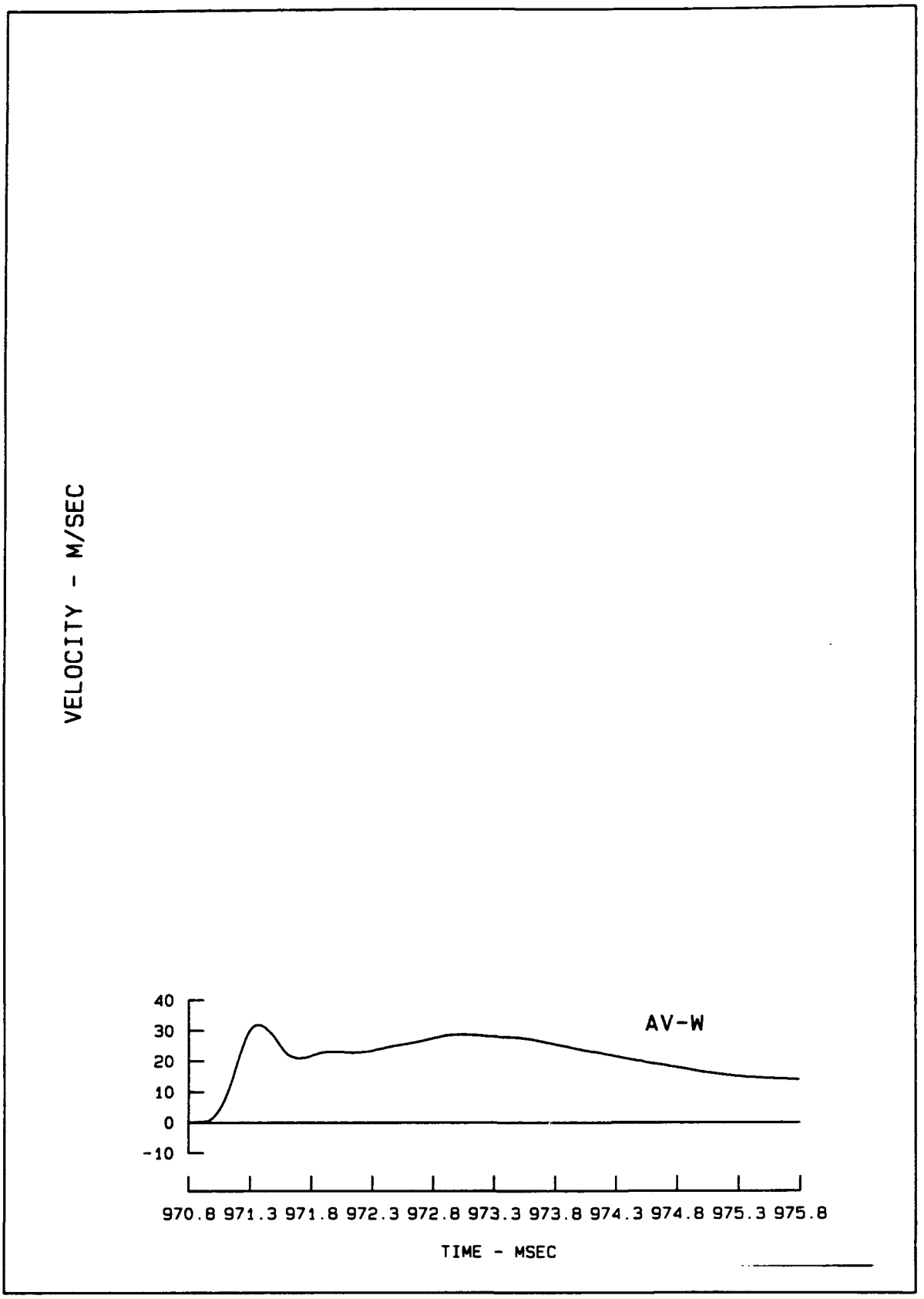

Figure D18. (Sheet 2 of 3)

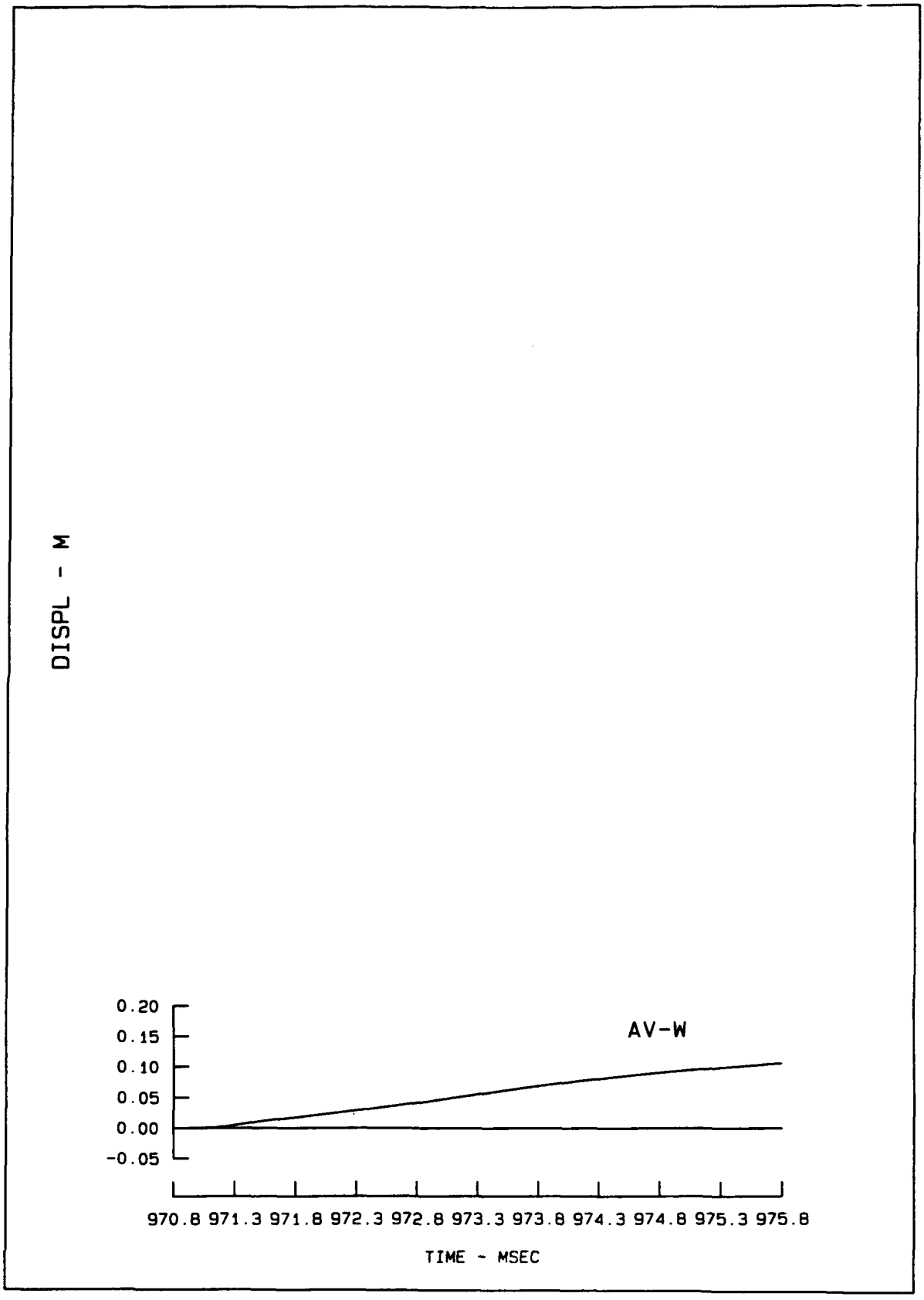

Figure D18. (Sheet 3 of 3)

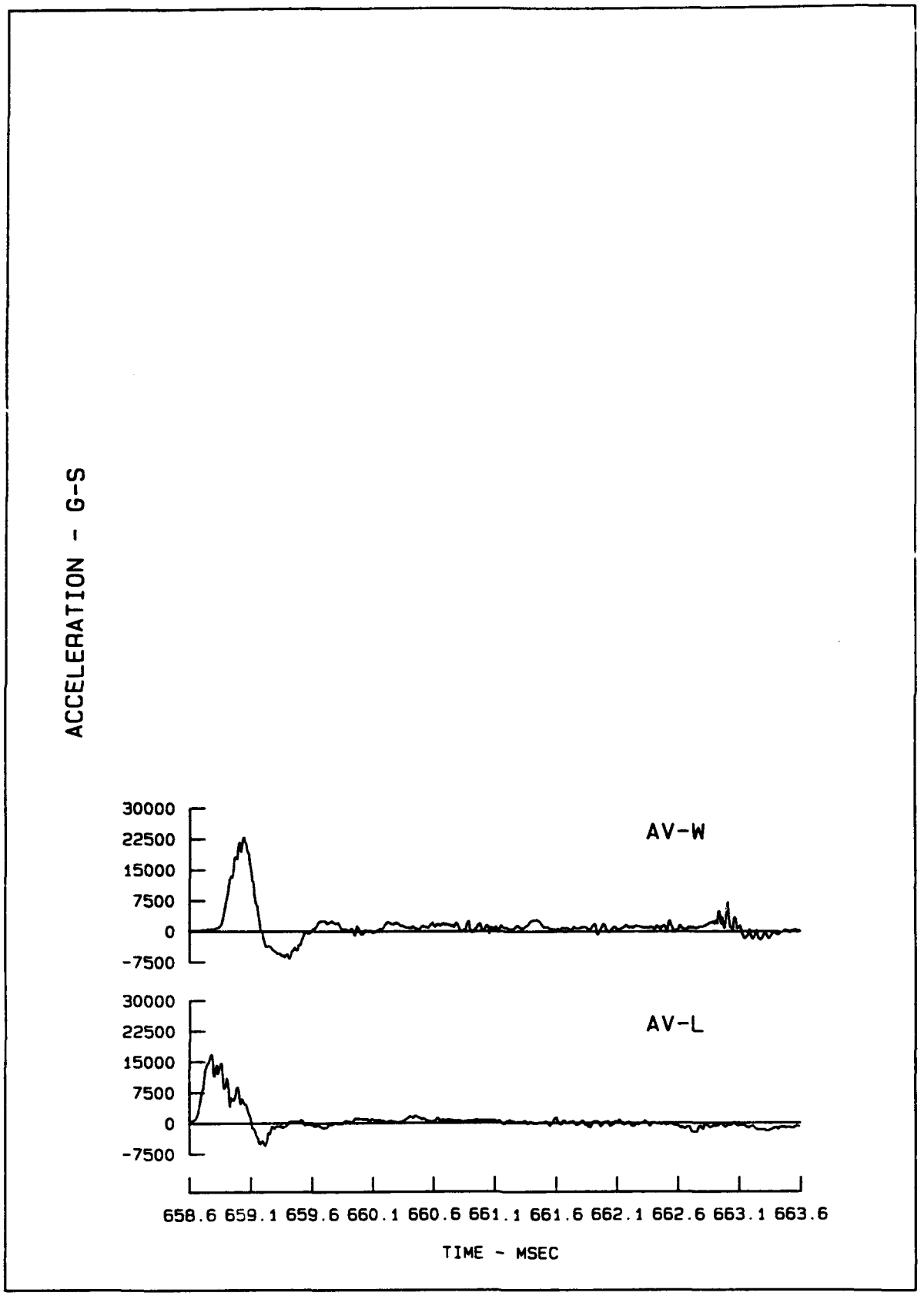

Figure D19. Acceleration, velocity, and displacement wave forms from Test 13 (Sheet 1 of 3)

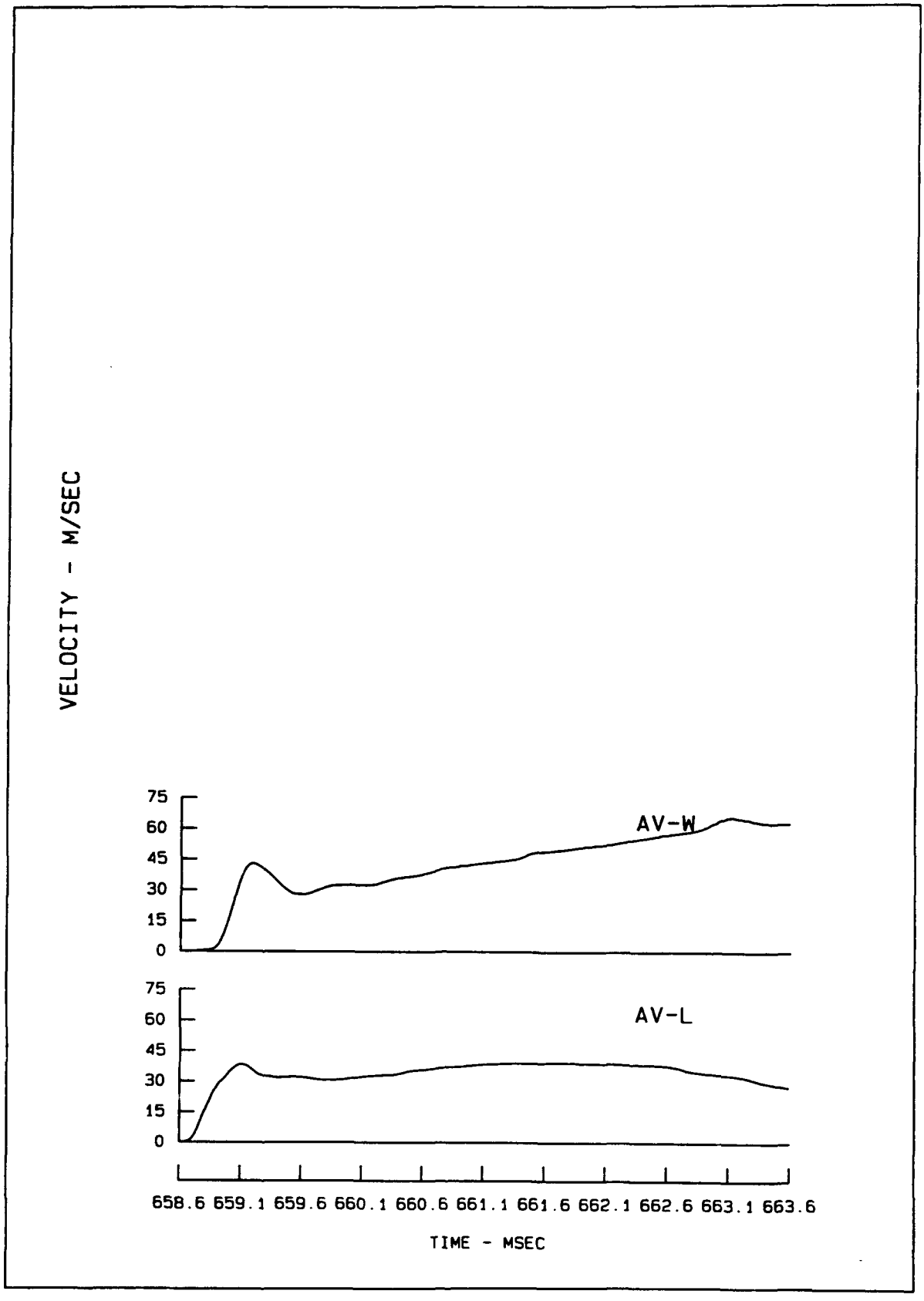

Figure D19. (Sheet 2 of 3)

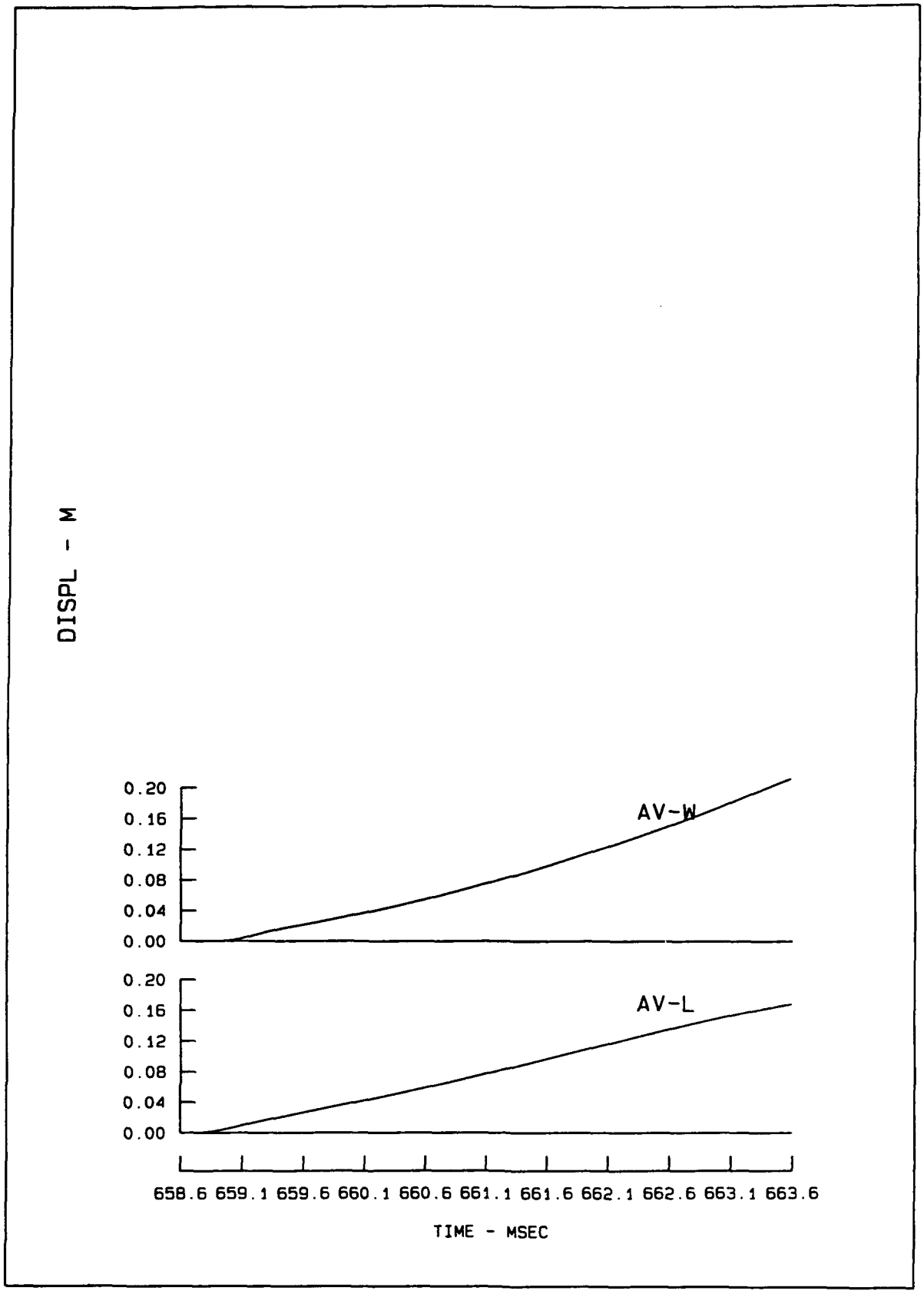

Figure D19. (Sheet 3 of 3)

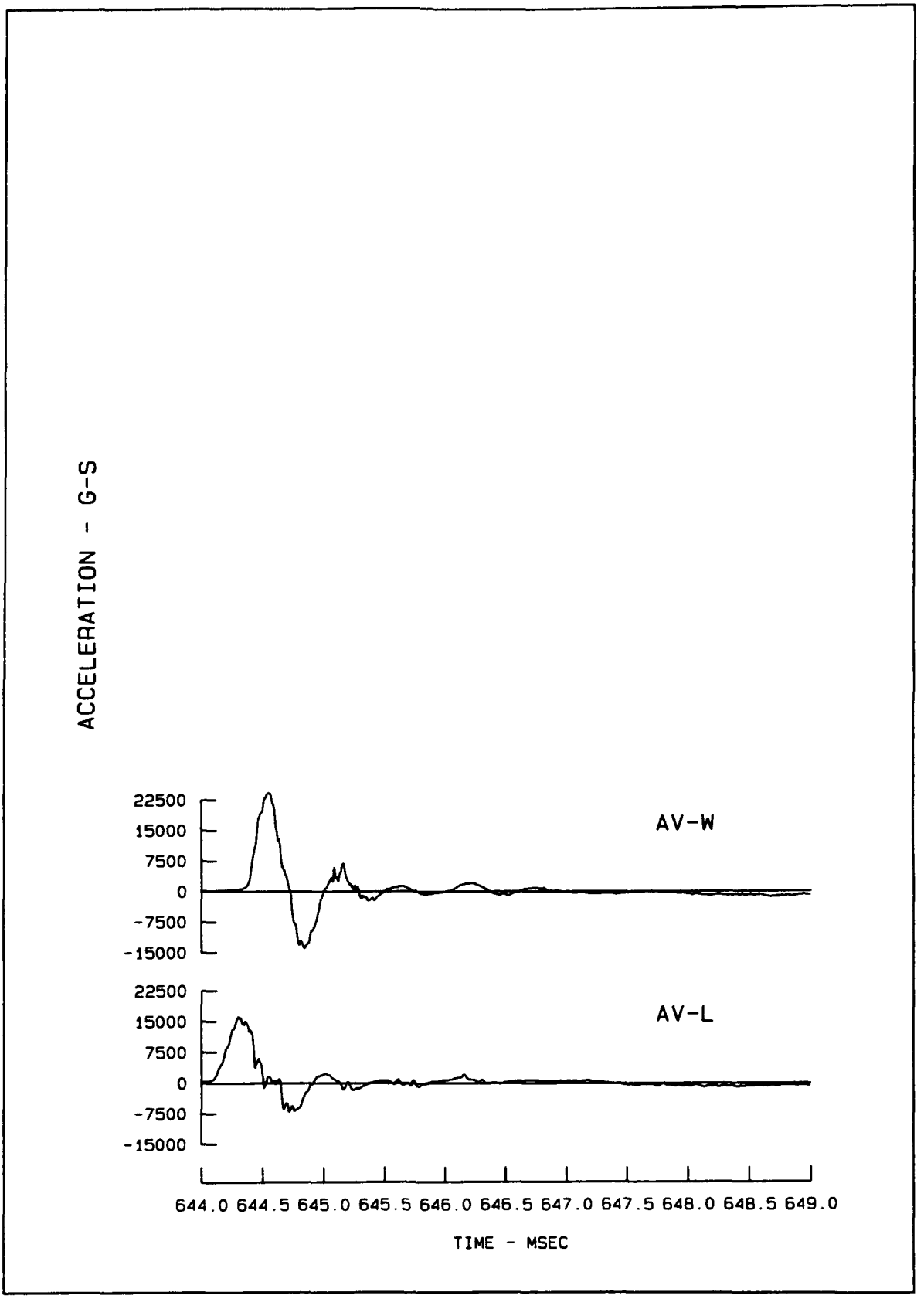

Figure D20. Acceleration, velocity, and displacement wave forms from Test 14 (Sheet 1 of 3)

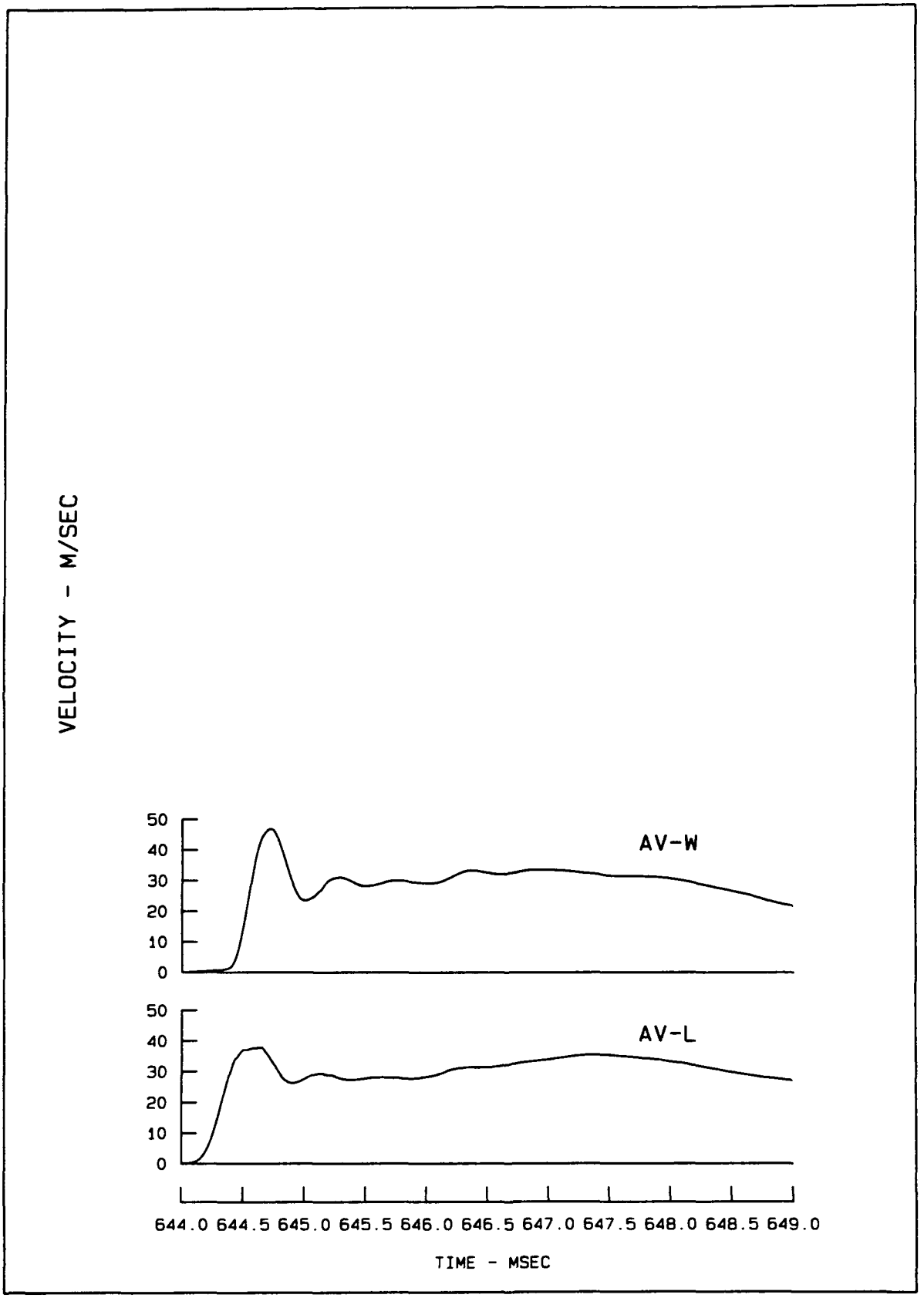

Figure D20. (Sheet 2 of 3)

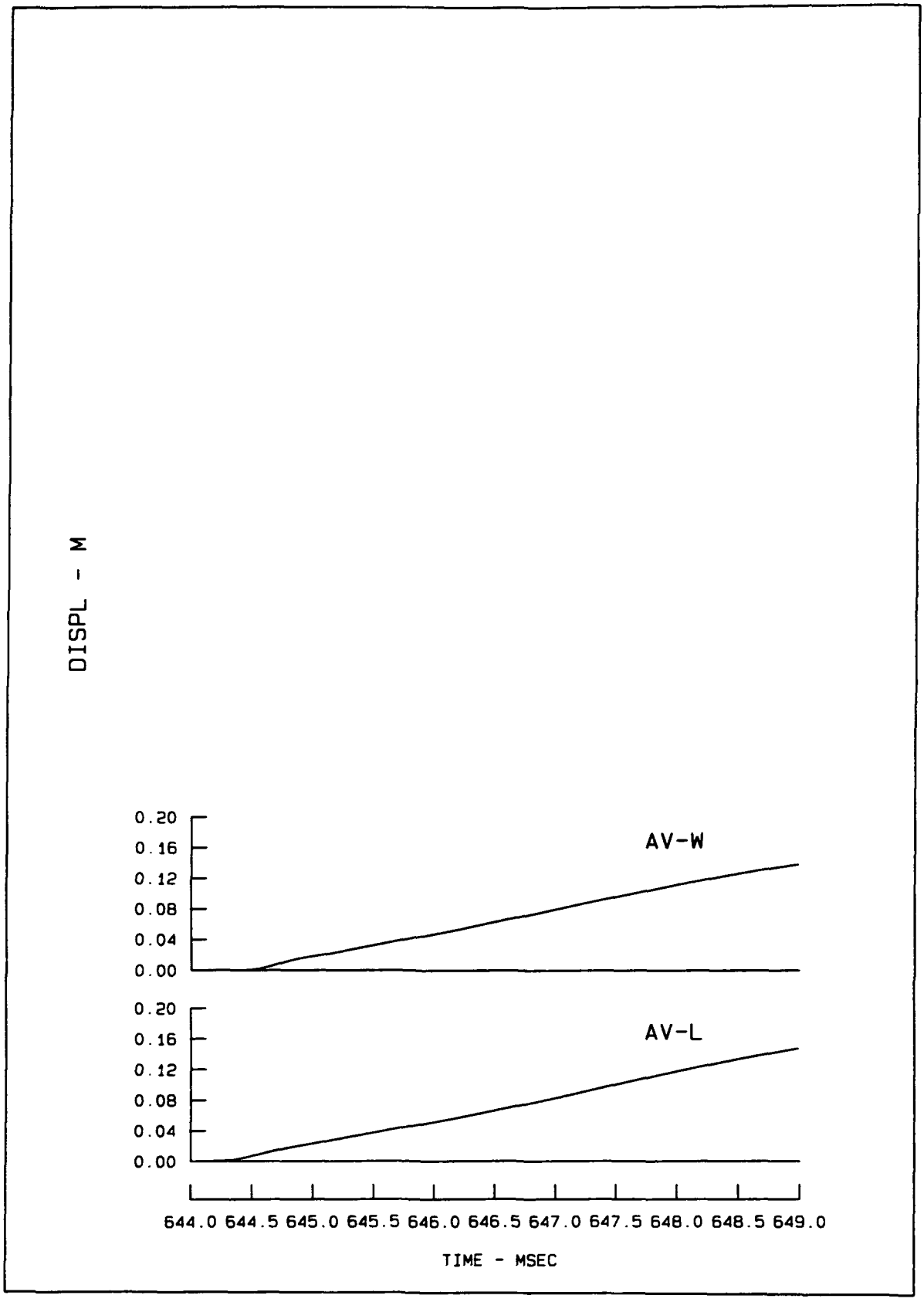

Figure D20. (Sheet 3 of 3)

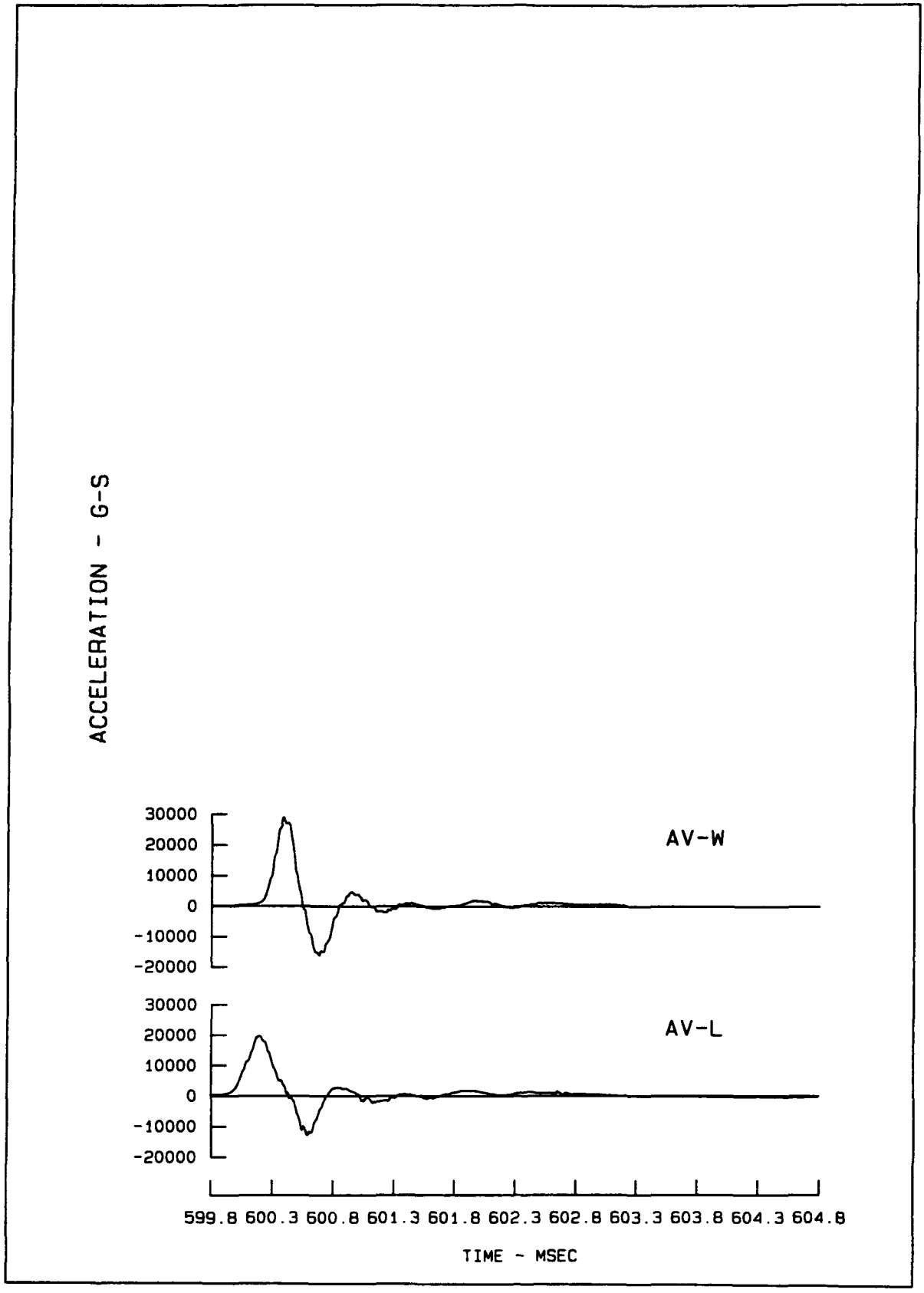

Figure D21. Acceleration, velocity, and displacement wave forms from Test 15 (Sheet 1 of 3)

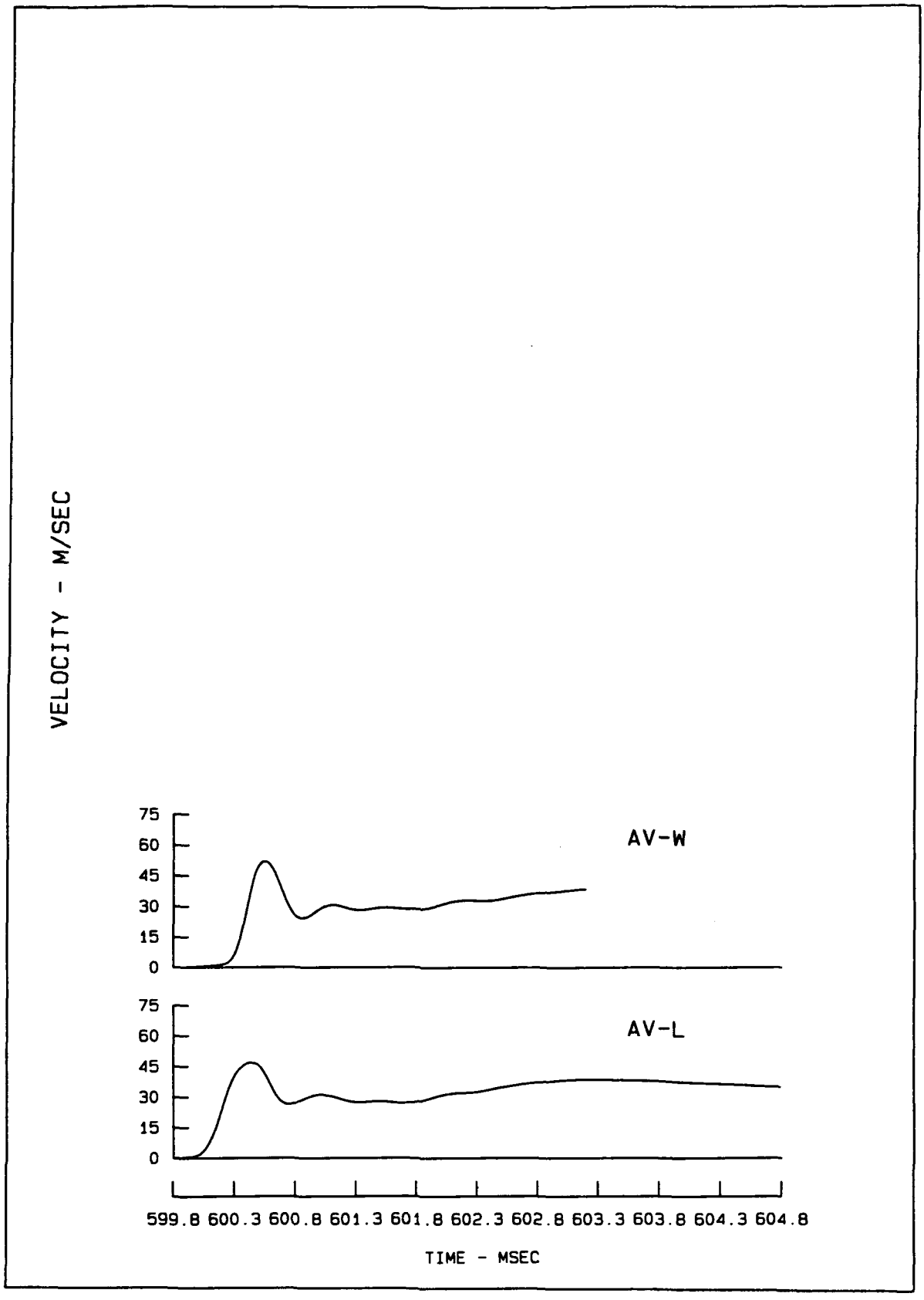

Figure D21. (Sheet 2 of 3)

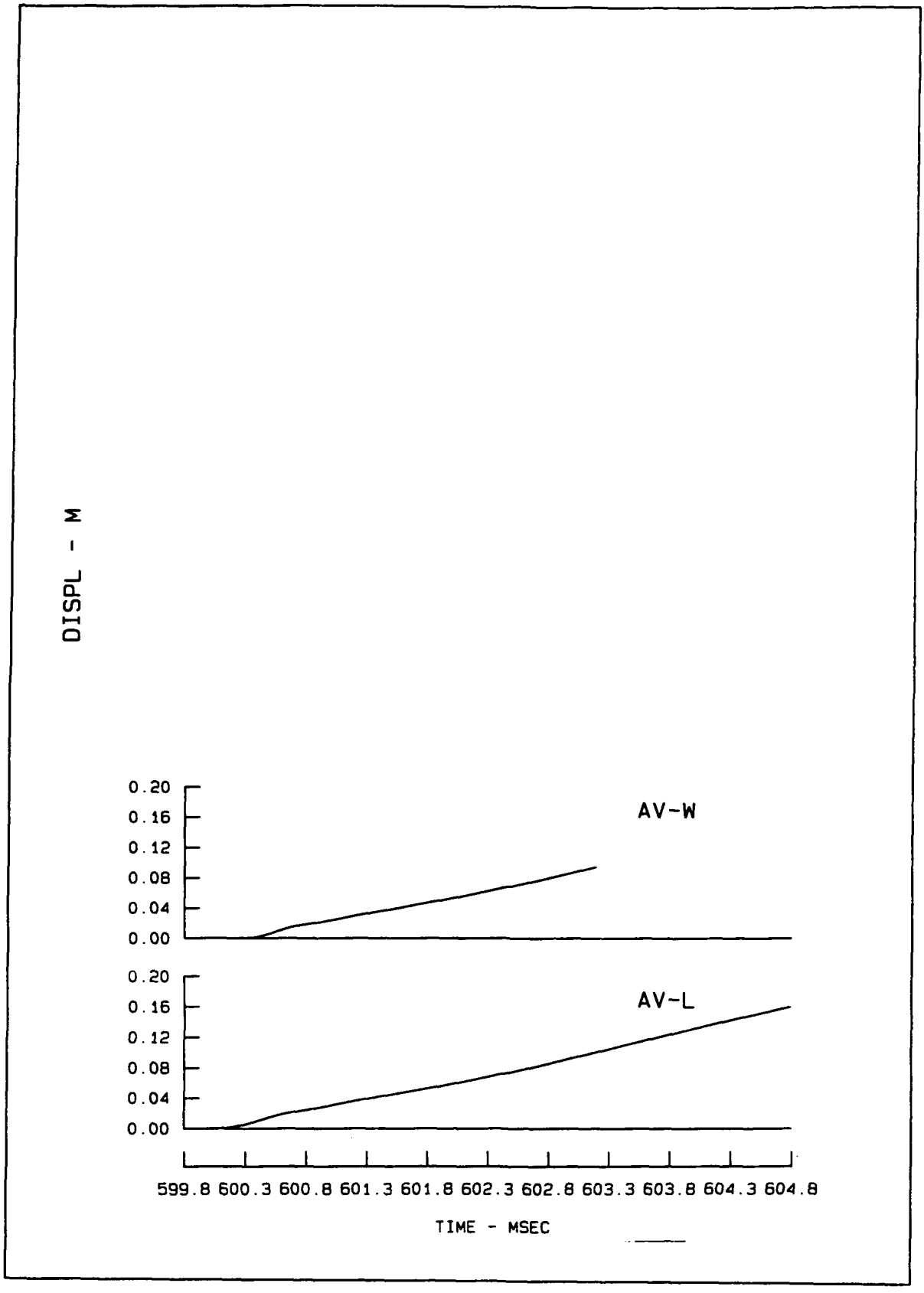

Figure D21. (Sheet 3 of 3)

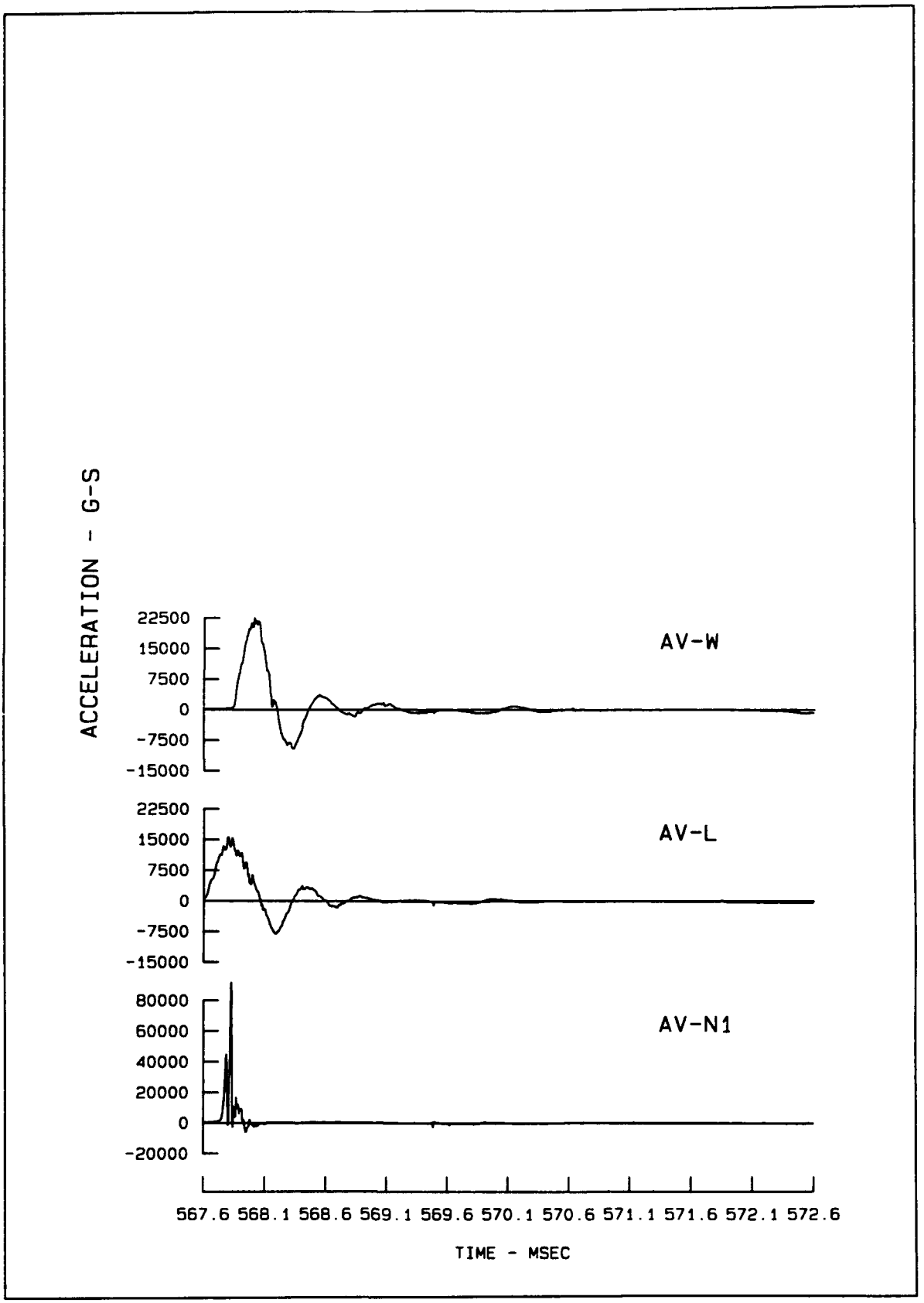

Figure D22. Acceleration, velocity, and displacement wave forms from Test 16 (Sheet 1 of 3)

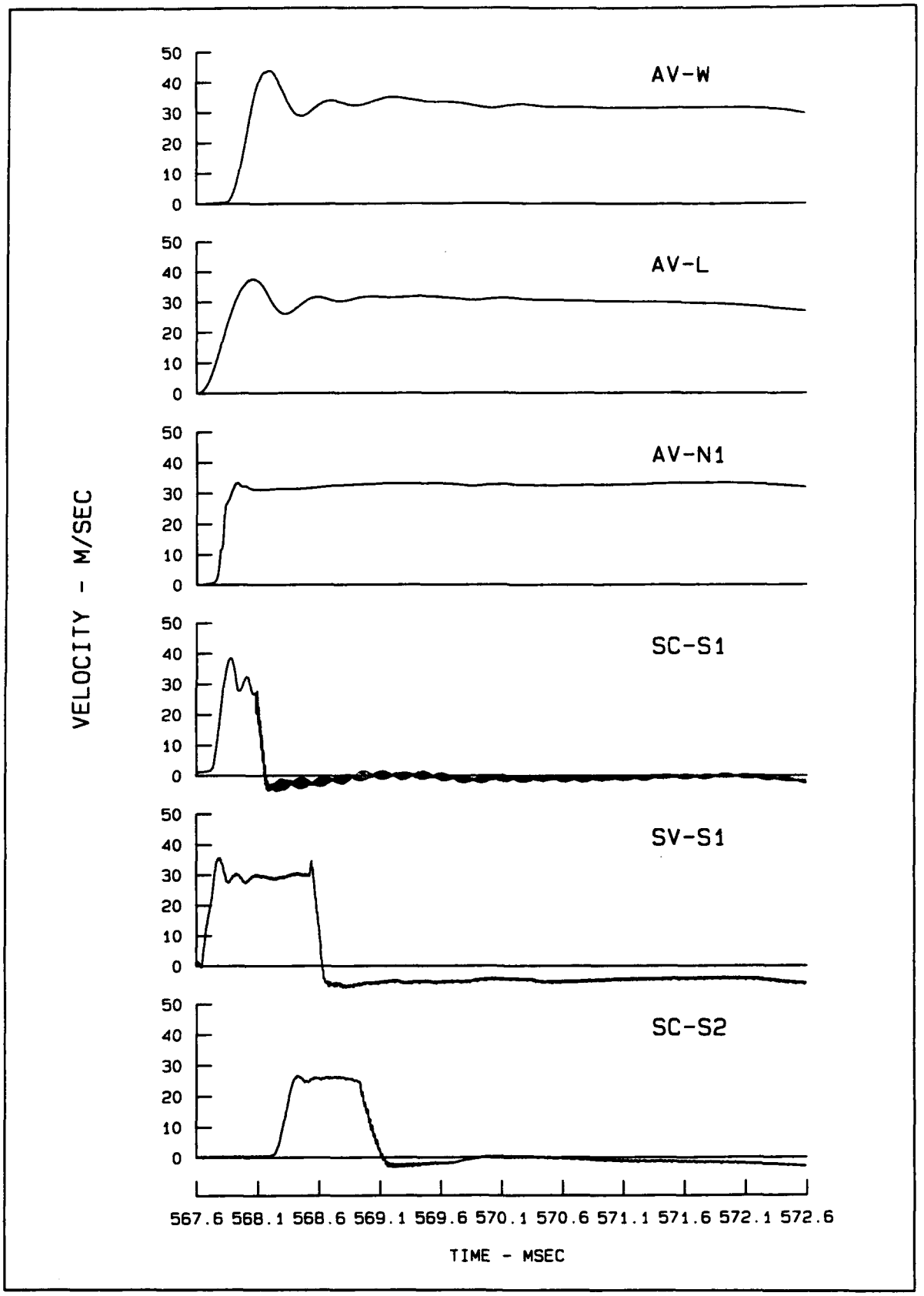

Figure D22. (Sheet 2 of 3)

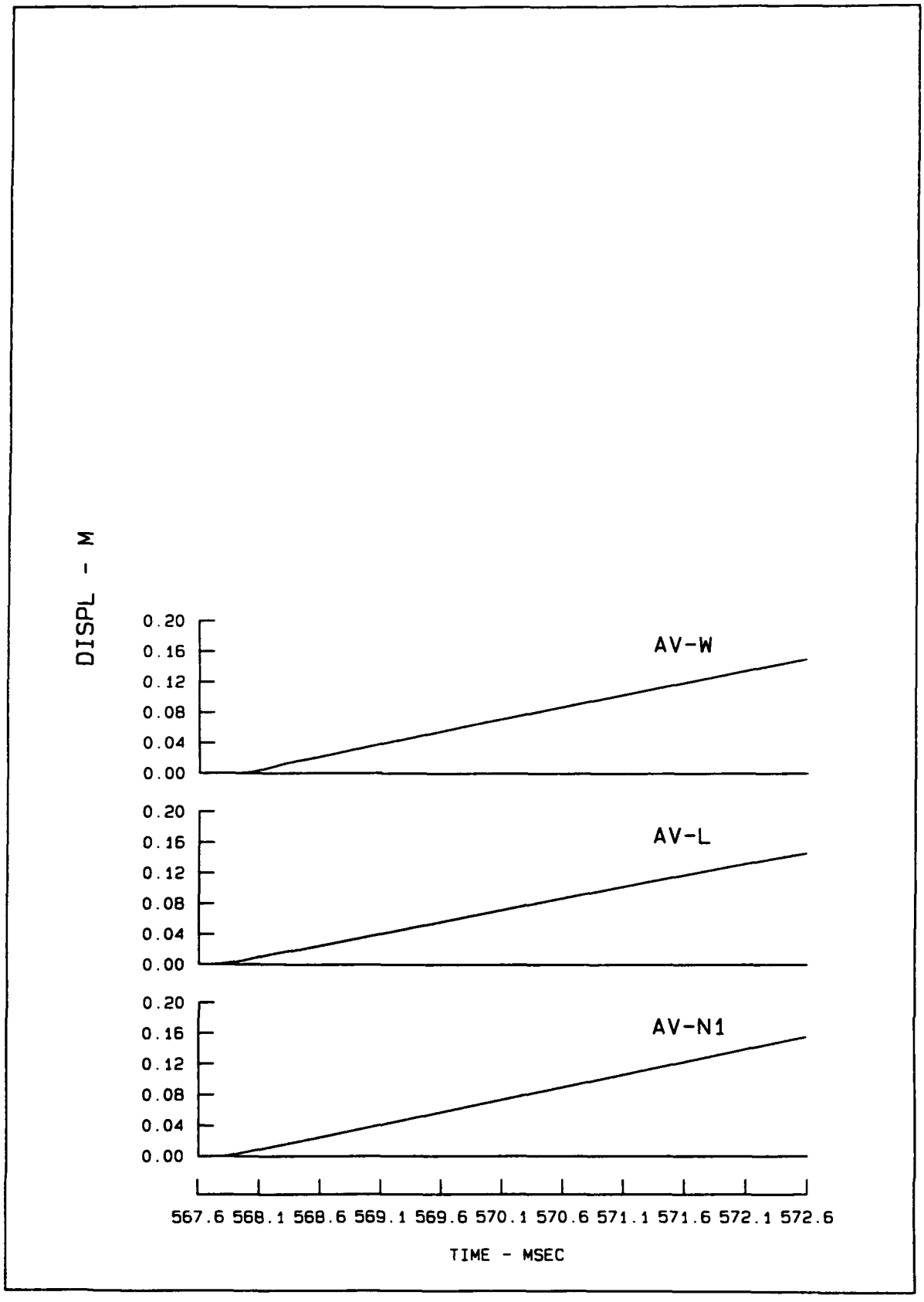

Figure D22. (Sheet 3 of 3)

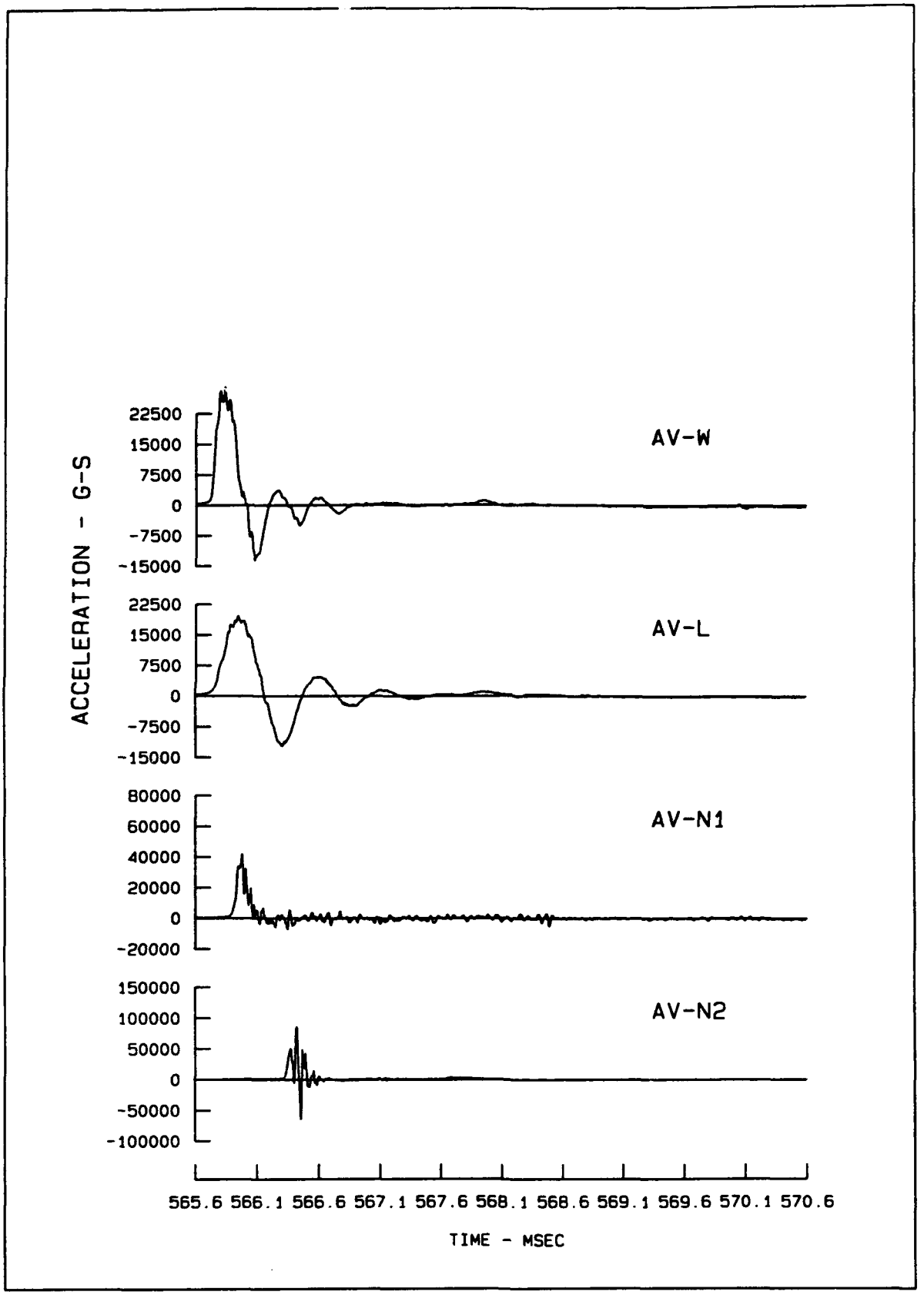

Figure D23. Acceleration, velocity, and displacement wave forms from Test 17 (Sheet 1 of 4)

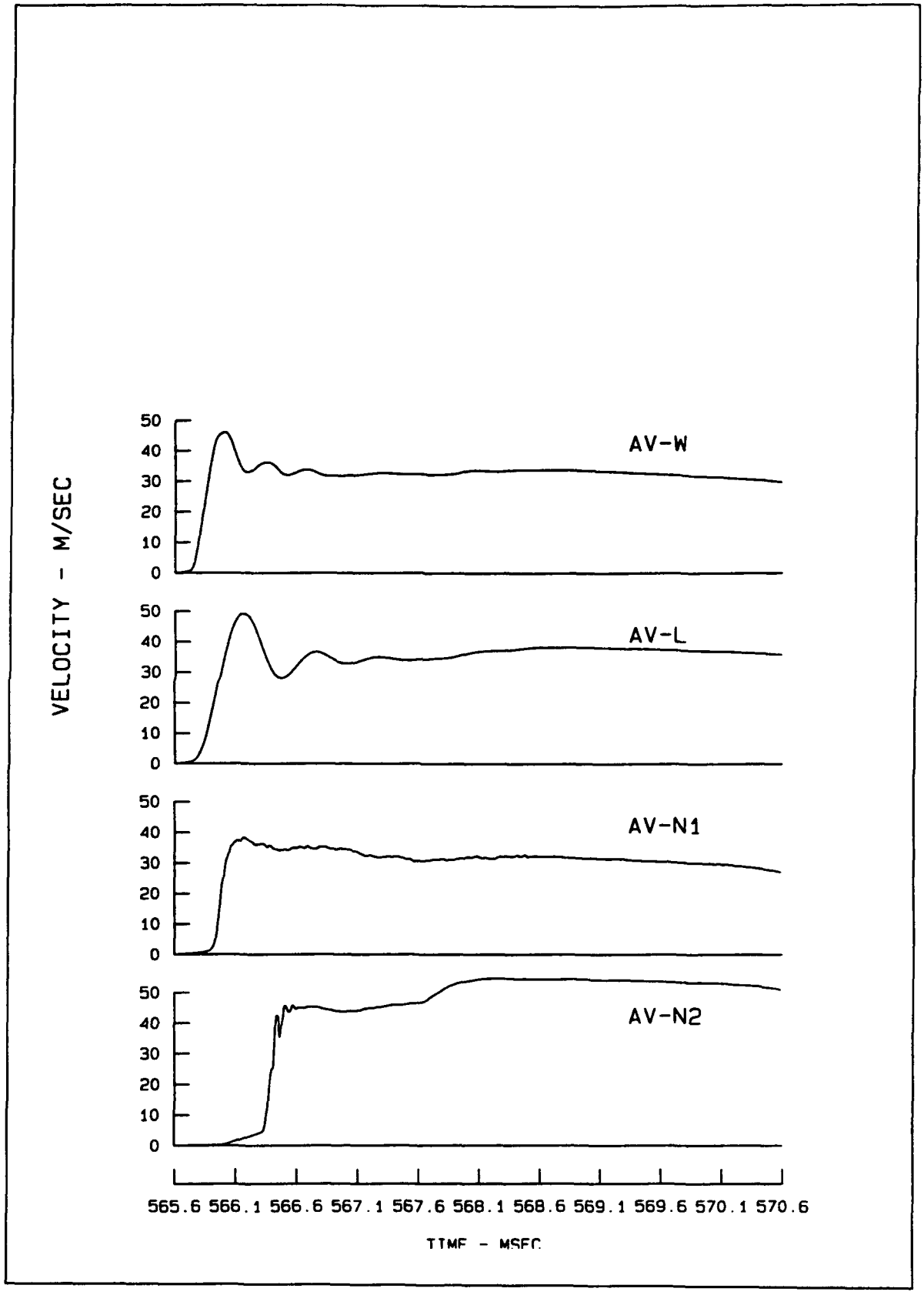

Figure D23. (Sheet 2 of 4)

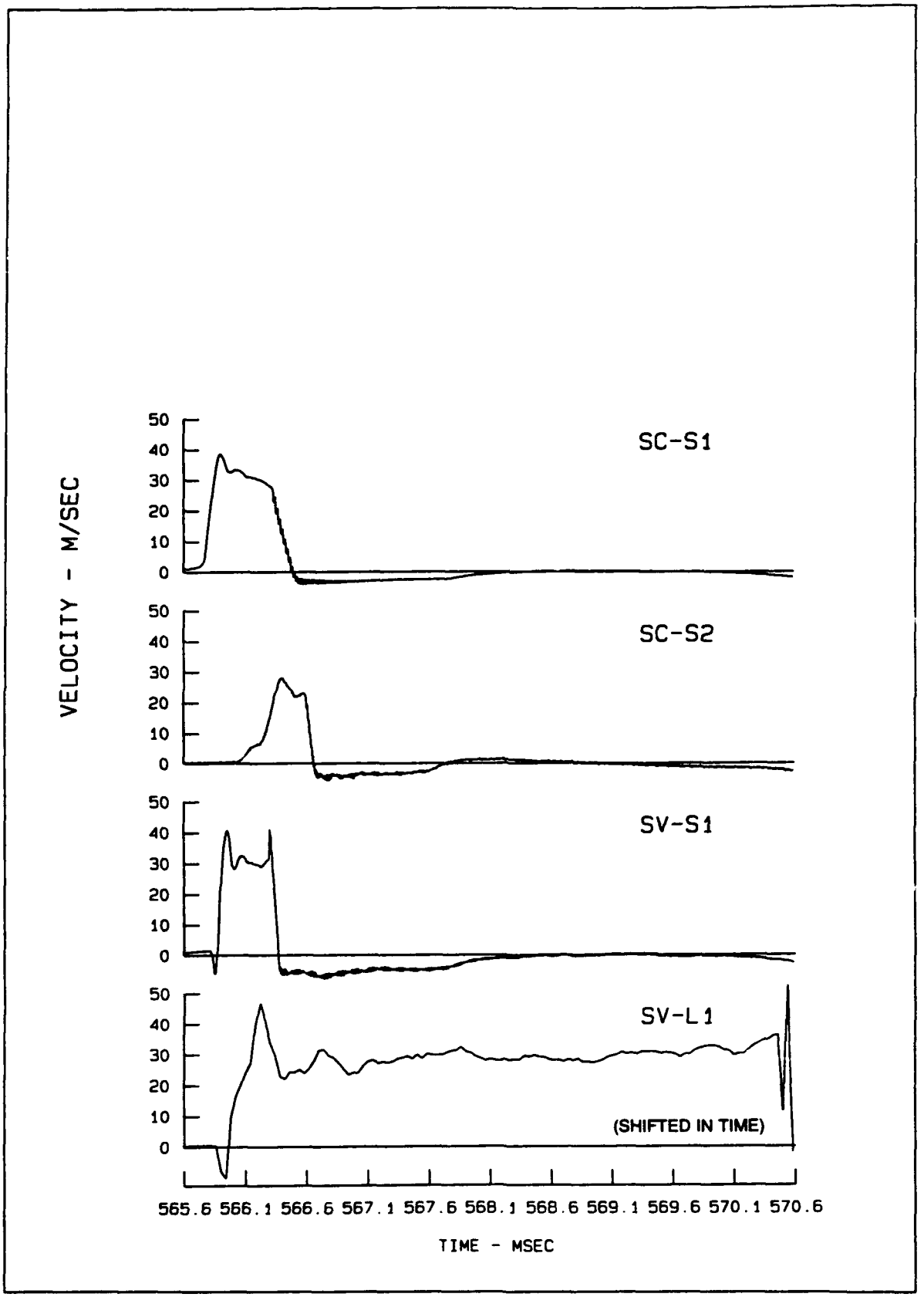

Figure D23. (Sheet 3 of 4)

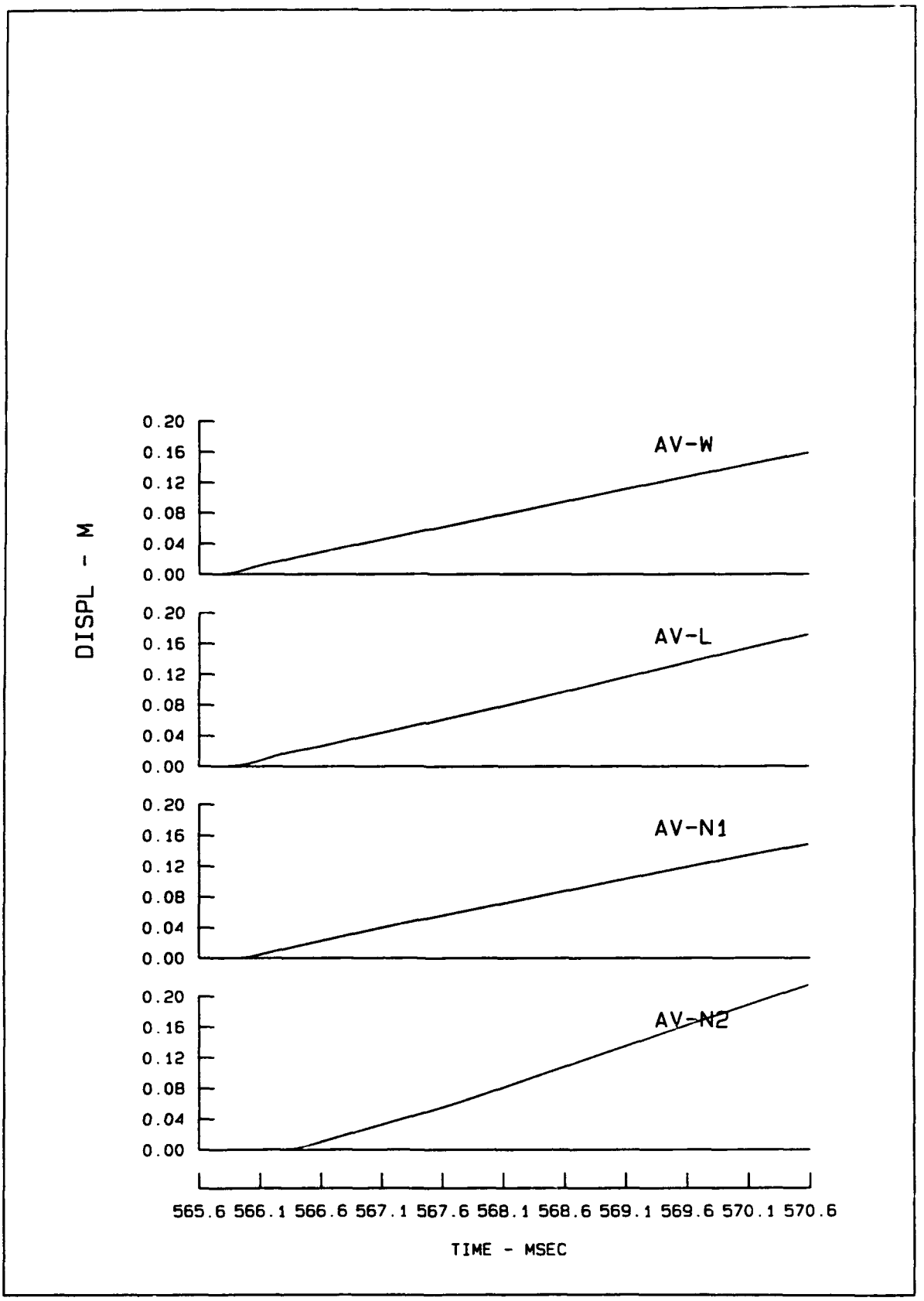

Figure D23. (Sheet 4 of 4)

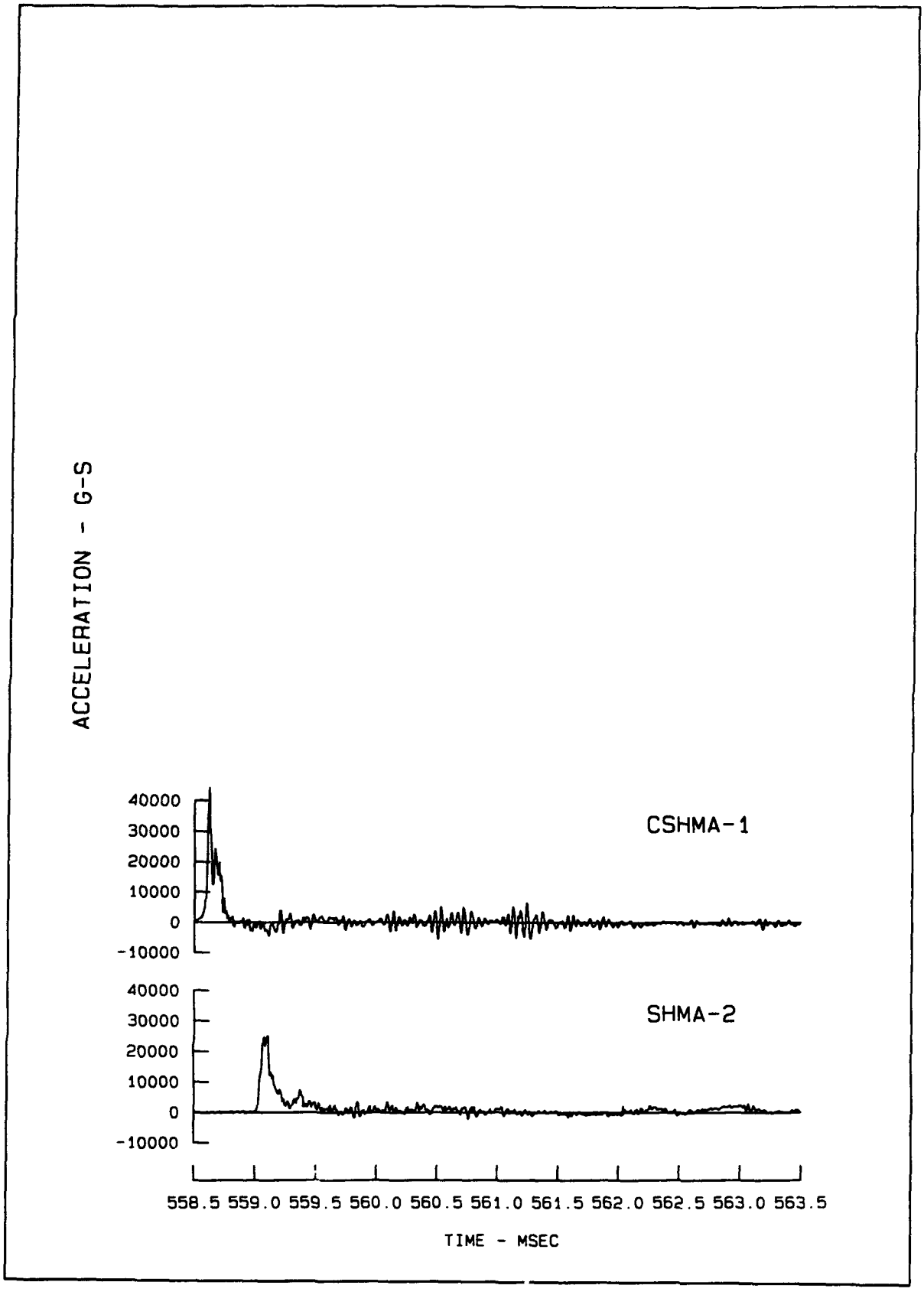

Figure D24. Acceleration, velocity, and displacement wave forms from Test 22 (Sheet 1 of 3)

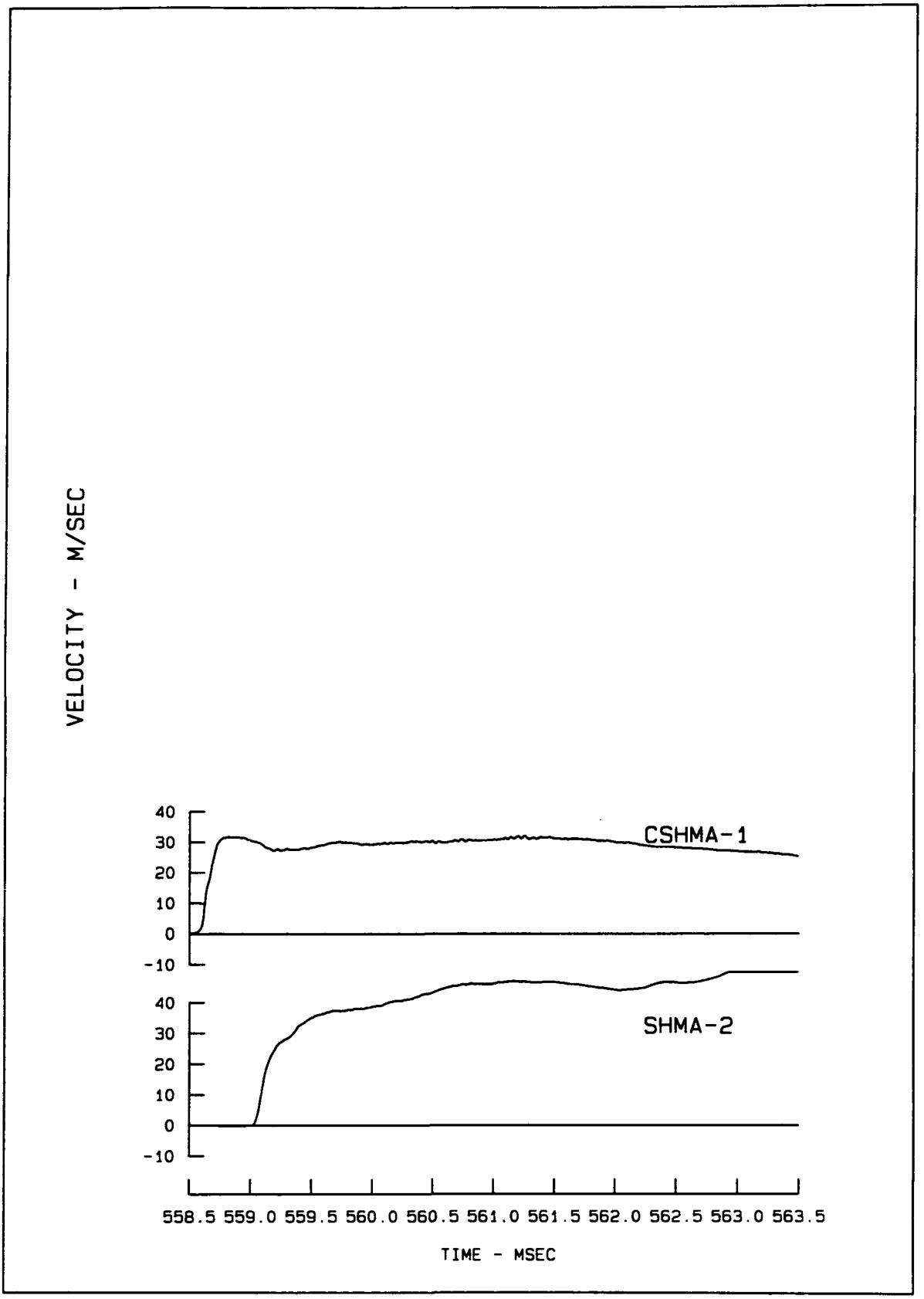

Figure D24. (Sheet 2 of 3)

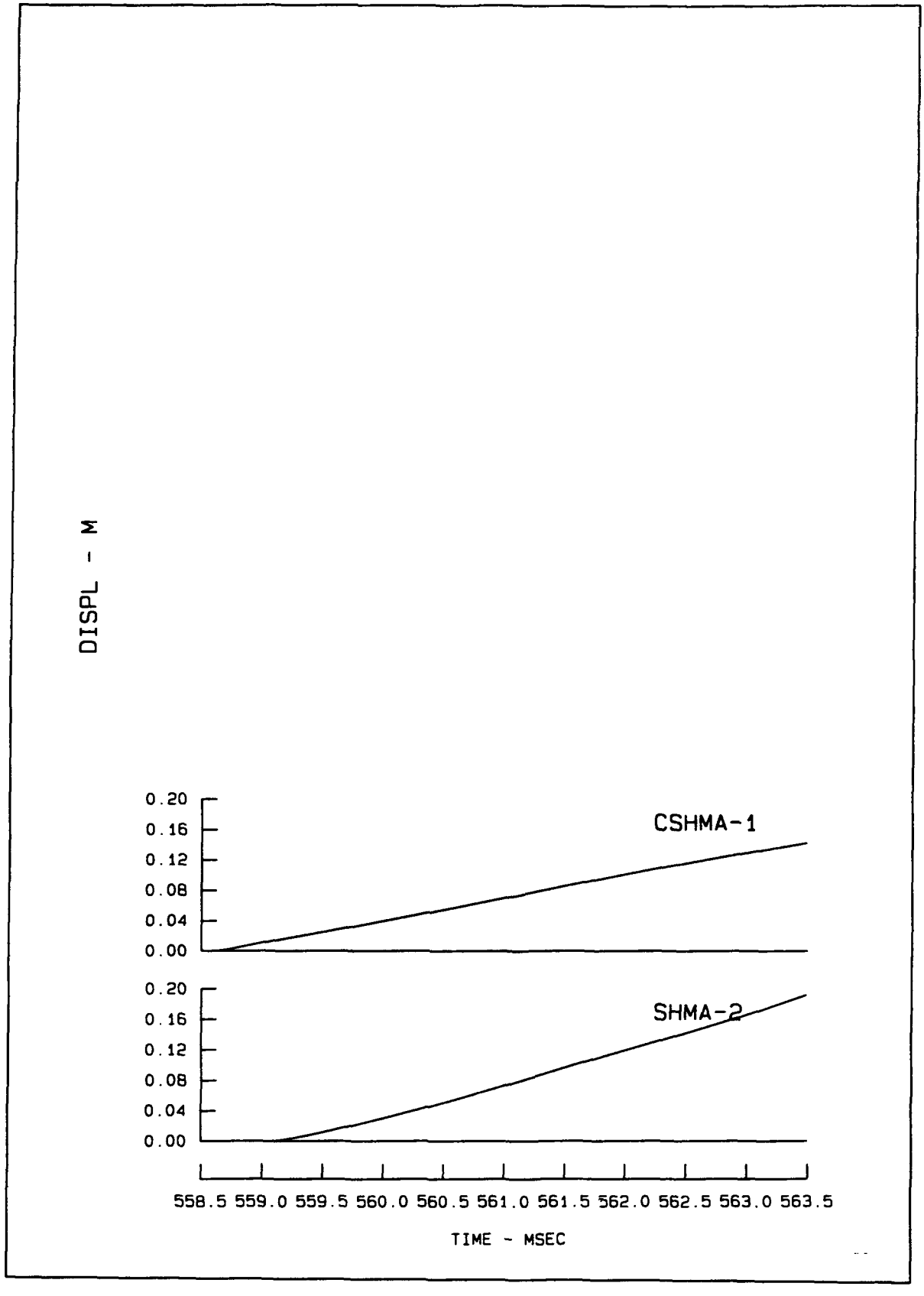

Figure D24. (Sheet 3 of 3)

REPORT DOCUMENTATION PAGE

Form Approved
OMB No. 0704-0188

Public reporting burden for this collection of information is estimated to average 1 hour per response, including the time for reviewing instructions, searching existing data sources, gathering and maintaining the data needed, and completing and reviewing the collection of information. Send comments regarding this burden estimate or any other aspect of this collection of information, including suggestions for reducing this burden, to Washington Headquarters Services, Directorate for Information Operations and Reports, 1215 Jefferson Davis Highway, Suite 1204, Arlington, VA 22202-4302, and to the Office of Management and Budget, Paperwork Reduction Project (0704-0188), Washington, DC 20503.

1. AGENCY USE ONLY (Leave blank)	2. REPORT DATE	3. REPORT TYPE AND DATES COVERED
	February 1994	Technical 900124-921231

4. TITLE AND SUBTITLE
DNA/WES Ground Motion Test Facility—Results and Analysis of Impact Tests Against Masonry and Socorro Plaster Sand Testbeds

5. FUNDING NUMBERS
C-MIPR 90-594
MIPR 91-571
MIPR 92-573
MIPR HDH02-1-A45V25
PE-4662
PR-RJ, AB

6. AUTHOR(S)
Howard G. White and John T. Byrne

7. PERFORMING ORGANIZATION NAME(S) AND ADDRESS(ES)
U.S. Army Engineer Waterways Experiment Station
Structures Laboratory, Explosion Effects Division
3909 Halls Ferry Road
Vicksburg, MS 39180-6199

8. PERFORMING ORGANIZATION REPORT NUMBER
Technical Report
SL-94-2

9. SPONSORING/MONITORING AGENCY NAME(S) AND ADDRESS(ES)
Defense Nuclear Agency
6801 Telegraph Road
Alexandria, VA 22310-3398
TDTR/Flohr

10. SPONSORING/MONITORING AGENCY REPORT NUMBER
DNA-TR-93-114

11. SUPPLEMENTARY NOTES
This work was sponsored by the Defense Nuclear Agency under RDT&E RMC Codes B4662 D RJ RI TDTR 5200 A 25904D, B 4662 D RJ RI TDTR 5200A 25904D

12a. DISTRIBUTION/AVAILABILITY STATEMENT
Approved for public release; distribution is unlimited.

12b. DISTRIBUTION CODE

13. ABSTRACT *(Maximum 200 words)*

The DNA/WES Ground Motion Test Facility is a vertical gas gun with a 4-ft diameter projectile. This report describes use of this facility for conducting tests with sand testbeds.

A description of testbed construction and testing procedures is discussed. Stress and velocity histories are presented from each test. Analysis of the data includes determination of the propagation velocity of the loading and rarefaction waves in a test article. A method for analyzing impacts for planarity and angle of impact is presented.

This test facility is a viable tool for instrumentation development studies. Investigations using the limited database available indicate that the gun provides a unique capability for determination of dynamic material properties for large geologic samples. These tests provided valuable information on the performance of weapons effects instruments prior to their use in large field tests. Analytic tools developed for analyzing test data will impact future tests by providing tolerances for various aspects of testing and by optimizing instrument arrays for cross correlation of stress and velocity data.

14. SUBJECT TERMS

Gas gun	Instrument calibration
Ground motion	Projectile impact
Ground shock	Planarity

15. NUMBER OF PAGES
153

16. PRICE CODE

17. SECURITY CLASSIFICATION OF REPORT	18. SECURITY CLASSIFICATION OF THIS PAGE	19. SECURITY CLASSIFICATION OF ABSTRACT	20. LIMITATION OF ABSTRACT
UNCLASSIFIED	UNCLASSIFIED	UNCLASSIFIED	SAR

5. FUNDING NUMBERS (Continued).
TA-RI, EA
WUDH082372

7. PERFORMING ORGANIZATION NAME(S) AND ADDRESS(ES) (Continued).

IIT Research Institute
10 West 35th Street
Chicago, Illinois 60616-3799

11. SUPPLEMENTARY NOTES (Continued).

B 4662 D AB EA TDTR 5200 A 25904D